2010

Cell Death Mechanisms in Drosophila Differentiated Photoreceptor Neurons

Alexis Robert Gambis

CELL DEATH MECHANISMS IN *DROSOPHILA* DIFFERENTIATED PHOTORECEPTOR NEURONS

A Thesis Presented to the Faculty of

The Rockefeller University

in Partial Fulfillment of the Requirements for

the degree of Doctor of Philosophy

by

Alexis Robert Gambis

June 2010

CELL DEATH MECHANISMS IN *DROSOPHILA* DIFFERENTIATED PHOTORECEPTOR NEURONS

Alexis Robert Gambis, Ph.D.

The Rockefeller University 2010

Apoptosis, or programmed cell death, is a form of physiological cell death that is essential for normal development and homeostasis. At the end of pupal development of the *Drosophila* retina, cell death terminates and photoreceptor neurons complete their differentiation process. We use these terminally differentiated photoreceptor neurons as a system to study neurodegeneration. We first adapt and develop fluorescent tools for photoreceptor visualization *in vivo*. These tools enable a recessive genetic screen to search for genes required for the survival of differentiated photoreceptors. Many redox and mitochondrial genes were found to protect photoreceptors from late cell death. Here, we focus on the iron-storage complex, Ferritin. *ferritin* mutations lead to caspase activation and photoreceptor neuronal death during development and sensitize adult photoreceptor neurons to cell death stimuli. *ferritin* mutations provide a robust model to study the role of iron and oxidative stress in

neurodegeneration. To further investigate the role of Ferritin in photoreceptor survival, we generate genetically-encoded *in vivo* iron and redox sensors.

In summary, by developing novel tools for photoreceptor cell visualization, we explore the neuro-specific mechanisms required for lifelong photoreceptor neuron survival. We perform a photoreceptor-specific genetic screen and characterize Ferritin's role in shielding photoreceptor cells from iron and oxidative stress-induced cell death.

Pour ma famille, Stephanie, les 2 autres tumbadores, Ehsan et Daniel

… et bien sûr Imagine Science Films

Imagination is more important than knowledge

Albert Einstein

ACKNOWLEDGEMENTS

A very special thanks goes to my adviser Hermann Steller for his support, inspiration and advice over the years. I would also like to thank Bertrand Mollereau for the on-sight training in the early stages of my project, and for his ongoing support overseas. A warm thank you goes to my committee members, Shai Shaham and Michael Young, for their guidance over the years. I also want to thank my external reader Claude Desplan for his time and commitment, and Cesar Mendes for guiding me during my first months in the laboratory. I am indebted to Ulrike Gaul for complementing a computationally trained young graduate student with the tools of molecular biology during my rotation in her lab. Thank you to Fanis Missirlis who gave me a crash course on the *Drosophila* iron and antioxidant regulation systems and invited me to give a plenary talk at the Fly Iron Meeting in London last year. A big hug goes to Samara Brown for her technical, fly and "editing" support in the laboratory from the very beginning. I thank all the past and present members of the Steller lab, and Pierre Dourlen who helped me with the genetic screen for a summer. Finally, this dedication will not be complete without loud stage applause to Cris at the Dean's Office for formatting/printing help, and all my friends, especially Ehsan, Daniel, Stephanie, Andy and Kate, who have been a great support over the years.

TABLE OF CONTENTS

LIST OF FIGURES

LIST OF TABLES

LIST OF ABBREVIATIONS

4E-BP	4E-Binding Protein
AD	Alzheimer's Disease
AO	Acridine Orange
AIF	Apoptosis Inducing Factor
ALD	Adrenuleukodystrophy
ALS	Amyotrophic Lateral Scelorsis
AMD	Age Macular Degeneration
ANTP	Antennapedia
A/P	Anterior/Posterior
APAF-1	Apoptosis Protease Activating Factor-1
APF	After Puparium Formation
APP	Amyloid Precusor Protein
Ark	Apaf-1 related killer
ASYN	Alpha Synuclein
BAX	Bcl-2-Associated-X
Bcl-2	B-cell lymphoma leukemia-2
BDGP	Berkeley *Drosophila* Genome Project
BH	Bcl-2 Homology
BH3	Bcl-2 Homology-3
BID	Bcl-2 Interaction Domain
BIR	Baculovirus IAP Repeat
Bgm	Bubblegum
CAD	Caspase Activated DNase
CARD	Caspase Activation and Recruitment Domain
Caspase	Cysteine Aspartate-specific protease

CAT	Catalase
Cdk	Cyclin-dependent Kinase
Ced	Cell death abnormal
C. elegans	*Caenorhabititis elegans*
Cp	Ceruplasmin
cpYFP	circularly permuted YFP
Cyt-c	Cytochrome-c
Dcp-1	Death caspase-1
DD	Death Domain
DED	Death Effector Domain
Dfd	Deformed
DIABLO	Direct IAP Binding Protein with Low PI
Diap1	*Drosophila* IAP-1
Diap2	*Drosophila* IAP-2
DNP	Dinitrophenylhydrazone
DNPH	2,4-Dinitrophenylhydrazine
Dp53	*Drosophila* p53
H99	Df(3L)H99
Dfh	*Drosophila* frataxin homologue
DGC	Dystroglycan-Dystrophin Complex
DISC	Death Inducing Signaling Complex
dPINK	*Drosophila* Pten-INduced Kinase 1
DR	Death Receptor
DTraf (1/2)	*Drosophila* TNFα Receptor Associated Factor (1/2)
Dtps1	*Drosophila* tretahalose-6-phosphase synthase 1
D/V	Dorsal/Ventral
EGFR	Epidermal Growth Factor Receptor

Egl	Egg laying defective
EM	Electron Microscopy
EndoG	Endonuclease G
ER	Endoplasmic Reticulum
eiF4A	Eukayotic Initiation Factor 4A
eIF4E	Eukayotic Initiation Factor 4E
Ey	Eyeless
FAC	Ferric Ammonium Citrate
FADD	Fas-Associated-Death-Domain
FALS	Familial ALS
FasL	Fas Ligand
Fatp	Fatty Acid Transport Protein
Fer1HCH	Ferritin 1 Heavy Chain Homologue
Fer2LCH	Ferritin 2 Light Chain Homologue
Fer3HCH	Ferritin 3 Heavy Chain Homologue
FRT	Flp Recombination Target Site
FHC	Ferritin Heavy Chain
FLC	Ferritin Light Chain
FLP	FLip Recombinase
GCLM	Glutamate-cysteine ligase modifier subunit
GH3	Grim Homology 3
GFP	Green Fluorescent Protein
GMR	Glass Multimer Reporter
GPX	Glutathione Peroxidase
HD	Huntington's Disease
Heph	Hephaestin
Hid	Head involution defective

HO-1	Heme Oxygenase-1
HYPER	Hydrogen PERoxide sensor
Htt	Huntington
IAP	Inhibitor of Apoptosis
IBM	IAP-Binding Motif
ICE	Interleukin 1-β-Converting Enzyme
ICAD	Inhibitor of CAD
IκB	Inhibitor of κB
IκK	Inhibitor of κB Kinase
IOC	InterOmmatidial Cell
IMS	InterMembrane Space
IRE	Iron Response Element
IRP	Iron Regulatory Protein
JNK	Jun-N-terminal Kinase
Ken	Ken and Barbie
LIP	Labile Iron Pool
Lolal	Lola-like
LPP	Lipid Phosphate Phosphatase
MAPK	Mitogen-Activated Protein Kinase
MEF	Mouse Embryonic Fibroblast
mRNA	messenger RNA
MODC	Mouse Ornithine DeCarboxylase
MOMP	Mitochondrial Outer Membrane Permeabilization
MST1	Mammalian Sterile-20-like Kinase-1
NF-kB	Nuclear Factor-κB
NFSA	No Flanking Sequence Available

NinaA	Neither inactivation nor activation A
NinaC	Neither inactivation nor activation C
Nmd	No mitochondrial derivative
Oho23B	Overgrown hematopoetic organs at 23B
PD	Parkinson's Disease
PANK2	Pantothenate Kinase 2
PINK1	Pten-Induced-Kinase-1
PRC	PhotoReceptor Cell
RE	Rh1-Gal4, EyFLP
Rh1	Rhodospin1
RHG	Reaper-Hid-Grim
RFeSP	Rieske Iron Sulfur Protein
RING	Really Interesting New Gene
RIP	Receptor Interacting Protein
RNA	Ribonucleic Acid
RNAi	RNA interference
ROS	Reactive Oxygen Species
S2	Schneider Cells 2 (*Drosophila* embryonic cell line)
Sens	Senseless
Sev	Sevenless
Sina	Seven-in-absentia
Svp	Seven-up
Sf-9	Spodoptera frugiperda-9
Skl	Sickle
SOD	SuperOxide Dismutase
SOP	Sensory Organ Precusor
SMAC	Second Mitochondria-derived Activator of Caspases

SOP	Sensory Organ Precursor
t(BID)	truncated (BID)
tdTomato	tandem dimer Tomato
Th	Thread
TRADD	TNFα Receptor Associated protein with DD
TRAF	TNFα Receptor Associated Factor
YFP	Yellow Fluorescent Protein
TNF	Tumor Necrosis Factor
TNFR-1	TNF Receptor-1
TUNEL	Terminal deoxynucleotidyl transferase mediated dUTP Nick End Labeling
UAS	Upstream Activating Sequence
UPR	Unfolded Protein Response
UTR	UnTranslated Region
UURCFR	UCLA Undergraduate Research Consortium in Functional Genomics
UV	Ultra Violet
VLCFA	Very Long Chain of Fatty Acids
Wun	Wunen
Wun2	Wunen2
XIAP	X-linked IAP

1 INTRODUCTION

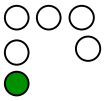

1.1 A Matter of Life or 'Programmed Cell Death'

Cell death is an important process in all organisms. It acts as a cellular quality control mechanism for proper development and function, and for the protection against diseases. Cell death actively removes unwanted or superfluous cells to sculpt parts of the body, such as the formation of digits by the removal of inter-digital cells, deletes unnecessary tissue as seen in the tadpole tail during amphibian metamorphosis, and adjusts cell-cell interaction such as the formation of proper connections between neurons and their targets. It also clears faulty or 'dangerous' cells, such as those infected by virus, undergoing unregulated division or auto-reactive lymphocytes, all of which may ultimately pose a threat to the organism (Jacobson et al., 1997).

Cell death is often coupled to cell proliferation. Excessive proliferation can provoke cell death (Evan et al., 1992), and dying cells can signal their replacement by transmitting mitogenic signals to neighboring cells (Ryoo et al., 2004). Both processes work together to meet the needs of development and maintain tissue homeostasis. However, deregulation of either process can cause an inappropriate gain or a loss of cells resulting in pathological conditions such as cancer, autoimmunity and neurodegeneration (Mattson et al., 2001; Thompson, 1995).

Virtually all cells have the ability to self-destruct by undergoing apoptosis. Elucidating the molecular mechanisms of how and when cells die is critical for understanding not only an organism's homeostatic development and physiology, but also the diseases that result from inappropriate cell death control, eventually leading to more effective and specific therapeutics.

While the first use of the term 'cell death' can be found in texts of Hippocrates, the first observations of the process date back to 1842 (Andre, 2003). Dying cells and tissue exhibit distinct features during embryogenesis and metamorphosis which caught the attention of 19th century biologists (Clarke and Clarke, 1996). German naturalist, Karl Vogt, described the disappearance of the notochord during toad metamorphosis. Later, in the rat retina, a link between cell death and proliferation was established (Tansley et al., 1937). In the developing nervous system, extra nerve cells were suggested to be eliminated by cell death (Hamburger and Levi-Montalcini, 1949). By the mid-20th century, it was clear that cell death was a naturally occurring process necessary for development (Glucksmann, 1965; Saunders, 1966).

The term 'programmed cell death' was introduced in 1964 during the characterization of inter-segmental muscle degeneration of the silkmoth.

This term defined cell death not as random or accidental in nature, but as a sequence of controlled steps leading to locally and temporally defined self-destruction (Lockshin and Williams, 1965). In a seminal publication by Kerr, Wylie and Currie, the term 'apoptosis' was first used to describe the stereotypical and morphological features culminating in the controlled self-destruction of a cell (Kerr et al., 1972). These distinct observed features are membrane blebbing, cell shrinkage, nuclear condensation and cytoplasmic compaction. Apoptosis was defined as a natural physiological process, active in both normal and diseased tissues, induced by a variety of signaling pathways and stimuli. Ultrastructural imaging further revealed a process by which apoptotic cells are frequently engulfed by surrounding cells, known as phagocytosis. Apoptosis was distinguished from necrosis, a passive and unspecific form of cellular death characterized by cell rupture and inflammation (Wyllie et al., 1980).

The first insights, supporting the hypothesis that apoptosis was a genetically-encoded process, came from studies in the nematode *Caenorhabititis elegans*. In this invertebrate organism, 131 cells out of 1091 were found to invariably die during the development (Sulston, 1983; Sulston and Horvitz, 1977). Due to its deterministic cell lineage, *C. elegans* became an ideal system to study cell death. A series of genetic screens brought about

the discovery of *ced-3*, *ced-4* and *egl-1* as the main executioners of cell death. Loss-of-function of one or more of these genes was shown to promote survival of the somatic cells normally programmed to die by apoptosis (Conradt and Horvitz, 1998; Ellis and Horvitz, 1986). Another gene, *ced-9*, was also recovered in these screens, but was revealed to have an opposing pro-survival role. *ced-9* loss-of-function mutations caused the ectopic death of cells that normally live while gain-of-function mutations prevented apoptosis (Hengartner et al., 1992). *ced-9* shares homology to the human *bcl-2* gene. Human *bcl-2* overexpression can rescue *ced-9* loss-of-function, giving significance to the characterization of the apoptotic pathway in *C. elegans* (Hengartner and Horvitz, 1994; Vaux et al., 1992). Not surprisingly, Sydney Brenner, Robert Horvitz and John Sulston received the Nobel Prize recognition in 2002 for their groundbreaking 'discoveries concerning genetic regulation or organ development and programmed cell death' (Brenner, 2003; Horvitz, 2003; Sulston, 2003).

1.2 Caspases

The discovery of *ced-3* paved the way to understanding the basic mechanisms of apoptosis. It was shown to share significant homology to the mammalian *interleukin-1-β-converting enzyme* (*ICE*), a cysteine aspartate-specific protease (caspase) important in the processing of the inactive

interleukin-1-β to the proinflammatory cytokine. The discovery of *ced-3/ICE* established the role of caspases as cell death effectors in the apoptotic pathway (Xue et al., 1996; Yuan et al., 1993). Genome comparative analyses revealed that both *ced-3* and *ICE* were part of a much larger family of genes, with four caspases in *C.elegans*, seven in *Drosophila melanogaster*, ten in mice and twelve in humans (Fig. 1.1B) (Lamkanfi et al., 2002; Shaham, 1998; Xue et al., 2006).

Caspases, generally synthesized as catalytically inactive or weak zymogens, typically contain an inhibitory N-terminal prodomain, followed by a large and small protease subunits (Fuentes-Prior and Salvesen, 2004). Caspase–mediated proteolytic cleavage leads to the release of the prodomain and the association of small and large subunits to form a catalytic hetero-dimer subunit (Shi, 2002). For proper caspase activation, two catalytic heterodimers need to form a heterotetramer (Fig. 1.1A). Once activated, caspases cleave substrates at specific tetra-peptide sites, usually after aspartic acid residues, but in some instances after glutamate residues as well (Nicholson, 1999).

Caspases involved in apoptosis fall into two classes, initiator and effector caspases, based in part on the lengths of their prodomain and how they are activated (Fig. 1.1B) (Degterev et al., 2003; Turk and Stoka, 2007).

Initiator caspases, such as Caspase-8 and Caspase-9 in humans and Dronc in *Drosophila*, are inactive monomers that rely on homotypic protein-protein motifs, such as the death effector domain (DED) and the caspase recruitment domain (CARD) for association with adaptor proteins and auto-activation. In mammals, Caspase-9 is recruited into a multimeric complex with Apoptotic-protease-activating-factor 1 (Apaf-1) via its prodomain. Once in the complex, pro-Caspase-9 is believed to auto-activate itself by virtue of its weak proteolytic activity. This auto-processing sets in motion a pro-apoptotic cascade event. Effector caspases typically have shorter prodomains, can exist in a dimer conformation in their inactive state and are activated by the proteolytic cleavage of upstream initiator caspases. These are referred to as the "executioners" because they are the key enzymes that carry out apoptosis (Degterev et al., 2003; Turk and Stoka, 2007).

The execution phase of apoptosis occurs rapidly, often lasting 20 minutes or less, in a process that can be visualized by light microscopy, both *in vivo* and *in vitro*. It is characterized by caspases cleaving hundreds of cellular substrates causing morphological changes, and ultimately leading to the irreversible demise of the cell. There are still uncertainties as to which substrates are functionally required in the apoptotic chain of events and which ones are mere bystanders of the process. Nevertheless, the apoptotic -

Figure 1.1 Caspase Activation, Structure and Domain Homology. (A) Caspases are synthesized as enzymatically weak precursors that undergo proteolytic maturation. The caspase precursor is composed of highly conserved large and small subunits (blue) and a weakly conserved prodomain (white). Two caspase precursors assemble into a hetero-tetrameric active enzyme. The N-terminal prodomain, which is highly variable in length (23 to 216 amino acids), is involved in he regulation of these enzymes (Thornberry and Lazebnik, 1998). **(B)** Domain architecture of caspases in *C.elegans*, *Drosophila* and mammals. Those caspases for which a clearly defined role in cell death has been demonstrated are labeled in bold. Initiator caspases contain pro-domain (black line) harboring motifs such as the CARD or DED, and are labeled in green. *Drosophila* have 7 caspases, 4 of which are known to be involved in cell death, Dredd, Dronc, Drice, and Dcp1. In mammals, 7 of the 11 identified caspases participate in apoptosis, including the initiator caspases, Caspase-2,-8,-9 and -10 and for executioner caspases, Caspase-3,-6, and -9. A possible role in cell death for other caspases cannot yet be excluded. Ced-3 behaves as both an initiator and executioner caspase. Approximate sites for proteolytic processing of zymogens after aspartic acids (Asp | X) are indicated by black arrows above Ced-3 (Kumar and Doumanis, 2000).

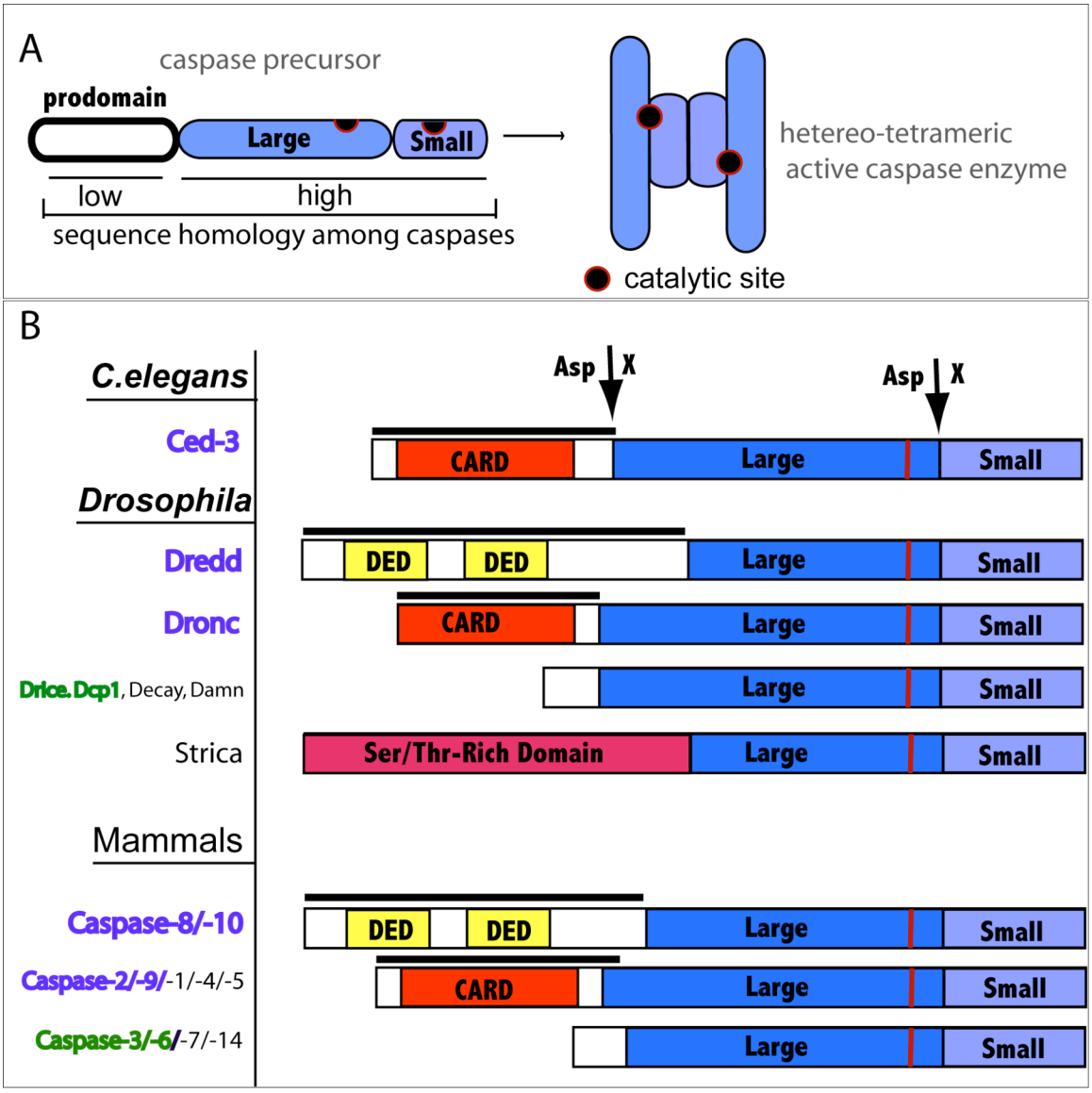

Figure 1.1 Caspase Activation, Structure and Domain Homology

relevance is well understood for a large number of caspase substrates. First and foremost, effector caspases can cleave initiator caspases, generating positive feedback loops and amplification of the cell death signal. One structural component of the cell, the nuclear lamin, is cleaved by caspases, which facilitates the orderly disassembly of the cell (Takahashi et al., 1996). The Inhibitor of the Caspase-Activated DNase (ICAD) is cleaved by caspases, relieving its inhibition of CAD and causing DNA fragmentation in apoptotic cells (Liu et al., 1997; Sakahira et al., 1998). Finally, caspases cleave β-catenin, promoting the loss of contact of the apoptotic cell with neighboring cells and thought to facilitate cellular clearance and engulfment (Brancolini et al., 1998). There are over 400 caspase substrates that have been identified (Luthi and Martin, 2007), and with recent advances in genomic analysis, many more will be characterized. Sequence analysis of identified caspase substrates will be invaluable to further understanding caspase function and specificity for both apoptotic and non-apoptotic functions.

While predominantly involved in cell death, caspases also function in non-apoptotic processes. In humans, the first caspase to be discovered, Caspase-1/ICE, cleaves the precursor forms of the inflammatory cytokine Interleukin-1β into active mature peptides; *caspase-1* mutant mice were

shown to be resistant to endotoxic shock (Li et al., 1995). A variety of mammalian caspases have also been demonstrated to have functions in a range of differentiation processes, including muscle specification (Fernando et al., 2002), terminal enucleation of red blood cells (Zermati et al., 2001), and lens epithelial cell development in the eye. In addition to its functions in cell death, *Drosophila* caspases have been involved in a myriad of cellular processes during development. These include cell migration, cell border migration, DNA repair, sperm differentiation, Sensory Organ Precursor (SOP) specification, and cell proliferation (Kuranaga and Miura, 2007; Montell, 2006).

Furthermore, we note that, while caspase-dependent apoptosis is the most well-characterized cell death pathway, it is certainly not the only form of active cell death. An illustrative example of caspase-independent cell death is the linker cell death during the development of *C. elegans*, which occurs independently of *ced-3*, the sole initiator and the executioner caspase in the intrinsic pathway of apoptosis (Abraham et al., 2007). Moreover, caspase-independent cell death is often associated with paraptosis, autophagy and nonlysosomal cell death (Mathiasen and Jaattela, 2002). The tumor suppressor P53, nuclease Endonuclease G (EndoG) and oxireductase Apoptosis Inducing Factor (AIF) have all been suggested to be key

mediators in caspase-independent pathways of cell death (Godefroy et al., 2004; Lipton and Bossy-Wetzel, 2002). Finally, other caspase (serine) proteases, notably cathepsins and calpains, have been implicated in caspase-independent pathways of cell death (Broker et al., 2005; Rozman-Pungercar et al., 2003). Nevertheless, still much remains to be understood about the underlying mechanisms governing caspase-independent forms of cell death.

1.3 Mechanisms of Caspase Activation

Intrinsic and extrinsic pathways can trigger caspase activation. The intrinsic or intracellular route of apoptosis is mediated at mitochondria and caspases are activated in response to internal signals such as genotoxic damage, oxidative stress, heat shock and developmental cues. The receptor-mediated pathway, historically referred to the "extrinsic pathway", acts at the cell surface, and is generally the pathway of choice for immune responses. Interestingly, the extrinsic pathway of caspase activation is less well defined in *C. elegans* and *Drosophila* than in mammals, suggesting a more recent evolutionary history of the apoptotic pathway (Chowdhury et al., 2006).

1.3.1 The 'Intrinsic' Pathway

The intrinsic pathway of apoptosis was first described with the discovery of the only initiator and executioner caspase, *ced-3,* in *C. elegans*. Genetic screens and epistasis experiments placed *ced-4, ced-9 and egl-1* upstream from *ced-3* in the apoptotic pathway. Ced-4 oligomerizes to promote Ced-3 processing and activation (Seshagiri and Miller, 1997; Yang et al., 1998). In the absence of apoptotic stimuli, Ced-4 is sequestered at the mitochondria and rendered inactive by direct interaction with mitochondrial-bound Ced-9, an anti-apoptotic member of the Bcl-2 family of proteins. Upon apoptotic induction, the pro-apoptotic BH3 (Bcl-2 Homology 3)-only protein, Egl-1, binds to Ced-9, triggering the release of Ced-4 from the mitochondria and its translocation into the cytosol (Lutz, 2000). Ced-4 then cleaves pro-Ced-3, inducing Ced-3 activation. Despite a few differences and added layers of complexity, the core intrinsic pathway of apoptotic activation in *C.elegans* is conserved in mammals and flies.

Caspase-9, a Ced-3 homolog, is one of the four mammalian initiator caspases and is considered to be the principal transducer of the intrinsic pathway of apoptosis. Mammalian adaptor protein, Apaf-1, is homologous to Ced-4 and commonly shares a CARD domain, which binds downstream initiator caspases to mediate apoptosome formation, and a nucleotide-

oligomerization binding domain, important for self-association. Several mammalian Bcl-2 family proteins share homology with Bcl-2 Homology (BH) domains of Egl-1, notably Bcl-2 Interaction Domain (BID) and Bcl-2 Associated-X protein (BAX). BID and BAX coordinate the cross-talk of death signaling primarily at the mitochondria but also at the nucleus and the Endoplasmic Reticulum (ER) (Danial and Korsmeyer, 2004; Hengartner and Horvitz, 1994).

The insect components of the intrinsic pathway of apoptosis share commonalities with both *C. elegans* and mammals. *Drosophila* Dronc, the Ced-3/Caspase-9 homolog, is the only initiator caspase and has been shown to be involved in virtually all forms of developmental apoptosis (Chew et al., 2004; Daish et al., 2004). Hac-1 is the homolog to Ced-4/Apaf-1, and associates with Dronc to form the apoptosome and mediate apoptosis. The *Drosophila* multi-domain Bcl-2 family members, Debcl and Buffy, have been shown to localize to the mitochondria and the ER respectively, and have pro- and anti-apoptotic functions in certain contexts. However, evidence for their role in the regulation of apoptosis remains limited (Doumanis et al., 2007; Igaki and Miura, 2004; Quinn and Richardson, 2004).

There are several mechanistic differences in the intrinsic pathway, especially pertaining to the factors and steps necessary for apoptosome formation and activation. In *C. elegans*, Ced-4 is activated when its interaction with the anti-apoptotic Ced-9 is disrupted by Egl-1. In mammals, activation occurs slightly differently; Apaf-1 requires Cytochrome-c (Cyt-c) to be released from the mitochondria. This release is a critical regulatory step of the mammalian apoptotic process, controlled by upstream Bcl-2 family members. Cyt-c interacts with the inhibitory WD40 domain of Apaf-1 and recruits the zymogen form of Caspase-9. Once activated, the apoptosome, comprising of Cyt-c, dATP, and Apaf-1, activates Caspase-9, which in turn cleaves and activates downstream caspases, including Caspase-3 (Bratton et al., 2001; Rodriguez and Lazebnik, 1999). The mechanisms that regulate the activation of Apaf-1 in mammals share several similarities with its homolog in *Drosophila*. Like Apaf-1, Hac-1 contains a series of WD40 repeats, which can bind to Cyt-c and induce caspase activation *in vitro*. Furthermore, the activation of Dronc requires the formation of an apoptosome-like complex. However, while required for all aspects of apoptotic cell death in mammals, Cyt-c is believed to be involved only in tissue- and context specific apoptotic paradigms in *Drosophila* (Dorstyn and Kumar, 2006).

In conclusion, we note that Ced-4/Apaf-1 can also participate in alternative pathways of cell death, notably in caspase-independent cell death (White, 2000). For example, in *C. elegans*, linker cell death can occur in the absence of the caspase, Ced-3. However, the linker cell is rescued from cell death in Ced-4 mutants, indicating that Ced-4 can promote cell death independently of Ced-3.

1.3.2 The 'Extrinsic' Pathway

The extrinsic pathway of cell death begins outside of the cell through the activation of specific pro-apoptotic receptors by molecules known as pro-apoptotic ligands. These ligands in turn relay intracellular signaling downstream and cause caspase activation. In mammals, Fas and Tumor Necrosis Factor (TNF) are integral membrane proteins with their receptor domains exposed at the surface of the cell. These Death Receptors (DRs) decorate the plasma membrane and harbor an extra-cellular cysteine-rich domain that recognizes cognate ligands and a cytoplasmic tail involved in the signaling transduction cascade. DRs bind their complementary death activators Fas Ligand (FasL) and TNF, which transmit signals into the cytoplasm and lead to the activation of apoptosis. An example of this extrinsic pathway is when cytotoxic T-cells bind their targets (e.g. virus-infected cells) during an immune response. The T-cells produce more FasL

at their surface, causing more binding of multiple Fas on the surface of the target cell, leading to target cell death by apoptosis (Suda et al., 1993).

In mammals, Fas activation leads to Fas receptor aggregation at the cell surface. Cytoplasmic Death Domains (DD) of trimerized Fas receptors recruit an adaptor protein known as the Fas-Associated Death Domain (FADD). In turn, FADD recruits one of the initiator caspases, Caspase-8, via its death effector domain (DED) which is recruited into a Death-Inducing Signaling Complex (DISC) with FADD (Ho and Hawkins, 2005; Park et al., 2007). Caspase-8 activation is not only regulated by the DISC assembly but also by an inhibitory factor, known as Flice [caspase-8]-like inhibitor protein. This protein also has a DED domain, and competes with the binding site of Pro-Caspase-8, inhibiting its activation. The recruitment of Pro-Caspase-8 to the DISC leads to Pro-Caspase-8 cleavage and activation (Donepudi et al., 2003). In a Type I pathway, Caspase-8 goes on to directly activate Caspase-3. In a Type II pathway, Caspase-8 cleaves BID into truncated (t)BID, which acts as a mitochondrial cue to oligomerize two other Bcl-2 family members, BAX and BAK, and the release of Cyt-c. Hence, in addition to its role in mediating the intrinsic apoptotic pathway mitochondrial components such as BID can amplify death signals from the

extrinsic pathway. This reveals a cross-talk between intrinsic (through the mitochondria) and extrinsic pathways (through DRs) of apoptosis.

The TNF pathway is considerably more complex than the Fas signaling pathway as it includes an intermediate chain of inhibitory and activating events. TNFα, a proinflammatory cytokine, exerts its biological activity by signaling with its receptor TNF Receptor-1 (TNFR-1) and by activating the transcription factor Nuclear Factor-κB (NF-κB), essential for survival in many cell types (Van Antwerp et al., 1996). For TNFR-1 activation by TNFα, the adaptor protein TNFα Receptor Associated protein with DD (TRADD) is brought to the receptor at the cell surface via a DD interaction. TRADD then recruits additional adaptor molecules like Receptor-Interacting Protein (RIP), TNFα Receptor Associated Factor (TRAF) and FADD (Micheau and Tschopp, 2003). These in turn recruit additional key components to TNFR-1 that are responsible for initiating an intracellular signal transduction cascade, such Mitogen-Activated-Protein Kinase (MAPK) and cell death-mediated mechanisms. TNFα causes apoptosis by recruiting pro-caspases into the high molecular TNFα factor complex in an apoptosome-like manner. Pro-caspases also play a role in turning off NF-κB survival signaling. In certain cell types, the TNFα pathway can promote survival instead of apoptosis by activating NF-κB,

which transcribes genes, such as antioxidants, whose products inhibit components of the apoptotic machinery. TNFα-induced NF-κB activity involves the five mammalian NF-κB/Relish transcription factors. In the absence of TNFα stimulation, NF-κB is associated with Inhibitor of κB (IκB) proteins in the cytoplasm. TNFα-induced activation of NF-κB relies largely on phosphorylation dependent ubiquitination and degradation of IκB proteins. The Inhibitor of κB Kinase (IκK) complex, a multiprotein kinase complex, is responsible for the TNFα-induced phosphorylation of IκB. The mechanism by which the decision between TNFα-induced cell death and survival is made is largely unknown.

In *Drosophila*, genetic screens have identified the first invertebrate TNF superfamily ligand, Eiger, and the TNFR-1 homolog, Wengen (Igaki et al., 2002; Kanda et al., 2002). *Drosophila* also has an ortholog of FADD, known as dFADD, which can bind to and activate the apical initiator caspase, Dredd (Hu and Yang, 2000). Two *Drosophila* TRAFs, dTRAF-1 and dTRAF-2, are proposed to function similarly to their mammalian counterparts. Collectively, this data suggest that *Drosophila* has a TNF-like pathway (Kauppila et al., 2003). However, extrinsic mechanisms of caspase activation remain elusive. Wengen is a type III membrane protein with a conserved cysteine-rich domain (TNFR homology domain) in the

extracellular domain, a hallmark of TNFR superfamily. However, Wengen lacks the intracellular DD motif, characteristic of the death receptor family. Also, dFADD/Dredd association has not been involved in programmed cell death but rather in the regulation of the innate immune response triggered by Gram-negative bacteria (Tanji and Ip, 2005). Nevertheless, Eiger is a strong pro-apoptotic inducer of cell death, especially in the nervous system. It can be cleaved and released from the cytosol as a soluble factor and does not require the activity of dFADD/Dredd, but is completely dependent on the Jun-N-terminal Kinase (JNK) pathway. Furthermore, dTRAF-2 and *Drosophila* inhibitor of apoptosis 1 (Diap1) were also shown to alleviate Eiger-induced apoptosis. (Igaki et al., 2002). Despite increasing evidence of an extrinsic pathway in *Drosophila*, there are significant differences with the mammalian pathway and the importance of the *Drosophila* TNF-like pathway in the apoptotic pathway remains limited.

In conclusion, we mention a variety of other apoptotic signals that act at the cell surface or via cell-to-cell interactions crucial. The Epidemal Growth Factor Receptor (EGFR) signaling pathway in *Drosophila* is activated by secreted ligands. The EGFR pathway leads to activation of the *Drosophila* Ras homologue and protects cells against apoptosis. This effect is in part mediated by the MAPK ERK, which phosphorylates the pro-apoptotic

protein Hid and thus induces its degradation (Bergmann et al., 1998). A second mechanisms to repress apoptosis downstream of EGFR signaling involves transcriptional repression of *hid* (Kurada and White, 1998). The Notch signaling, mediated by Notch transmembrane receptor and ligands, inhibits apoptosis by direct interference with XIAP in mammals and Diap1 in *Drosophila* (Thompson et al., 2008). Finally, the extracellular matrix and cell-to-cell adhesion/interactionare important trophic and survival factors (Cheresh and Stupack, 2008).

1.4 The Discovery of the RHG Protein Family

Both *C. elegans* and *Drosophila* are powerful genetic systems to study the genetic determinants and mechanisms of cell death. However, in contrast to *C.elegans*, cell death in *Drosophila* is more of a stochastic process and not solely determined by lineage. *Drosophila* cells exhibit developmental plasticity as well as non-stereotypical and regulatory complexities similar to mammals. *Drosophila* cell death is dynamic in particular but it is also largely replicable on a global scale. Collectively, these traits underline *Drosophila* as an attractive model for the analysis of non-autonomous regulators of apoptosis from both genetic and molecular perspectives.

Drosophila cell death has been characterized in a variety of developmental contexts, from the early-staged embryo to late-staged pupa. A

first study of early developmental cell death in *Drosophila* revealed a wave of dying cells at embryonic stage 11, roughly seven hours after egg-laying (Abrams et al., 1993) becoming widespread as embryogenesis proceeds. Dying cells can be visualized using the vital live dye Acridine Orange (AO), a fluorescent quencher of dying cells. A deficiency screen using this characterized embryonic paradigm of cell death uncovered a startling result in embryos homozygous for the deficiency *Df(3L)H99* (spanning the interval 75C1-2 and referred to as H99) : deletion of this region virtually abolished all signs of programmed cell death in the developing *Drosophila* embryo. Since that discovery, developmental apoptosis in *Drosophila* was revealed to be primarily regulated by three pro-apoptotic genes contained within the H99 cell death locus: *reaper* (*rpr*), *hid* (*head involution defective*, also known as *wrinkled*) and *grim*, collectively referred to as RHG (*reaper-hid-grim*) (Chen et al., 1996; Grether et al., 1995; White et al., 1994). Subsequent studies revealed that RHG genes are expressed in virtually all cells that undergo apoptosis; the loss of one or more of these genes in the locus only partially blocks embryonic cell death, suggesting a vital cooperative function in the execution of apoptosis. Intriguingly, the RHG genes share very little homology except for a 14 amino-acid sequence in the N-terminus named the RHG motif. By performing genome-wide sequence

analyses, other RHG-like proteins have been identified. *sickle* (*skl*), immediately proximal to *reaper*, encodes a 30 amino acid Trp-block (or Grim-Helix 3, GH3) in addition to the RHG-motif, and is able to induce apoptosis by itself and is upregulated in response to a variety of insults including ionizing radiation (Christich et al., 2002; Srinivasula et al., 2002; Wing et al., 2002). The thioredoxin peroxidase and ER resident, *jafrac-2* also encodes a RHG motif and is rapidly released into the cytosol following apoptotic induction (Tenev et al., 2002). *dOmi*, a *Drosophila* homolog of the mitochondrial serine protease *htrA2/Omi,* was recently identified and demonstrated to be released into the cytosol during certain conditions of apoptosis (Challa et al., 2007). In contrast to RHG protein family, the general involvement of *skl*, *jafrac-2* and *dOmi* in the pro-apoptotic pathway remains to be established and may only to be required in context-specific forms of cell death and/or in response to certain stimuli.

Biochemical studies show cell death action of RHG proteins occurs by mediating caspase activation through Diap1 inhibition via their binding to the RHG motif. Based on these studies, Reaper, Hid and Grim are referred to as IAP antagonists, and their RHG motifs as IAP-Binding Motifs (IBM). When overexpressed in a variety of tissues and cell culture, *Drosophila* IAP antagonists can induce ectopic cell death (Steller, 2008). Interestingly, cell

death also occurs when they are misexpressed in mammalian system, indicating a universal role of these RHG proteins in cell death (McCarthy and Dixit, 1998; White et al., 1996). While no orthologs have been identified in mammals, mouse and human Caspase-9, mitochondrial Inter-Membrane Space (IMS) Smac/Diablo and HtrA2/Omi all harbor a homologous IBM-like motif. Smac/Diablo and HtrA2/Omi, can bind to IAPs and promote caspase activation when overexpressed in transfected cells (Srinivasula et al., 2000), but unlike the *Drosophila* IAP antagonists, there is scant evidence to date that they are important regulators of apoptosis in more physiological circumstances. It is still unclear as to whether these factors are 'IAP-interacting' proteins, or true 'IAP-antagonists'. Nevertheless, promising evidence for a mammalian IAP antagonist came with the *in vivo* characterization of ARTS, a splice form of the Septin mitochondrial protein, shown to decrease X-linked IAP (XIAP) protein levels, induce caspase activation, and promote caspase-mediated removal of cytoplasm during terminal sperm differentiation in mice (Gottfried et al., 2004; Kissel et al., 2005; Larisch et al., 2000).

1.5 Inhibitors of Apoptosis and IAP-Mediated Caspase Inhibition

To prevent caspase activation, the apoptotic pathway is fastened with inhibitory regulatory belts. As mentioned, the sequestration of pro-apoptotic

factors at the mitochondria is one of the inhibitory mechanisms of caspase activation. In *C. elegans*, Ced-9 sequesters pro-apoptotic Ced-4 at the mitochondria (Yan et al., 2005). In mammals and flies, upstream Bcl-2 family proteins and WD40 repeats of Apaf-1 play inhibitory roles on the pro-apoptotic function of Apaf-1 (Danial and Korsmeyer, 2004).

Another fundamental mechanism of inhibition introduces a novel class of proteins that inhibit caspases. The first of such proteins discovered was the baculoviral P35 protein, shown to suppress host cell death responses to viral infection in Baculoviridae (Clem et al., 1991; Friesen and Miller, 1987). Biochemical studies further revealed its mode of action: P35 binds to the catalytic sites of active caspases inducing a conformational change that locks the protease into an inactive form and thereby preventing cell death. With no homology to proteins outside of the Baculoviridae family, P35 was subsequently shown to be a broad caspase inhibitor in several species and was quickly adapted as an invaluable tool for apoptosis research (Bump et al., 1995; Xue and Horvitz, 1995). Interestingly, the ectopic expression of baculoviral P35 blocks apoptosis in mammalian cells, suggesting a common mechanism of inhibition in bacteria and mammals. Inhibitory of Apoptosis Proteins (IAPs), were later discovered based on their ability to substitute for P35 (Birnbaum et al., 1994; Crook et al., 1993).

IAPs usually contain one to three N-terminally tandem Baculoviral IAP Repeats (BIRs), each approximately 80 amino acids in length and containing a unique zinc-finger motif (Crook et al., 1993). In flies and mammals, the BIR domain acts as a switch between cell death and cell survival. A tug-of-war exists between RHG proteins and caspases, each competing to bind to the BIR domains. Caspase binding to BIR inhibits caspases and RHG motif binding to BIR causes IAP inactivation and caspase release. IAPs are also regulated a third way, using the ubiquitin pathway and depending on their C-terminal Really Interesting New Gene (RING) domain (Steller, 2008). The RING-dependent IAP regulation is further discussed in section *1.6*.

Since their discovery in baculoviruses, a large number of cellular IAP-like proteins have been identified in a wide variety of organisms. Cellular IAPs, cIAP-1 and c-IAP-2, were biochemically isolated in human cells as the binding partners of TRAF2 in TNF-α induced apoptosis (Rothe et al., 1995). XIAP was discovered by sequence homology to other IAPs (Duckett et al., 1996). Other mammalian IAPs include melanoma IAP (ML-IAP) (Vucic et al., 2000), Bruce/Apollon (Chen et al., 1999), Survivin (Ambrosini et al., 1997), and testis-specific IAP (ts-IAP) present in great apes (Richter et al., 2001). All of these IAPs bear at least one BIR domain, while cIAP-1,

cIAP-2, XIAP, ts-IAP and ML-IAP also harbor a RING domain. cIAP-1 and cIAP-1 also contain a CARD domain. In *C. elegans*, a *Survivin*-like gene has been identified but has not been shown to be involved in cell death (Lens et al., 2006). The *Drosophila* Inhibitors of Apoptosis Protein 1 (Diap1) and 2 (Diap2) each contain two BIR domains and a RING motif. *diap1* loss-of-function leads to early unrestrained caspase-dependent embryonic cell death, revealing *diap1's* essential function for cell survival (Ryoo et al., 2004). *diap2* was postulated to be required primarily for the innate immune responses to Gram-negative bacterial infection and to be dispensable for cell survival (Huh et al., 2007; Leulier et al., 2006). Genetic screens have also revealed a third IAP gene, *dBruce*, a functional homolog of mammalian *Bruce,* important for apoptosis and caspase regulation. *dBruce*-null flies suppress *reaper*- and *grim*-induced cell death in the eye, and cause the hyper-activation of caspases during spermatogenesis resulting in improper sperm differentiation and male sterility (Agapite and Steller, 2002; Arama et al., 2007). However, the role of *dBruce* in other tissues, and its general function in the apoptotic pathway still remains unclear.

The presence of multiple IAPs begs the question of why more than one IAP exists and what, if any, are their individual roles. It is postulated that different IAPs may have different caspase specificity and specific

effects in differing cell types. Alternatively, multiple IAPs may work together to inhibit cell death. For example, mammalian XIAP, cIAP-1 and cIAP-2, have been shown to prevent apoptosis by binding the initiators and the effectors Caspase-3, -7, and -9 but not Caspase-1, -6, -8 or -10 (Deveraux et al., 1998; Roy et al., 1997). *XIAP*-null mice are completely normal and have no detectable defects in apoptosis. However, there is a compensatory up-regulation of cIAP-1 and c-IAP-2, implying that XIAP function may be redundant with other family members (Olayioye et al., 2005). In *Drosophila*, dBruce and Diap2 have both been suggested to promote Diap1 degradation, highlighting the cooperative functions of IAPs as a means of amplifying the cell death signal (Herman-Bachinsky et al., 2007; Yoo, 2005).

1.6 IAP Ubiquitination and Degradation

In addition to BIR domains, highly conserved zinc-finger RING domains are present in certain IAPs and bestow substrate specificity to the ubiquitin system (Joazeiro and Weissman, 2000). The ubiquitin system is the principal system for actively regulating the abundance of proteins in eukaryotic cells (Glickman and Ciechanover, 2002). Ubiquitin-ligase can target proteins for degradation by assembling ubiquitin polymers on specific substrates. Polyubiquitination chains are assembled through the sequential

activity of three highly conserved classes of enzymes. In the first step, the E1 ubqiutin-activing enzyme forms a high energy intermediate between an active site cysteine side chain and ubiquitin polymer. This step requires energy in the form of ATP. The activated ubiquitin is then transferred to an active site cysteine in the E2 ubiquitin-conjugating enzyme. The E3 ubiquitin-ligase simultaneously binds its cognate E2 and the substrate to be ubiquitinated, and juxtaposes the two to promote ubiquitin transfer between the E2 and an internal lysine on the substrate.

RING domains in IAPs encode E3 ubiquitin ligase activity, revealing that the ubiquitin-mediated protein degradation pathway is involved in IAP function and apoptosis. The RING motif can bind pro- and anti-apoptotic factors, thereby acting as a switch between life and death. In *Drosophila*, Diap1 can bind, mediate ubiquitination and inactivate both Dronc and the RHG proteins via its RING motif (Chai et al., 2003; Wilson et al., 2002). Conversely, RHG proteins can stimulate the poly-ubiquitination and the degradation of Diap1 by recruiting Diap1's E3 RING motif and E2 conjugases, notably UbcD1 and Diap2 (Herman-Bachinsky et al., 2007; Ryoo et al., 2002). In mammals, the RING-containing XIAP has been demonstrated to ubiquitinate Smac/Diablo, Caspase-3, Caspase-9, AIF as well as itself by autoubiqutination (Morizane et al., 2005; Riedl et al., 2001;

Suzuki et al., 2001; Wilkinson et al., 2008; Yang et al., 2000). Recent work in the laboratory by *Schile et al*. shed light on the function of the RING domain of XIAP by generating a knock-out mouse containing a RING-deleted XIAP. Mouse Embryonic Fibroblasts (MEFs) derived from this mouse are highly sensitized to TNFα-induced apoptosis. Furthermore, deletion of the RING in XIAP reduces the incidence of leukemia and prolongs the survival of mice in a Eμ-myc lymphoma background. The authors demonstrated using irradiated MEFs that the deletion of the *XIAP* RING domain results in reduced caspase ubiquitination and concluded that the ubiquitinating activity of XIAP is important for its role as a negative regulator of apoptosis (Schile et al., 2008). Collectively, studies in mammals and *Drosophila* have indicated an essential role of the RING domain for IAP stability and for cellular survival.

1.7 Cell Death Action at the Mitochondria

The intrinsic pathway of apoptosis is mediated by mitochondrial factors in mammals and its activation is defined by mitochondrial-mediated events: Mitochondrial Outer Membrane Permeabilization (MOMP), release of Cyt-C, and Apaf-1 apoptosome-mediated caspase activation. Hence, the mitochondria is a major mediator of physiological apoptosis in vertebrates. In the invertebrate organisms, such as *C. elegans* and *Drosophila*, much

remains to be learned about the precise role of the mitochondria in the regulation of apoptosis. Nevertheless, we note a few noteworthy insights.

Ced-9 sequestration of Ced-4 occurs at the mitochondrial surface, thereby revealing the mitochondria as a major platform for apoptotic regulation in *C. elegans*. In *Drosophila*, Buffy and Debcl also localize to the mitochondria, reinforcing the importance of the mitochondria in invertebrate apoptosis. RNA interference (RNAi) studies of these genes demonstrate they can act simultaneously in anti- and pro-apoptotic ways depending on stress stimuli (Brachmann et al., 2000; Colussi et al., 2000; Quinn et al., 2003). Loss-of-function phenotypes have further revealed a role of Buffy/Debcl in pruning cells in the developmental nervous system. Nevertheless, still much remains to be learned about Buffy/Debcl as active effectors of programmed cell death.

In contrast to mammals, previous studies suggest that MOMP and Cyt-c release does not occur in *Drosophila* (Dorstyn et al., 2004; Varkey et al., 1999; Zimmermann et al., 2002), despite the existence of Debcl and Buffy at the mitochondria (Igaki and Miura, 2004). Moreover, Hac-1 reportedly does not require Cyt-c for its activation and is constitutively active in cells, where it binds to and continuously processes the initiator caspase, Dronc (Dorstyn et al., 2004; Muro et al., 2002; Zimmermann et al.,

2002). Similarly, *C. elegans* Ced-4 is constitutively active without Cyt-c involvement (Yan et al., 2005).

An intriguing 'mitochondrial' observation is that *Drosophila* caspases Dronc and Drice seemed to be cleaved and activated in the vicinity of the mitochondria (Dorstyn et al., 2002). Recent reports also show that Cyt-c in *Drosophila* may have tissue-specific and stage-specific functions. For example, Cyt-c is required for Hac-1-dependent caspase activation in sperm differentiation (Arama et al., 2006). In the pupal retina, Cyt-c-dependent apoptosome activation plays an "accelerating" role in the elimination of InterOmmatidial Cells (IOCs), a sculpting process which is delayed in the absence of Cyt-C (Mendes et al., 2006).

Finally, *Drosophila* IAP antagonists, Reaper, Grim and the recently identified dOmi, all contain the conserved GH3 domain, a motif required for their localization to the mitochondria. It has also been suggested that the GH3 motif was further required for 'efficient' cell killing (Claveria et al., 2002; Freel et al., 2008), as its deletion leads to the diminished pro-apoptotic potency of these genes (Freel et al., 2008). Hence, in *Drosophila*, the localization of pro-apoptotic genes at the mitochondria may have an 'enhancing' but not essential role on the execution of cell death.

1.8 The *Drosophila* 'Gas and Brake' Model

Identification of RHG proteins, caspases and IAPs brought about the proposal of the "gas and break model" of cell death (Fig. 1.2). The 'gas' branch pushes the pedal on cell death via the Apaf-1/Cyt-c/Dronc apoptosome formation. The 'brake' is mediated by Diap1, which holds the caspases in an inhibited state. Under normal non-apoptotic conditions, Diap1 binds to the unprocessed form of Dronc via its BIR domain, preventing caspase and apoptotic activation. Diap1 also promotes Dronc ubiquitin-mediated degradation (Chai et al., 2003; Zachariou et al., 2003). In response to apoptosis, RHG are expressed, their N-termini bind to the BIR domain of Diap1, 'releasing the brake' of Diap1 on Dronc (Chai et al., 2003). Now liberated, Dronc enters the apoptosome through CARD-CARD interactions with Hac-1. An activated apoptosome 'puts on the gas' by triggering a cascade of caspase cleavage/activation, leading to apoptosis. Even though additional factors involved in cell death have been identified, the streamlined 'gas and brake model' accurately portrays the canonical apoptotic pathway and its essential role in controlling cellular life and death decisions (Fig. 1.2) (Steller, 2008).

Figure 1.2 The *Drosophila* Gas and Brake Model of Apoptosis. The model highlights the forward drive of caspase activation by oligomerization of caspases within the apoptosome (the Gas) and the inhibition of the active caspase by IAPs (The Brake). Diap1 can be depressed to release the caspase Dronc by IAP antagonists/RHG proteins. The Eiger/Wengen-mediated pathway is the invertebrate equivalent of the 'extrinsic pathway' found in mammalian systems. P53/JNK pathways have been shown to cause caspase-dependent and –independent cell death. The core components of the intrinsic 'Gas and Break' model of apoptosis are labeled in blue.

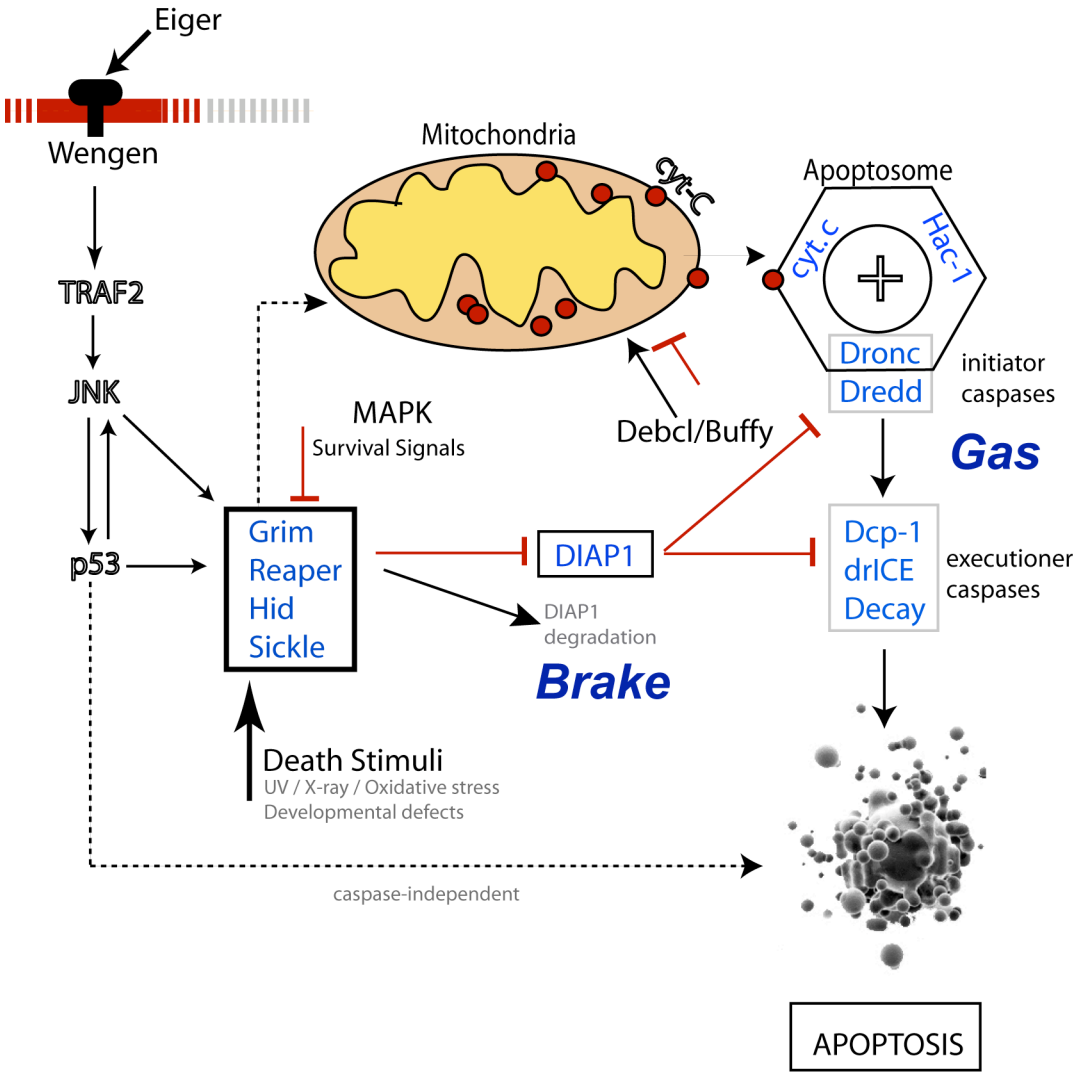

Figure 1.2 The *Drosophila* Gas and Brake Model of Apoptosis

1.9 A Fly Eye's View on Cell Death

Virtually all of the genes required for proper *Drosophila* eye development are highly conserved, and many perform similar functions in a wide range of species. Thus, the *Drosophila* eye has proven to be an excellent model system for identifying new genes involved in developmental processes (Fig. 1.3). Furthermore, the presence of such a large number of neurons (>6000), the highly reproducible and consistent nature of ommatidial development, the potential for easily observable phenotypes and the power of genetics makes the *Drosophila* eye an extremely useful tool to find new genes in the apoptotic pathway.

1.9.1 Structure and Early Development of the *Drosophila* Eye

Each insect eye is composed of approximately 800 individual light-sensing units, called ommatidia, arranged in a highly regular hexagonal array. The number of cells, their identities and functions within each ommatidium is invariant. Each adult ommatidium consists of 19 cells, including 8 Photoreceptor Cells (PRCs) (R1-R8), 4 cone cells (homologous to the vertebrate lens), 6 pigment cells, and a mechanosensory bristle cell at alternate ommatidial vertices (Fig. 1.3A-C).

The adult eye develops from an epithelial bilayer, called the eye imaginal disc, which is derived from a group of about 20 cells set-aside during embryonic development. During the first two larval instar stages, cells of the eye disc remain undifferentiated but undergo repeated divisions to produce almost all of the cells that will form the adult eye. In the third and final larval instar, PRC differentiation begins at the posterior margin of the eye disc, proceeds anteriorly following a dorso-ventral groove, termed the morphogenetic furrow. The morphogenetic furrow marks the boundary between differentiating and undifferentiated cells. While cells anterior to the furrow are not undergoing differentiation and do not express neural markers, they are already committed to become retinal tissue (Fig. 1.3D) (Ready et al., 1976; Tomlinson, 1985).

The order in which PRCs differentiate within an ommatidium is invariant and begins with the R8 PRC. R2/R5, R3/R4 and R1/R6 PRCs are then sequentially recruited in a pair-wise fashion via the stimulation of the Epidermal Growth Factor Receptor (EGFR) signaling pathway (Dominguez et al., 1998; Freeman, 1996). The R7 PRC is recruited last; in addition to EGFR signaling, R7 differentiation requires Seveneless (Sev) (Hafen et al., 1987; Tomlinson and Ready, 1986) and the Notch receptors (Cooper and Bray, 2000) (Fig. 1.3D). It is well established that PRC fate is irreversibly

established during larval development, when each of PRC expresses a particular set of transcriptional regulators and sends its projection to different layers of the optic lobe. We refer to PRC formation in the *Drosophila* retina as a 'two-step process'. In the first step, during larval development, the PRCs become committed and send their axonal projections to their targets in the brain. In the second step, terminal differentiation is executed during pupal development and the PRC adopt their final cellular properties (Mollereau et al., 2001). The end result is the formation of 8 PRCs in each ommatidium with each PRC identity determined by the combination of expressed genes and projections in the brain. All PRCs contain microvillar structures known as rhabdomeres, which capture light and span the whole depth of the retina. The outer PRCs R1 to R6, equivalent to the vertebrate rods, are involved in motion/image detection and project axonally to the lamina part of the optic lobe. Furthermore, R1 to R6 express Rhodopsin 1 (Rh1), a light-sensing protein, which accumulates in the rhabdomeres. The inner PRCs, R7 and R8, analogous to the mammalian cone cells, are used for color discrimination and project their axons into the medulla of the same optic lobe (Cook and Desplan, 2001). The R7 spans only the apical half and R8 the basal half of the retina. R7 expresses rhodopsins 3 (Rh3) and 4 (Rh4) while R8 expresses rhodopsins 5 (Rh5) and

Figure 1.3 Structure and Differentiation of the *Drosophila* Eye. (A) Scanning electron microscopy of the *Drosophila* retina reveals a multi-faceted structure. **(B)** Rhodopsin 4 (blue) and phalloidin (red) stain respectively the inner R7 PRC and outer R1-R6 PRCs of the wild-type retina (whole-mount retina dissection). **(C)** Outer PRC autofluorescence visualized using the cornea neutralization technique (Pichaud and Desplan, 2001). A UV-sensing associated pigment, present in the outer PRCs, can be excited with a 600-660 excitation cube followed by a UV filter. **(D)** Differentiation of the eye imaginal disc starts post-morphogenetic furrow with R8 fating (dark orange), which then triggers differentiation of R1-R6 PRCs (white) ending in R7 PRC (yellow) recruitment. **(E)** Cross-section of the retina reveals structure of a group of ommatidia with cornea at the apical end and light-sensing rhabdomeres elongated throughout the entire section. **(F)** Schematic of a single *Drosophila* adult ommatidium, showing the arrangement of PRCs, accessory cells and lens. The light-sensing rhabdomeres are specialized tube-like organelles of the PRCs that serve as a wave-guide for incident light collected by the lens cornea. The outer R1-R6 PRC rhabdomeres are labeled in green and inner R7 and R8 are labeled in yellow and red, respectively. **(G)** Transmission electron microscopy image of a tangential section of an ommatidium with larger outer PRC R1-R6 rhabdomeres and a smaller inner PRC R7 rhabdomere. *(Images A and B, courtesy of Samara Brown).*

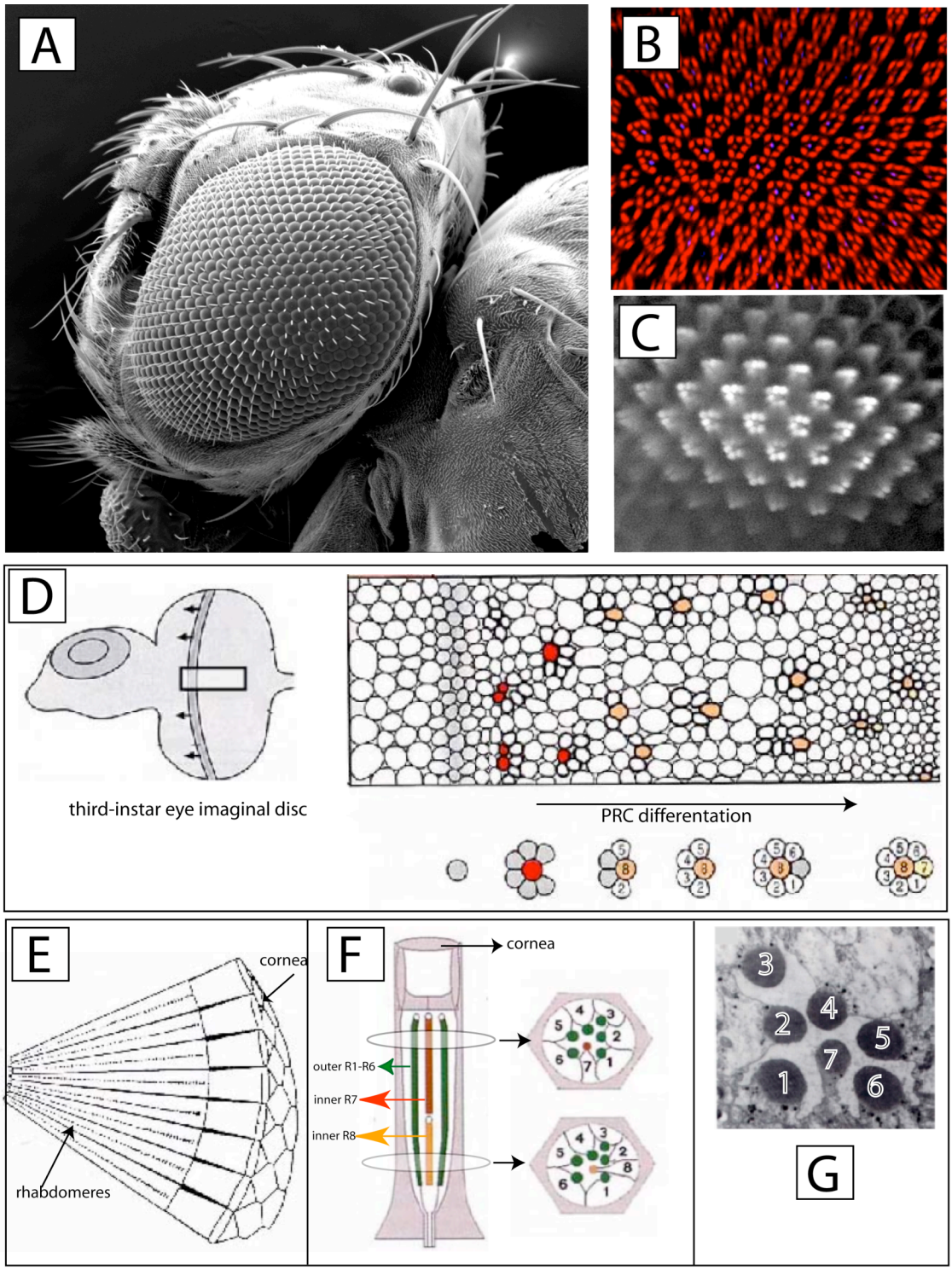

Figure 1.3 Structure and Differentiation of the *Drosophila* Eye

6 (Rh6) (Fig. 1.3E-G) (Chou et al., 1996; Chou et al., 1999; Fortini and Rubin, 1990; Huber et al., 1997; Montell et al., 1987; Papatsenko et al., 1997).

1.9.2 Pupal Cell Death in the Developing *Drosophila* Eye

The beautiful, almost crystalline, appearance of the adult *Drosophila* retina requires selective cell death of a subset of support cells that make up the 'interommatidial lattice'. Developmental studies by *Ready et al*. laid the foundations for understanding retinal cell death. (Cagan and Ready, 1989b; Wolff and Ready, 1991). As a final step in patterning, IOCs recruited from the epithelia start to cluster around newly differentiated PRCs and cone cells (Tomlinson, 1985). IOCs are organized into an interweaving hexagonal lattice of nine secondary and tertiary pigment cells that pattern the ommatidial array. Emergence of this lattice represents a balance between recruitment of IOCs into pigment cells and the selective elimination of about one-third 'surplus' of IOCs. Similar to the elimination of inter-digital cells during limb formation in human fetal development or the neuronal pruning in the developing human nervous system, cell death in the *Drosophila* pupal eye occurs because of an excess production of cells generated by successive rounds of cell divisions earlier in development (Cagan and Ready, 1989b; Cordero et al., 2004; Monserrate and Brachmann, 2007; Wolff and Ready,

1991; Yu et al., 2002). Pupal death in the retina has been reported to occur in two major waves. The early-stage cell death takes place between 20 and 24h After Puparium Formation (APF) and the late-stage between 26 and 36h APF (Monserrate and Brachmann, 2007) (Fig. 1.4B-C). However, studies on eye-specific mutants have revealed cell death defects and the presence of extra cells occurring as early as 18h APF (Cordero et al., 2004) (Fig. 1.4B). Also, a spike of cell death has been found to occur as late as 37h APF to eliminate the peripheral IOCs and incomplete ommatidia at the border of the pupal eye disc.

IOC death in the developing retina is dependent on the conserved intracellular Notch signaling pathway (Cagan and Ready, 1989a; Miller and Cagan, 1998; Parks et al., 1995) (Fig. 1.4A). Temperature-sensitive *notch* mutations cause an increase in IOCs during pupal development. Intriguingly, Notch inhibition also leads to supernumerary PRCs (up to 14) instead of the normal 8 PRCs. This suggests that the lack of cell death in *notch* mutants may favor ectopic cells to transform into PRCs. Further studies indicated that IOC death occurs through apoptosis. Indeed, antibody staining and epistasis revealed a caspase-dependent apoptosis in the pupal eye dependent Hid for IOC elimination. Indeed, *hid*-mutant retinas exhibit excess IOCs at 18-hour APF (Cordero et al., 2004). Furthermore EGFR -

Figure 1.4 IOC Elimination during Pupal Development. IOC elimination occurs in two stages that can be visualized by comparing IOC organization and number at specific pupal stages. The eight-PRCs are located below the IOC layer and are thereby not visible at this level. **(A-C)** Staged wild-type retina stained against Armadillo (arm, white) protein to outline IOC cells. **(A'-C')** Corresponding schematic ommatidium containing four cone cells (orange cells labeled 'c'), two primary pigment cells (yellow cells, labeled '1°'), three bristle cells (dark yellow cells labeled 'b') and several IOCs (purple cells). (**from A to B**) 18-26 hours: the first stage of death in which approximately 1.8 IOCs per ommatidium die by apoptosis, accompanied simultaneously with IOC sorting; **(from B to C)** 26-42-hours: during the second stage of death, an average of 1.7 IOCs per ommatidium are eliminated and the remaining IOCs differentiate as secondary and tertiary pigment cells. **(B')** One of the two IOCs marked with an asterisk will be eliminated between each pair of bristle cells surrounding the ommatidial cluster. **(C')** By 42h APF, the elimination of IOCs is completed and each ommatidium is surrounded by six secondary, three tertiary, and three bristle cells. *Images B-D courtesy of Cesar Mendes*

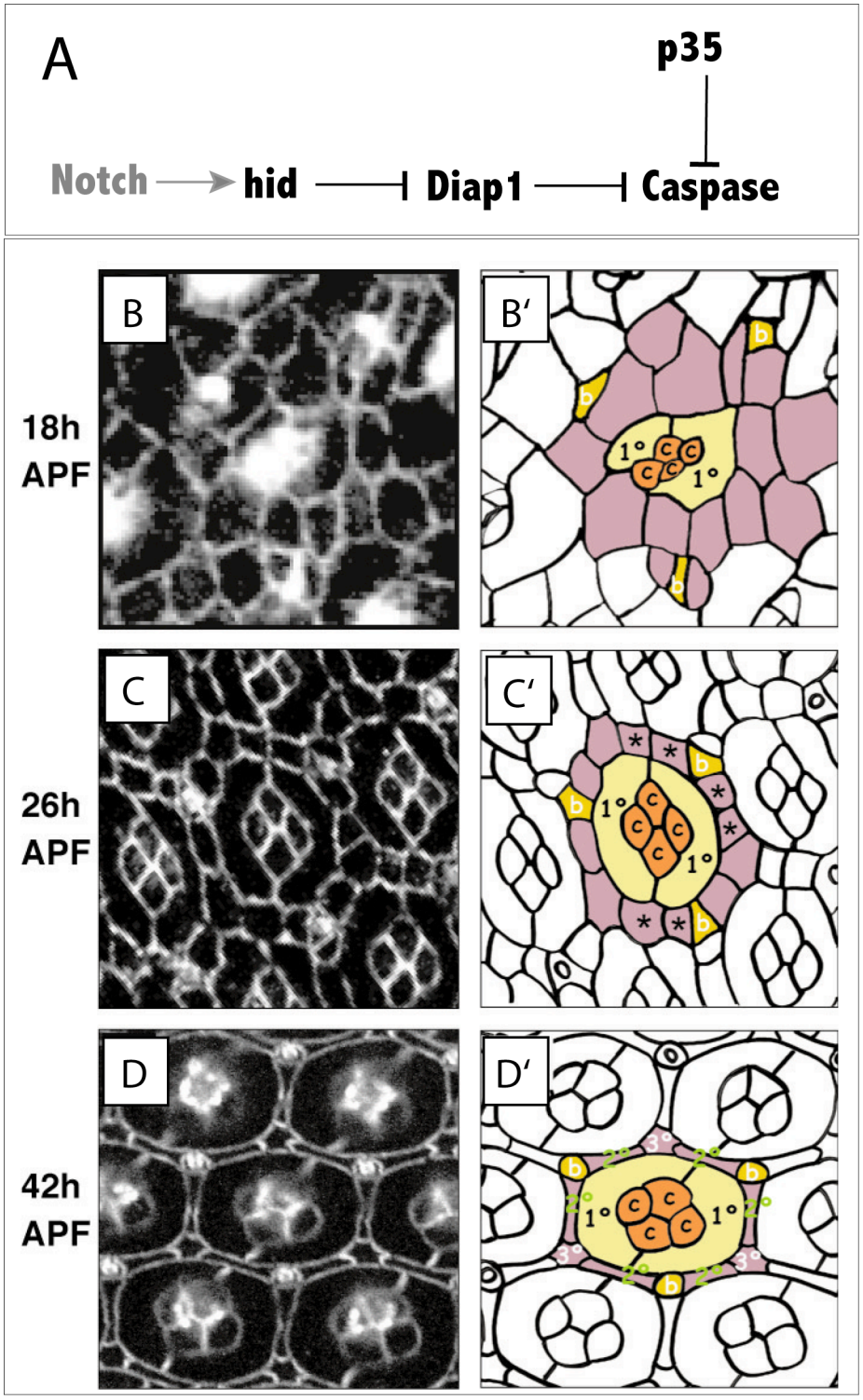

Figure 1.4 IOC Elimination during Pupal Development

activation promotes IOC survival at least in part by negatively regulating *hid* levels (Kurada and White, 1998). Overexpression of P35 and Diap1, were subsequently both shown to rescue virtually all aspects of pupal IOC death (Hay et al., 1994).

1.9.3 The Fly Eye: Use of a Misexpression System to Study Cell Death

The *Drosophila* eye is non-essential for organismal viability. It therefore provides an ideal platform to study gene function, cell death and disease without any deleterious effects on the organism's survival.

The discovery of numerous retinal specification genes marked the birth of 'eye-inducible expression' systems. Other tissue-inducible expression systems in the wing and in the embryo have since been characterized but the range of manipulation is far more extensive in the eye. In common to other tissue-specific promoters, the *Drosophila* eye promoters have two characteristics: they can trigger expression at specific stages in development and in a subset of retinal cells. The most widely used promoter is the Glass Multimer Reporter (GMR), designed by mutimerizing a site-specific DNA binding domain from the zinc finger protein, *glass*, required for normal PRC development in *Drosophila*. GMR is expressed only after the morphogenetic furrow in all differentiating cells of the eye imaginal disc, including PRCs and IOCs, and persists throughout adulthood (Moses et al.,

1989; Moses and Rubin, 1991). An early eye promoter is the transcription factor *eyeless* (*ey*), expressed only in undifferentiated cells of the eye imaginal disc prior to the morphogenetic furrow. *ey* is a 'master control gene' of early eye development and its targeted expression in various imaginal disc primordia can induce ectopic eye structures in tissues such as the wing, leg and antennae. Intriguingly, the ectopic eyes appear morphologically normal, often consisting of groups of fully differentiated ommatidia with complete sets of PRCs (Halder et al., 1995). *ey* is commonly used to express recombinases in the early-undifferentiated cells of the larval eye and thereby generate clones by mitotic recombination (Newsome et al., 2000). The recombinase-based technique for clonal analysis using *ey* is further developed later in this section. Finally, the rhodopsin1 (*rh1*) promoter turns on at around 70% pupal stages and drives expression specifically in outer R1-R6 PRCs. The *rh1*-inducible system to express pro-apoptotic genes and fluorescent genes in terminally-staged PRCs for visualization is extensively described and used in subsequent chapters. Finally, other promoters are used to induce expression only in a subset of PRCs, including the receptor tyrosine kinase, *sevenless* (*sev*) expressed in inner R7 PRCs, and the orphan nuclear receptor, *seven-up* (*svp*), which displays weak expression in R1/R6 and strong expression in R3/R4. Using

the eye-inducible promoters described above, pro-apoptotic genes can be expressed in the developing *Drosophila* eye, leading to an adult eye that is morphologically abnormal, disorganized and oftentimes reduced in size. In general, the severity of the eye phenotype is based on two factors: the potency and onset of expression of the pro-apoptotic stimulus. For the latter, the general rule is that the earlier in development the onset of ectopic cell death, the more severe the eye ablation. Ectopic expression of *reaper* using the *GMR* promoter leads to a 'rough' eye phenotype. In contrast, *reaper* overexpression using the *rh1* promoter leads to age-dependent and selective degeneration of PRCs without any visible eye phenotype (Chapter 2). Using the GMR-induced eye ablation phenotype, genetic screens have been designed to find mutations that would aggravate the phenotype or restore the eye to normal. In a landmark cell death screen (Agapite and Steller, 2002), point mutations were dominantly screened for an effect on the GMR-*reaper*-induced rough eye phenotype. Of note are the *diap1* alleles, which both dominantly enhance and suppress the eye phenotype. In addition, co-expression of P35 and Diap1 block GMR-*reaper* cell death and restores a nearly wild-type eye.

The *Drosophila* retina also provides the genetic tools to study the loss-of-function consequences of genes. Through mitotic recombination,

homozygous mutant 'clones' can be generated in the eyes of flies that are heterozygous for lethal mutations. The production of clones by mitotic recombination can be stimulated with X-rays. However, X-rays are unspecific in consequences and have proven to be impractical for large-scale genetic analyses. Recent advances have introduced genes and sites that are used in recombination in yeast to trigger mitotic recombination in *Drosophila*. 'Where' and 'when' mosaic clones are produced during development can be controlled using tissue-specific promoters to drive recombinase enzymes that recognize specific sites engineered into the genome. A widely used eye-specific promoter to generate clones is *ey*, which can be used to drive a yeast-specific FLP (FLiPpase) recombinase. A general rule is that the earlier FLP is expressed in development, the larger the clones produced later in the adult. Upon expression, FLP recombinase recognizes two FRT (Flp-Recognition Target) sites and catalyzes rec(Steller, 2008)iprocal exchange between these sites (Newsome et al., 2000). The FRT sites, which are recognized and cleaved by FLP recombinase to initiate crossing-over between the two sites, have been placed near the centromeres on all *Drosophila* chromosomal arms using P-element transposition and such lines are readily available for general use.

Loss-of-function consequences of a variety of genes have been studied in the *Drosophila* retina. A classical cell death example is the loss-of-function analysis of *diap1*. Homozygous clones of *diap1* loss-of-function mutations leads to 'cell lethal' clones, which die because of unrestrained caspase activation. Overexpression of P35 can rescue cell-lethal *diap1* mutant clones (Agapite and Steller, 2002; Ryoo et al., 2004). Furthermore, in a screen for recessive suppressors of *hid*-induced apoptosis using the FLP/FRT technique, over thirty *hac-1* loss-of-function alleles were identified and characterized by a reduction of developmental apoptosis (Srivastava et al., 2007).

1.10 Mechanisms of Neurodegeneration

1.10.1 Insights into Neuronal Cell Death

Neurodegenerative diseases, characterized by accelerated or otherwise inappropriate neuronal loss, are caused by both genetic and environmental factors. Previous studies have observed that dying neurons exhibit a range of pathological features including the presence of damaging free reactive metals, oxidative stress, protein misfolding/aggregation, protein degradation defects, and ER stress (Bredesen et al., 2006; Mattson et al., 2001). Nevertheless, many studies have been mostly correlative, instilling

uncertainty as to whether features mentioned above play a causative role or are merely by-products of the neuronal loss (Andersen, 2004).

Some insights into the cause of neurodegeneration have been possible by studying the phenotypic and biochemical consequences of loss-of-function mutations of disease-related genes. Mutations in the antioxidant *superoxide dismutase* (*SOD*) gene favor a susceptibility to the onset of Amyotrophic Lateral Sclerosis (ALS), characterized by higher levels of oxidative stress and a progressive fatal motor neuron loss (Beckman et al., 1993). Mutations associated with familial hereditary forms of Parkinson's Disease (PD) have been shown to cause an aggregation of α-synuclein, increase in iron, defects in protein turnover and mitochondrial dysfunction. These mutations have also been suggested to be important causes of dopaminergic neuron loss and PD onset (Barnham and Bush, 2008; Dexter et al., 1991; Jellinger et al., 1990; Lang, 2007). In PD models, there has also been indication of cell death activation. 6-OHDA, a neurotoxin that can reproduce many characteristic features of PD in animals, induces Caspase-3 dependent apoptosis in culture cells (Hartmann et al., 2000; Zigmond and Stricker, 1984). Finally, iron chelators, antioxidant supplementation, and caspase inhibitors all improve neuronal survival in a variety of neurodegeneration paradigms (Bantubungi et al., 2005; Du et al., 2001; Kaur

et al., 2003; Wang et al., 2006; Yuan et al., 1993). However, many of these studies are performed in cultured cells *in vitro* and do not always recapitulate the environment of neurodegeneration.

The development of cellular animal models of neurodegenerative disease, notably in *Drosophila*, has fueled progress into the basic mechanisms neurodegeneration. Specifically, the *Drosophila* retina recapitulates the environment in human neurodegenerative diseases (Bilen and Bonini, 2005) and the retinal (photoreceptor) neurons develop in a very stereotyped manner allowing convenient investigation (Mollereau and Domingos, 2005).

Genetic screens and epistasis experiments in the *Drosophila* retina have shed lights on mechanisms of neuronal cell death and offered insights into potential therapeutic drug targets in neurodegeneration diseases. For example, *hac-1* mutations suppress a *Drosophila* Huntington's Disease (HD) model characterized by expansion of polyglutamine (polyQ) tract. *p53* knockout suppresses neurodegeneration induced by the expanded polyQ repeats (Bae et al., 2005). Increased antioxidant Glutathione *S*-transferase (GST) activity rescues dopaminergic and PRC loss in a *Drosophila* model of PD (Whitworth et al., 2005). Finally, mutations in PINK1 (Pten-INduced-Kinase-1), a gene required for mitochondrial function and linked to PD,

when fed with SOD and Vitamin antioxidant medium displayed amelioration in the PINK1-induced retinal degeneration (Clark et al., 2006; Wang et al., 2006). Loss-of-function analysis of disease-related genes has also shed light on mechanisms inherent to neurodegenerative disorders. We highlight a recent study in *Drosophila* revealing that the loss of function of *DJ-1A*, associated with familial PD, leads an increase in Reactive Oxygen Species (ROS), sensitivity to oxidative stress stimuli and PRC degeneration (Yang et al., 2005).

1.10.2 Oxidative Stress: Mediator of Neuronal Cell Death

It has been postulated that oxidative stress may be a primary mechanism by which neurons die. In eukaryotes, the main source of oxidative stress and oxygen radicals is at the mitochondria. ROS, by-products of respiration in aerobic organisms, are highly reactive and can oxidize and modify other intracellular molecules. ROS formed from both exogenous and endogenous sources, includes superoxide anions (O_2^-), hydrogen peroxide (H_20_2), and hydroxyl anions (OH^-). A variety of defense mechanisms protects cell against excess ROS. The organism fights ROS with specialized substances generally called antioxidants. The primary antioxidant enzymes include SOD, Catalase (CAT), and Glutathione peroxidase (GPX) (Curtin et al., 2002; Fleury et al., 2002). SOD catalyzes-

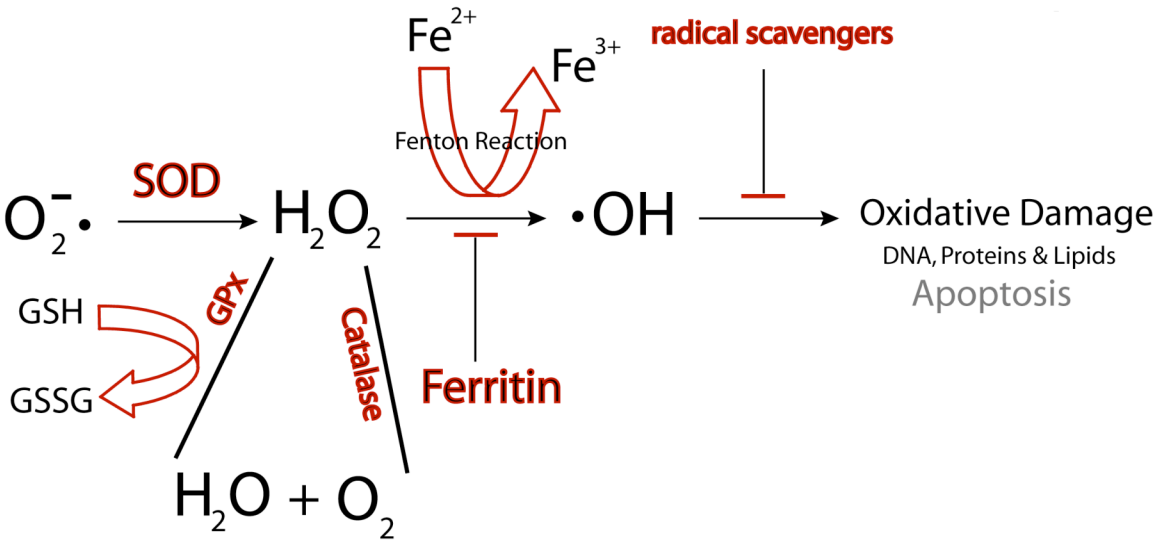

Figure 1.5 Intracellular Antioxidant Defense System. The primary antioxidant defense network protecting the cell from oxidative stress-induced damage and apoptosis. SOD catalyzes the dismutation of superoxide anions into oxygen and hydrogen peroxide. CAT catalyzes the decomposition of hydrogen peroxide into water and oxygen. GPx the major antioxidant in the brain, requires reduced GSH, which is oxidized (GSSH) during the conversion of hydrogen peroxide to water and oxygen. Metals participate in the generation of reactive oxygen species. In the Fenton Reaction, ferrous iron (II) is oxidized by hydrogen peroxide to ferric ion (III), a hydroxyl radical and a highly reactive hydroxyl anion. Metal chelators, notably Ferritin, can sequester ferrous iron and promote its conversion to a less reactive ferric state. Because of their iron-storage capacities, Ferritin complexes are potent intracellular antioxidants.

the dismutation of superoxide into oxygen and less reactive H_20_2 while CAT and GPX catalyzes the decomposition of H_20_2. Another essential defense procedure is the action of metal chelators, notably the primary iron-storage complex Ferritin, useful in for trapping ferrous ions, which can otherwise initiate via the production of hydroxl radicals and downstream lipid peroxidation and DNA damage via the Fenton Reaction (Fig. 1.5) (Gutteridge, 1994).

Oxidative stress is often associated with neurodegenerative diseases such as PD, Alzheimer's Disease (AD), HD or ALS. Indeed, neurons are particularly vulnerable to increases in ROS levels. With age, these cells lose their capacity to detoxify ROS. It is well established that oxidative stress is involved in the aging process, which in turn contributes to the link between neurodegenerative diseases and old age, probably due to progressive neuronal attrition (Droge, 2003). Therefore, the study of the pathways that transform normal cellular constituents, such as ROS, into death effectors constitutes an important aspect of current research in neuroprotection (Droge, 2002). Furthermore, therapies targeting oxidative stress by upregulating intracellular antioxidant defense systems hold great promise.

A large number of studies indicate that high concentrations of ROS can induce cellular damage and be an underlying factor of cell death. The

conserved signaling pathway implicating the Mammalian Sterile-20-like Kinase-1 (MST1/*Drosophila* homolog, Hippo) and FOXO transcription factors mediate oxidative-stress induced neuronal death in mammalian cells (Lehtinen et al., 2006). Oxidative stress also activates the JNK signaling pathway and sustained JNK activation triggers apoptosis. It has been suggested that ROS accumulation plays a causative role in JNK activation, notably in TNFα-induced apoptosis. Furthermore, the anti-apoptotic activity of NF-κB in TNFα-signaling involves suppressing the accumulation of ROS. One such mechanism of the antioxidant and protective activities of NF-κB is the Ferritin upregulation, which prevents sustained JNK activation and cell death (Pham et al., 2004).

While a few critical mediators have been put forward, most studies are performed in mammalian cell culture and much still remains to be understood about the mechanisms of oxidative stress-induced neuronal apoptosis in an *in vivo* context.

1.11 A Prologue to the Study of PRC Death Mechanisms

Despite huge gains in the understanding of cell death, especially during development, the mechanisms of neuronal cell death remain obscure. Neurons are post-mitotic cells, and by their mere nature have acquired novel resistance mechanisms to fend themselves from exogenous stress. The study

described here seeks to understand the nature of the anti-apoptotic network in neurons using *Drosophila* PRCs as a model system. We used misexpression tools, forward genetic screens, and *in vivo* stress-specific sensors to further uncover the molecular mechanisms of PRC death. Some general questions we addressed are: Do PRCs die in a caspase-dependent or –independent pathway? How do pathways in neuronal cell death differ from characterized paradigms of developmental cell death? Which genes are enriched in PRCs? Which PRC-specific genes protect neurons from apoptosis? And which pathways dictate the decision between PRC survival and death?

The work presented relies on numerous mutations and transgenes of a suite of cell death genes that are currently available in the laboratory and in the field of *Drosophila* apoptosis. The next chapters describe sequentially the tools built for PRC analysis, a PRC-specific recessive genetic screen, and the characterization of Ferritin, an iron-storage complex, shown to be essential for PRC viability and the protection against caspase-dependent apoptosis.

2 *DROSOPHILA* PHOTORECEPTOR CELLS: A MODEL TO STUDY NEURONAL CELL DEATH

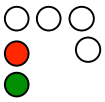

2.1 Summary

Programmed cell death is an important mechanism in both development and homeostasis in adult tissues for the removal of either superfluous, infected, transformed or damaged cells by activation of an intrinsic suicide program. Although virtually all cells constitutively express all the apoptotic components, cells differ dramatically in their susceptibility to undergo apoptosis at different developmental stages. To understand the mechanisms controlling cell death in terminally differentiated neurons, we use adult *Drosophila* PRCs as a model system. We adapted and developed novel fluorescent-based methods to visualize and study PRC death *in vivo*. We show that the differentiated PRCs undergo progressive degeneration when exposed to a variety of apoptotic stimuli. At earlier larval time-points, these cells respond immediately to a given apoptotic stimuli. However, the same apoptotic stimuli in late pupal stages leads to progressive and late-staged degeneration, indicating a resistance to cell death. We revisit pro-apoptotic *reaper*-induced and *Drosophila p53* (*dp53*)-cell death. Both *reaper* and *dp53* overexpression kills PRCs in an age-dependent. Caspase inhibitor P35 overexpression in *dronc* loss-of-function mutant clones further reveals that *reaper* induces caspase-dependent PRC degeneration while *dp53* is only partially dependent on caspases for PRC killing.

2.2 Introduction

Programmed cell death is an important terminal pathway for cells of multicellular organisms, and is involved in a variety of biological events that include morphogenesis, maintenance of tissue homeostasis, and elimination of harmful cells. Dysfunction of programmed cell death leads to a range of various diseases in humans, including neurodegeneration.

The core apoptotic pathway was first discovered in *C.elegans* and has since been found to be conserved across all lineages (Danial and Korsmeyer, 2004; Kaufmann and Hengartner, 2001; Tittel and Steller, 2000). The higher-order complexity in multicellular organisms has lead to redundancy in the pathway as well as tissue-specific discrepancies. However, molecular and biochemical analyses on simple and less redundant organisms have helped to strip down the core components of the apoptotic machinery.

Drosophila is as an attractive model system to study cell death since it presents an intermediate level of complexity between *C.elegans* and vertebrate systems. *Drosophila* has a fully sequenced genome and provides powerful genetic tools to study both the loss- and gain-of-function in a tissue-specific manner (Ashburner and Bergman, 2005; Brand and Perrimon, 1993). Moreover, the core components of the apoptotic pathway have been well characterized in *Drosophila*, paving the way for further exploration into

a variety of stresses inputs that trigger or suppress the apoptotic pathway, and how the programmed cell death machinery is differentially activated in a variety of paradigms.

Although most cells endogenously express the components of the apoptotic pathway and have the ability to trigger the cell death machinery, their susceptibility differs in a tissue- and stage-dependent manner. For instance early-stage 6 embryos exposed to UV-C irradiation are dependent on *hac-1* rather than *reaper* to promote apoptosis. However, in later stage 10-11 embryonic stages, *reaper* acts independently of *hac-1* in the same UV-C-induced cell death paradigm (Zhou and Steller, 2003). The dependence of certain pro-apoptotic factors also changes based on the developmental cell death paradigm. *reaper* is required to sculpt the joint part of the leg while the proper elimination of IOCs during eye formation is predominantly dependent on *hid* (Manjon et al., 2007; Yu et al., 2002). In the pupal retina, previous studies have revealed a phase of heightened UV sensitivity dependent on *dp53* (Jassim et al., 2003). The degree of responsiveness to a cell death stimulus also varies depending on the stage of cell cycle and differentiation. The ectopic expression of *reaper* in the embryo or third instar larva induces massive induction of cell death while the pupa is more resistant to cell death when exposed to the same *reaper*

stimulus (White et al., 1996). This suggests that cells at later stages of differentiation that are no longer cycling are more resistant to ectopically induced cell death.

The *Drosophila* eye is a non-essential organ, in which the loss- or gain-of-function of genes does not alter the insect's development or viability. Traditionally, the adult eye has been widely used to score the pro-apoptotic potency of certain genes and to measure the degree of genetic interactions. For example, it has been readily used to identify and to analyze components of the canonical cell death pathway. However, traditional cell death studies using the *Drosophila* retina rely on the misexpression of pro-apoptotic genes in the developing eye at a stage when cells are still undergoing mitosis and differentiation (Ellis et al., 1993; Hay et al., 2004). Therefore, the apoptotic onset in these misexpression systems interferes with differentiation.

In order to investigate the mechanisms regulating adult cells notably neurons, a cellular system is required in which cells have completed differentiation. We use the terminally-staged photoreceptor neurons as a system of choice. Adult PRCs in the *Drosophila* retina are active, post-mitotic differentiated neurons. A large array of studies has focused on the differentiation, morphology and behavior of these cells over the course of

development (Mollereau and Domingos, 2005). In addition, PRCs are an established neurodegenerative model, in which cellular degeneration can be followed and quantified over time (Ahmed et al., 1998; Nishimura et al., 2004).

In addition to gain-of-function studies described above, loss-of-function analysis is equally important to understand the anti-apoptotic cell death mechanisms vital for PRC viability. Loss-of-function analysis during late-staged development or in the adult is often rendered difficult by the early lethality of gene mutations in a recessive state. However, recombination can be used as a method to generate loss-of-function clones in an otherwise heterozygous background for a given lethal mutation. Recombination between homologous chromosomes is well known to occur during meiosis. It can also occur during mitosis, although usually at a very low frequency. In flies, it is possible to increase the rate of mitotic recombination by the FLP/FRT recombination system. Recombinase FLP induces mitotic recombination between FRT sites on homologous chromosomes (Xu and Rubin, 1993). Cell markers have been engineered in this system to label mutant clones in both developing tissues and adult cuticle. In the adult retina, the FLP/FRT system has used the red-eye pigment of the white gene as a marker for wild-type cells. Loss of red

pigment has been commonly used to visualize loss-of-function clones. Similarly, loss of GFP fluorescence has been used to study clones in the eye imaginal disc (Newsome et al., 2000). These marked clones in mosaic *Drosophila* retinas have been used extensively to answer developmental questions. The use of the FLP/FRT system has also allowed for the high-frequency production of mosaic animals for 95% of *Drosophila* genes.

The wealth of knowledge and tools available provide the foundations for the work presented henceforth, which investigates the underlying pathways regulating the survival and the demise of post-mitotic differentiated PRCs. The objective of this chapter is in three parts. First, we introduce and characterize the fluorescent-based system to visualize PRCs *in vivo*. Second, we investigate the degeneration kinetics in differentiated PRCs subject to a battery of apoptotic insults. Third, we focus on *reaper*- and *dp53*-induced PRC degeneration and study its dependence on the core caspase-mediated pathway of apoptosis in PRCs. Work here provides the groundwork for future genetic screens and for the characterization of novel genes required for adult PRC survival.

2.3 Experimental Procedures

2.3.1 Fly Stocks and Genetics

Flies were maintained in a 12-hour light/dark cycle and crosses were carried out at 25°C, except for the *reaper* and *dp53* in time-course analysis in which flies were raised at 18°C and switched to 25°C post-eclosure. Canton-S was used as the wild-type strain. For PRC live imaging, we used flies with the genotype *rh1-Gal4; UAS-GFP*^{ninaC}, obtained from Dr. Claude Desplan (Pichaud and Desplan, 2001). *rh1* is a strong minimal promoter, which targets expression specifically to the outer PRCs (R1-R6). GFP is expressed specifically in rhabdomeres by appending the N-terminal localization motif myosin-related gene, *neither inactivation nor activation C* (*ninaC*). To induce PRC degeneration, we used a *UAS-reaper* transgene on second chromosomes (Zhou et al., 1997). *UAS-dp53* on the second chromsome was kind gift from M. Young (Jin et al., 2000). For *dronc* loss-of-function analysis, we use the previously described null *FRT82B, dronc*^{I29}, which harbors a Gln53-to-Stop point mutation in the CARD domain of *dronc* and was recovered as a recessive suppressor by the *Bergmann* laboratory in a *GMR-hid* recessive screen (Xu et al., 2005).

GMR-(w+)RNAi, provided by Tiffany Cook, is an RNAi construct developed using the optimized RNAi pWIZ vector (Lee and Carthew, 2003). It is under the control of GMR and is raised against the *white* gene. It partially removes of red eye pigmentation and thereby, enables immunostaining on semi-thin tangential cryosections, which otherwise would be challenging to perform due to pigment background autofluorescence (Fig.2.3G-H). Finally, *FRT80 (w+)* was used to generate 'empty clones' as a way of introducing the double-fluorescent FLP/FRT recessive technique (Fig. 2.4D-E).

2.3.2 Design of FLP/FRT Stocks for Clonal Analysis

The *rh1-tdTomato*^{ninaC} expresses red fluorescence in the outer (R1-R6) adult PRCs. It was designed by fusing the minimal promoter *234(-152+82)-rh1* sequence to the *tandem dimer (td)Tomato* coding region, a kind gift from the Tsien Lab (Fig. 2.4A) (Shaner et al., 2004). *tdTomato* is derived from *mRFP1*, a monomeric mutant of *DsRed* by directed mutagenesis. It is a genetic fusion of two copies of the *dTomato* gene, which was specifically designed for less aggregation. Its tandem dimer plays an important role in the exceptional brightness of *tdTomato*. *tdTomato*'s emission wavelength (581nm) and brightness make it the fluorescent gene of choice for live animal/*in vivo* imaging (Appendix 6.1). The 140-base pair, myosin-related

neither inactivation nor activation (ninaC) N-terminal localization signal, was appended in-frame to the C-terminus of the *tdTomato* sequence for targeted fluorescence into the rhabdomere compartments of PRCs (Fig. 2.4A) (Montell and Rubin, 1988). *ninaC* allows for better live visualization of PRCs using the cornea neutralization technique described in *Exp. Proc. 2.3.3*. $tdTomato^{ninaC}$ was first built in a pBluescript vector (Stratagene) and positive clones were selected based on red fluorescence and colony PCR. $tdTomato^{ninaC}$ was then inserted at sites BamH1/EcoR1 into a $CHAB_{\Delta XbaI}$ vector containing the *rh1* promoter and a SV40 polyA (Wimmer et al., 1997).

Twenty-four independent *rh1-*$tdTomato^{ninaC}$ transgenes, recovered after injection, were screened *in vivo* for strong expression and for accurate rhabdomere visualization using the live-imaging method described in *Exp. Proc. 2.3.3*. Four independent lines, corresponding to each arm of the second and third chromosomes, were meitotically recombined onto neomycin-resistant FRT chromosomes. Recombination was performed in 180µl neomycin G418-supplemented (Invitrogen, Geneticin®) food medium to recover FRT flies, which were subsequently screened for red fluorescence in the pseudopupil. We also meitotically recombined previously characterized *eyFLP* and *rh1-Gal4* transgenes on the X chromosome to produce the

eyFLP, rh1-Gal4 allele, which we refer to as RE. The four respective FRT/FLP lines used to generate clones on the chromosomal arms of the second and third chromosome are the following: **2L:** *RE; FRT40A, rh1-tdTomato^{ninaC}; UAS-GFP^{ninaC}* // **2R:** *RE; FRT42D, rh1-tdTomato^{ninaC}; UAS-GFP^{ninaC}* // **3L:** *RE; UAS-GFP^{ninaC}; FRT80A, rh1-tdTomato^{ninaC}* // **3R:** *RE; UAS-GFP^{ninaC}; FRT82B, rh1-tdTomato^{ninaC}*. For the *reaper* and *dp53* time-dependent study in clones (Fig. 2.5), we meitotically recombined *UAS-reaper* and *UAS-dp53* transgenes with *UAS-GFP^{ninaC}* on the second chromosome.

2.3.3 Live Fluorescent Imaging of PRCs

Flies were selected according to their genotype and anesthetized with CO_2 for approximately 15 minutes. Anesthetized flies were placed in a 35mm cell culture dish half filled with 1% agarose at 60ºC. Eyes were arranged in an upward direction to increase field of vision and optimize rhabdomere visualization. The agarose solidified at room temperature in a CO_2 atmosphere chamber. Water at 4ºC was poured onto agarose plates and kept in CO_2 chamber for 15 to 30 minutes. The water enables immersion imaging and allows to maintain the effects of the CO_2 anesthetic. For both GFP and tdTomato imaging, flies were examined using an upright confocal fluorescent microscope (Axioplan; Zeiss) equipped with a 40X water

immersion lens with a 1.0 optical aperture and a working distance of 3.61mm. Excitation wavelengths were 485nm (EGFP) and 554nm (tdTomato). Images were acquired using a digital camera (AxioCam Hrc, Zeiss) and acquisition software (Zeiss LSM 510).

For the study of age-dependent study of PRC death in clonal analysis (Fig. 2.5), each individual fly was detached from the agarose by gently prying the fly body with a brush, dried on the surface of a Kimwipe tissue and subsequently transferred it to a regular new vial. For age-dependent analysis, agarose gel temperature was set to a lower temperature of 55ºC facilitating rescue of flies after imaging. Sometimes, especially after immersion imaging, the flies required more than 15 minutes to recover. However, we did not observe significant effects of this procedure on the lifespan or fertility of the rescued flies (data not shown).

2.3.4 Retinal Plastic Sections

Flies were decapitated under anesthesia, cut by the anterior/posterior axis and fixed in 2% glutaraldeyde in phosphate buffer for 30 minutes under constant agitation (for electron microscopy analysis, retinas were sent a this stage to Helen Shio at the Electron Microscopy Imaging Facility). After a quick wash in phosphate buffer, eyes were incubated with 1% Os_2O_4 solution in phosphate buffer for approximately 2 hours. Eyes were further

dehydrated in successive 10-minute incubations with ethanol (50%, 70%, 95% and 100%). Following two successive 10-minute washes with 100% propylene oxide, the eye samples were incubated overnight with a 1:1 mixture of propylene oxide and Durcupan resin. Eyes were then incubated for two hours with pure resin, mounted in molds and baked overnight at 70ºC. 500nm plastic sections were cut on a microtome (Ultracut UCT, Leica), stained with toluidin blue and mounted. Slides were observed using a transmission microscope (Axioskop 2 plus; Zeiss) equipped with a 60X oil immersion lens. Images were acquired using a digital camera (AxioCam Hrc, Zeiss) and acquisition software (AxioVision Ac).

2.3.5 Immunostaining on Cryosections

Flies were decapitated under anesthesia, mounted in molds, embedded in Tissue-Tek O.C.T. and frozen for 30 minutes. 10μm sections (Micron HM 505E) were transferred to slides, dried and fixed in 4% paraformaldehyde for 20 minutes. After three washes with PBST (1xPBS + 0.3% Triton x-100), primary antibodies were incubated in BNT (1xPBS, 1% BSA, 0.1% Tween 20, 250 mM NaCl) overnight at 4°C. Primary antibodies were Rabbit anti-Human active caspase-3 1:50 (Cell Signaling) and rat anti-ELAV 1:20 (Developmental Studies Hybridoma Bank). Samples were washed three times with PBST and incubated with appropriate secondary antibodies: FITC

1:200 and Cy3 1:400 (Jackson Immuno-Research Laboratories) for 2 hours at room temperature. Samples were mounted in Vectashield with DAPI and analyzed on an upright Zeiss LSM 510 Confocal microscope.

2.4 Results

2.4.1 Live Imaging of PRCs

In order to study cell death, it is important to have a robust system where cells can be visualized and cellular loss can be easily quantified. We use a fast and reliable fluorescent-based system to visualize PRCs, study their morphology and quantify their degradation in an age-dependent manner. The simplest and fastest method for PRC visualization relies on the Upstream Activating Sequence (UAS)/Gal4 system, the *rh1* promoter and enhanced Green Fluorescent Protein (GFP) (Pichaud and Desplan, 2001). The UAS/Gal4 system allows the ectopic expression of transgenes in a tissue- and time-specific manner by modulating the expression of Gal4 under the control of a defined promoter (Brand and Perrimon, 1993). *rh1* promoter driving Gal4 allows to overexpress genes specifically in the outer PRCs at a terminally-differentiated stage starting at 70% pupation onwards (O'Tousa et al., 1985; Zuker et al., 1985). This targeted expression in late-staged differentiated PRCs contrasts with the early eye promoter *GMR*

expressed in all retinal cells starting in first instar larval stages (Fig. 2.1C). We specifically used the *rh1* minimal promoter known for being a strong promoter and thereby leading to high expression of Gal4 and any gene under the control of UAS. We express GFP under the control of UAS. To allow better image, GFP is specifically targeted to the rhabdomeres with a portion of the gene *ninaC*, tagged to its C-terminus (Fig. 2.1D) (Montell and Rubin, 1988). This characterized motif of 40 amino acids from the C-terminus of the NinaC protein corresponds to the *myosin-1* domain, necessary for the protein's anchoring to the rhabdomeres (Kumar and Ready, 1995; Matsumoto et al., 1987; Porter et al., 1992).

For live GFP imaging of PRCs, the retina is imaged using the cornea neutralization technique, which consists of immersing the compound eye in agarose then water (Pichaud and Desplan, 2001; Stark and Thomas, 2004) (Fig. 2.1A-B). Using this technique, we can distinguish individual rhabdomeres of the ommatidia expressing GFP under *rh1* promoter. The method is unique because it allows to visualize and to measure semi-quantitatively PRC degeneration using the loss of GFP as an indicator. Furthermore, the imaging procedure is non-invasive allowing for recovery of flies after imaging.

Figure 2.1 Live Imaging of PRCs: Experimental Design. **(A)** Diagram of the experimental setup for live imaging of PRCs, consists of a single fly immobilized in agarose with one eye facing upwards and immersed in water. Imaging is performed using a 20X or 40X immersion lens. **(B)** Photography of live imaging set-up using a Confocal LSM Zeiss upright microscope and a 40X immersion lens. Close-up reveals the agarose-water Petri dish containing flies. **(C)** The onset of *rh1* is in outer PRCs of late stage pupae (70% APF, green line), in contrast to GMR (red line), which is expressed in all differentiating retinal cells (PRCs, pigment and sensory cells) starting in larval stages. As PRCs become more differentiated from larva, through pupal stages, to adulthood, they acquire a greater resistance to apoptosis (dark blue). **(D)** Schematic representation of the wild-type *Drosophila* eye under GFP immersion. *Left panel*: the UAS/Gal4 system drives the expression of GFP under the control of *rh1* promoter. GFP contains a rhabdomere *ninaC* localization signal (yellow) for better rhabdomere visualization. *Middle panel*: the adult eye with GFP-expressing ommatidia. *Right panel*: in a single ommatidium, only outer PRCs, R1-R6, express GFP, excluding inner PRCs (R7-R8, gray) and IOCs (white). **(E)** Schematic representation of the degenerating *Drosophila* eye under GFP immersion. *Left panel*: the UAS/Gal4 system drives the expression of both GFP and pro-apoptotic stimulus (light blue) under the control of *rh1*. *Middle panel*: representation of the adult eye in degenerative conditions with approximately 50% loss of GFP fluorescence. *Right panel*: A single ommatidium, which succumbs to pro-apoptotic stimulus, causing distortions (R4, green), shrinkage (R6, green) and ultimately disappearance (R1) of outer PRCs, 50% GFP loss, leaving inner PRCs (gray) and pigment cells (white) unaltered. D: dorsal, V: ventral.

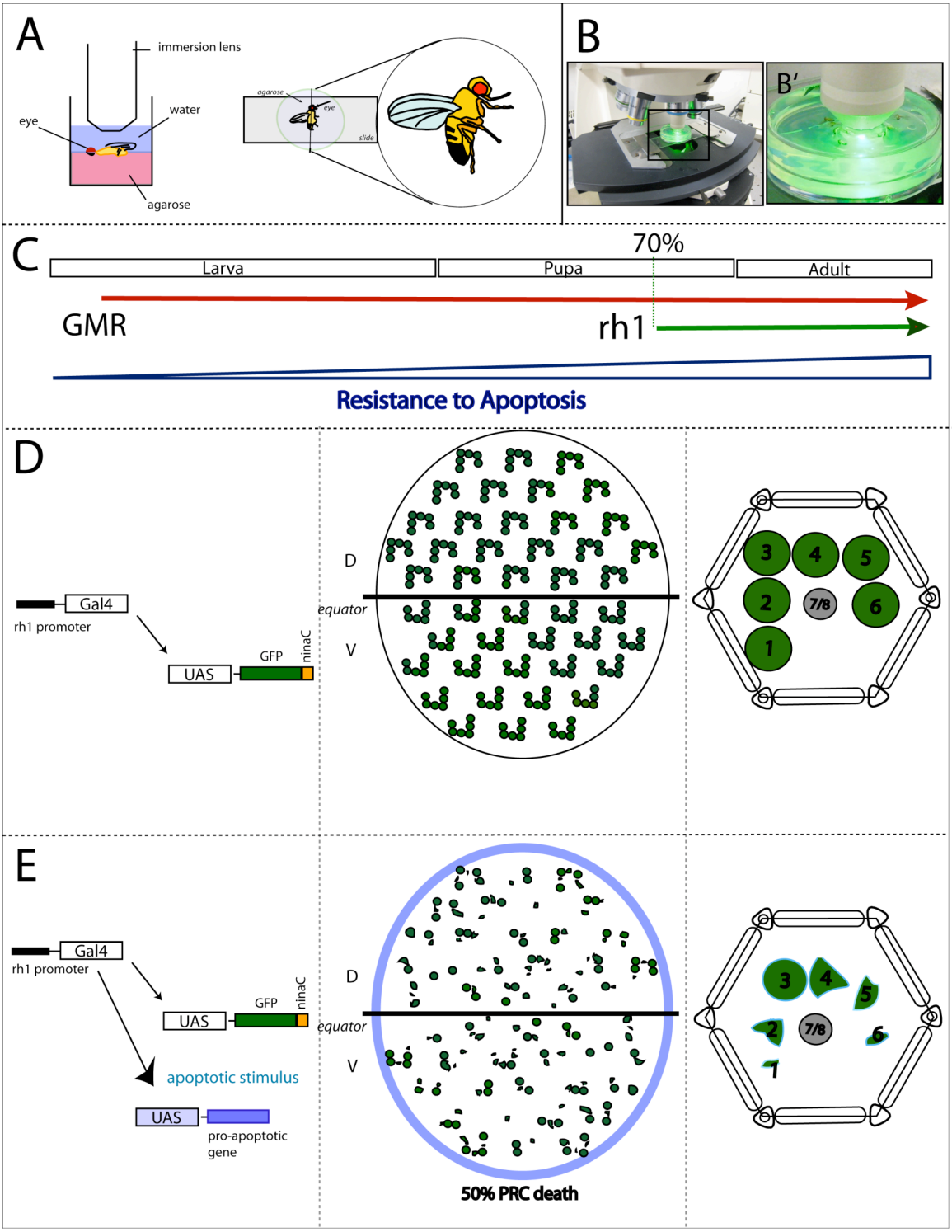

Figure 2.1 Live Imaging of PRCs: Experimental Design

2.4.2 Response of PRCs to Different Apoptotic Stimuli

Flies expressing pro-apoptotic genes under the control of the *rh1* driver are viable and undergo PRC degeneration over time at a rate determined by nature and dosage of pro-apoptotic stimulus. Ectopic expression of pro-apoptotic genes such as *dp53*, *reaper*, and *hid*, under the control of the *rh1* promoter induces complete PRC degeneration starting at late pupal stages or 1-day post-eclosure and ending in less than 2-weeks into adulthood. Other pro-apoptotic stimuli, such as dominant-negative mutants or RNAi silencing of genes involved in neurodegeneration, notably $a\beta^{142}$ (AD model) and *DJ-1A RNAi* (PD Model), displayed little to no PRC degeneration, even after 30 days of continuous and sustained stimulus (Table 2.1).

We also observe that PRCs are especially vulnerable at late stages of pupal development, when *rh1* expression begins. Indeed, *dp53* induces PRC degeneration in approximately 10 days with approximately 20-30% degeneration at day 1 (data not shown). *reaper* induces PRC degeneration in 3 days with already 50% degeneration observed at day 1 post-eclosure (Fig. 2.3D). Even more dramatically, JNK kinase *hep* induces the complete loss of all PRCs at 1-day post-eclosure, revealing hypersensitivity of PRCs to JNK activation in late pupal stages (Table 2.1).

Table 2.1 Ectopic Cell Death in Outer PRCs. Time course for cell death induced by different stimuli under the expression of *rh1* and visualized by GFP live imaging. The onset of PRC loss represents the timepoint during which we note the first indication of GFP loss in R1-R6 PRCs. The time required for PRC loss is determined by the amount of days it takes for complete GFP disappearance. Flies were imaged daily between 1 and 5 days and then every 5 days until 1 month (5, 10, 15, 25, 30).

	rh1-Gal4/rh1-Gal4; UAS-GFP:ninaC/CyO		
UAS-	***chr.***	***onset of PRC loss***	***complete PRC loss (days)***
rpr [3]	2	1	3
rpr [14]	3	1	2
hid [4]	2	1	3
hid^{ala5} [48]	2	1	2
reaper,hid		-	1
dronc	3	1	4
drice	2	1	5
dcp-1	2	1	4
dp53	3	2	10
hep	2	-	1
hep	3	1	2
bax	2	2	3
bax	3	2	4
ras^{DN}	2		*no GFP loss after 30 days*
Htt^{128}			*no GFP loss after 30 days*
tau ^{RWO46}	2	5	*> 50% GFP-+ PRCs after 30 days*
DJ-1A RNAi	2	15	*> 50% GFP-+ PRCs after 30 days*
MJD^{Q78}	3	20	*> 50% GFP-+ PRCs after 30 days*
Ab^{142}	2		*no GFP loss after 30 days*
rh1^{G69D}	2	15	*> 50% GFP-+ PRCs after 30 days*
dPINK1			*no GFP loss after 30 days*
hPINK			*no GFP loss after 30 days*

The degeneration of a PRC rhabdomere is represented by a series of stereotypical morphological changes. Under apoptotic stimuli, PRC rhabdomeres become distorted, elongated, shrink and ultimately fall basally to their demise. With the fluorescent live imaging method, PRC degeneration is determined by the progressive loss of GFP in the rhabdomeres (Figs. 2.1E, 2.2B). For confirmation and higher ommatidial resolution, retinal plastic sections are performed and reveal interommatidial disarray and inter-cellular vacuoles, indicative of retinal degeneration (Fig. 2.2D). Furthermore, EM analysis offers an even higher resolution of PRC degeneration. In wild-type conditions, ommatidia display stereotypical oval-shaped rhabdomere morphology with the outer PRCs slightly larger than the inner ones. The rhabdomeres appear as highly ordered stack of microvilli, in which rhodopsin molecules are arranged (Fig. 2.2E). In PRCs exposed to *dp53* at day 3, these same rhabdomere lose their structure due to the loss of the microvillar orderly structure. We also observe, in degenerating ommatidia with EM analysis, the hallmarks of apoptosis, including condensation of nuclei and cytoplasm and appearance of vesicles. Since overexpression of *dp53* is performed using the *rh1* promoter, only outer PRCs undergo and the inner PRC rhabdomere remains unaltered (Fig. 2.2F).

Figure 2.2 Wild-type and Degenerating PRCs. (A, C, E) are wild-type retinas and **(B, D, F)** are retinas expressing *dp53*, both at day-3 post-eclosure. **(A)** Visualization of a wild-type retina using live imaging at 20X magnification reveals ommatidia expressing GFP in outer PRCs. **(B)** White-boxed region in (A) highlights a 40X-magnified area with the six outer R1-R6 PRCs of each ommatidia expressing GFP. **(C)** Visualization of a retina expressing *rh1>dp53* leads to degeneration, indicated by the loss of GFP. **(D)** White-box region in (C) highlights a 40X-magnified area. Loss of GFP in ommatidia indicates PRC degeneration due to overexpression of *dp53*. **(E-F)** Retinal plastic sections reveal PRC integrity **(E)** and PRC degeneration **(D)** as well as IOC integrity or lack there of. **(E)** The orderly organization of ommatidia with surrounding IOCs is stereotypical of a wild-type retina. **(F)** The presence of inter-cellular vacuoles (red asterisks) as well as missing and distorted rhabdomeres (red arrows) indicate retinal degeneration. **(G-H)** Electron microscopy further highlights the rhabdomere structure of PRCs in wild type and pro-apoptotic conditions. Under wild-type conditions **(G)**, rhabdomeres are large, intact and organized around the inner R7 PRC. In *dp53*-degenerative conditions **(H)**, they are elongated, smaller or disorganized around the inner unaltered R7 PRC. R7 PRC is labeled '7'. EM analysis reveals feature of apoptotic cell death including membrane blebbing (yellow arrows), nuclear condensation and cytoplasmic compaction. *(Images G and H, courtesy of Helen Shio at the Electron Microscopy Facility, Rockefeller University)*.

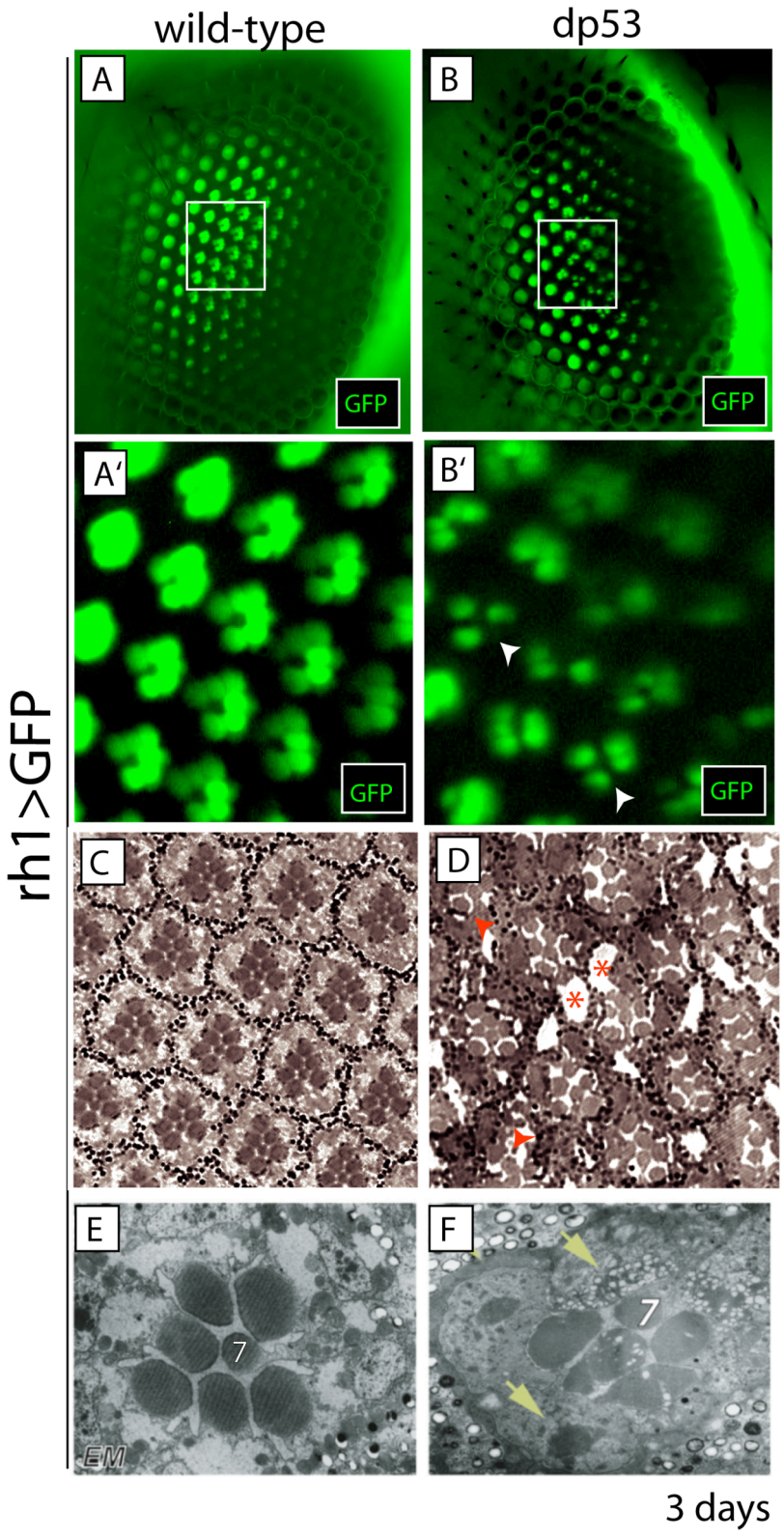

Figure 2.2 Wild-type and Degenerating PRCs

2.4.3 *reaper* Triggers PRC Degeneration in a Caspase-Dependent Manner

We then studied the effects of pro-apoptotic RHG gene *reaper* and in relationship to the caspase-dependent apoptotic pathway. The expression of *reaper* using the early *GMR* promoter also leads to PRC degeneration but with a 'rough eye' phenotype (Fig. 2.2A). *reaper* under the control of *rh1* triggers approximately 50% of PRC loss, indicated by the approximate 50% loss of GFP fluorescence (Fig. 2.2C). P35 rescues both the rough eye surface of *GMR>reaper* and the PRC loss of *rh1>reaper* retinas (Fig. 2.3B,F). We further characterized *reaper*-induced PRC degeneration in horizontal retinal sections. In wild-type conditions, the outer PRCs are arranged at the apical edge of the retina. Inner PRCs, notably R7, are arranged more basally and closer to the optic lobe (Fig. 2.3G1-G2). Wild-type retinas do not exhibit caspase activation in PRCs (Fig. 2.3G3). In contrast, *rh1>reaper* retinal sections at day-1 post-eclosure reveal distinctive PRC degeneration features. First, outer PRCs lose their apical arrangement and fall basally towards the optic lobe (Fig. 2.3H1-H2). Second, degenerating and 'falling' outer PRCs become caspase-positive (Fig. 2.3H3). Third, occasional PRC nuclei display fragmented morphology, a hallmark feature of apoptotic progression (Fig. 2.3H1'-H3').

Figure 2.3 *reaper*-induced PRC degeneration is Mediated by Caspases. All retinas were imaged at 1-day post-eclosure. **(A-C)** Overexpression of *reaper* in the developing eye leads to an adult rough eye **(B)**. P35 overexpression suppresses *reaper*-induced eye ablation **(C)** and restores a nearly wild-type eye **(A)**. **(D-F)** Using *rh1* promoter, *reaper* triggers approximately 50% PRC degeneration, indicated by the loss of GFP **(E)**. *reaper*-induced PRC degeneration is rescued by the overexpression of the caspase inhibitor P35 **(F)** and restores the six outer PRCs of each ommatidia as in the wild-type retina **(D)**. **(G-H)** Cryosection of a control *(rh1>lacZ)* **(G)** and *rh1>reaper* retina **(H)**. PRC nuclei are marked with DAPI (green) and ELAV (blue). Caspase staining is marked with CM1 (red). **(G1-G2)** *rh1>lacZ* retina reveals the tightly packed arrangement of outer PRCs at the apical edge (yellow bracket, **G1**) and inner PRCs in the middle of the retinal section. **(G3)** Little to no detectable CM1 staining. **(H1-H2)** *rh1>reaper* retinas reveal outer PRC disorganization and degeneration due to *dp53* overexpression. PRC fall basally and lose their apical integrity (yellow bracket). **(H3)** Degenerating outer PRCs, labeled with DAPI and ELAV, co-localize with CM1 staining. White box region in (H1-H3) highlights pkynotic or fragmented PRC nuclei (H1'-H2'), which co-localize with CM1 (H3') (yellow arrows). **(G)** Quantification of *reaper*- and *dp53*-induced PRC death with and without P35 overexpression. *reaper*-induced PRC degeneration is rescued by P35 overexpression at 1-day post-eclosure. *dp53* is only partially suppressed by P35 overexpression at 3-days post-eclosure (~%20 rescue).

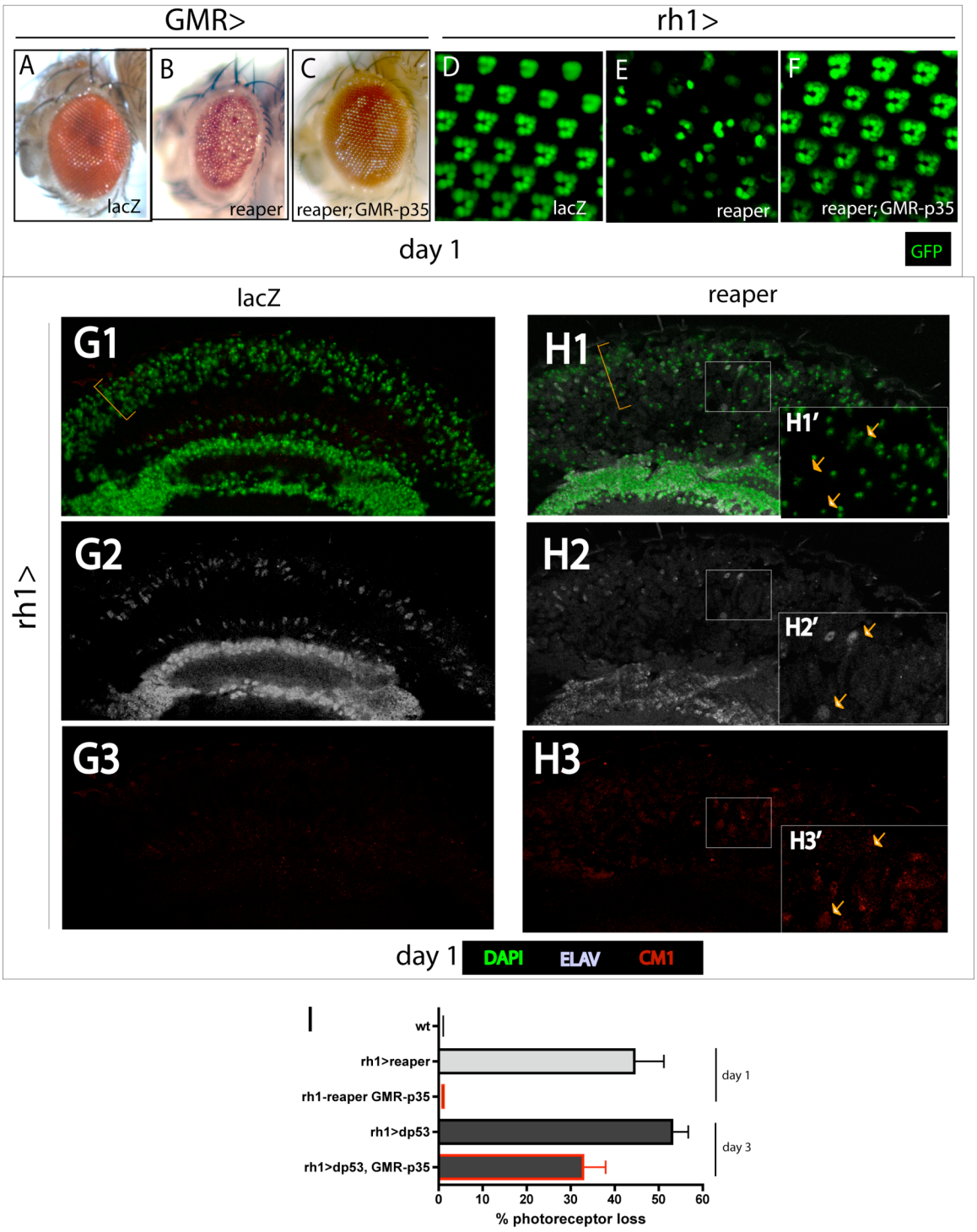

Figure 2.3 *reaper*-induced PRC degeneration is Mediated by Caspases

Similarly to *reaper*-induced PRC degeneration, *dp53* also triggers caspase activation and subsequent PRC degeneration (data not shown). However, in contrast to *reaper*, *dp53* is only partially rescued by P35, revealed by approximately 20% PRC rescue at day-3 post-eclosure (Fig. 2.3I).

2.4.4 A FLP/FRT System for Loss-of-Function Analysis

Based on the FLP/FRT technique, we developed a method for the generation and for imaging of lethal mutations in a recessive state in adult PRCs *in vivo*. For this purpose, we engineered a transgenic 'red' fluorescent construct targeted to the outer PRCs to complement the existing GFP construct. In combination, we present the first double-fluorescent system for *in vivo* imaging of mosaic PRCs in the *Drosophila* retina.

Preliminary efforts focused on choosing the best red fluorescent gene, which would allow for efficient rhabdomere visualization using the cornea neutralization technique. The criteria for selection were 1) fluorescent brightness for rhabdomere visualization, 2) fluorophore stability for *in vivo* time-course analysis and 3) absence of fluorphore aggregate formation for imaging of individual rhabdomeres within the ommatidia. *tdTomato*, a tandem dimer modified version of *RFP*, presents strong brightness, stability and lack of aggregation, thereby making it the red fluorescent gene of choice

(*Exp. Proc. 2.3.1* and *App. 6.1*) (Shaner et al., 2005). The *rh1-tdTomato* construct with a *ninaC* rhabdomere localization signal (Montell and Rubin, 1988) was assembled (Fig. 2.4A) and then recombined onto wild-type FRT chromosomes. Flies carrying both *GFP* and *tdTomato* constructs on FRT chromosomes, the *rh1* promoter, and the *eyFLP*/FRT technique were used to perform loss-of-function analyses in the *Drosophila* retina (Fig. 2.4B) (Newsome et al., 2000). tdTomato labels the wild-type and heterozygous PRCs whereas *GFP* is expressed in all PRCs. The absence of tdTomato (red) fluorescence represents the PRC clonal patches. In the schematic representation of a mosaic retina (Fig. 2.4C), R5-R6 PRCs are wild-type and outer R1-R4 PRCs are mutant PRCs. We visualized these clonal patches using the cornea neutralization technique (*Exp. Proc 2.3.2*). No visible PRC defects were detected because clones were generated with a wild-type FRT chromosome. Hence, clones exhibit the normal morphology and number of outer PRCs (Fig. 2.4D). Pseudopupil imaging of the mosaic eye further reveals the tdTomato (red) and GFP (green) pseudopupils of the mosaic retina (Fig. 2.4E1-E3).

Figure 2.4 A PRC Double-Flourescent Method for Recessive Analysis. **(A)** Structure of the *rh1-tdTomato*^{ninaC} construct to visualize PRCs by (red) fluorescent imaging. The (genomic -252+18) minimal *rh1* promoter (black) is fused to *rh1-tdTomato* (red, 472bps). The *ninaC* sequence (white, 150bps) was appended in-frame to *rh1-tdTomato* for the localization of the fluorescence to the rhabdomere. The construct was inserted into a $\Delta Chab_{Xba1}$ vector (~9kb). **(B)** The FLP/FRT technique enables the generation of homozygous clones from a progenitor heterozygous cell by mitotic recombination induced by the recombinase *FLP*, which is driven by the promoter *ey*. The chromosomal arm exchange is rendered possible by the presence of *FRT* sites on the pair of homologous chromosomes (Newsome et al., 2000). **(C)** Schematic representation of the mosaic eye with wild-type and mutant PRCs. D: dorsal. V: ventral. **(C')** Close-up reveals, at a single-cell resolution, that outer R1-R2 are mutant PRCs (green) and R3-R6 are either wild-type or heterozygous PRCs (red). **(D)** The mosaic adult retina with *FRT[w+]* clonal patches of PRCs indicated by the absence of red. Merge of both GFP (green) and tdTomato (red). **(D1-D3)** White-box in **(D)** highlights a 40X-magnified mosaic region in the adult retina **(D1)**. Wild-type and heterozygous PRCs are labeled in red **(D2)**. All PRCs are labeled in green **(D3)**. We note mosaic ommatidia (red and green) at the edge and *FRT[w+]* clonal ommatidia at the center (only green). No PRC defects are observed because clonal patches were generated with an empty 'wild-type' *FRT[w+]* chromosome. **(E1-E3)** Pseudopupil imaging of the mosaic eye in **(D)**.

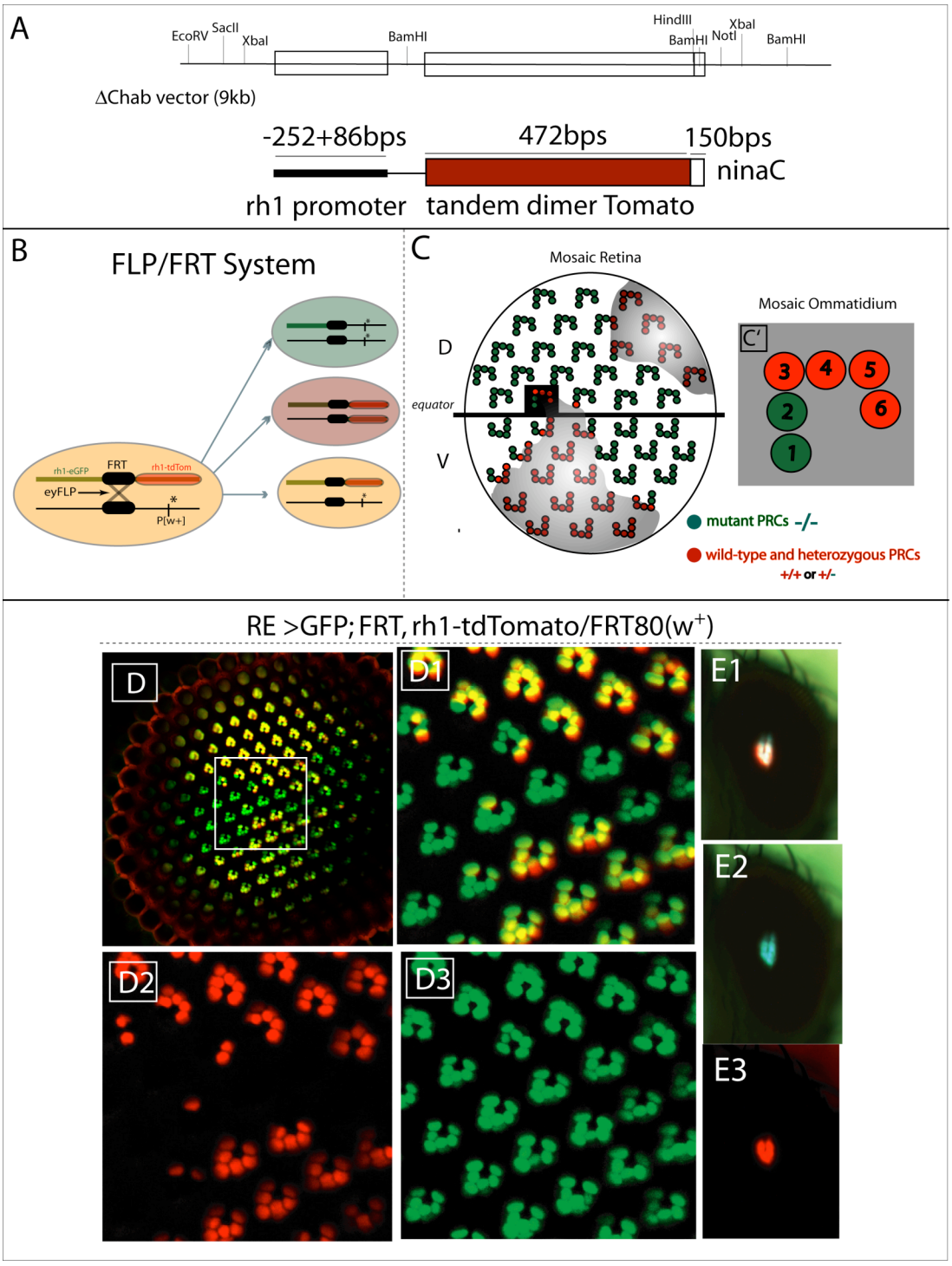

Figure 2.4 A PRC Double-Fluorescent Method for Recessive Analysis

2.4.5 Age-Dependent *reaper*- and *dp53*-Induced PRC Death is Delayed in *dronc* Loss-of-Function Clones

Relying on these newly developed gain- and loss-of-function tools, we further explore *reaper*-induced and *dp53*-induced PRC degeneration in a time-dependent study. We generated loss-of-function clones of $dronc^{I29}$ mutations and investigated cell death kinetics of *reaper* and *dp53* in mosaic retinas under *rh1*. To mitigate *reaper* and *dp53* cell death activity under *rh1* in pupal stages and monitor PRC death in the adulthood, flies were raised at 18°C and switched at 25°C post-eclosure. Three different scenarios were predicted: *dronc* loss-of-function mutations suppress, delay or have no effect on apoptotic-induced PRC death in the adulthood (Fig. 2.5G). The same mosaic patch of PRCs was imaged at days 1, 4 and 7 to follow the progression of *reaper*-induced cell death (Fig. 2.5A-C) and days 1, 4 and 10 to follow the progression of *dp53*-induced cell death (Fig. 2.5D-F).

reaper overexpression leads to PRC loss in approximately 1-week in the population of wild-type and heterozygous PRCs. Starting at day 1 (Fig. 2.5A), *reaper* leads to approximately 30% degeneration at day 4 (Fig. 2.5B) and over 90% by day 7 (Fig. 2.5C). Conversely, the presence of *dronc* mutant clones suppresses *reaper*-induced cell death, indicated by the persistence of mutant PRCs despite the enduring *reaper* stimulus. However,

we note an occasional loss of PRCs in *dronc* mutant tissue at later adulthood stages. While no visible PRC loss is revealed up until day 4, a low frequency (5%) of PRC loss is revealed at day 7 in *dronc* mutant tissue (Fig. 2.5H). Sporadically, we also detect *dronc* mutant ommatidia with very small rhabdomeres at day 7 (Fig. 2.5C1'), indicating both degeneration and the forthcoming demise of these PRCs. Overall, these results indicate that *reaper*-induced PRC death is primarily dependent on caspase initiator *dronc* with occasional PRCs, overexpressing *reaper*, which undergo *dronc*-independent killing.

In contrast to *reaper*, *dp53* killing reveals a more prominent caspase-independent pathway of PRC death. Indeed, *dp53*-induced PRC degeneration kinetics is only delayed by a few days in *dronc* loss-of-function conditions. In *dp53* overexpression conditions, we observe approximately 25% PRC loss at day 4 in wild-type and heterozygous PRCs while no evidence of PRC loss in *dronc* mutant PRCs (Fig. 2.5E,I). However, at day 7, we detect over 60% degeneration in wild-type PRC and 20% degeneration in mutant PRCs (Fig. 2.5F,I). These results accord with P35 overexpression studies, which similarly show only a partial rescue of *dp53*-induced PRC death by blocking caspases.

Figure 2.5 An Age-Dependent Analysis of *reaper*- and *dp53*-Induced Cell Death in *dronc* Loss-of-Function Clones. In **(A-F)** panels, wild-type and heterozygous PRCs are represented in red and mutant homozygous *dronc I29* PRCs are revealed by the absence of red. All PRCs (wild-type and *dronc* mutant PRCs) are labeled in GFP. For every timepoint, merge, green and red channels are shown. **(A-C)** panels represent *rh1>reaper* induced PRC death with homozygous clones of *dronc I29*. **(D-F)** panels represent *rh1>dp53* induced PRC death with homozygous clones of dronc I29. 40X magnification. **(A-C)** *reaper* induces progressive degeneration of PRCs. Three timepoints highlighted are day 1 (**A1-A3)**, day 4 **(B1-B3)** and day 7 **(C1-C3)**. **(A1'-C1')** White-box region in A-C highlights close-up of *dronc* mutant and wild-type PRCs. White arrows point to *dronc* mutant ommatidia which display PRC loss or degeneration from day 1 to day 7. **(D-F)** *dp53* induces progressive degeneration of PRCs. Three timepoints highlighted are day 1 (**D1-D3)**, day 4 **(E1-E3)** and day 10 **(F1-F3)**. **(D1'-F1')** White-box region in A-C highlights close-up of *dronc* mutant and wild-type PRCs under the expression of *dp53*. **(G)** Potential effects of mutant clones on PRC degeneration induced by apoptotic stimuli (violet). Red PRCs are wild-type or heterozygous PRCs with apoptotic stimuli. Absence of red labels mutant PRCs. Green labels all PRCs with apoptotic stimui. *Suppression:* mutant PRCs are resistant to apoptotic-induced PRC death. *Delay:* mutant PRCs degenerate at a slower rate than wild-type PRCs to apoptotic stimulus. *No effect*: mutant PRCs degenerate with same kinetics as wild-type PRCs to apoptotic stimulus. **(H-I)** Quantification of PRC loss in wild-type + heterozygous (red) versus mutant (green) PRCs for *reaper*- **(A-C)** and *dp53*- **(D-E)** induced PRC degeneration.

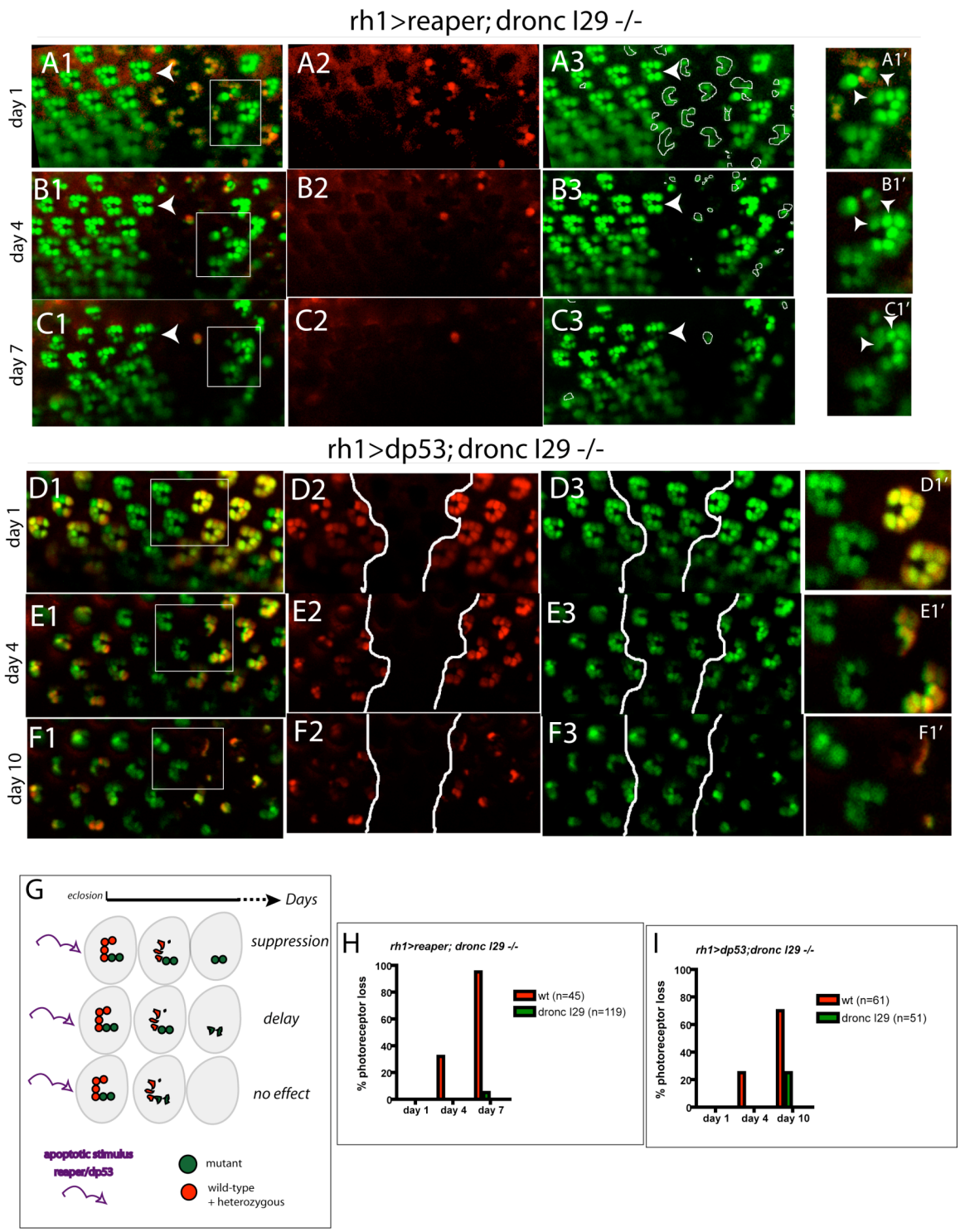

Figure 2.5 An Age-Dependent Analysis of *reaper*- and *dp53*-Induced Cell Death in *dronc* Loss-Of-Function Clones

2.5 Discussion

2.5.1 A New PRC Visualization Approach for Gain- and Loss-of-Function Analysis

Rapid and high throughput live methods, such as deep pseudopupil analysis, only account for the integrity of all PRCs within the ommatidia; they do not allow for a precise quantification of cell viability in a single ommatidium, thus lacking cellular resolution (Kurada and O'Tousa, 1995). While the UV imaging method allows the live visualization of individual ommatidium relatively quickly (Fig. 1.3C), the epi-fluorescence needs to be captured within a few seconds, rendering image focus and acquisition a challenge. On the other hand, retinal plastic section, EM analysis and whole-mount retinal dissections all provide a very high retinal resolution, but the protocols are time-consuming and do not permit the study of progressive degeneration.

We report a robust fluorescent-based system to visualize and study PRC integrity with a simple, fast and non-invasive approach. This method was originally described as a method to analyze the spectral properties of pigments in bigger (*Musca domestica*) flies (Franceschini et al., 1981). It was later readily used to study PRC morphology and differentiation in *Drosophila*. Here, we have used this system for the study of cell death in

differentiated PRCs (Pichaud and Desplan, 2001). Indeed, using GFP under *rh1*, we can visualize outer PRCs *in vivo* and account in a semi-quantitative manner the extent of PRC degeneration in response to apoptotic stimuli.

We have added a new layer of visualization to the GFP-based method by introducing *tdTomato* red fluorescent labeling of PRCs. Combining the double-fluorescent system and the genetic FLP/FRT tools for clone induction allows the visualization of a mixed population of PRCs: mutant, heterozygous and wild-type PRCs. We highlight the advantages of the double-fluorescent based method.

First, it is a fast and reliable amenable for high throughput recessive screening for genes affecting PRC survival, morphology and differentiation. Indeed, mutants can be studied in a loss-of-function manner and subsequently recovered for further analysis, thereby circumventing the need for time-consuming invasive retinal plastic section procedures or whole-mount retinal dissections.

Second, it provides a single-cell resolution, whereas individual PRC mutant cells and mosaic ommatidium can be visualized and the phenotypic consequences assessed. For example, the method can gauge PRC sensitivity to apoptosis in a context-specific manner. Mutant PRCs surrounded by wild-type PRCs in mosaic ommatidia as opposed to mutant PRCs embedded in

completely mutant ommatidia may respond differently to cell death. Such cell non-autonomous interplay in mosaic tissue has already been suggested in cell competition studies in *Drosophila* developing tissue (de la Cova et al., 2004).

Third, it allows for transgenic overexpression in loss-of-function clones. Transgenes and promoter driving these transgenes typically harbor the *white* gene as a markers, which confers red-eye color to flies. Hence, transgenic overexpression in loss-of-function clones is not feasible using standard retinal plastic section procedures, which resort to red pigment or absence of as a marker for clones (Newsome et al., 2000). On the other hand, using the fluorescent-based system, both pro-apoptotic players and inhibitors can be overexpressed in mutant clones, thereby allowing for epistasis analyses as well as the identification of suppressors and enhancers in cell death sensitized backgrounds.

Last but not least, the non-invasive technique enables to track loss-of-function clones *in vivo* and monitor PRC changes in a time-dependent manner. Hence it is as an invaluable system to study age-dependent PRC degeneration and a model to understand the mechanisms of adult-onset and progressive neurodegenerative human diseases.

2.5.2 Modeling Neurodegeneration: an Age-Dependent and Progressive PRC Degeneration

Ectopic expression of pro-apoptotic genes reveals that terminally-differentiated PRCs are refractory to cell death and degenerate in an age-dependent manner. Core intrinsic pro-apoptotic players, such as IAP antagonists *reaper* and *hid*, under *rh1* expression induce PRC degeneration in 3 days or less. On the other hand, *dp53* induces PRC degeneration in approximately 10 days. This suggests *dp53* may initiate a more complex cascade of events. In addition to its pro-apoptotic function, *dp53* also elicits a pro-survival response, including the upregulation of antioxidant genes and the arrest of cell cycle and proliferation for DNA repair (Jassim et al., 2003; Sablina et al., 2005; Sax and El-Deiry, 2003). While speculative, we propose that the *dp53* pro-survival pathway may mitigate the pro-apoptotic activity of *dp53* and subsequent degeneration of PRCs. Finally, we observed that genes involved in neurodegeneration, such as the silencing of *DJ-1A* and *dPINK* genes involved in the familial genetic form of PD lead to very slow PRC degeneration. Hence, they mimic the late onset of symptoms and slow progression of most human neurodegenerative diseases. We further point out that PRC degeneration is not only dependent on the nature of the apoptotic insult but also on dosage. For example, additional copies of *reaper* transgene

expression or the combinatorial effects of *reaper* and *hid* dramatically enhance the kinetics of PRC degeneration.

In contrast to the age-dependent cell death during the adulthood, we detect that PRCs are acutely sensitive to apoptosis in late pupal stages. Indeed, when *reaper* or *dp53* are overexpressed, a massive PRC loss is revealed already at day-1 post-eclosure. Hence, we identify a late-pupal window of heightened sensitivity to apoptosis of terminally-staged PRCs. Other studies have also identified stages of apoptotic sensitivity during pupal development. Indeed, IOCs in the pupal retina are especially vulnerable to UV insults between 18-25-hour APF, a sensitivity diminished with the progression of pupal development and non-detectable in the adult retina (Jassim et al., 2003).

We contrast the age-dependent cell death in mature PRCs with an imminent and massive cell response in differentiating PRCs. Indeed, in the developing eye, *dp53* and *reaper* under *GMR* induce cell death signals in a matter of hours while in our terminally-staged PRC system, the same apoptotic insults under *rh1* induces apoptosis over a few days and thereby mimic slowly progressive course of neurodegeneration. Moreover, our PRC system allows us to mimic morphological features of progressive neuronal degeneration. Under degenerative conditions, outer PRC rhabdomeres

become distorted, smaller, abnormal, lose their apical integrity and eventually disappear, replicating the hallmarks of onset/progression of neurodegenerative diseases (ex: ALS): cellular atrophy, axonal swelling and impairments, and eventual neuronal loss.

While harboring distinct progressive and age-dependent post-mitotic cell death features, degenerating PRCs also display common morphological and biochemical apoptotic-like features, thereby providing us with a system to further explore and understand mechanisms of apoptosis in differentiated cells. Revisiting *dp53* and *reaper*-induced cell death in PRCs has identified hallmark apoptotic-like events including caspase activation, nuclear fragmentation, membrane blebbing and cytoplasmic compaction.

2.5.3 Blocking Caspases: A Delay in Neurodegeneration

An issue of controversy in the literature is the role of caspases in neurodegeneration. While caspase activation has been shown to occur in dying neurons in diseases, the causative involvement of caspase has yet to be established (Bredesen et al., 2006). We revisited the role of caspases in *reaper* and *dp53*-induced PRC degeneration models. IAP antagonist *reaper* has been extensively studied in development. In the *Drosophila* cells, Reaper-induced cell death is completely dependent on caspases as co-transfected in *Drosophila* cells with viral caspase inhibitor P35 rescued

virtually all apoptosis (Zhou et al., 1997). Similarly, in the developing eye, Reaper-induced retinal degeneration was blocked by P35 (White et al., 1996). On the other hand, tumor suppressor P53 has been shown to cause apoptosis in both caspase-dependent and –independent pathways (Godefroy et al., 2004). In *Drosophila*, *dp53* has been shown to activate Reaper and downstream caspase activation in radiation-induced apoptosis (Brodsky et al., 2000). However, P53 also has been shown cause caspase-independent cell death in many types of neuronal injury such as brain ischemia and excitotoxicity (Cregan et al., 2002). In our PRC system, we show that *reaper* and *dp53* overexpression lead to caspase activation. Indeed, at day-1 and day-3 post-eclosure, we observe caspase activation in degenerating PRCs of *reaper*- and *dp53*-stimulated retinas. Furthermore, P35 overexpression fully rescues *reaper*-induced PRC death at day-1 post-eclosure. However, it only partially suppresses (20%) *dp53*-induced PRC death at day-3 post-eclosure, confirming a prominent caspase-independent branch of *dp53*-induced cell death.

A time-dependent analysis of *reaper* and *dp53*-induced cell death in *dronc* mutants provided us with a higher resolution on the role of caspases in these models. In *dp53*-induced PRC degeneration, we observe a progressive degeneration. Until day 4, *dronc* mutant PRCs are resistant to *dp53*-induced

cell death but eventually succumb to cell death, evidenced at day 10. On the other hand, *reaper*-induced PRC loss is almost completely suppressed in *dronc* mutant clones. However, we detect at day 7, when all wild-type PRCs have already succumbed to *reaper*-induced cell death, the evidence of the initial stages of PRC degeneration. Indeed, we note 5% PRC loss in mutant tissue and occasional rhabdomeres that display degenerative phenotypes. Hence, this implies that *reaper*-induced cell death may harbor a Dronc-independent cell death pathway in adult PRCs. A Dronc-independent pathway of apoptosis has already been postulated. Indeed, in a *dronc* mutant embryo developmental cell death is significantly reduced but not completely blocked (Xu et al., 2005).

With these studies, we introduce the concept of 'delay' to explain the role of caspases in neuronal cell death. Based on time-dependent results, *dronc* inactivation leads to a moderate delay in *dp53*-induced PRC death and a very strong delay (nearly suppression) in *reaper*-induced PRC death. A longer time-course analysis is necessary to gauge the full 'delay' of PRC degeneration delay in both models. We radically propose that caspase inhibition provides a temporal delay but may not be sufficient to completely suppress neuro-degeneration. Supporting this hypothesis, mammalian studies have shown that caspase inhibition effectively inhibits caspases but

only delays disease onset and mortality in neurodegenerative conditions (Chen et al., 2000). We further suggest that the nature and the onset of the pro-apoptotic stimulus in neurons may dictate the potency of delay by caspase inhibition.

In conclusion, with the characterization of *reaper*- and *dp53*-induced, we highlight the advantages of the newly developed double-fluorescent method for dissecting PRC death mechanisms. These and other recent reports support the growing idea that both caspase-dependent and –independent pathway may mediate cell death in adult neurons at specific ages and after particular kinds of perturbations (Broker et al., 2005).

3 GENETIC SCREENS TO IDENTIFY GENES INVOLVED IN PHOTORECEPTOR CELL DEATH

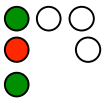

The work presented in this chapter was performed in collaboration with the Mollereau Laboratory at the École Normale Supérieure de Lyon. With the help of Pierre Dourlen, a visiting postdoctoral fellow under my supervision and training, the entire PRC recessive screen and part of the secondary P35 screen were conducted in our laboratory. Pierre Dourlen along with other members of the Mollereau Laboratory are now finishing the P35 secondary screen, which was started here, and are currently involved in the characterization of a select number of (P35-)recovered candidates.

3.1 Summary

The success of *Drosophila melanogaster* as a model organism is largely due to screens that identify genes involved in various biological processes. Traditional cell death screens have led to the discovery of many of the core anti- and pro-apoptotic regulators of the *Drosophila* apoptotic pathway. Using the newly devised double-fluorescent technique described in Chapter 2, we performed a recessive cell death genetic screen to search for genes that specifically affect PRC viability. The screen's results revealed a myriad of recessive mutations that cause PRC differentiation defects and degeneration, leaving 50% with minor or no PRC defects. Of the PRC degeneration phenotypes, we could distinguish two different classes. The first class is composed of mutations that trigger severe PRC degeneration, accompanied by secondary polarity defects and rough/glossy eye phenotypes. The second class is composed of mutations that cause selective and moderate PRC loss with no polarity defects or eye morphology phenotypes. The latter class, enriched in mitochondrial and redox-related genes, is of particular interest because it seemingly represents a subset of genes that are important in PRC survival either late in development or post-eclosure. To uncover mutations triggering caspase-dependent cell death, we further sub-categorized the PRC degeneration phenotypes in a second

screen, based on their ability to be rescued by the caspase inhibitor, P35. After the double-screening process, we made a note of redox-related genes which, when mutated (such as *fatty acid transport chain*, *fatp*), lead to age- and caspase-dependent PRC degeneration versus others when mutated (such as *ferritin light chain homologue, fer2LCH*), are also caspase-dependent but cause a punctual PRC degeneration. By analyzing the PRC degeneration phenotypes and their connection to the caspase-dependent apoptotic pathway, we have gained a better understanding of the pathways governing PRC-specific cell death.

3.2 Introduction

3.2.1 Cell Death Genetic Screens in *Drosophila*

Drosophila is a powerful genetic system, suitable for the execution of large-scale forward genetic screens. The forward genetic approach in *Drosophila* has been successfully used to identify molecular components of the canonical apoptotic pathway. The induction of apoptosis requires the activity of three closely related genes, *reaper*, *hid*, and *grim*, together known as the RHG protein family. The function of these genes was revealed in a deficiency screen, spanning 85% of the genome. The deficiency line, H99, which covers the RHG locus, was shown to abolish all signs of naturally

occurring programmed cell death during embryogenesis. The cloning of *reaper*, *hid* or *grim* and their subsequent ectopic expression confirmed their pro-apoptotic activity; they were able to elicit apoptosis in the developing *Drosophila* eye and give rise to a reduced adult eye (White et al., 1994). Based on the discovery of RHG family proteins, sensitized genetic screens were designed to isolate modifiers of this reduce-eye phenotype and successfully identify novel regulators of cell death. Especially noteworthy was the recovery of several loss- and gain-of-function mutations of the caspase suppressor, *diap1*, able to both enhance and suppress the eye ablation phenotype induced by either *hid* or *reaper* (Agapite and Steller, 2002; Goyal et al., 2000). The characterization of these mutations paved the way to understanding the mechanisms of action of the RHG protein family; These proteins were shown to inhibit anti-apoptotic Diap1, earning their prestigious title as "IAP antagonists".

A prerequisite for the successful recovery of potential candidates from dominant screens is that the reduction of gene dosage by 50% is sufficient to induce a phenotype. However, most genes require a complete reduction of 100% (homozygous mutant conditions) for any phenotypic consequences. Recessive mutations usually cause lethality, making it impossible to study their effects in late development and in the adult. To overcome this hurdle,

clonal analysis using the FLP/FRT technique has been particularly useful to study genes that are lethal in a homozygous mutant state and to recover essential genes in cell death screens (Golic and Lindquist, 1989; Newsome et al., 2000). For example, the isolation of novel mutations in the initiator caspase *dronc*, were identified in a *GMR-hid* recessive screen. Loss-of-function *dronc* mutants were shown to recessively suppress the eye ablation phenotype caused by eye-specific overexpression of *hid* (Xu et al., 2005). In this chapter, we describe a novel recessive screen based on similar FRT/FLP technique for clonal analysis, which aims to find novel anti-apoptotic factors required for PRC survival.

3.2.2 Convergence between Cell Death and Differentiation

Developing cells on the way to becoming differentiated cells and those on a route to suicide, travel a similar course. The determinants in their course are caspases. Caspases have been shown to play a leading role in both differentiation and apoptosis. They required for proper sperm differentiation and for proper SOP development (Arama et al., 2003; Kanuka et al., 2005). Killer caspase enzymes are also required for the controlled dismantling of the cell during apoptosis.

A causative relationship also exists between cell differentiation and death. Cells that do not properly differentiate undergo apoptosis, a

phenomenon that is referred to as “death by frustration”. Work performed by a former graduate student, Ann Tang, in our laboratory has shown that pro-apoptotic *reaper* is transcriptionally turned on in improperly differentiated embryos (Tang and Steller, 2007). Other studies have suggested a role of Hox genes, known to be required for regional differentiation along the anterior-posterior axis, to trigger apoptosis. The Hox gene *Deformed* (*Dfd*) maintains the boundary between the maxillary and mandibular head lobes by activating *reaper* (Lohmann et al., 2002). Another Hox gene, *Antennapedia* (*ANTP*), known to regulate differentiation of the leg, induces apoptosis when misexpressed in certain areas of the eye imaginal disc (Plaza et al., 2001). Cell differentiation factors can also play an anti-apoptotic role. The *Drosophila* EGFR had a dual role in both cell proliferation and differentiation. A gain-of-function mutation in *ras*, integral to EGFR pathway, was recovered as strong suppressors of *hid*-and *reaper*-induced apoptosis (Gafuik and Steller, 2008).

The link between cell death and differentiation in *Drosophila* PRC development has also been suggested but remains unclear. An example of this is the mutant ommatidia of *senseless* (*sens*), a zinc transcription factor. In the ommatidium, R8 is the first photoreceptor to form and appears to recruit and support other PRCs. In *sens* mutant ommatidia, R8 PRCs are

absent, with occasional outer PRCs are also missing. To explain the presence of photoreceptors in the absence of R8 in *sens* mutant retina, one hypothesis is that the R8 photoreceptor could differentiate, begin the process of photoreceptor recruitment, and then die. While dying, R8 could also send death signals to its neighboring PRCs. Intriguingly, this anti-apoptotic role of *sens* has already been suggested in *Drosophila* in earlier development. *sens* prevents programmed cell death in *Drosophila* embryos and in salivary glands by repressing *reaper* and possibly *hid*. Furthermore, the loss of *sens* is rescued by the loss of pro-apoptotic genes or by overexpression of the caspase inhibitor protein, P35 (Chandrasekaran and Beckendorf, 2003).

Similar to *sens*, other differentiation mutants have been previously described to exhibit PRC loss or degeneration in the *Drosophila* retina. This begs the question as to whether the PRC differentiation perturbations can activate PRC death in the *Drosophila* retina. We address this in a two–step screening process. First, we isolated differentiation mutations with missing outer PRCs and second, we assess the ability of the caspase inhibitor P35 to rescue PRC loss. We also sought to isolate mutations that solely affect PRC survival without differentiation or other developmental defects.

3.2.3 An Enhancer-Trap Screen to Identify Genes with PRC Expression

Prior to exploring mechanisms underlying terminally differentiated PRC death, a search for genes that are preferentially expressed or enriched in PRCs was undertaken in the laboratory by the *Mollereau* Group. The assumption is that differentiated PRCs highly express distinctive genes, which are not or are weakly expressed earlier in developmental. Furthermore, a subset of genes specific to differentiated PRCs should promote the survival of PRCs, which when mutated would plausibly cause the degeneration of these cells.

In order to identify genes that are expressed in outer PRCs, *Philippe Loiseau*, a visiting summer student and *Cesar Mendes*, a former graduate student in the laboratory, took advantage of the Berkeley *Drosophila* Genome Project (BDGP), comprised of a collection of seven P-element mutagenesis screens, associated with 40% of the *Drosophila* genome (Bellen et al., 2004). From this collection, they distinguished two classes of P-elements used: P[Z] and P[lacW], each carrying the *E.coli lacZ* gene encoding the β-galactosidase as a reporter, fused to a minimal promoter (Fig. 3.1A). These P-element lines are recessive lethal lines, because they mostly integrated into the 5' untranslated regions (UTRs) or in the coding regions of

the genes, inactivating them. In addition, the insertion leads to the activation of the LacZ reporter regulated by enhancer regions of the targeted region. β-galactosidase expression pattern reflect the endogenous expression patterns of genes near the sites of P-element insertion (Mlodzik and Hiromi, 1992). It is strongly suggested that the P-element mimics the normal transcriptional gene expression with β-galactosidase, allowing further study of the expression patterns of the disrupted gene. The P[Z] and P[lacW] subsets from BDGP comprises over 2,500 stocks. These stocks were individually cryo-sectioned and analyzed for β-galactosidase activity in outer PRCs (Fig. 3.1B) (Rantnakumar and Loiseau, 2002). 149 lines revealed *lacZ* expression in outer PRCs, corresponding to 107 unknown genes, 6 uncharacterized genes (CGs), 1 line not mapped, and 33 cytogenes (mapped only by broad cytological locations). An example of the latter group is Bloomington Stock 10827 which correspond to cytogene *l(2)06270*. Early in my thesis, work was accomplished to find the exact location of this P-element insertion by performing inverse PCR reactions. Of the 3 lines tested, the resulting amplicon containing flanking sequence of cytogene *l(2)06270* was successfully sequenced and blasted against the *Drosophila* genome (Fig. 3.1C). The sequence corresponds to a fragment in the 5' UTR of the gene *thor* (Figure 3.1D). Thor is a member of the 4E-Binding Proteins (4E-BP)

Figure 3.1 P-element Enhancer-Trap Screens for PRC Expression. (A) Structures of the *P[Z]* and the *P[lacW]* transposable elements. Both P-elements contain a *LacZ* reporter, an *hsp70* minimal promoter, and a bacterial origin of replication (Ashburner and Bergman, 2005). Distinctively, *P[Z]* contains a *rosy*$^{+}$ marker and *P[lacW]* a mini-white w^{+} marker. P-element lines were used as source of mutant lines for genetic screens described in this chapter. **(B)** PRC nuclei are labeled DAPI (turquoise) and P-element lacZ expression by X-galactosidase activity (X-Gal, dark blue). Example (*crumbs*) of a vertical cryosection of an adult eye exhibiting *lacZ* expression (green arrow) in outer PRCs at the apical edge of the retinal section. **(C)** A diagram depicting the inverse PCR strategy for recovering P-element flanking sequence information. The strategy is a 5-step process: RsaI restriction enzyme, self-ligation, 2 rounds of PCR and sequencing. **(D)** Sequence analysis of sequenced fragment against the Drosophila genome *(BLAST, Flybase, GBrowser)* reveals that P-element *l(2)06270* is inserted into the 5'UTR region of the *thor* gene.

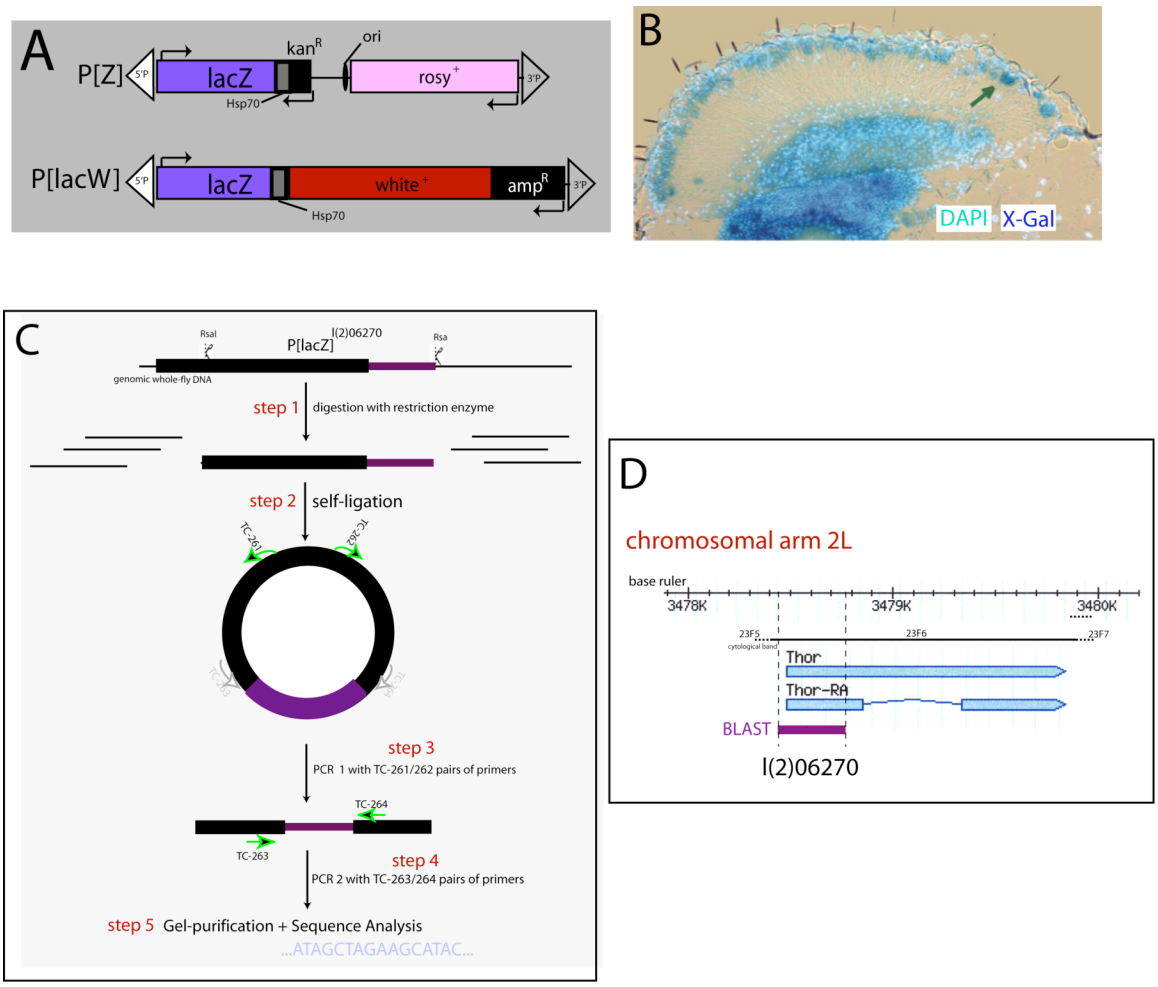

Figure 3.1 P-element Enhancer-Trap Screen for PRC Expression

family, which in *Drosophila* and mammals, has been defined as critical regulators in a pathway that control initiation of translation through binding eukaryotic Initiation Factor 4E (eIF4E). Thor has been implicated in host immune defense, oxidative stress regulation and insulin-dependent starvation responses (Bernal and Kimbrell, 2000).

Interestingly, the number of P[Z] lines with detectable PRC expression (99 out of 500, approx 20%) is highly superior to the P[lacW] (50 out of 2000, 2.5%), suggesting that the LacZ reporter included in the P[Z] transposon is more responsive and/or more influenced by regulatory regions. The 149 P-element lines and affected genes, which reveal PRC expression in the enhancer-trap screen results, are summarized and presented in Table 3.1.

3.2.4 A Dominant Screen for Modifiers of *dp53*-Induced PRC Death

In order to monitor PRC loss, the GFP-based system for PRC live imaging, described in Chapter 2, was used. *dp53* induces PRC loss in approximately 10 days, starting one day after eclosure and slowly progressing until no outer PRCs are visible after ten days. The early onset and slow progression of degeneration facilitates the analysis of possible modifiers of the cell death phenotype induced by *dp53*. Around day 3 or 4, approximately half of the outer PRCs are lost, presenting an ideal time point to detect modification of the progression of cell death. The kinetics of -

Table 3.1 P[Z] and P[lacW] Lines with LacZ Expression in PRCs

P[Z]

P-element #	Gene	P-element #	Gene	P-element #	Gene
10183	crebA	11452	l(2)44DEa	11629	emc
10184	abl	11463	ter94	11632	l(2)04521
10236	CG16765	11481	l(2)06270	11633	rdp3
10326	orb	11483	fer2LCH	11638	l(3)04713
10343	Toll	11486	osa	11654	hsromega
10827	l(2)00231	11491	mo25	11666	sc2
10827	lilliputian	11493	slmb	11668	l(3)05697
10827	eflalpha48D	11494	atg1	11669	sar1
10827	eIF-5A	11502	mpcp	11677	l(3)05967
11053	kekkon-1	11509	l(3)00720	11681	stat92E
11056	mesk2	11512	l(3)00836	11683	jumu
11062	CG30497	11513	sanpodo	11688	atx2
11073	dve	11520	lip	11697	syx1A
11183	l(2)02321	11528	kst	11698	l(3)06743
11193	mts	11533	atpα	11707	msn
11200	retained	11536	syntaxin 13	11711	cdi
11201	lobe	11544	pum	11712	eip75B
11244	ken	11548	smij	11718	l(3)07207
11261	l(203050	11549	l(3)01859	11722	l(3)07615
11278	numb	11563	baldspot	11728	l(3)08126
11295	spen	11564	tropomysoin1	11729	rols
11336	aats-val	11567	l(3)02404	11731	sgl
11346	l(2)03728	11581	eIF-5C	11734	l(3)09070
11349	ter94	11582	l(3)03076	11735	eIF5B
11356	calmodulin	11585	grappa	11742	l(3)10112
11359	aop	11590	ctbp	11743	bitesize
11369	rhoGEF2	11609	regena	11752	string
11374	crol	11612	modulo	11525	put
11379	eb1	11617	csp	11749	vn
11384	iam	11623	dlc90F	11756	blw
11385	doc	11624	mub	11716	corto
11403	smooth	11626	trn	11744	pros
11409	inscuteable	11627	akt1	11763	cyt c-d

P[lacW]

P-element #	Gene	P-element #	Gene	P-element #	Gene
10154	bantam	10320	gclm	12054	raspberry
10162	msn	10331	crumbs	12064	hsp83
10180	l(3)0499	10674	l(2)k07509	12113	l(1)G0087
10481	thor	10694	NFSA	12121	puckered
10491	l(2)k01103	11218	Tor	12141	top1
10515	lola-like	11470	act5c	12161	takr99D
10555	l(2)k08770	11499	sop	12211	ldh
10583	vrille	11588	cop	12222	l(3)L7160
10646	split ends	11809	lnx2	12228	ctp
11127	CG8674	11812	CG12113	12232	l(1)G)226
11995	raspberry	11813	CG17255	12273	act5C
12207	l(2)k00808	11825	act5c	12275	neuroglian
12387	l(2)k08317	11855	l(1)G0254	12287	flap wing
10095	arm	11975	cut-up	12293	unc-76
10281	l(3)L1231	12024	cut-up	12294	inx2
10286	Hsc70-4	12026	CG6606	12803	alh
10315	l(3)L3560	12027	raspberry		

degeneration observed in *dp53*-stimulated PRCs is in contrast with a faster degeneration kinetic seen with *reaper*-stimulated PRCs, or the extremely slow degeneration observed in *rh1* (*ninaE*) mutants (Table 2.1).

P-element lines with expression in outer PRCs, correspond to loss-of-function alleles, and therefore may modulate the killing effect of *dp53*. The crossing scheme is illustrated in Fig. 3.1A and explained briefly in the *Exp. Proc. section 3.3.4*. From the 149 lines tested, 32 alleles were identified as dominant modifiers of *dp53*-induced cell death, corresponding to 21% of the total number of lines tested. From these, 21 are classified as *suppressors*, thus putative pro-apoptotic genes, and 11 as *enhancers*, thus putative anti-apoptotic genes (Table 3.2).

Initial characterization of the *dp53*-induced cell death phenotype in outer PRCs showed that caspase activation only accounts partially for the degenerative phenotype (Fig. 2.3I). Moreover, *reaper* acts downstream of *dp53* and is at least partially responsible for the execution of apoptosis (Brodsky et al., 2000). In order to determine if the identified alleles act directly on *dp53* or simply on general cell survival, a secondary screen was carried out using *reaper* by *Cesar Mendes* and with my assistance in the final stages (Table 3.2). Approximately 60% of the alleles showed the same affect, both for *dp53*- and *reaper*-induced cell death, indicating that these

mutations either act downstream of *reaper*, or indirectly affect cell survival. Moreover, *ninaE* alleles (~30%) did not affect *reaper*-induced apoptosis, suggesting that the corresponding genes act epistatically between *dp53* and *reaper*.

The screen results brought about three different projects in the laboratory. *cyt-c* mutations dominantly suppress *dp53*-induced PRC degeneration, which later led to the characterization of Cyt-c in PRC death and IOC developmental apoptosis (Mendes et al., 2006). Cyclophilin ER-resident *neither in nor activation A* (*ninaA*) mutations retard *dp53*-induced cell death, a mechanism that was later attributed to a mild protective ER stress signaling (Mendes et al. 2009). Finally, *fer2LCH* mutations dominantly enhanced *dp53*-induced cell death and established a role for iron and broader antioxidant regulation in PRC protection. The characterization of the iron-storage complex Ferritin in PRC viability is further developed in Chapters 4 and 5.

3.3 Experimental Procedures

3.3.1 Fly Stocks and Genetics

Flies were maintained at 25ºC and in a 12-hour light/dark cycle. Canton S (CS) was used as the wild type strain.

Figure 3.2 *dp53*-Induced PRC Death Modifier Genetic Screen. (A) The crossing scheme for the *dp53*-induced PRC modifier genetic screen. Fifteen female virgin flies expressing GFP and *dp53* under the control of *rh1* driver are crossed with five males with *P[lacZ]* mutation or wild-type. *dp53* induces progressive degeneration with approximately 50% loss of PRCs at 3 days post-eclosure. In this sensitized background, individual P-element mutations, *P[lacZ],* are dominantly screened for suppression or enhancement of the *dp53*-induced 50% PRC death. **(B-F)** panels represent images of PRCs visualized by GFP imaging. **(B)** Wild-type retina with normal six outer PRCs in each ommatidium. **(C)** *dp53* overexpression leads to 50% PRC death revealed by the loss of GFP-positive PRCs. P-element mutations in *fer2LCH* **(E)** dominantly enhance while *cyt-c-d* **(D)** and *ninaA* **(F)** mutations dominantly suppress 50% *dp53*-induced PRC death at day-3 post-eclosure. *Images B-F, courtesy of Cesar Mendes.*

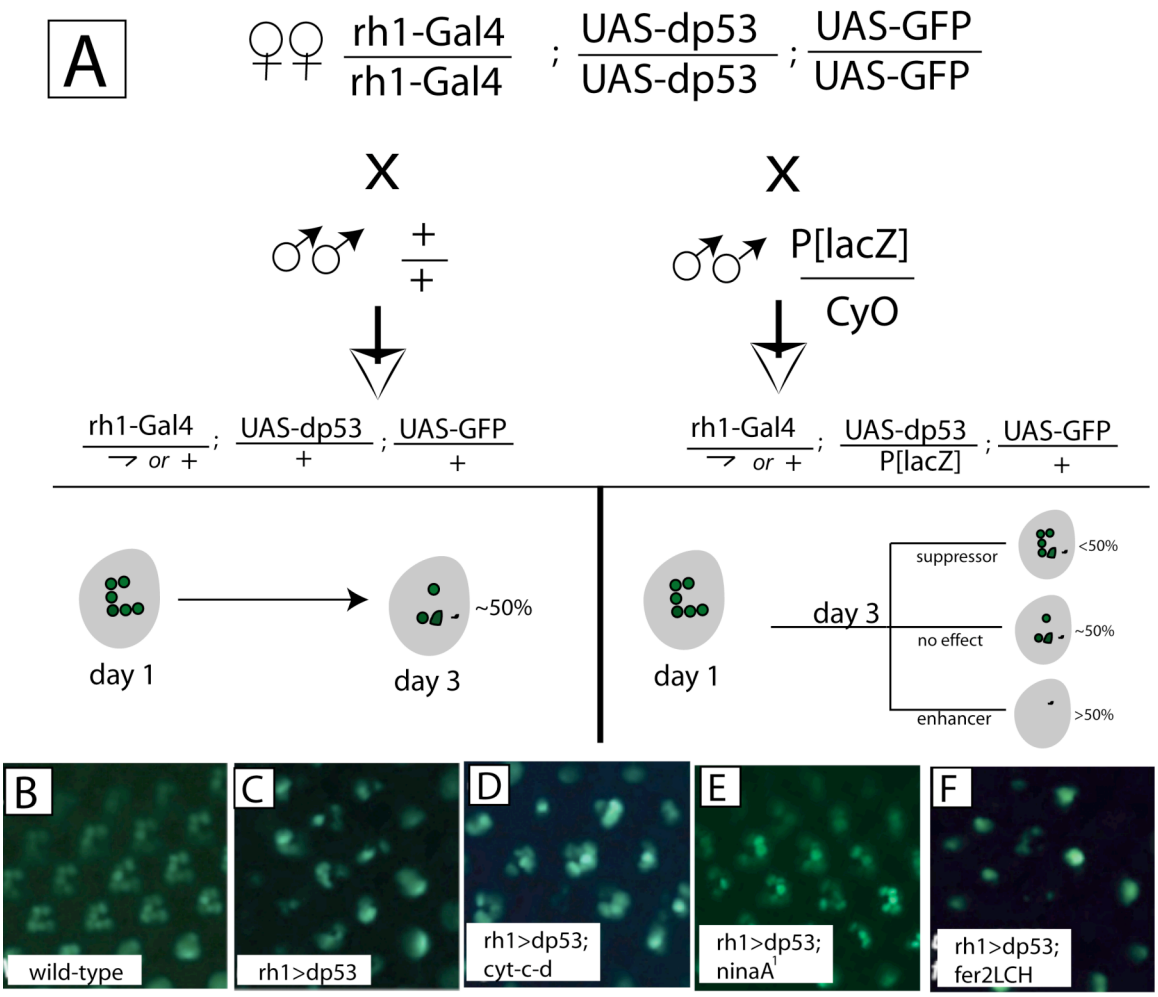

Figure 3.2 *dp53*-Induced PRC Death Modifier Genetic Screen

Table 3.2 Dominant Modifiers of *dp53*- and *reaper*-Induced PRC Death. P[LacZ] mutations (with *lacZ* expression in PRCs) were screened for a dominant effect on *dp53*-induced PRC death at day-3 post-eclosure. Lines, which enhanced or suppressed *dp53*-induced PRC death, were subsequently screened in a *reaper*-induced PRC paradigm at day-1 post-eclosure. **+**, enhancement; **-**, suppression; **0**, no effect; **ND**, non-determined. Line labeled in violet represents *thor*, identified by inverse PCR (*Exp. Proc. 3.3.5*).

P-element #	Disrupted Gene	*Effect on rh1>dp53*	*Effect on rh1>rpr*
10944	*liliputian*	-	-
11053	*kekkon-1*	-	-
11062	*CG30497*	-	-
11200	*retained*	-	-
11336	*aats-val*	-	-
11356	*calmodulin*	-	-
11403	*smooth*	-	-
11494	*atg1*	-	-
11626	*tartan*	-	-
11633	*rpd3*	-	-
11681	*stat92E*	-	-
11743	*bitesize*	-	-
11763	*cyt-c-d*	-	-
11809	*lnx2*	-	ND
11812	*CG12113*	-	0
12287	*flap wing*	-	0
10095	*armadillo*	-	-
12141	*topoisomerase 1*	-	0
10180	*l(3)0499*	-	+
10481	*thor*	-	0
3530	*ninaA*	-	-
11073	*dve*	+	0
11053	*fer2LCH*	+	0
11062	*osa*	+	-
11512	*mpcp*	+	0
11585	*grappa*	+	0
11711	*center divider*	+	-
11729	*rolling pebbles*	+	0
11749	*vein*	+	-
10694	*unknown*	+	+
10331	*crumbs*	+	+
11681	*puckered*	+	+

For both PRC Enhancer-Trap and *dp53*-modifier screens, a collection of 1,250 P-element lines from the Bloomington Stock Center was used. These P-elements (P[Z]/P[lacW]) contain a *lacZ* gene, a marker gene ($rosy^+$ for P[Z] and w^+ for P[lacW]), a minimal Hsp70 minimal promoter, and a bacterial origin of replication (Fig. 3.1A).

For the PRC Recessive Screen, we used 456 FRT P-element lines established by the UCLA Undergraduate Research Consortium in Functional Genomics (UURCFG), a Howard Hughes Medical Institute-sponsored project led by the UCLA Banerjee laboratory (Chen et al., 2005). These lines are derived from P-elements on second and third chromosomes from the Bloomington and Szeged Stock Centers. The *mini-white* transgene in the P-elements usually confers yellow or orange eye color to adult *Drosophila* and these lighter colors were crucial to the identification and characterization of mosaic eyes by the UURCFG. Most of the Bloomington lines have sequence information on the flanking genomic region of each P-element insertion but a few have No Flanking Sequence Available (NFSA). Each individual line of the 456 P-element mutation collection was meiotically recombined onto an FRT-containing chromosome (*FRT40A* for *2L*, *FRT42D* for *2R*, *FRT80B* for 3L and FRT82B for 3R) by an undergraduate student from the UURCFR at the Banerjee Laboratory. Out of the collection, we make note of FRT lines

FRT82, fer2LCH and *FRT42, fatp* recessive that displayed moderate and selective PRC degeneration and were subject to further analysis.

For the generation of homozygous *(P[w$^+$]/P[w$^+$])* mutant eyes in a heterozygous and viable animal, each *FRT, P[w$^+$]* of the UURCFR Collection was crossed with a corresponding *FRT* stock 'screen' lines which contains corresponding FRT motifs, the eye-specific source of FLP recombinase, *ey-flp*, and fluorescent (GFP/tdTomato) markers to visualize PRCs. GFP (green) marks all PRCs while the absence of tdTomato (red) marks clonal regions. As an example, a chromosomal 3R *FRT82, P[w+]* mutation was crossed to the corresponding *RE; UAS-GFP^{ninaC}; FRT82B, rh1-tdTomato^{ninaC}* (Fig. 3.4A) This crossing scheme also applies for mutations on 3L (FRT80B), 2L (FRT40A), and 2R (FRT42B). The four stock lines used are: **2L:** *RE; FRT40A, rh1-tdTomato^{ninaC}; UAS-GFP^{ninaC}* // **2R:** *RE; FRT42D, rh1-tdTomato^{ninaC}; UAS-GFP^{ninaC}* // **3L:** *RE; UAS-GFP^{ninaC}; FRT80A, rh1-tdTomato^{ninaC}* // **3R:** *RE; UAS-GFP^{ninaC}; FRT82B, rh1-tdTomato^{ninaC}.*

For the secondary screen, 203 (47%) lines displaying mild to severe PRC degeneration were subsequently screened with caspase inhibitor P35. To rapidly determine P35 rescue in a single cross, 'P35-screen' stocks were generated by meitotically recombining *rh1-GFP^{ninaC}* with *GMR-p35* stocks

on the second and third chromosomes. A first selection of potential recombinants was determined by selecting flies with stronger red-eye color, as a product of transgenic combination. For confirmation, *rh1-GFP^{ninaC}*, *GMR-p35* potential recombinants were crossed to *GMR-hid^{10}* and analyzed for both green fluorescent pseudopupil and rescue of the *hid*-ablated eye phenotype in the progeny. Recombinants on both second and third chromosome were kept and used to generate the following four lines for the secondary P35 screen: **2L:** *RE; FRT40A, rh1-tdTomato^{ninaC}; rh1-GFP^{ninaC}, GMR-p35* // **2R:** *RE; FRT42D, rh1-tdTomato^{ninaC}; rh1-GFP^{ninaC}, GMR-p35* // **3L:** *RE; rh1-GFP^{ninaC}, GMR-p35; FRT80A, rh1-tdTomato^{ninaC}* // **3R:** *RE; rh1-GFP^{ninaC}, GMR-p35; FRT80A, rh1-tdTomato^{ninaC}*.

For validation of the PRC recessive screen, a collection of eye-specific FRT-recombined loss-of-function mutations previously described to induce degeneration, polarity defects and ectopic D/V axes in the *Drosophila* retina were used. These include *FRT40A, Def(Sal)* (Barrio et al., 1999), *FRT82B, svp^{e22}* (Begemann et al., 1995; Mlodzik et al., 1990), *FRT80A, crumbs* (Pellikka et al., 2002), *FRT80A, iroC^{DMF3}* (Cavodeassi et al., 1999; Dominguez and de Celis, 1998) and *FRT82, pdsw* (Owusu-Ansah et al., 2008), For P35 rescue validation, we use two *diap1* alleles, *th^{5}* and *th$^{jc5.}$* The loss-of-function allele in *diap1* mutation, *FRT80, th^{5}*, bears a

substitution of a tryptophan into an early stop codon at position 273 (W273-stop) leading a premature truncation with the deletion of several amino acids at the C-terminus of Diap1(Goyal et al., 2000; Hay et al., 1995). *FRT80, th*^{jc58} is an enhancer trap *P[lacW]* insertion considered to be a null or lethal strong hypomorphic line, inserted in the 5' UTR of *diap1* close to transcription start site; it was obtained from Bloomington.

3.3.2 β−galactosidase and DAPI Staining of Cryosections

Fly heads were embedded in O.C.T Tissue Tek compound and sectioned in cryostat as described in *Chapter 2, Exp. Proc. 2.3.5*. Samples were fixed in 4% paraformaldehyde in coplin jar for 30 minutes and then washed three times (5-minute washes) in PBS 1X. The β-galactosidase activity was revealed by adding 97µl of prewarmed LacZ staining buffer (Na_2HPO_4, 7.2mM; NaH_2PO_4, 2.8mM; NaCl, 150mM; $MgCl_2$, 1mM; $K_3(Fe(CN)_6$, 2mM) mixed with 3µl 30X X-Gal solution (Chemicon, Millicore) to individual slides with tissue sections. Slides were then placed at 37ºC overnight. They were subsequently washed in PBS 1X and mounted in Vectashield (glycerol) DAPI medium. UV light microscope was used to look at DAPI staining of nuclei.

3.3.3 Live Fluorescent Imaging of PRCs

Please refer to *Chapter 2, Experimental Procedures, 2.3.3*

3.3.4 Design of the Genetic Screens

For the PRC Enhancer-Trap screen, 15 flies for each P-element line were cryosectioned and screened for expression in PRCs. Typically, 10 P-element lines were screened for each run. For the *dp53*-modifier-screen, virgin females carrying the *rh1* driver and the *dp53/GFP* transgenes under the control of UAS sequence were crossed to males carrying P-element recovered from the enhancer-trap screen. In order to minimize variability in the death phenotype due to age variations and simultaneously allow the harvest of a reasonable number of offspring, flies eclosing within a period of approximately six hours were collected for future analysis. Since half the PRCs are lost during days 3 to 5, this was the time point chosen to perform the analysis. Flies expressing GFP and *dp53* under the control of the *rh1* driver were compared with flies of the same genotype but with a dominant mutation caused by a P-element in a gene expressed in outer PRCs (Figure 3.2). For each screening session, a group of at least five flies were analyzed. Only after three independent experiments with similar results, an allele was

considered to be included as a modifier. Recovered *dp53* modifiers were then subsequently screened with *reaper* using the same strategy.

For the PRC recessive screen, the 456 FRT P-element line males were crossed to the FRT stock lines as described above. The direct progeny of these flies exhibited mutant clones of varying sizes revealed by the absence of red fluorescence. Flies were kept for 7 days in a vial, leaving a population of 1 to 7-day-old flies. We introduced this delay between fly eclosure and screening in order to evaluate the scope of PRC degeneration and capture mutants where PRCs degeneration occurs only after a few days. Ten to fifteen flies were screened and at least five images were taken for each line to determine the phenotype with confidence phenotype. Sample preparation and imaging are described in *Exp. Proc. 2.3.3*.

3.3.5 Inverse-PCR for Recovering Flanking Sequences of P-elements

Genomic DNA Extraction - 15 frozen flies (with genotype $Pz^{l(2)06270}$) were homogenized on ice using a cordless pestle pellet motor in a 1.5µl eppendorf tube with 200µl of Buffer A (100mM Tris, pH 7.5, 100mM EDTA, 100mM NaCl, 0.5% SDS). Homogenate was then incubated for 30 minutes at 65ºC. When cooled to room temperature, 400µl of Buffer B (5M KOAc, 6M LiCl) was added to the homogenate. After centrifiguation for 15 minutes at room temperature, supernatants were transferred to a fresh

eppendorf tube. Phenol-chloroform extractions (1:1, 500µl phenol-chloroform mixture) were repeated twice and DNA was precipitated by 0.7ml of isopropanol. After another round of centrifugation, the supernatant was discarded and the pellet was washed with 70% ethanol. The pellet was air-dried and dissolved in 75µl H_20 and stored at -20ºC for future use.

Digestion, Ligation and PCR – 10µl of genomic DNA was digested in 30µl restriction digest mix using 10 U (units) of AluI (New England BioLabs Buffer 2) and RsaI (New England Biolabs Buffer 1) for 3 hours and subsequently heated to 65ºC for 20 minutes. To 5µl of digested DNA, 353µl H_20, 40µl T4 DNA ligase buffer (10X) were added. Ligation was performed overnight at 16ºC using 2µl T4 DNA ligase. DNA was concentrated by ethanol precipitation for 1 hour at -20ºC. DNA was then subject to two rounds of PCR (polymerase chain reaction). **1º PCR**: 95ºC for 5', (95ºC for 30'', 60ºC for 1', 72ºC for 2')x40, 72ºC for 7') using 15µl DNA, 5nmol of dNTPs (0.ul of 10mM mix), 5 µl 10x Taq polymerase buffer, 5 U of Taq polymerase (1µl Promega Taq) and 20pmols of primers (2µl). The pair of primers are: TC-261 - 5'-GAGTCTGAGTGAGACAGCGATATGATTGTTG – 3' and TC-262 - 5'-CTTTCACTCACACTTATTGCAAGCATACGT-3'. **2º PCR** -95ºC for 5', (95ºC for 30'', 60ºC for 1', 72ºC for 2')x35, 72ºC for 7')) using 2µl PCR

product and primers in this second PRC reaction are: TC-263 – 5'-CCCTTAGCATGTCCGTGGGGTTTGAATTAAC – 3' and TC-264 – 5'-GATGTCTCTTGCCGACGGGACCACCTTATGT – 3'.

Sequence Analysis - DNA fragments were sequenced directly using primers TC-263 and TC-264. They confirmed a 512 base-pair fragment comprising the 5' UTR and coding region of *thor* by BLAST (Blast Local Alignment Search Tool, http://flybase.org/blast/). Protocol was kindly provided by *C. Arzu and C. Desplan*.

3.4 Results

3.4.1 Validation of the PRC Recessive Screen

We revisited loss-of-function mutants previously shown to have retinal cell death and differentiation phenotypes. This survey serves as a validation for the subsequent PRC recessive screen, which aims to find novel components required for PRC survival. In *spalt* complex mutant clones, we observe ectopic *rh1*-positive inner PRCs (Mollereau et al., 2001), and misoriented ommatidia (Fig. 3.3A) (Domingos et al., 2004). Loss-of-function mutations in orphan nuclear receptor *svp* leads to missing outer PRCs and alignment defects revealed by the loss of GFP and disorganized placement of remaining GFP-positive outer PRCs in mutant clones (Fig. -

Figure 3.3 Analysis of PRC Death and Differentiation Mutants using the Double-Fluorescence Visualization Method. For all panels, we show merge (1), red (2), and green channels (3). Merge reveals mosaicism with clonal and wild-type regions. *tdTomato* (red) labels wild-type and heterozygous PRCs (2). *GFP* (green) labels all PRCs and white line highlights boundary of mutant clonal regions (3). **(A1-A3)** *Def(Sal)* clones cause supernumerary PRCs (up to 7) to express GFP (*rh1*) (white arrows). **(B1-B3)** svp^{e22} clones display moderate PRC loss with ommatidia containing 3 or less GFP-positive outer PRC (white arrows). **(C1-C3)** $iroC^{DMF3}$ clones at the boundaries with wild-type tissue display ectopic Dorsal/Ventral axes highlighted by the white dashed lines. **(D1-D3)** *crumbs* clones display abnormal GFP-labeled PRC morphology with enlarged, elongated and smaller rhabdomeres (white arrows). **(E1-E3)** *pdsw* clones reveal empty regions with little (white arrows) to no GFP-positive PRCs remaining.

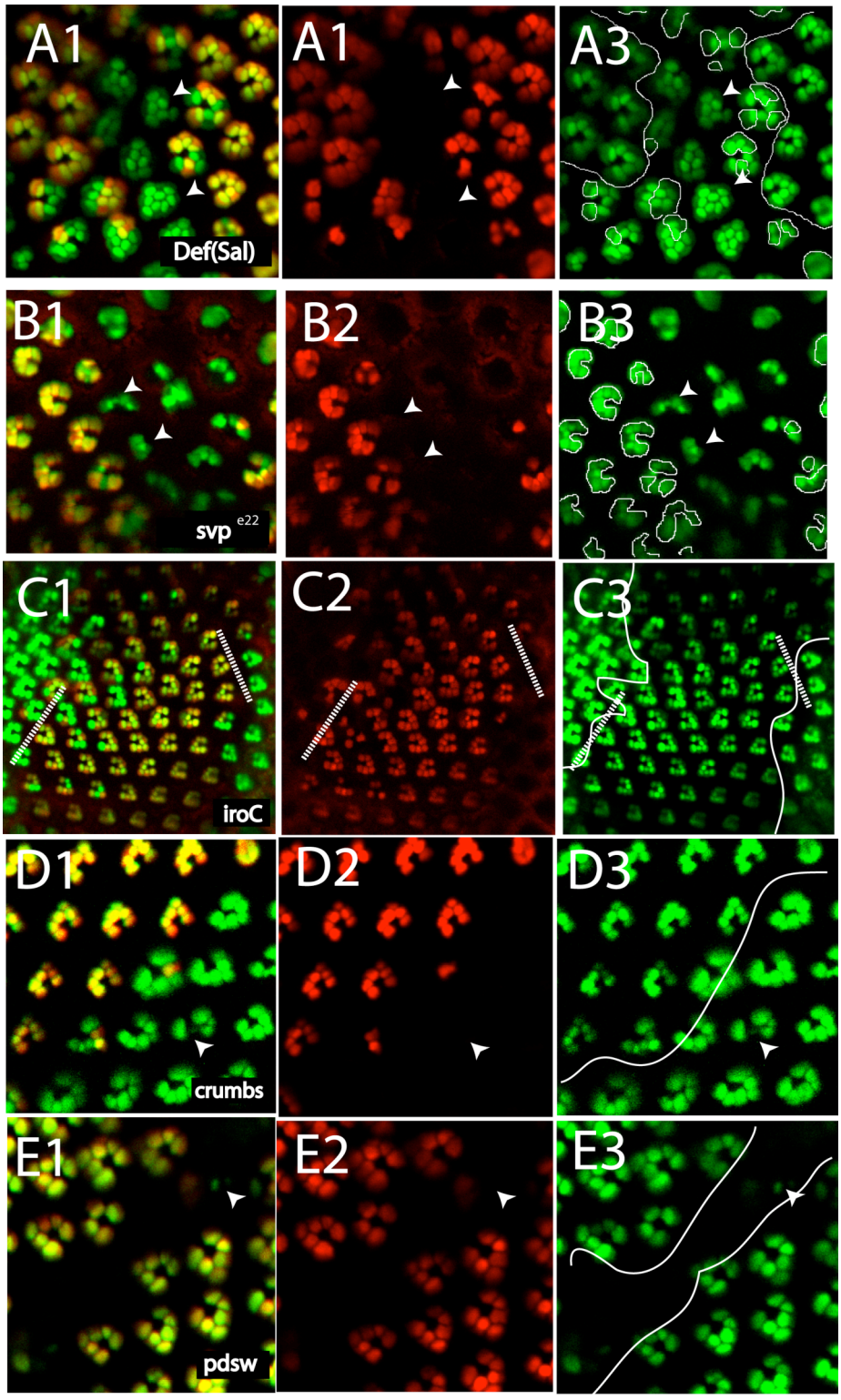

Figure 3.3 Analysis of PRC Death and Differentiation Mutants using the Double-Fluorescence Method

3.3B) (Miller et al., 2008), (Domingos et al., 2004). Mutant patches for the *Iroquois Compex iroC* exhibit ectopic D-V axes (Fig. 3.3C) (Cavodeassi et al., 1999). Mutant PRCs for transmembrane protein *crumbs* exhibit distinct rhabdomere morphology with either faint and small or enlarged GFP-positive cells (Fig. 3.3D) (Izaddoost et al., 2002). Finally, electron transport chain 1-encoded gene *pdsw* mutant clones do not contain any PRCs, revealed by the absence of GFP in mutant clones and ommatidial gaps in the adult retina (Fig. 3.3E) (Owusu-Ansah et al., 2008).

3.4.2 A Classification of PRC Phenotypes

We then screened for PRC phenotypes in the 456 available UUCFRG FRT-P-element lines. Each FRT P-element was crossed to flies harboring *GFP*, *tdTomato*, *eyFLP*, and the corresponding FRT site, all necessary components for the visualization and induction of mutant clones (Fig. 3.4A). The classification of PRC degeneration phenotypes proved to be challenging because of the frequent pleiotropic effects of a variety of recessive mutations on PRC integrity. For example, mutant tissue with severe PRC degeneration was often accompanied with ommatidial alignment and PRC morphology defects. Furthermore, we note that the previously described exterior eye phenotypes in the UUCFRG collection do not always reflect the

degeneration at the PRC resolution. In other words, a wild-type eye does not indicate that there is no PRC phenotype and vice-versa.

Of the 456 FRT P-element alleles screened, we isolated a collection of recessive mutations, which exhibited defects in PRC degeneration, differentiation, morphology as well as a combination of these effects (Fig. 3.4G). The 'no defects' class represents 128 mutations (29.4%) with no apparent PRC changes in number, morphology or survival. Mutations such as *lola-like (lolal)*, which results in a rough eye but exhibits no PRC loss, were also included in this class. In the 'minor defects' class, we regroup 103 mutations (23.4%), which display very rare PRC defects in mutant clones such as occasional missing PRCs or ommatidial misalignment. Typically these types of mutations did not reveal significant phenotypic consistency. In the 'clonal size defects' group, we catalog 27 mutations (6.3%), which generate adult mutant clones that are smaller or larger than corresponding wild-type (twinspot) clones. The 'moderate PRC degeneration' group includes 52 (11.9%) mutations, which exhibit moderate PRC loss with typically 1 to 2 missing PRCs in mutant ommatidia. The 'severe PRC degeneration' class includes 78 (17.9%) mutants, which lead to massive retinal degeneration, affecting both PRCs and ommatidial integrity. On occasion, some of these mutations triggered the complete loss of all PRCs

(ex: *pdsw*). Typically, these mutations caused exterior eye phenotypes (ex: rough or glossy). The class of 'polarity and alignment defects' regroups 26 (6.0%) mutations, which cause PRC alignment (ex: *iroC*) or ommatidial orientation defects; mutations in this class occasionally display PRC degeneration. Finally, the 'other' class includes the 21 (4.8%) mutations, which display PRC morphology, identity and expression alterations.

After the screening process and the classification, we note a high degree of pleiotropic effects of many mutations on PRC survival, morphology, and differentiation. However, a select number of mutations led to more specific alterations of PRCs; such mutations uncovered novel functions of their respective genes and corresponding pathways. The breakdown of PRC phenotypes is represented in Fig. 3.5A. We also provide the complete list of screen results and a selection of images/phenotypes in Appendix 6.3. In an effort to dissect pathways of PRC survival, we focused specifically on mutations that caused PRC degeneration phenotypes.

3.4.3 The PRC Degeneration Phenotypes

The three major classes of PRC degeneration are mild, moderate and severe PRC degeneration (Fig. 3.6A-C). We add a second layer of classification for the PRC degeneration phenotypes. These are the following criteria: alignment defects in the mosaic retina, effects of mutant degenera-

Figure 3.4 The PRC Recessive Screen. (A) The genetic crossing scheme for the PRC recessive screen on chromosomal arm 3R (FRT82). Fifteen virgin females expressing *GFP* and *tdTomato* in the outer PRCs and harboring the eye-specific FLP recombinase, *eyFLP*, are crossed to five males with FRT-recombined P-element males from UUCFRG. **(B)** Representations of a series of single mosaic ommatidia with mutant PRCs (green) and wild-type or heterozygous PRCs (red). Using the UUCFRG collection, the possible output phenotypes from the PRC recessive screen. The focus of the screen will be on mutants with PRC mild-to-severe degeneration (degenerating green PRCs, blue scale). The screen will also identify mutations, which cause polarity and alignment defects as well as mutations, which lead to distinct morphological defects (*abnormal shaped, sub-divided*) and (*rh1*) expression variations in the PRCs.

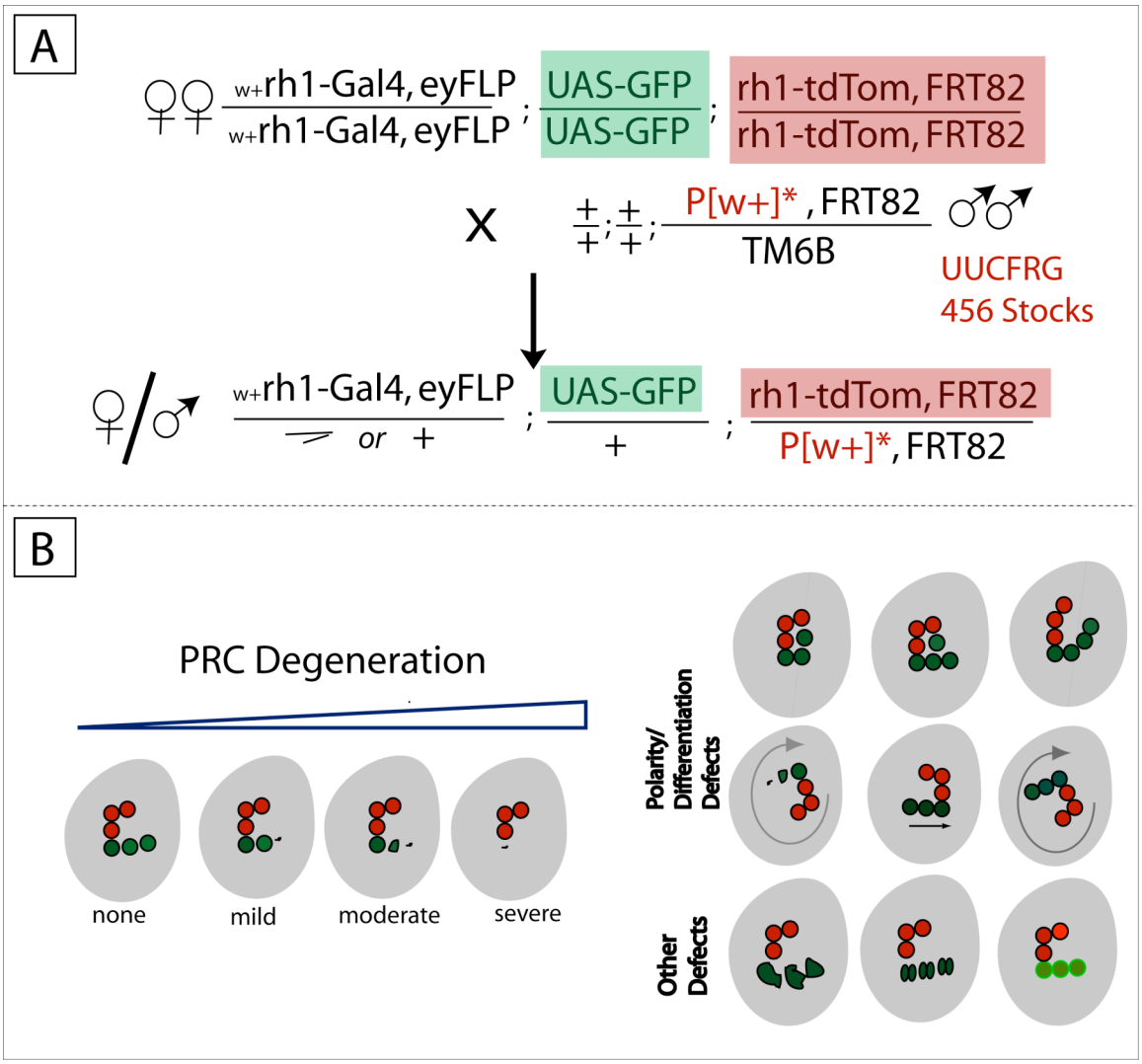

Figure 3.4 The PRC Recessive Screen

Figure 3.5 Summary of PRC Recessive Screen and PRC Degeneration Phenotypes. (A) Breakdown of PRC phenotypes in the PRC recessive into 5 categories with a focus on PRC degeneration: minor defects (23.7%), no defects (29.4%), clone size defects (6.3%), moderate PRC degeneration (11.9%), severe PRC degeneration (17.9%), polarity and alignment defects (6.0%) and other (4.8%). PRC degeneration phenotypes account for 47% (203) of the total 456 FRT UUCFRG collection. **(B)** PRC degeneration with no developmental defects (5.4%) represent recessive mutations with no exterior eye phenotype ('wild-type'). PRC degeneration mutants recovered by P35 include both partial and complete P35 rescue (14.3%).

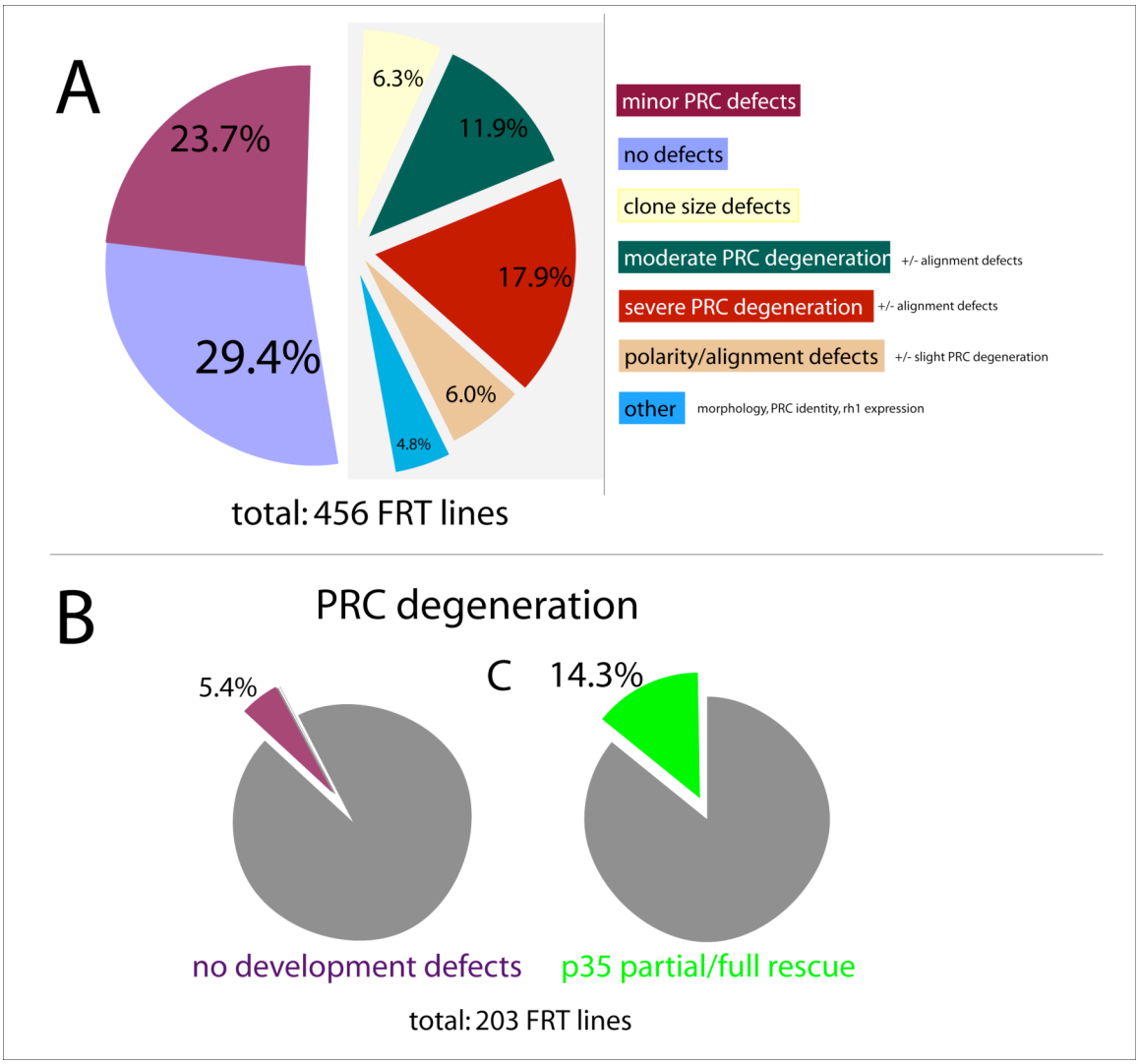

Figure 3.5 Summary of PRC Recessive Screen and PRC Degeneration Phenotypes

Figure 3.6 Classification of PRC Degeneration Phenotypes. For all panels, we show merge (**1**), red (**2**), and green channels (**3**). Merge reveals mosaicism with clonal and wild-type regions. *tdTomato* (red) labels wild-type and heterozygous PRCs (**2**). *GFP* (green) labels all PRCs (**3**). **(A)** *Mild PRC Degeneration* – NFSA mutant clones exhibit ommatidia with occasional loss of 1 or 2 PRCs (white arrows). **(B)** *Moderate PRC Degeneration*: *RFeSP* mutant ommatidia a range of degeneration with PRCs either unaffected, degenerated or missing. No apparent ommatidia disorganization or alignment defects are detected. **(C)** *Severe PRC Degeneration*: *Ebi* mutant clones display severe degeneration with few mutant PRCs remaining. **(D)** *squid* mutant clones display severe PRC degeneration accompanied with alignment defects. **(E)** *PRC Degeneration with Cell Non-Autonomous Effects*. *eiF4A* mutant clones display severe degenerating, affecting wild-type PRCs as well, as seen by degenerating or missing wild-type (red) PRCs. **(F)** *PRC Degeneration with Cell Lethality*: Mutant ND (non-determined) are non-existent. We observe occasional missing PRCs (white arrows), indicative of single-cell mutant clones with missing PRCs.

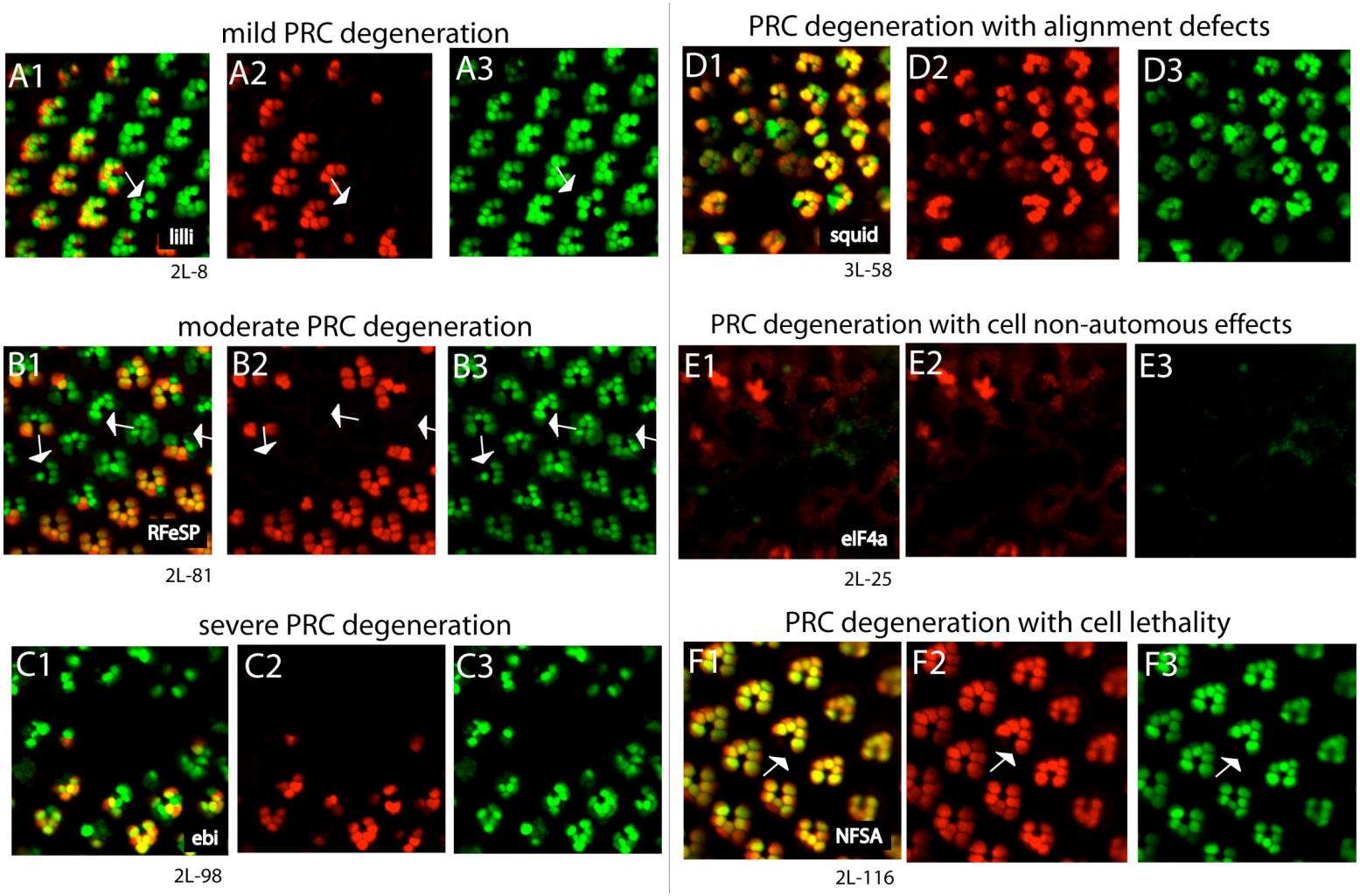

Figure 3.6 Classification of PRC Degeneration Phenotypes

Table 3.3 PRC Degeneration with No Developmental Defects. FRT P-element lines with PRC degeneration but no developmental defects, revealed by an exterior wild-type eye phenotype. Red represents genes involved in oxidative stress regulation. Yellow highlights gene *fer2LCH*, which exhibits a moderate PRC degeneration and is further described in subsequent chapters.

Table 3.3 PRC Degeneration with No Developmental Defects

Selective PRC degeneration with no development defects (wild-type eye)				
Screen Stock #	P-element #	Disrupted Gene	Gene Function	PRC Degeneration Phenotype
3L-23	12096	mitochondrial Ribosomal Protein S34	*Component for the protein synthesis/Ribosomal activity within the mitochondrial*	*high degeneration/polarity defects*
3R-68	11483	fer2LCH	*Detoxification and storage of iron/antioxidant*	*moderate PRC degeneration, especially in mosaic ommatidia*
2L-13	10446	rab-protein 6	*Protein quality control, vesicule trafficking*	*missing PRCs (but no rough eye), sometimes inner PRCs missing*
2L-29	10539	threonyl-tRNA-synthetase	*Threonyl-tRNA-synthetase*	*massive PRC degeneration, enlarged, smaller rhabdomeres/missing PRCs, no real polarity defects, wild-type eye (very interesting)*
2L-50	10673	CG9523	*N/A*	*slight PRC degeneration*
2L-71	10988	fatty acid (long chain transport chain)	*Metabolism/carrier of very long chains of fatty acids*	*deformed, flattened rhabdomeres and moderate PRC degeneration. Age-dependent.*
2L-81	11048	rieske iron sulfur protein	*iron sulfur protein part of the mitochondrial oxidative phosphorylation systems*	*PRCs are deformed, enlarged and occasionally missing but moderate PRC degeneration.*
2L-121	12809	lethal (2) 35Di	*Mitochondrial electron transport*	*moderate PRC dgeenration - frequently missing PRCs - GFP sometimes brighter in mutant clones*
2R-63	10677	ribonuclease H1	*Ribonuclease activity*	*moderate (age-dependent?) PRC degeneration*
2L-162	14898	vasa	*RNA helicase activity*	*missing PRCs, especially in mosaic ommatidia*
2R-157	13519	tim10	*Translocase of inner mitochondria membrane*	*(age-dependent) slight PRC degeneration/no polarity defects*

-tive tissue on neighboring wild-type PRCs, mutant clonal size and effects of mutant tissue on the exterior eye surface.

In the first group, we note that severe PRC degeneration also result in alignment defects and misaligned ommatidia. For example, RNA-binding protein *squid* triggers severe retinal degeneration and gross alignment defects (Fig. 3.6D). In the second group, mutations in genes such as *eukaryotic initiation factor 4A (eiF4A)* induce PRC degeneration accompanied by 'cell-autonomous effects'. This is revealed by a collateral wild-type PRC degeneration (Fig. 3.6E). The third group represents PRC degeneration accompanied with cell lethality, as seen in NFSA (2L-12) mutants.

Finally, the last group highlights 'selective' PRC degeneration mutations 'without any developmental defects' (Table 3.3, Fig. 3.5C). These mutations affect specifically late-staged PRC survival leaving surrounding IOCs unaltered and resulting in morphologically normal (wild-type) retinas. Among such PRC-specific mutations, we find enrichment (6 out of 10) in redox-related components such as mitochondrial, iron-regulated and antioxidant genes, all of which are involved in preventing the accumulation of oxidative-related stress and oxidative-related cellular damage. For example, mutation in the mitochondrial gene *Rieske iron sulfur protein*

(RFeSP) triggers moderate PRC degeneration (Fig. 3.6B). Similarly, mutation in iron-storage Ferritin subunit *fer2LCH* caused occasional PRC loss, more pronounced in mosaic ommatidia (Fig. 3.8J).

3.4.4 Caspase Inhibitor P35 Rescues Clonal Size and PRC Degeneration in *diap1* Mutant Clones

The secondary screen consisted of overexpressing viral caspase inhibitor P35 in candidates to determine the caspase-dependent component of PRC degeneration phenotypes. As proof of principle for the P35 secondary screen, we first characterized the *diap1* loss-of-function PRC degeneration phenotype and P35 rescue. Previous studies have established that *diap1* mutant clones in the developing eye disc are 'cell lethal' because of 'uninhibited' caspase activation (Ryoo et al., 2004).

Loss-of-function PRC clones of *diap1* (th^5) did not survive to adulthood. Mosaic retinas for th^5 display wild-type and heterozygous PRCs with no visible mutant PRC clones. Nevertheless, we occasionally detect individual missing PRCs (Fig. 3.7A), a feature indicative of PRC loss in single-cell mutant clones. On the other hand, retinas mutant for the strong hypomorphic mutation th^{jc58} tended to exhibit small clones and PRCs revealed frequently degenerative rhabdomere, indicated by smaller rhabdomere morphologies (Fig. 3.7C).

Figure 3.7 P35 Rescues Clonal Size and PRC Degeneration in *diap1* Mutants. For all *diap1* mosaic retina panels, we show merge (**1**), red (**2**), and green channels (**3**). Merge reveals mosaicism with clonal and wild-type regions. *tdTomato* (red) labels wild-type and heterozygous PRCs (2). *GFP* (green) labels all PRCs (3) and white line outlines the border of the mutant clones (absence of red). **(A)** Loss-of-function th^{5} mutant clones are small to non-existent (cell-lethal) and exhibit PRC loss (white arrows). **(B)** P35 overexpression in th^{5} loss-of-function mosaic retina leads to an adult retina with an increased mutant clonal size (white border outline) and no apparent PRC loss. **(C)** Strong hypomorph th^{J5C8} mutant clones are also small and tend to be in mosaic ommatidia. Mutants PRCs are viable but occasionally smaller and degenerative (white border outline). **(D)** Similarly as in panel B, th^{J5C8} mutant clones are larger and exhibit no signs of PRC degeneration with the expression of P35 (white border outline).

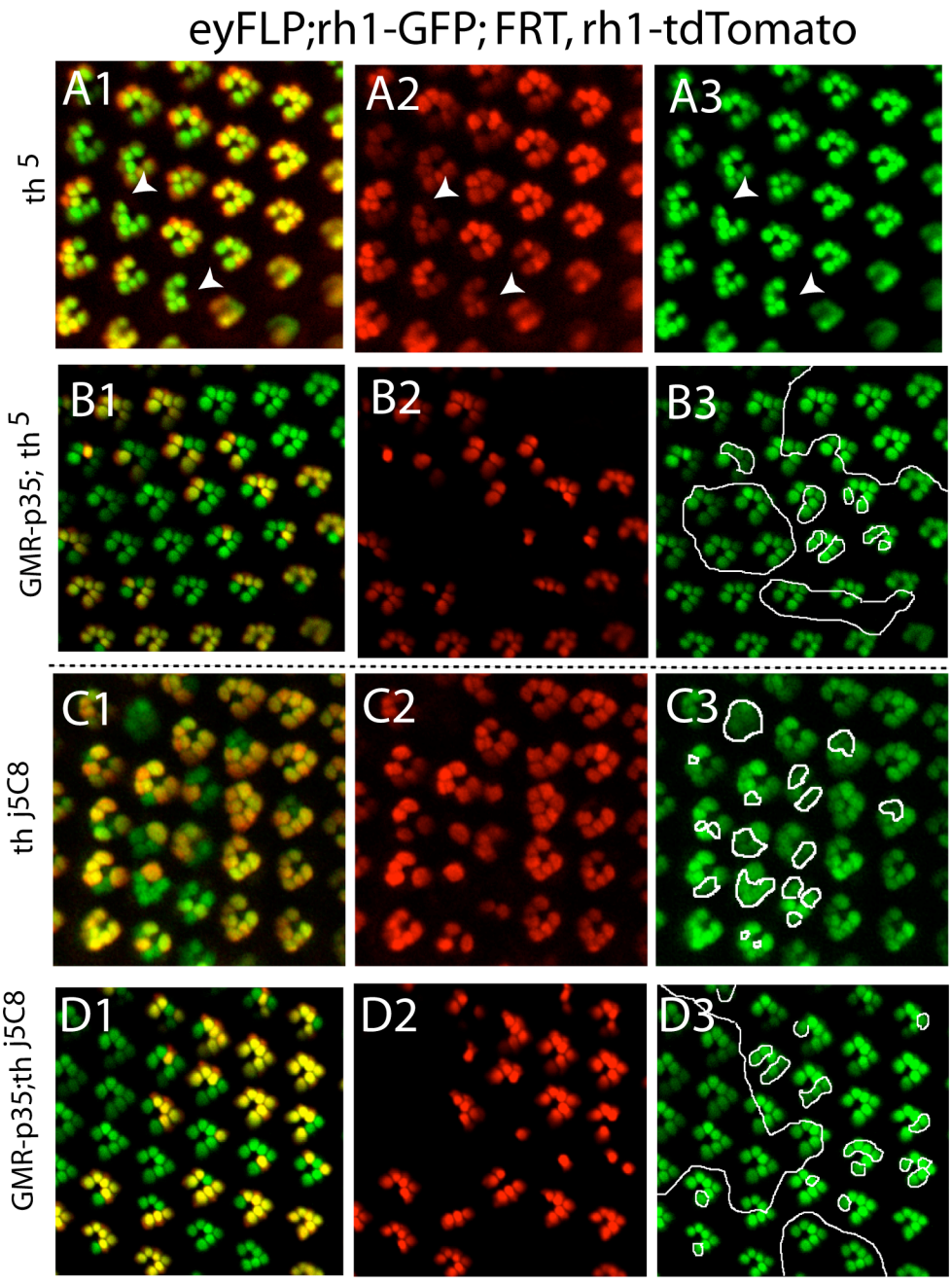

Figure 3.7 P35 Rescues Clonal Size and PRC Degeneration in *diap1* Mutants

The expression of P35 resulted in large mutant clonal patches comparable in size to twin-spot wild-type tissue and no detectable PRC degeneration in both th^{5} and th^{jc58} mosaic retinas (Fig. 3.7B,D). Hence, the *diap1* mutant analysis provided us with a framework to find novel mutations, which are similarly rescued by P35. We note that the previously described cell differentiation and death mutants, such as *svp*, *sens*, *flamingo* and *pdsw*, previously shown to have missing PRC phenotypes, did not present any detectable rescue by P35 (data not shown).

3.4.5 Recovery of Caspase-Dependent PRC Degeneration Phenotypes

Of the 120 lines with PRC degeneration tested (of the 200 PRC degeneration phenotypes, Fig. 3.8A), 29 of them presented either a partial or a complete rescue with P35. Similarly as *diap1* clones, CG8165 (unknown gene) has single-cell clones with missing PRCs (Fig. 3.8B). P35 overexpression simultaneously rescued both the size and PRC degeneration in these clones (Fig. 3.8C).

Mutations in the lipid phosphate phosphatases (LPPs), *wunen* (*wun*) and *wunen2* (*wun2*) were also rescued by P35. Moderate PRC degeneration in *wun* mutants was fully rescued by P35. *wun2* mutants revealed one missing PRC per ommatidia (Fig. 3.8H) in the absence of P35. With P35, only 5% to 10% of the mutant ommatidia displayed missing PRCs (Fig.

3.8H). Along with *wun2*, we identified 6 other mutants with P35 partial suppression of PRC degeneration. Two examples are the putative transcription factor *ken and barbie (ken)* and ribosomal protein *overgrown hematopoetic organs at 23B (oho23B)*. *ken* exhibits PRC degeneration and enlarged rhabdomeres when mutated (Fig. 3.8D). Surprisingly, P35 rescues PRC degeneration but mutant PRCs still exhibit abnormal rhabdomere morphology (Fig. 3.8E). *oho23B* causes both PRC degeneration and alignment defects. Intriguingly, P35 expressions restored ommatidial alignment, by presumably rescuing IOCs, but mutant clones still exhibited PRC degeneration and loss (data not shown).

We highlight two other distinct phenotypes rescued by P35. *fatp* mutations exhibited a progressive and late PRC degeneration. At day 1, *fatp* mutants typically exhibit 1 missing PRCs. This initial degeneration enhances with age from day 1 to day 14 with over 40% PRC loss between day 4 and day 8 interval (Fig. 3.8F). The progressive PRC degeneration is completely rescued by P35 (Fig. 3.8G). *fer2LCH* mutant retinas also exhibit moderate (1-2 missing PRC per mutant ommatidia) yet non-progressive PRC degeneration, prevalent in mosaic ommatidia and fully rescued by P35.

In conclusion, of the 29 genes (Table 3.4), 18 were fully recovered and 11 were only partially recovered by P35. Five genes are involved in the

Figure 3.8 Caspase-Dependent PRC Degeneration Mutants. For panels **B-K**, we show the merge image with clonal and wild-type regions. *tdTomato* (red) labels wild-type and heterozygous PRCs. *GFP* (green) labels all PRCs. White line arrows point to ommatidia with missing PRCs. Panels **B-K** are represented as pairs of mosaic retinas with and without overexpression of *P35*. **(A)** The crossing scheme for the secondary P35 genetic screen to recover caspase-dependent PRC degeneration mutant on chromosomal arm 3R (FRT82). 120 of 203 lines with PRC degeneration phenotypes, isolated from the first PRC recessive screen, were subsequently screened for rescue with P35. **(B-C)** CG8165 mutant clones are non-existent. The occasional missing PRCs (white arrows) suggest PRC loss in single-cell mutant clones **(B)**. P35 overexpression leads to a mutant clone of size comparable to twin-spot and rescues PRC loss **(C)**. **(D-E)** *ken* mutant clones reveal ommatidia with enlarged PRC rhabdomere morphology and typically 3 missing PRCs. P35 overexpression rescues PRC loss but PRCs in mutant ommatidia still display abnormal elongated rhabdomere morphology. **(F-G)** *fatp* mutant clones without **(F)** and with P35 overexpression **(G)**. Hexagon, octagon and circle follow a mosaic ommatidia, a mutant ommatidia and a wild-type ommatidia respectively in panel **F**. Hexagon and circle follow complete mutant and wild-type ommatidia respectively in panel G. **(F1-F4)** *fatp* mutant clones display progressive degeneration with less than 10% PRC degeneration at day 1 **(F1)**, 30% PRC degeneration at day 4 **(F2)**, 40% PRC degeneration at day 7 (F3) and finally 60% PRC degeneration at day 14 **(F4)**. We note in octagon- and hexagon-outlined ommatidia, the presence of all mutant PRCs at day 1 (F1) and the complete absence of mutant PRCs at day 14 (F4). (G1-G4) Overexpression of P35 rescues progressive PRC loss in *fatp* mutant clones seen in panel **F**. No loss is seen highlighted mutant and wild-type ommatidia. (H-I) *wun2* mutant clones reveal missing ommatidia with 3 or more missing PRCs. Overexpression of P35 leads to a partial rescue of PRC loss resulting in a partial rescue with mutant ommatidia displaying on average 1 missing PRC. **(J-K)** *fer2LCH* mutant clones typically display a moderate PRC degeneration with on average 1 missing PRC in mutant ommatidia **(J)**. P35 overexpression fully rescues the moderate PRC degeneration. *Images D,E,F,G,H, I, courtesy of Simon Courobe and Pierre Dourlen.*

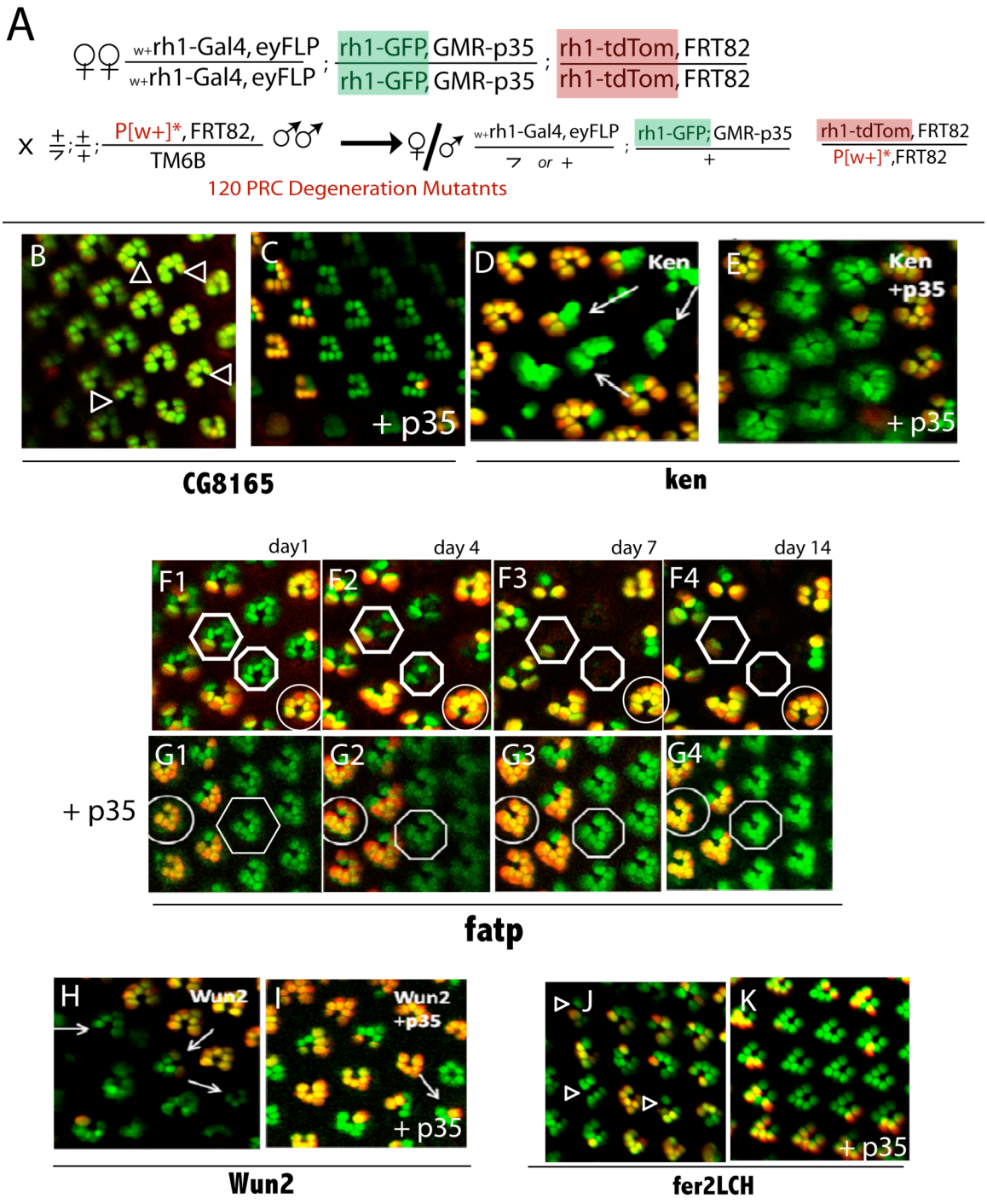

Figure 3.8 Caspase-Dependent PRC Degeneration Mutants

Table 3.4 PRC Degeneration Mutants Rescued by P35. FRT P-element lines which display PRC degeneration and are rescued, either partially or completely by P35 (29 genes). Red highlights **6** genes involved in oxidative stress regulation. Blue highlights **5** genes, which are part of the DGC complex. Yellow highlights mutants recovered by P35, which are shown in Fig. 3.8. Two first alleles of *diap1*, th^{5} and th^{Jc58}, serves as validation examples and are denoted as '**V**' lines. All mutations above the dashed line (**21**) exhibit a complete PRC rescue by P35 and ones below the dashed line (**8**) reveal only a partial rescue of retinal degeneration.

Table 3.4 PRC Degeneration Mutants Rescued by P35 – page 1/2

Rescue of PRC Degeneration With p35 - page 1/2				
Screen Stock #	P-element #	Disrupted Gene	PRC Degeneration Phenotype	p35 Rescue Phenotype
V	th5	diap1/thread	missing PRCs in very small clones	full rescue of PRCs and clone size (~ twinspots)
V	thJ5c8	diap1/thread	ocassionally degenerating PRCs/very small clones/mosaic ommatidia	full rescue of PRCs and clone size (~ twinspots)
3L-2	10017	sallimus	*slight PRC degeneration/polarity defects*	*full rescue of PRCs and polarity defects*
3L-6	10166	CG14821	*slight degeneration/polarity defects*	*full rescue of PRCs and polarity defects*
3R-16	10305	Daughters against dpp	*very minor PRC defects*	*full rescue of minor defects/PRCs*
3R-19	10320	Glutamate-cysteine ligase modifier subunit	*slight degeneration/polarity defects*	*full rescue of PRCs*
3R-39	12133	squid	*massive degeneration or very small rhabdomeres*	*full rescue of high PRC degeneration*
3R-52	12304	NFSA	*occasional missing cells*	*full rescue of PRCs*
3R-65	14488	CG8165	*missing PRCs in very small clones*	*full rescue of PRCs and clone size (~ twinspots)*
3R-68	11483	fer2LCH	*occasional missing PRCs and alignment defects. Defects especially in mosaic ommatidia*	*full rescue of PRCs*
2L-14	10448	U2 small nuclear riboprotein auxiliary factor 38	*frequent missing outer/inner PRCs especially in very big clones accompanied polarity defects. Small clones, only PR missing*	*full rescue of inner/outer PRCs*
2L-15	10451	turtle	*little defects/occasional missing PRCs but IOC mostly affected because misaligned/shifted ommatidia*	*full rescue of PRCs and alignment (IOCs)*
2L-36	10580	v(2)k05816	*from few missing PRCs to no defects.*	*full rescue of PRCs*
2L-46	10652	NG	*variable PRC degeneration (50% slight defects, 50% no defects)*	*full rescue of PRCs*
2L-47	10656	A kinase anchor protein 200	*minor PRC defects*	*full rescue of PRCs*
2L-54	10690	NG	*frequently missing PRCs*	*full rescue of PRCs*
2L-58	10838	Trehalose-6-phosphate synthase 1	*very few missing PRCs*	*full rescue of PRCs*

Table 3.4 PRC Degeneration Mutants Rescued by P35 – page 2/2

Rescue of PRC Degeneration With p35 - page 2/2				
Screen Stock #	P-element #	Disrupted Gene	PRC Degeneration Phenotype	p35 Rescue Phenotype
2L-71	10988	Fatty acid (long chain) transport protein	*age-dependent PRC degeneration - deformed rhabdomeres to missing PRCs*	*full rescue of PRCs*
2R-13	10420	ken and barbie	*deformed/enlarged/missing PRCs/slight polarity defects*	*no PRC degeneration but still deformed PRCs*
2R-39	10541	muscleblind	*frequently few missing PRCs, especially in big clones*	*full rescue of PRCs*
2R-116	11161	bancal	*very small (or no) clones with missing PRCs and polarity defects*	*full rescue of PRCs and clone size (~ twinspots)*
2R-122	11225	fused lobes	*occasional missing PRCs with slight alignment/polarity defects*	*full rescue of PRCs and alignment/IOC*
2R-139	12347	mastermind	*deformed rhabdomeres but little PRC degeneration/slight polarity defects*	*full rescue of PRC morphology and loss*
2R-140	12382	wunen	*PRC degeneration/cell non-autonomous defects but sometimes no PRC degeneration - heterogenous*	*full rescue of PRCs*
3L-11	10186	fringe connection	*deformed/shrunken/elongated/missing rhabdomeres*	*PRC degeneration is reduced and rhabdomeres appear normal*
2L-1	10357	NFSA	*deformed rhabdomeres but no PRC loss*	*rhabdomeres appear normal*
2L-11	10435	no mitochondrial derivative	*massive degeneration, wild-type seems to be affected (cell non-autonomous?)*	*PRC degeneration is reduced wild-type PRs are not affected*
2L-17	10457	overgrown hematopoietic organs at 23B	*degeneration and rough eye but curiously very little PRC degeneration. Degeneration affects pigment/IOCs. Misalignment*	*rescue of IOCs/no mislaignment*
2L-29	10539	Threonyl-tRNA synthetase	*massive PRC degeneration, enlarged, smaller rhabdomeres/missing PRCs, no real polarity defects, wild-type eye (very interesting)*	*PRC degeneration is reduced*
2R-90	11015	wunen-2	*masive degeneration and polarity defects*	*PRC degeneration is reduced*
2R-101	11077	Kinesin heavy chain	*deformed (a few missing) rhabdomeres*	*no PRC degeneration but still deformed PRCs*

Dystroglycan-Dystrophin Complex (DDC) important in establishing a link between the cytoskeleton and the extracellular matrix, and four genes have functions in oxidative stress pathways.

3.5 Discussion

We conduced two successive screens to first isolate PRC degeneration phenotypes and second, to probe the ability of P35 to rescue PRC loss. We relied on the UURCFG collection of 456 FRT-recombined P-element lethal lines. These lines were initially described by UURCFG based on the exterior eye phenotypes; adult mosaic retinas were categorized as rough, glossy, cell lethal and wild-type using light microscopy and EM analysis. Using our double-fluorescent PRC imaging method, we were able to obtain a finer PRC resolution of the mutant degeneration phenotypes and overexpress transgenes in clones, not feasible using the standard retinal plastic sections because of the presence of red pigmentation in both mutant and wild-type clones.

3.5.1 Assessing the Cell Death Contribution in PRC Phenotypes

Overall, our PRC screens helped separate PRC death from a multitude of developmental defects. In *svp*, *seven-in-absentia (sina)* and *sens* mutant retinas, we detected missing outer PRCs. However, P35 did not rescue the

missing PRCs, confirming that these mutations are involved in differentiation and observed PRC loss is due to the mis-specification of PRCs rather than ectopic cell death of existing PRCs.

Mutations in *mastermind* displayed both supernumerary (up to 7) PRCs when mutated and moderate PRC loss. Moderate PRC degeneration in one of the alleles of *mastermind* was rescued by the P35 overexpression, but supernumerary PRCs were still detected. *mastermind* is a putative activator of Notch signaling, which stands as a point of convergence between cell death and differentiation in pupal retinal development (Cagan and Ready, 1989a; Petcherski and Kimble, 2000). Hence, caspase inhibitor P35 was seemingly able to dissociate Notch-dependent apoptosis from Notch-dependent differentiation in PRCs.

We also identified mutations, which triggers both PRC morphology defects and degeneration. In *ken* mutants, P35 rescued PRC degeneration but mutant PRCs still displayed abnormal morphology. Based on previous studies, *ken* has already been indirectly linked to cell death. *ken* mutants have rotated genitalia in adult flies, a stereotypical phenotype of apoptosis present in loss-of-function mutations such as *hid*, *dronc* and flies that express P35 (Lukacsovich et al., 2003; Macias et al., 2004; White et al., 1994). Ken has been shown to be a positive regulator of JAK/STAT pathway

(Hombria and Sotillos, 2006). Intriguingly, a recent study has suggested that *Drosophila* STAT, STAT92E, is a positive regulator of Diap1 and protects against radiation-induced apoptosis (Betz et al., 2008). Based on previous work, we speculate that *ken* mutants may repress JAK-induced STAT92E activation and Diap1 inhibition, leading to caspase-dependent apoptosis. Further analysis is required to understand the dual role of Ken and the broader JAK/STAT pathway in regulating both PRC survival and morphology.

We then searched for mutations, which specifically led to late-staged and selective PRC death without an external eye phenotype. Typically, morphological and alignment defects in the adult retina are caused by early loss of IOCs, cone cells and subsequent ommatidial integrity. Strengthening this argument, we note that the overexpression of a pro-apoptotic stimulus with the early eye promoter GMR leads to massive ommatidial disarray and a resulting rough ablated eye (White et al., 1996). On the other hand, the overexpression of same pro-apoptotic stimulus using the late-eye PRC-specific promoter *rh1* induces PRC degeneration without an exterior eye phenotype. The recovery of 10 mutations (4.3%) with selective PRC degeneration phenotypes provided further insight into survival mechanisms

specific to PRCs. In this category, we note again a significant enrichment (6 out of 29) in genes involved in oxidative stress regulation.

3.5.2 Oxidative Stress and Caspases in PRC Death

The mechanisms underlying neuronal cell death in neurodegenerative diseases remains not well-understood. Currents concepts of this process suggest the involvement of free radical species and oxidative stress. Biochemical markers of oxidative stress, such as lipid peroxidation, protein carbonylation, depleted glutathione levels and altered iron metabolisms are prevalent in neurodegenerative diseases. Moreover, the presence of these cellular alterations in early-stages of neurodegeneration models, suggest that they may be early markers pathology and may provide a clue to the primary causes of oxidative-stress induced neuronal cell death (Andersen, 2004).

The results from our PRC-specific screens highlight the importance of ROS in neuronal dysfunction and further implicate caspases as mediators of ROS-induced PRC death. Indeed, among the PRC degeneration phenotypes rescued by P35, we detect a significant over-representation of genes involved in the protection against oxidative stress. *Drosophila no mitochondrial derivative* (*nmd*) gene is required for proper mitochondrial aggregation and integrity (Hales, 2004). Mutations of *nmd* trigger mitochondrial alterations, which in turn generates mitochondrial-derived

free radicals. *Drosophila* Tretahalose-6-phosphase Synthase 1 (Dtps1) has been shown in several organisms, notably *S. cerevisae*, to cause the accumulation large quantities of the antioxidant trehalose, known to protect both proteins and lipids from oxidation. Not surprisingly, mutations in *tps1* lead to an acute sensitivity to oxidative stress (Pereira et al., 2001). Glutamate-cysteine ligase modifier subunit (GCLM) is important for the augmentation of glutathione known as a primary intracellular antioxidant to protect cells from oxygen radicals. The GLCM knockout mice exhibits a 80% to 90% reduction in glutathione and increased sensitivity to oxidative stress (Yang et al., 2002). Fatp is a plasma membrane transporter for Very Long-Chain Fatty Acids (VLCFAs) and displays antioxidant capacities (Schaffer and Lodish, 1994). No mutations in human FATP or studies in *Drosophila* have been reported. However, we expect elevated VLCFAs, a hallmark feature of oxidative perioxisomal disorders, which triggers lipid peroxidation by enhancing superoxide anion generation (Dhaunsi et al., 2005). Finally, Fer2LCH is one of the subunits of the Ferritin complex, involved in iron sequestration and detoxification. The disruption of the iron-storage Ferritin complex triggers the release of ferrous iron, which participates in the generation of iron-induced oxidative stress (Arosio and Levi, 2002). Finally, we mention a recent study in *Drosophila* has also

shown that ROS-induced apoptosis caused by impairments in selenoproteins is also mediated by caspase-dependent pathways (Morey et al., 2003).

Whether ROS-inducing factors induce caspase-dependent or –independent pathways of apoptosis has been an issue of great debate. Our screen results shed light on this controversy. We reveal caspase-directed PRC death primarily occurs as a result of redox de-regulation. Indeed, mitochondrial alterations, glutathione depletion, and iron accumulation, caused by the above-mentioned mutations, trigger caspase-dependent PRC death. Mammalian neuronal studies have also suggested that caspases may be involved in such ROS-induced cell death paradigms. Glutathione depletion leads to caspase-3 activation and motor-neuron-like cell death in mouse *in vitro* and *in vivo* studies (Chi et al., 2007). Drugs decreasing mitochondrial membrane potential causes mitochondrial dysfunction and induces caspase-dependent apoptotic pathways in cultured cortical rat neurons (Cunha-Oliveira et al., 2006). Finally, iron chelators have been suggested to have neuro-protective effects by diminishing caspase-3 activation and neuronal cell death in brains of PD patients (Kaur et al., 2003; Xu et al., 2008).

While ROS insults frequently trigger caspase-dependent PRC death, we also isolated mutations that induce caspase-independent pathways of

PRC death. Indeed, *pdsw*, which encodes a subunit of the mitochondrial complex I (Owusu-Ansah et al., 2008), and mitochondrial ribosomal proteins (S34, L17, L4 – Appendix 6.3) elevate ROS levels resulting in severe PRC degeneration, not recovered by P35. Collectively, these findings corroborate with mammalian studies indicating that oxidative stress can induce both caspase-dependent and –independent apoptosis. We present two models for the dual effects exerted by ROS production. In the first model, we propose that only a type of free radicals trigger caspase-dependent apoptosis. It is indeed well established that free radicals have different effects on DNA. Oxidative damage to DNA is solely the result of interaction of DNA with hydroxyl radicals specifically; superoxide and hydrogen peroxide are normally not reactive towards DNA. In turn, oxidative DNA damage has been shown to selectively activate caspase-dependent apoptosis (Albright et al., 2003; Morey et al., 2003). Hence, we infer that the isolated redox-related mutations, which trigger caspase-dependent PRC degeneration, may share a common and specific oxidant response. In the second model, we propose that the levels of ROS dictate the choice between caspase-dependent versus –independent pathways of apoptosis. Previous results show that low concentrations of H_20_2 ranging from 10μM to 100μM induce predominantly apoptosis whereas high concentrations of H_20_2 ranging

1mM to 10mM induced predominantly necrosis in mammalian cells (Teramoto et al., 1999). Based on this second model, the severity of PRC degeneration may be a good indicator for both the degree of ROS generation and the dependence to the caspase-dependent machinery. In our results, we observe that redox gene mutations with moderate PRC death often result in caspase-dependent cell death. Conversely, greater redox perturbations accompanied with severe PRC degeneration tend to not be suppressed by caspase inhibitor P35.

In total, the low frequency of P35 rescue (14.3%) strongly implies that PRCs preferentially undergo caspase-independent pathways of cell death. The vast mammalian literature on neurodegeneration periodically also highlights the prominence of caspase-independent pathways in diseases. Indeed, other proteases besides caspases such as serine proteases, cathepsins and calpains have been shown to be involved in neuronal cell death in neurodegenerative conditions (Broker et al., 2005).

In conclusion, despite the pleiotropic effects of mutants on PRC survival, we successfully identified a select number of mutant phenotypes rescued by P35. These mutations provide insights into novel pathways regulating caspase activation and survival of PRCs. We particularly focused on the Ferritin subunit *fer2LCH* mutant phenotype for our future work.

Based on the wealth of knowledge on the iron-storage complex Ferritin across lineages, we infer that iron accumulation occurs in *fer2LCH* mutations and preferentially sensitizes late-staged PRCs to caspase activation and apoptosis. *fer2LCH* mutations provide an ideal model to further study the interplay between iron, oxidative stress and apoptosis, still not well understood.

4 LACK OF FERRITIN CAUSES PHOTORECEPTOR CELL DEATH DURING DEVELOPMENT

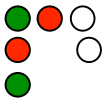

4.1 Summary

While iron is essential for many biological processes, excess labile amounts may be harmful for many tissues, notably the brain and the retina. Based on the results of the PRC recessive screen in Chapter 3, we show that the loss-of-function mutations in the *fer2LCH* subunit of the iron-storage Ferritin complex causes moderate PRC death which is rescued by caspase inhibitor P35. In this chapter, we further characterize the role of Ferritin in the retina and reveal an expression in PRCs. Furthermore *ferritin* mutant retinas trigger caspase activation and an increase in free iron in late pupal retinal stages. They also exhibit higher levels of oxidative stress. We suggest that Ferritin-dependent iron regulation plays a protective role in developing PRCs. With the Ferritin characterization in PRCs, we develop novel fluorescent-based transgenic sensors to measure oxidative stress and labile iron *in vivo*.

4.2 Introduction

The genetic screen results of Chapter 3 suggest that PRCs are especially vulnerable to oxidative stress. This is implied by the recovery of a battery of genes involved in oxidative metabolism, mitochondrial function and the intracellular antioxidant network, which when mutated, trigger

selective PRC degeneration. Of particular interest, *fer2LCH* loss-of-function mutations were shown to induce moderate PRC degeneration in a caspase-mediated manner. We now focus our attention on the characterization of the Ferritin complex in *Drosophila* PRCs.

4.2.1 Iron Management and Regulation

Iron is an essential co-factor in heme and nonheme-containing enzymes. The presence of iron is necessary for carrying out numerous vital biological reactions, but because of its highly reactive nature, iron is toxic if its concentrations are not tightly regulated intracellularly. The divalent state of iron (ferrous iron) makes it highly toxic, as it can rapidly react with hydrogen peroxide and molecular oxygen to produce free radicals (Curtin et al., 2002; Torti and Torti, 2002). Free radical formation can promote lipid peroxidation, DNA strand breaks, and modifications or degradation of biomolecules, eventually leading to cell death (Fig. 1.5).

Cells have evolved a sophisticated mechanism consisting of an array of proteins, notably Ferritin, that regulate the amount of free iron in cells by modulating its uptake, storage and export. Together, these proteins provide a state of cellular equilibrium, whereby iron is readily available for all metabolic functions but sheltered from taking part in cytotoxic ROS-generating reactions (Arosio and Levi, 2002; Torti and Torti, 2002).

4.2.2 Ferritin: The Primary Iron-Storage Complex

Ferritin has two main functions: intracellular iron storage and detoxification of iron. Ferritin complexes are found in nearly all bacteria and plants as ubiquitous, symmetrical 24-subunit heteropolymer holospherical, which can store up to 2,000 atoms of iron (Harrison and Arosio, 1996).

Across all lineages, they are composed of stereotypical heavy and light chain subunits. Iron is converted from a reactive ferrous state to non-reactive ferric state via the ferroxidase enzymatic activity integral to the Ferritin Heavy Chain (FHC) subunit. The Ferritin Light Chain (FLC) is important for the nucleation of the iron into the complex (Boyd et al., 1984; Chou et al., 1986; Hentze et al., 1986).

Mammalian Ferritins are preferentially localized in the cytosol. However, depending on tissue type, the ratio of heavy chain and light chains subunits varies in mammalian systems. Furthermore, vertebrate Ferritins exist in many variants and have specialized to cope with various tissue-specific functions. For example, mammalian iso-Ferritin variants exist in the liver, spleen, heart, lung, and brain (Fisher et al., 2007). In agreement with the phenotype in PRCs from Chapter 3, we also make note of a mammalian Ferritin sub-type localized in the retina, preferentially in rod bipolar cells and photoreceptors (Hahn et al., 2004a; Tawara, 1986).

4.2.3 The *Drosophila* Ferritin Complex

Insight into Ferritin function and regulation has come from studies in insects. The *Drosophila* Ferritin complex is only encoded by two genes, *fer2LCH* and *ferritin heavy chain homologue* (*fer1HCH*) closely clustered on position 99F of the third chromosome, and their transcriptional regulation appears to be co-regulated (Dunkov and Georgieva, 1999). The lack of redundancy and juxtaposition of both chains on the same locus makes the *Drosophila* system an attractive system to dissect Ferritin regulation and function.

Insect Ferritin molecular distinctively maintain a 1:1 ratio of the two subunits ensuring the presence of 12 heavy and 12 light chains in the symmetrical 24-subunit complex (Hamburger et al., 2005). Unlike in mammals, insect Ferritins have been shown to be predominantly present in intracellular-membrane compartments of the vacuolar system. The secretory nature of the fly Ferritin complex has led to suggestions that it is involved in systemic iron trafficking between tissues through the hemolymph. A third mitochondrial ferritin (Fer3HCH) also exists in *Drosophila* and when overexpressed is shown to protect mitochondria from iron overload (Lind et al., 2006).

Studies on *Drosophila* iron metabolism have shed light on the importance of iron management in the antioxidant defense system and in neuronal protection. *Drosophila* Fer1HCH has been suggested to play a role to combat oxidative stress. Its expression increases when flies are fed the oxidative agent paraquat, a transcriptional control solely mediated by the JNK pathway (Wang et al., 2003).The involvement of iron overload has also been implicated in *Drosophila* models of neurodegeneration. The suppression of the *Drosophila frataxin homologue* (*dfh*) by RNAi results in diminished activities of Ferritin, numerous heme and iron-sulfur-containing enzymes, and increased susceptibility to iron toxicity (Anderson et al., 2005).

4.2.4 Post-Transcriptional Cellular Iron Control: IRP-IRE Interaction

From insects to mammals, the post-transcriptional control of iron uptake, storage, and utilization is mediated by the interaction of iron-responsive elements (IREs) and iron regulatory proteins (IRPs). The IRE is a well-conserved RNA stem loop found in the UTRs of iron-regulated genes , first identified in human *ferritin* mRNA, and IRP is a cytosolic RNA-binding protein (Hentze et al., 1987; Rouault et al., 1988). When cellular iron levels are high, IRP binds and silences IRE-containing genes. When cellular iron levels are low, IRP relieves its inhibition of IRE-containing

genes, thereby promoting their expression to cope with high levels of iron. In addition to iron, the IRE/IRP regulatory system is modulated by hydrogen peroxide and nitric oxide revealing a link between oxidative stress and iron metabolism. Hence, the IRE-IRP system is a vital mechanism of cellular protection against genotoxic stress.

In mammalian cells, the iron-regulatory proteins are IRP1 and IRP2. IRP2 is the dominant iron sensor under normoxia, but IRP1 is the more ancient protein in evolutionary terms and has an additional function as a cytosolic aconitase (Haile, 1999; Meyron-Holtz et al., 2004). IRE sequences exist in a variety of mammalian genes. We note the presence of IRE motifs in the 5' UTRs of FLC and FHC as well as 3' UTR of the transferrin receptor (Goossen et al., 1990). More recently putative IRE-like sequences were found in the Parkinson's Alpha Synuclein (ASYN) transcript and the Amyloid Precursor Protein (APP), hinting to a causative role of iron regulation in neurodegenerative diseases (Cahill et al., 2008).

As in vertebrates, the IRE/IRP system functions in *Drosophila* (Missirlis et al., 2003; Rothenberger et al., 1990). IRP homologs, IRP-1A and IRP-1B, share 86% sequence similarity and are expressed in the fly, (Muckenthaler et al., 1998), although only IRP-1A has been shown to bind

to IREs from both *Drosophila* and mammals (Lind et al., 2006; Missirlis et al., 2007). Furthermore, ubiquitous and muscle-specific overexpression of IRP-1A, but not of IRP-1B, resulted in pre-adult lethality, underscoring the biochemical difference between the two proteins. Nevertheless, both IRP-1A and IRP-1B possess cytosolic aconitase activity. A functional IRE is present in the 5' UTR of the *fer1HCH* mRNA, but only in certain splice variants that are preferentially encoded under iron-limiting conditions (Georgieva et al., 1999; Lind et al., 1998). In contrast, no IRE is present in *fer2LCH* mRNA (Fig. 4.1A) (Georgieva, 2002).

The IRE-IRP regulatory system, IRE sequence, and IRPs are well conserved from insects to mammals (Casey et al., 1988). Not surprisingly, the system has been hijacked to study labile iron levels in the cell. A GFP-based system has been engineered in mammalian cells, whereby the Ferritin rat IRE sequence has been inserted upstream of GFP (Macchi et al., 2003). Hence, the levels of GFP fluorescence reflect cellular iron levels. In mammalian cells, the iron fluorescent sensor, IRE-GFP, was widely used in mammalian cells to probe responses to iron treatment and study endogenous iron levels in intracellular compartments. IRE-GFP sensor is induced upon iron sources, including Hemin and FAC and reduced using iron chelators, deferoxaminemesylate salt; it was also successfully adapted to measure

mitochondrial iron level variations in erythrocytes (Gu and Rossi, 2005; Paradkar et al., 2009).

The classical method for demonstrating iron in tissue is the *Perl's* histochemical procedure, which consists of the reaction of potassium ferrocyanide with ferric iron from iron-binding proteins, such as Ferritin (Perl and Good, 1992). Calcein has also been used to fluorescently measure cellular iron in mammalian cells (Thomas et al., 1999). These methods measure ferric iron stored within iron-binding proteins and thus, proved to be irrelevant for our studies since the objective was to measure an increase labile 'ferrous' iron levels in tissue devoid of Ferritin. Hence, we adapted a transgenic version of the mammalian IRE-GFP sensor to assay labile iron levels in *ferritin* mutant retinas in *Drosophila (Exp. Proc. 4.3.5)*.

4.2.5 Iron And Cell Death

Iron overload plays a role in the pathogenesis of a number of retinal neurodegenerative diseases. In mammals, ferrinopathy (neuroferrinopathy) has been identified as an autosomal, dominant disease affecting the central nervous system. It is caused by mutations in exon 4 of the *FLC* gene on chromosome 19. Degenerating neurons have been shown to be iron-positive and immuno-reactive to Ferritin antibodies. Recent mouse studies have also

implicated the role of iron-containing enzymes ferroxidases, Ceruplasmin (Cp) and its homolog Hephaestin (Heph), in retinal degeneration. While in normal conditions, Cp and Heph are localized to the Muller glia and retinal pigment epithelium, mice deficient in these enzymes had a striking increase in retinal iron followed by photoreceptor degeneration (Hahn et al., 2004a).

Ferritin's involvement in the apoptotic pathway was first put forward in a study of NF-κB transcriptions factors, which antagonize cell death induced by tumor necrosis factor TNFα. FHC was identified as a NF-κB target and revealed to act as a novel anti-apoptotic player by inhibiting ROS accumulation and preventing sustained JNK activation. The knockdown of FHC by short interference RNA hairpins also causes an increase in JNK activation induced by TNFα. Furthermore, the brake on ROS accumulation by FHC was shown to occur via iron sequestration (Pham et al., 2004).

While previous studies implicate iron in cell death mechanisms, the data remains mostly correlative. In this study, we generate the first loss-of-function of the entire *ferritin* complex in *Drosophila*. We provide evidence indicating that *ferritin* mutant PRCs promote iron-mediated oxidative stress and then engage in a caspase-regulated cell death pathway during the late stages of retinal development in *Drosophila*.

4.3 Experimental Procedures

4.3.1 Fly Stocks and Genetics

Flies were maintained at 25ºC and a 12-hour light/dark cycle. Canton S (CS) was used as the wild type strain. The *fer2LCH*^{Pz0035}, *fer1HCH*^{Pz0451}, *fer1HCH*^{EP1038} alleles are P[lacZ] enhancer trap lines obtained from the Bloomington Stock Center. FRT82, *fer2LCH*^{Pz0035} was part of the UURCFG stocks. P-element allele *fer1HCH*^{Pz0451} was meiotically recombined on the FRT82 chromosome for recessive analysis. *UAS-Fer1HCH*, *UAS-Fer2LCH, UAS-Fer1HCH/Fer2LCH and UAS-Fer1HCH*^{ferroxidase*} (*, ferroxidase-defective) are kind gifts of Dr. Fanis Missirlis (School of Biological and Chemical Sciences, Queen Mary University of London). *UAS-Fer1HCH RNAi* was obtained from the RNAi Collection generated by the Barry Dickson Laboratory (Dietzl et al., 2007). *fer2LCH-gal4* was generated by P-element Gene-Switch, which consisted of the conversion of the P-element *LacZ* enhancer-trap *Pz*^{0035} in *fer2LCH* locus to a Gal4 line. (Sepp and Auld, 1999). *fer1HCH-GFP* is a GFP enhancer trap, kindly provided by Lynn Cooley (Kelso et al., 2004). Intron/exon donor and acceptor splice sites flank the GFP sequences on the P-element; consequently all *fer1HCH-GFP* mRNA types (IRE +/-) are predicted to contain the GFP exon, which encode GFP in frame with the Fer1HCH protein. Fer1HCH-GFP assembles *in vivo*

with Fer1HCH to form functional fluorescent ferritin. Furthermore, the full-length mature polypeptide is predicted to translocate to the ER and contain the GFP attached to the N-terminus, after the signal peptide is cleaved (Missirlis et al., 2007).

The stock *hsFLP; tub FRT>GFP>FRTGal4* was a kind gift from Gary Struhl and was a used to generate *FLP*-out gain-of-function clones of misxpressed tagged Ferritin complexes in the gut and eye imaginal disc (Struhl and Basler, 1993). The '>' denotes an FRT site. To generate clones, flies were left to lay eggs for 2 days and then transferred to a new vial. Embryos were heat-shocked for 37ºC for 1 hour and then dissected at third-instar larval stage for midgut and eye imaginal disc stainings. *eyFLP;; FRT82, ubiGFP* and *eyFLP;;FRT82, GMR-hid* lines were respectively used to generate mosaic (Xu and Rubin, 1993) and whole-eye clones (Stowers and Schwarz, 1999) in third-instar and 42-hour APF eye imaginal discs. The *Δ2-3* transposase (Robertson et al., 1988) was used to perform 'P-element hopping' and by imprecise excision generate deletions strains in the *ferritin* locus. The stock *RE; UAS-GFP^{ninaC}; FRT82, rh1-tdTomato^{ninaC}* was used for generating and visualizing homozygous clones of *ferritin* mutations in the outer (R1-R6) adult PRCs using the live PRC imaging method (*Chapter 2,*

Exp. Proc. 2.3.2 and 2.3.3). The ubiquitous *arm-Gal4* promoter for broad organismal expression was obtained from the Bloomington Stock Center.

4.3.2 Generation of Ferritin Deletion Line by P-element Excision

The P-transposon insertion EP^{1038}, localized in the exon 2 of *fer2LCH* was mobilized by crossing to flies bearing the *Δ2-3* transposase (Robertson et al., 1988). 412 male progeny from this cross, which lost the $white^{+}$ P-element marker and indicative of an excision event, were crossed to a *TM6B* balancer strain. To isolate deletions truncating both *ferritin* genes, P-element excision alleles were crossed to another P-element transposon insertion in the adjacent *fer1HCH* locus. 7 (1.7%) putative *ferritin* deletions were selected based on (homozygosity) lethality confirmed by crossing them to the original P-element transposon *fer2LCH* EP^{1038} and the 3R deletion *Df(3R)tll-8*, deleting the entire *ferritin* locus (from Bloomington Stock Center, BL2599, break information from John Merriam).

To determine the extent of the deletion, individual *ferritin* excision lines trans-heterozygous lethal over the $fer1HCH^{Pz0451}$ and $fer2LCH^{Pz0035}$ alleles, were subsequently screened by Southern Blotting. For this purpose, we used a 312-bp probe left to the P-element insertion site and in the intronic region of *fer2LCH* locus. The extent of these deletion created by

imprecise excision was determined by Southern Blot analysis on BamH1-digested genomic DNA. (Forward primer: 5'-CGGGCTTTTTCACAGGC-AGAGTAA-3'; reverse primer sequence 5'-CGCCCTCTTAAATGCAATAACCAACAA- 3'; PCR annealing and Southern hybridization at 55°C). The Southern Blot revealed all seven *ferritin* deletion lines represented the same 2.2kb truncation referred to as *Df(3R)Fer*. In order to determine the exact breakpoints of the deletion *Df(3R)Fer*, PCR was undertaken on heterozygous flies with the putative 2.2kb deletion. PCR revealed an excision event, which left 10 bases (corresponding to a inverted repeat sequence) of the original P-element and excised a 2.2kb region, comprising portions of the first exons of *fer2LCH* and *fer1HCH*. *Df(3R)Fer* was subsequently recombined onto a *FRT* chromosome to study its loss-of-function phenotype.

4.3.3 Live Fluorescent Imaging of PRCs

Please refer to *Chapter 2, Experimental Procedures, 2.3.3*

4.3.4 Retinal Plastic Sections

Adult mosaic retinas/eyes were collected and then sectioned and stained following the protocol described in *Chapter 2, Experimental Procedures, 2.3.4*.

4.3.5 Design of GFP-Based Free Iron Sensor

We decided to use the previously described mammalian IRE-GFP sensor for *in vivo* iron measurements in *Drosophila* tissue based on the following reasons. First, the IRE-GFP sensor has been readily used in mammalian cell culture and shown to successfully mimic iron levels in cellular context and upon exogenous iron administration (Gu and Rossi, 2005; Macchi et al., 2003; Paradkar et al., 2009). Second, IREs are conserved from insects to mammals; the rat IRE has been shown to not only bind mammalian IRPs but also *Drosophila* IRP-1A (Lind et al., 2006; Missirlis et al., 2007; Piccinelli and Samuelsson, 2007). Third, the regulation of IRE is dependent on its position from the translation start site of targeted gene. The function and distance for effective action of the IRE in the longer splice variant of *Drosophila* Fer1HCH in still unclear. However, in mammals, it has been well established that IRE needs to be at close proximity (approximately 30-base pairs) to the translational start site for the IRP-IRE system to function efficiently (Goossen et al., 1990; Koloteva et al., 1997).

The UAS-IRE-GFP construct is an *in vivo* transgenic labile iron reporter designed by inserting the IRE-d2EGFP construct in a *Drosophila* pUAST Casper vector. IRE-d2EGFP was digested using EcoR1/Not1 sites

from plasmid pcDNA.3(+)-IRE-d2GFP given by Sangwon F. Kim, PhD, from the Department of Neuroscience at John Hopkins University. IRE is a 28 base-pair rat Iron Response Element (5'-GAATTCCTGCTTCAACAGTGCTTGGACGGAATCCCGGGGATCC-3') which forms a stem-loop hairpin and is a RNA-binding motif; it is located 30 base pairs from the transcriptional start site of d2EGFP. d2EGFP (Clontech) is a destabilized unstable form of EGFP, where residues 422-461 of Mouse Ornithine DeCarboxylase (MODC) were fused to the C-terminus of EGFP. The destabilized EGFP allows for a high turnover of GFP fluorescence and thereby accurate measurements of free iron levels in the cell at a given time-point.

The levels of basal fluorescence of 25 independent insertions were determined by crossing to *GMR-Gal4* followed by chicken-GFP antibody (Aves Lab, 1:1000) staining. Two lines of levels of basal fluorescence were selected: weak *UAS-IRE-GFP*[6] to study upregulation and a strong *UAS-IRE-GFP*[10] to study down-regulation of free iron.

To study iron levels in *ferritin* mutants, we built the line *eyFLP, GMR-Gal4; UAS-IRE-GFP*[6]*; FRT822, UAS-DsRed* based on the original stock *eyFLP, GMR-Gal4; Sco/CyO; FRT82, UAS-DsRed*, a kind gift of Joe Rodriguez in the laboratory. Pupal eye discs aged to 42-hour APF were

dissected and stained with anti-chicken-GFP (1:1000, Aves Lab), anti-mouse-DsRed (1:1000, Clontech), and anti-rat ELAV (1:20, DHSB).

4.3.6 Measuring Hydrogen Peroxide *in vivo*

The *UAS-HyPer* construct is the first animal oxidative stress (H_2O_2) transgenic sensor; it was built by cloning the *HyPer* (Hydrogen Peroxide cytoplasmic, purchased through EVROGEN) probe into a fly vector, pUAST Casper. *HyPer* is the first genetically-encoded fluorescent indicator for the intracellular detection of hydrogen peroxide that can be used for imaging of H_2O_2 production by cells under various physiological and pathological conditions. Previous results suggest that *HyPer* can serve as a promising tool in the detection of H_2O_2 in mammalian cells. As an ROS indicator, *HyPer* allows the generation of a real-time image series that give precise information about the time course and intensity of H_2O_2 changes in any compartment of interest. The probe *HyPer* was previously constructed by inserting a *circularly permuted Yellow Fluorescent Protein* (*cpYFP*) into the regulatory domain of *oxyR*, a prokaryotic *H_2O_2* –sensing protein (Appendix 6.4, Fig. 6.4A) (Belousov et al., 2006).

Thirty-seven independent insertions were recovered after injection and individually crossed to *GMR-Gal4* flies to assess basal fluorescence using live GFP imaging. Two lines with weak basal expression and two lines

with strong basal expression, respectively on second and third chromosomes, were selected for further usage.

For validation of the *HyPer* probe, we crossed the weak *UAS-HyPer*^{13} to *GMR-Gal4*. Eye imaginal discs were dissected from third instar larvae, placed in Schneider growth medium for 30 minutes. Batches of five eye discs connected by the mouth hook were placed in one 50µl drop of 1X PBS on a slide. H_2O_2 was added to a final concentration of 0.5µM and the increase of fluorescence was monitored immediately before and after the addition of H_2O_2 by real-time imaging using an upright Lumar GFP fluorescent microscope and the AxioVision 5.1 Real-Time imaging software (Appendix 6.4, Fig. 6.4B).

To study H_2O_2 levels based on the *Hyper* probe, we built the line *eyFLP, GMR-Gal4; UAS-HyPer*^{13}*; FRT822, UAS-DsRed* based on the original stock *eyFLP, GMR-Gal4; Sco/CyO; FRT82, UAS-DsRed*, a kind gift of Joe Rodriguez in the laboratory. Eye imaginal discs were dissected, placed in Schneider growth medium for 30 minutes and then transferred onto slides and mounted with Vectashield glycerol medium. *In vivo* imaging on *ferritin* clones (absence of red) with *HyPer* probe (green) was done immediately after mounting using an upright Zeiss Confocal microscope.

HyPer was imaged using a GFP filter (473nm) and *ferritin* clones were visualized using a Cy3 filter (520nm) (Appendix 6.4, Fig. 6.4C).

4.3.7 Generation of Transgenic Flies with Tagged Ferritin Constructs

Tagged ferritin constructs *UAS-FLAG-Fer1HCH* and *UAS-myc-Fer2LCH* were generated by inserting *FLAG* (5'-GACTACAAGGACGACGATGACAA-3') and *c-myc* (5'-GAGCAGAAACTCATCTCTGAAGAGGATCTG-3') peptide tags respectively at the N-termini of Fer1HCH and Fer2LCH. The tags were inserted immediately following the predicted cleavage sites of the ER target leader sequence (Nichol and Locke, 1999). *FLAG* was inserted following aspartic acid 22 of Fer1HCH and *myc* following cysteine 23 of Fer2LCH in a *Drosophila* pCasper-UAST vector. Similarly, *EGFP* and *mCherry* Open Reading Frames were tagged to *Fer1HCH* and *Fer2LCH* respectively, to generate *UAS-GFP-Fer1HCH* and *UAS-mCherry-Fer2LCH* (Fig. 4.6A). These fluorescent tag constructs were used study the localization of the Ferritin *in vivo*. *mCherry* is derived from *mRFP1* and is considered the best general-purpose monomer for protein fusion, owing its superiority to its photostability (Appendix 6.1).

4.3.8 Western Blot Analysis

Whole flies, fly heads, and dissected retina were homogenized in lysis buffer in the presence of protease inhibitors. Protein extracts were loaded into a Tris-HCL gel (BioRad), and transferred to PVDF nitrocellulose membranes. For Ferritin protein quantification in whole-flies and dissected retina, the following primary antibodies were used: rabbit anti-Fer1HCH (1:1000; gift from Fanis Missirlis), rabbit anti-Fer2LCH (1:1000, gift from Fanis Missirlis); rabbit β-Tubulin from (1:1000, DSHB, University of Iowa, USA), and mouse anti-HRP (Horse Radish Peroxidase, Jackson Laboratories, 1:10,000). For GFP quantification, 30 fly heads were homogenized for each sample and the following antibodies were used: mouse-GFP (1:1000, Molecular Probes), mouse anti-β-actin (1:1000, DSHB, University of Iowa, USA) and rabbit anti-HRP (Jackson Laboratories, 1:10000).

4.3.9 Protein Carbonylation Assay

Protein carbonylation was measured using the OxyBlot™ protein detection kit following manufacturer's recommendations (Chemicon/Millipore, France). Briefly, thirteen dissected retina mutant for both *fer1HCH*^{Pz0451} and *fer2LCH*^{Pz0035} , were homogenized in lysis buffer

(50mM Tris-HCL pH7,4, 150mM NaCl, 1% IGEPAL, 2mM DTT, Sigma, France) on ice. After centrifugation, protein supernatant extracts were treated with 2,4-dinitrophenylhydrazine (DNPH). The reaction of DNPH with carbonylated proteins allows the formation of 2-4-dinitrophenylhydrazone (DNP) that can be detected with an anti-DNP. Extracts were loaded on 12% polyacrylamide gel and transferred overnight onto 0.45μM nitrocellulose membrane (Whatman, Schleicher and Schuell, Germany). DNP groups were immunodetected with a rabbit anti-DNP followed by secondary anti-HRP antibodies and ECL revelation. For a loading control, α-tubulin was detected using an anti-α-tubulin antibody (Sigma, France).

4.3.10 *ferritin in situ* RNA Hybridization of Embryo and Larval Tissue

fer1HCH and fer2LCH full length ORFs were used as template for RNA *in situ* probes and amplified from *Drosophila* genome by PCR. For *fer1HCH*, we used the following set of primers: forward primer sequence: 5'-GGAATTCGCCACCATGGTGAAACTAATTGCTAGCC-3' reverse primer sequence: 5'-CTAGTCTAGACCTTACAGGGTCTTGTCGAACA-GGAA-3'. For *fer2LCH*, we used the following set of primers: forward primer sequence: 5'-GGAATTCGCCACCATGGTGAAACTAATTGCTAG

CC-3'; reverse primer sequence 5'-CTAGTCTAGATTACTGCTTCTGCA-GATACTC-3'. The full-length EcoR1/Xba1-digested cDNAs were subsequently subcloned into pBluescript SK+. The T3 and T7 promoters of the pBluescript were used to generate DIG-labeled riboprobes for *in situ* hybridization of embryos and larval tissue using standard protocols. Secondary antibody alkaline phosphatase followed by NBT/BCIP reaction was used for further analysis.

4.3.11 Ferritin Immunostaining on Larval Tissue and Schneider-2 Cells

Third instar larval, 42-hour APF eye discs and larval midguts were dissected in 1X PBS and fixed for 15 minutes in 4% formaldehyde. After three 10 minute successive washes in 1X PBS/0.3% Triton (PBST), fixed tissue was stained with the following antibodies: rabbit anti-Myc (Santa Cruz, 1:200), anti-FLAG (Clontech, 1:1000), chicken-GFP (Aves Lab, 1: 1000) and anti-DsRed (Clontech 1:1000), anti-Svp (1:500, a kind gift from Y. Hiromi) and rabbit-CM1 (1:50) Incubations were performed overnight at 4C. Incubations with secondary antibodies rabbit-FITC (1:200), mouse-Cy3 (1:400) and rat-Cy5 (1:500) were performed for 2 hours at room temperature. After three PBST washes, samples were mounted on slides in VectaShield with DAPI and imaged using Zeiss Confocal LSM upright microscope.

For Schneider Cells 2 (S2 cells), *UAS-mCherry-Fer2LCH* and *UAS-GFP-Fer1HCH* were co-transfected with *actin-Gal4* expression plasmids and were immunostained and imaged following a similar procedure as above. The following antibodies were used: mouse anti-DsRed (Clontech, 1:1000) for mCherry and chicken anti-GFP (Aves Lab, 1:1000) for GFP.

4.4 Results

4.4.1 Disruption of the Ferritin Complex Triggers Moderate PRC Degeneration

The PRC recessive genetic screen revealed that a mutation in the *fer2LCH* subunit of the Ferritin complex by a P-element insertion in exon 1 of the coding region leads to moderate PRC death (Fig. 4.1A). Furthermore, overexpression of caspase inhibitor P35 rescues this PRC death (Fig. 4.1B). We further use *ferritin* mutations to study the link between iron deregulation and the apoptotic pathway in PRCs. The *ferritin* locus spans a region of approximately 5kbps and harbors *fer2LCH* and *fer1HCH* genes in close proximity. Both genes are approximately 700 nucleotides in length and share overlapping 5' UTRs. The locus is riddled with P-element insertions in both *ferritin* coding regions, intronic regions and UTRs (Fig. 4.1C). We present the *ferritin* locus and highlight P-element alleles which were further used to

study Ferritin deregulation in Fig. 4.1C. We took advantage of a P-element mutations in the *fer1HCH* locus, notably the P-element insertion Pz^{0451} inserted in the second intron, to study the consequences of the disruption of the Fer1HCH subunit (Fig. 4.1C). Trans-heterozygotes $fer2LCH^{Pz00035}/fer1HCH^{Pz00451}$ are viable; however homozygotes for $fer2LCH^{Pz00035}$ or $fer1HCH^{Pz00451}$ are embryonic lethal. Nevertheless, we observe a few first instar larval escapers in $fer2LCH^{Pz00035}$ homozygote flies that display evidence of iron accumulation (Appendix 6.5). The placement of Pz^{0035} in exon 1 of *fer2LCH* suggests that it is a loss-of-function allele. Furthermore, dominant mutations in $fer2LCH^{Pz003}$ reduce significantly levels of Fer2LCH. Similarly, $fer1HCH^{Pz0451}$ dominant mutations reduce Fer1HCH protein levels. We also note that mutations of one subunit dominantly affect the protein levels of the other subunit, revealing the co-dependent translational regulation of the Ferritin complex (Fig. 4.1D).

During the early stages of the Ferritin characterization in PRCs, a primary goal was to generate a loss-of-function allele of the entire Ferritin complex. For this purpose, we used an EP element line, with a $white^{+}$ gene, inserted in exon 1 of *fer2LCH* as a tool to generate a genomic deletion –

Figure 4.1 The *ferritin* Locus, P-element Mutations and Deletion by P-element Excision. For panels **A-B**, tdTomato (red) highlights wild-type and heterozygous PRCs and absence of tdTomato represents *fer2LCH*^{Pz0035} homozygous clones. GFP (green) labels all PRCs. (A) *fer2LCH*^{Pz0035} mutant clones display moderate PRC loss (white arrowheads) compared to wild-type ommatidium (red circle). **(B)** P35 overexpression rescues *fer2LCH*^{Pz0053} moderate PRC degeneration. **(C)** The structure of the *ferritin* locus reveals the close proximity of *fer1HCH* and *fer2LCH* with common regulatory regions and a 5,017 base-pair region (blue line). Four P-element alleles (*fer2LCH*^{Pz0035}, *fer2LCH*^{EP1038,} *fer1HCH*^{Pz0451}, *fer1HCH*^{EP3383}) and their insertions are highlighted in the schematic representation of *ferritin* locus. From the PRC recessive screen, *fer2LCH*^{Pz0035} (green triangle) is inserted in the first exon of *fer2LCH* locus. The span of the deletion *Def(3R)Fer* is indicated by the red line and was generated by imprecise excision of P-element *EP1038* (red triangle) in *fer2LCH* locus. IRE (green line) is present in one splice variant of *fer1HCH*. 312-base-pair Southern probe (red) corresponding to intronic region after exon 2 of *fer2LCH* was used for Southern blot analysis on a 3.7 kbps BamH1-digested fragment. (D) Western blot analysis of heterozygous flies containing P-element mutations, *fer2LCH*^{Pz0035} show reduced protein levels of Fer2LCH and Fer1HCH compared to wild-type control *(Image courtesy of Fanis Missirlis)*. (F) Southern blot analysis of heterozygous flies harboring a series of P-element mutations in *ferritin* locus and against BamH1-digested DNA. *Def(3R)Fer* is represented by the lowest 1.5kbps DNA molecular band. Higher DNA molecular bands correspond to BamH1-digested wild-type (3.7kb) and P-element fragments (>3.7kbps).

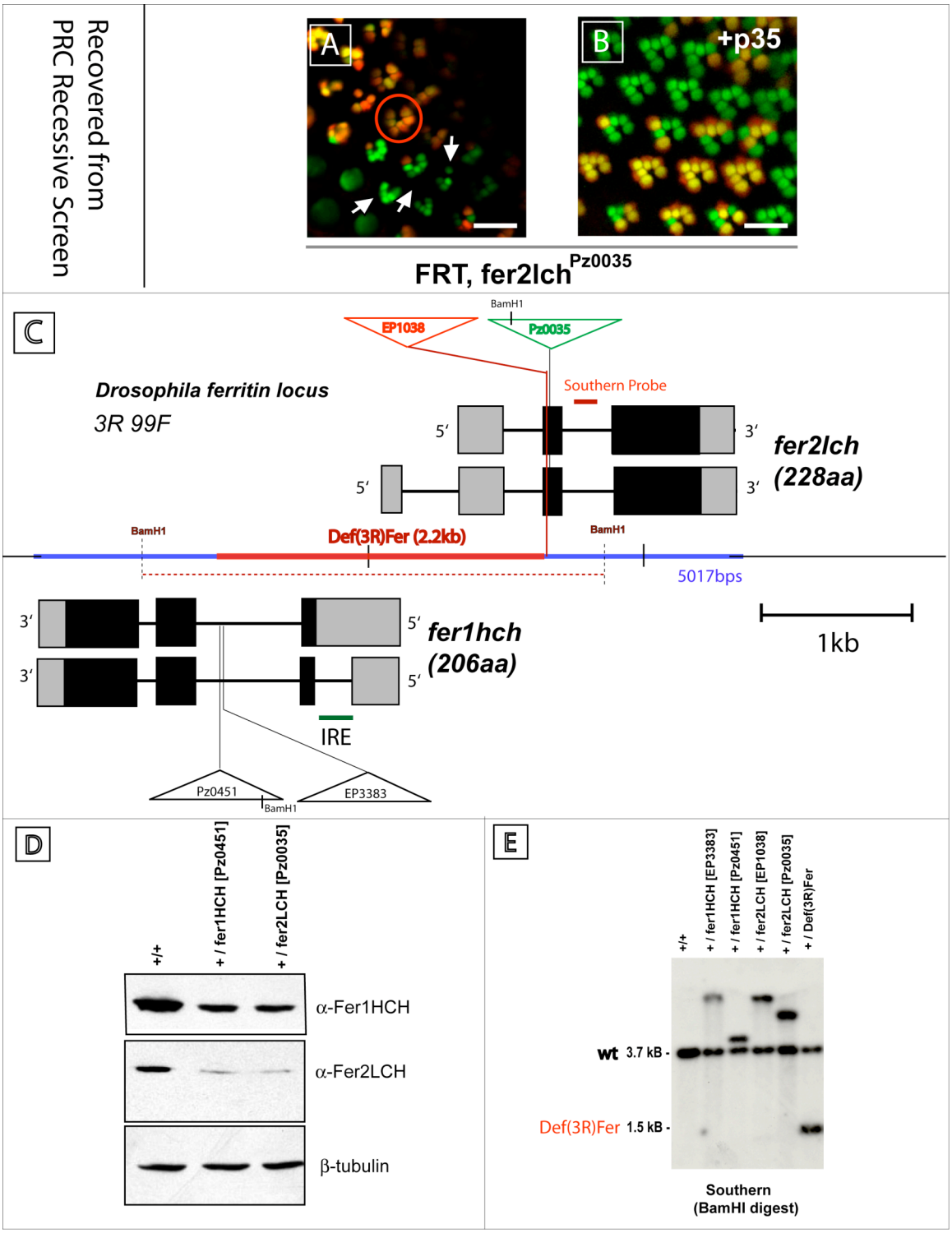

Figure 4.1 The *ferritin* Locus, P-element Mutations and Deletion by P-element Excision

spanning coding regions of both *fer1HCH* and *fer2LCH*. By imprecise excision/P-element hopping of $fer2LCH^{EP1038}$, we generated a 2.2kb deletion truncating parts of the first exons of *fer1HCH* and *fer2LCH* (Fig. 4.1C,E). A putative deletion, denoted *Def(3R)Fer*, was initially inferred by performing complementation analyses with P-elements in both *fer1HCH* and *fer2LCH* and a chromosomal deletion *Def(3R)tll-8* line spanning the entire ferritin locus (*Exp. Proc 4.2.3*). It was ultimately confirmed by Southern Blot analysis and breakpoints were identified by PCR sequencing (Fig. 4.1E). Collectively, $fer2LCH^{Pz0035}$, $fer1HCH^{Pz0451}$ and *Def(3R)Fer* were used as our tools to study the consequences of Ferritin disruption on PRC survival.

All three *ferritin* alleles were recombined on FRT chromosomes in order to analyze PRC phenotypes in recessive conditions. *ferritin* mutant retinas exhibited missing PRCs at 1-day post-eclosure. The phenotype is variable and seems to be enhanced in mosaic ommatidia as first indicated in the PRC recessive screen. Mutations of either one or both subunits, inactivating the Ferritin complex, generated a similar degree of PRC degenerating ranging from 10-20% (Fig. 4.2A-C,E). An *RNAi* line raised against Fer1HCH displayed a slightly higher level of PRC degeneration (25%) (Fig. 4.2D,E). In addition to PRC loss, *ferritin* mutants exhibit inter-cellular vacuoles and misaligned ommatidia, indicative of IOC death and

Figure 4.2 Lack of the Ferritin Complex Leads to PRC Degeneration. All retinal images were taken at 1-day post-eclosure. **(A-D)** Plastic tangential sections of mosaic retinas, *fer2LCH*^{Pz0035}, *fer1HCH*^{Pz0451}, *Def(3R)Fer* and *GMR>Fer1HCH RNAi* highlight occasional missing PRCs and vacuoles (V), both indicative of retinal degeneration. Absence of red pigment denotes mutant clones. Yellow arrowheads highlight mutant ommatidia with at least one missing PRC and the red arrowheads highlight corresponding wild-type ommatidia (surrounded by red pigment cells). **(E)** Quantitative bar graph analysis of the PRC loss represented in (A-D). 3 mosaic retinas per genotype were analyzed for quantification. **(F)** Live PRC imaging of *Def(3R)Fer* clones reveals moderate PRC loss (white arrowheads). **(G)** P35 overexpression rescues *Def(3R)Fer* degeneration. **(H)** Overexpression of the Ferritin complex (using *UAS-Fer1HCH* and *UAS-Fer2LCH* transgenes conjointly) rescues moderate PRC loss in *Def(3R)Fer* clones. **(I)** Lethality rescue of *ferritin* mutants. Overexpression of *Ferritin* transgenes under the control of ubiquitous promoter, *arm-Gal4*, rescues lethality of *ferritin* mutants. Overexpression of both transgenes *UAS-Fer1HCH* and *UAS-Fer2LCH* is necessary to rescue embryonic lethality of *Def(3R)Fer* flies.

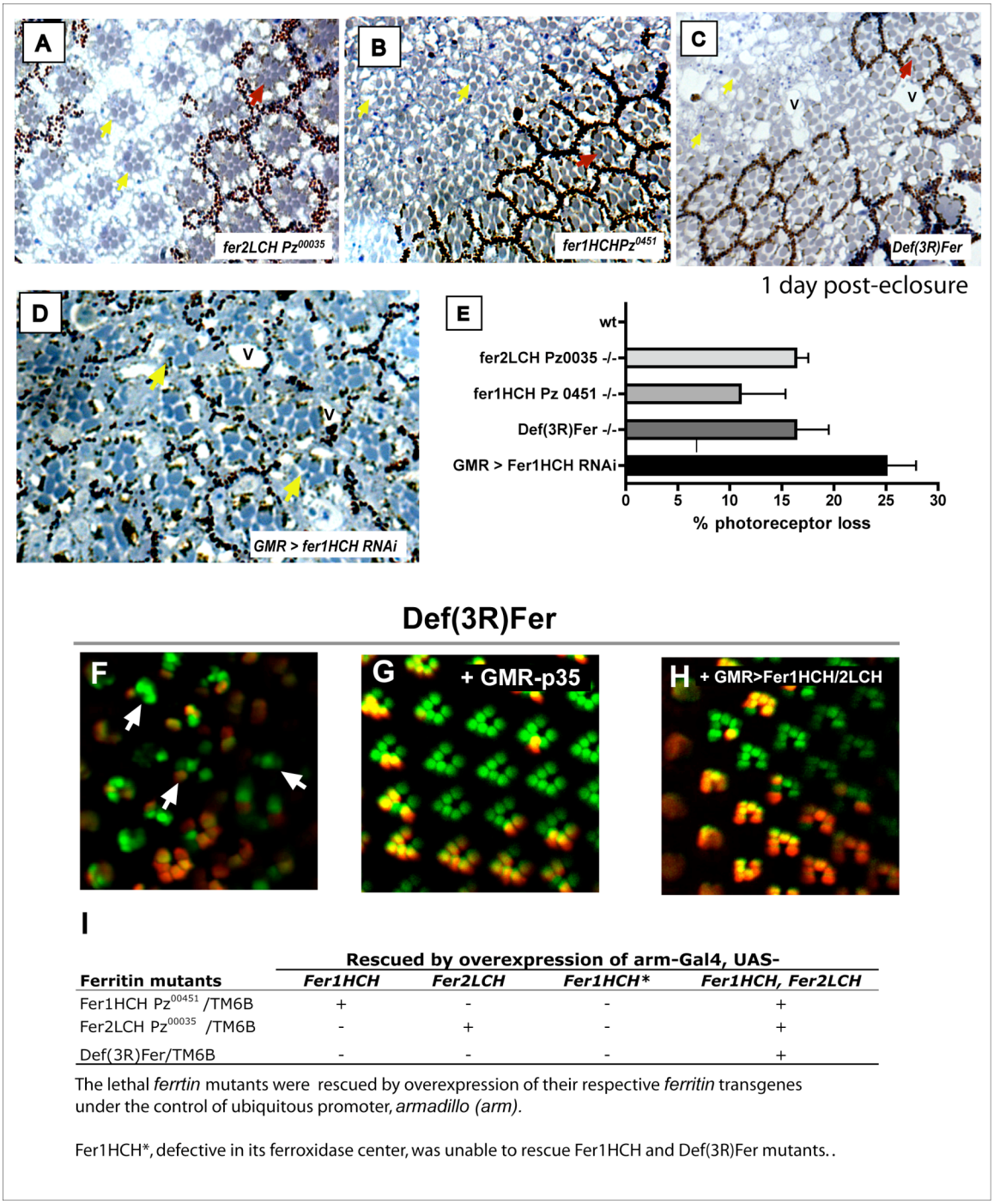

I

Ferritin mutants	Rescued by overexpression of arm-Gal4, UAS-			
	Fer1HCH	*Fer2LCH*	*Fer1HCH**	*Fer1HCH, Fer2LCH*
Fer1HCH Pz^{00451} /TM6B	+	-	-	+
Fer2LCH Pz^{00035} /TM6B	-	+	-	+
Def(3R)Fer/TM6B	-	-	-	+

The lethal *ferrtin* mutants were rescued by overexpression of their respective *ferritin* transgenes under the control of ubiquitous promoter, *armadillo (arm)*.

Fer1HCH*, defective in its ferroxidase center, was unable to rescue Fer1HCH and Def(3R)Fer mutants..

Figure 4.2 Lack of the Ferritin Complex Leads to PRC Degeneration

entire mutant ommatidia collapse during pupal development. The vacuoles and ommatidial alignment defects are especially prominent in *Def(3R)Fer* deletion loss-of-function clones (Fig. 4.2C). In all cases, *ferritin* mutations triggered late-onset PRC degeneration during development, revealed by a wild-type eye surface.

Using the double-fluorescent PRC imaging technique described in Chapter 2, we confirmed PRC loss in *Def(3R)Fer* and its rescue by caspase inhibitor P35 (Fig. 4.2F,G). PRC loss and embryonic lethality was also rescued in *Def(3R)Fer* mutants by the conjoint overexpression of both *ferritin* transgenes (Fig. 4.2H). A similar rescue of PRC loss (data not shown) and lethality were also detected in *Fer2LCH* and *Fer1HCH* mutants by the overexpression of the respective transgenic subunits (Fig. 4.1I). Together, this confirms that the PRC degeneration is caused by *ferritin* mutations and not by potential background mutations on the FRT (3R) chromosome.

4.4.2 *ferritin mRNA* Expression During Development

We performed an expression analysis in embryos and larval using RNA probes raised against the cDNAs of *fer1HCH* and *fer2LCH* (*Exp. Proc 4.3.10*). *In situ* mRNA hybridization studies reveal an expression of *fer1HCH* and *fer2LCH* ubiquitously expressed in early staged embryos (data

Figure 4.3 ***In situ*** **RNA Expression of** ***ferritin*** **in Embryos and Larval Tissue.** *In situ* hybridization against *ferritin* mRNA in embryos and larval tissue using AntiSense (AS) RNA probes. Control staining using Sense (S) RNA probes are shown in bottom left former for panel A-F and top for panels G-H. For all panels, *fer1HCH* and *fer2LCH* mRNA expression reveal similar patterns. **(A-B)** A 16-hour embryo shows *fer2LCH* **(A)** and *fer1HCH* **(B)** mRNA expression primarily in the embryonic midgut (red arrowheads). **(C-D)** Expression profiling in the third-instar larval midgut reveals strong stainings for both *fer2LCH* **(C)** and *fer1HCH* **(D)**. **(E-F)** Both *fer2LCH* **(E)** and *fer1HCH* **(F)** reveal strong expression in the larval brain, notably in neurons arranged concentrically in the optic lobes. **(G-H)** Stainings in the third-instar larval eye disc shows *fer2LCH* **(G)** and *fer1HCH* **(H)**, slightly preferentially anterior to the morphogenetic furrow in the PRC region (red arrowheads).

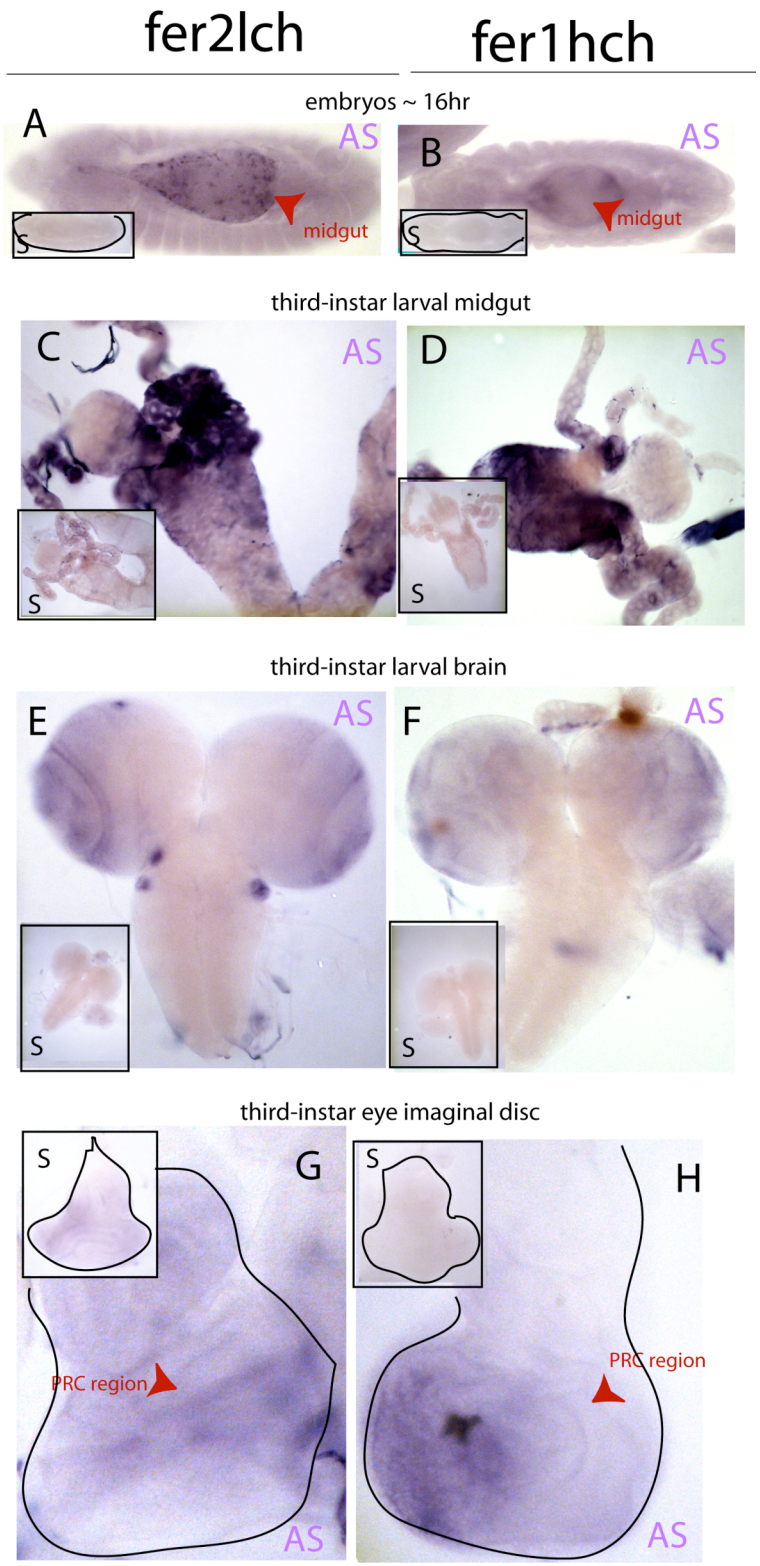

Figure 4.3 *In situ* RNA Expression of *ferritin* in Embryos and Larval Tissue

not shown). 16-hour embryos reveal a prominent mRNA expression in the midgut and amnioserosa for both subunits (Fig. 4.3A,B). In third-instar larva, the strongest *ferritin* expression for both chains was revealed in the midgut (Fig. 4.3C,D); however, we also detected very distinctive expression patterns in the brain and in the larval discs. In the larval brain, *fer1HCH* and *fer2LCH* expression was detected in concentrically organized neurons in the optic lobes (Fig. 4.3E,F). For *fer2LCH*, an additional punctuate pattern is observed in the ventral cord (Fig. 4.3E). *ferritin* expression was also seen in the larval discs, notably the wing, leg (data not shown) and eye discs. Of interest, we observed, for both *fer1HCH* and *fer2LCH*, an *mRNA* expression through the eye imaginal disc but slightly enhanced in the PRC region post-morphogenetic furrow (Fig. 4.3G,H). Overall, the expression of *fer2LCH* and *fer1HCH* exhibit similar patterns of expression.

4.4.3 The Ferritin Complex is Expressed in PRCs

To further dissect the expression of *ferritin* transcript and protein levels in the developing and adult *Drosophila* eye, we resorted to readily available *ferritin* reporters (*Exp. Proc. 4.3.1*). GFP staining in *fer2LCH>GFP* eye imaginal disc reveals a PRC-enriched *fer2LCH* transcript expression in the post-morphogenetic furrow region (Fig.

4.4A,A'). A 42-hour APF, *fer2LCH* transcript expression is further revealed in PRCs but also in surrounding IOCs (Fig. 4.4B,B').

Fer1HCH protein expression was determined using a previously characterized GFP-containing P-element line integrated into the second intron the *fer1HCH*, referred to as *fer1HCH-GFP* (Kelso et al., 2004). Using this protein reporter, we reveal a membrane-bound and cytoplasmic localization of the Fer1HCH (Fig. 4.4C,C'). At 42-hour APF, we highlight the membrane-bound localization of the Fer1HCH subunit in the developing PRCs (Fig. 4.4D,D').

Using Ferritin antibodies on eye imaginal discs, we confirm a membrane-bound localization for Fer2LCH. While unconfirmed, we also detect a potential axonal staining of Fer2LCH in the PRCs (Fig. 4.5A). On the other hand, Fer1HCH antibody staining reveals a nuclear staining, mostly likely not recapitulative of the Fer1HCH protein localization (Fig. 4.5B).

We further note that the *lacZ* enhancer trap P-element line *fer2LCH*^{Pz0035}, recovered from the PRC recessive screen, displays β-galactosidase expression in the adult PRCs in semi-thin horizontal eye sections (Fig. 5.1E-F). It was also one of the P[Z] candidates recovered in the P-element expression profile screen in search for genes expressed in

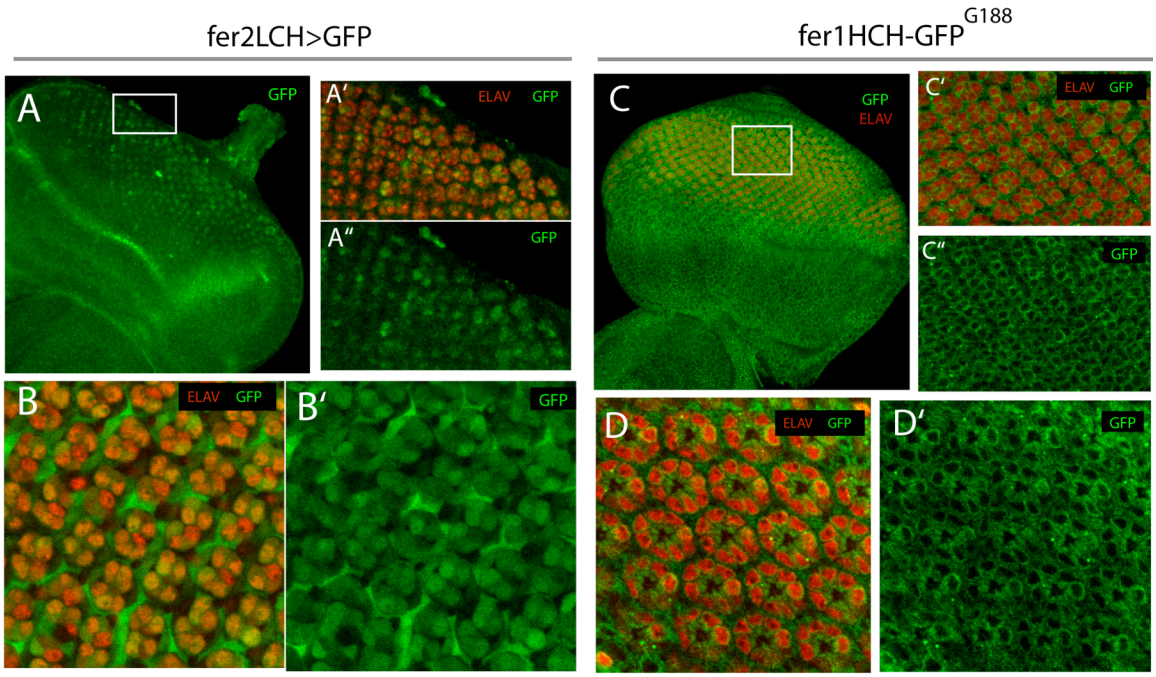

Figure 4.4 Ferritin Transcript and Protein Reporters. For all panels, GFP (green) and ELAV (red) stainings were performed on third-instar and 42-hour APF pupal eye discs **(A-B)** *fer2LCH-Gal4* promoter was used to express *GFP* in the third-instar **(A)** and 42-hour APF pupal eye disc **(B)**. **(A)** *fer2LCH* transcript pattern is preferentially in the developing PRC region and white-box region **(A')** reveals *fer2LCH* expression in developing PRCs, indicated by the overlap of GFP with ELAV. **(B)** Similar staining at 42-hour APF in the pupal eye confirms *fer2LCH* expression in differentiated PRCs and further reveals expression in surrounding IOCs. **(C-D)** *fer1HCH-GFP* was used to monitor protein levels of *fer1HCH* in the third-instar **(C)** and 42-hour APF pupal eye disc **(D)**. **(C)** GFP reveals a ubiquitous staining through the eye imaginal disc, including in developing PRCs (ELAV). **(C')** White-boxed region reveals a membrane-bound non-nuclear staining in developing PRCs. **(D-D')** 42h APF staining reveals a similar staining as in panel C in differentiated PRCs.

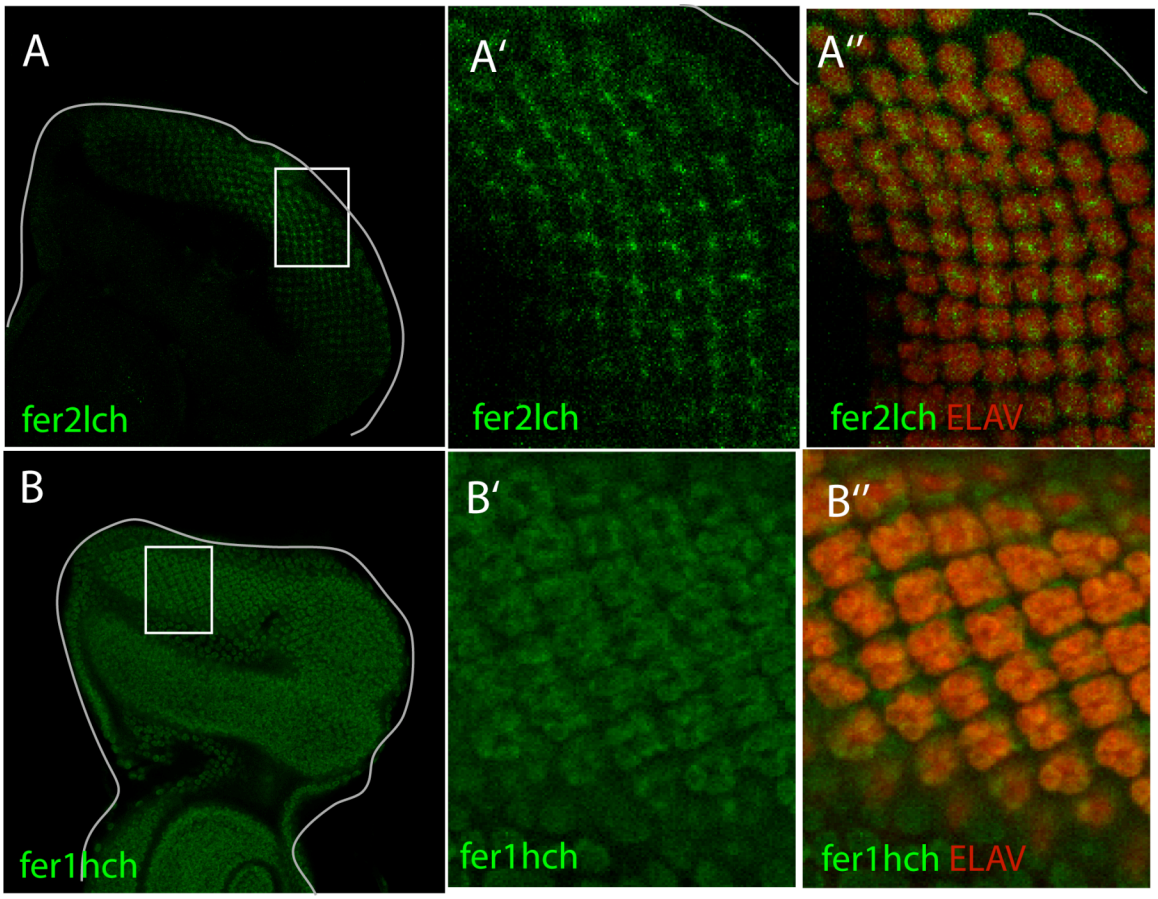

Figure 4.5 Ferritin Protein Expression in Eye Imaginal Discs. Ferritin immunostainings using respectively Fer2LCH and Fer1HCH antibodies are represented in green and PRC labeling using ELAV are labeled in red. **(A)** Fer2LCH antibody staining reveals protein expression preferentially anterior to the morphogenetic furrow. **(A'-A'')** White-box region highlights Fer2LCH (green) membrane-bound staining in PRCs (ELAV, red). **(B-B'')** Fer1HCH antibody staining reveals a ubiquitous and nuclear (un-specific) protein expression, which co-localizes with ELAV **(B'')**.

PRCs described in Chapter 3. The *fer2LCH*^{Pz0035} *lacZ* reporter is used in Chapter 5 to assess Ferritin's response in adult PRCs to a variety of environmental and pathological stresses.

Collectively, we provide strong evidence for a previously unrecognized endogenous expression of Ferritin in PRCs of the *Drosophila* retina.

4.4.4 Ferritin Assembles into a Hetero- and Non-Secreted Complex In the *Drosophila* Retina

In order to further understand the dynamics, regulation and localization of the Ferritin complex, we generated tagged Ferritin subunit transgenes constructs (Fig. 4.6A). We confirmed that tagged *FLAG-Fer2LCH* and *myc-Fer1HCH* transgenes, when overexpressed with ubiquitous promoter *arm*, were able to rescue embryonic lethality of *fer1HCH*^{Pz0451} and *fer2LCH*^{Pz0035} homozygous flies (data not shown). We also note a partial functionality of fluorescently tagged Ferritins. However two copies of these transgenes were required to overcome lethality in the *ferritin* mutants. This is probably due to the larger size of the fluorescent tags, which partially impedes with Ferritin function and assembly. However, mCherry-Fer2LCH and GFP-Fer1HCH, while only supplying partial

functionality, successfully incorporate *in vivo* into the holo-Ferritin complex (data not shown, *correspondence from Fanis Missirlis*).

When overexpressed using GMR promoter, both fluorescently tagged Ferritin chains in the eye imaginal disc co-localize (Fig. 4.6B). Furthermore, overexpression of the same constructs in S2 cells confirms the co-localization and further reveals the cytoplasmic localization of the complex (Fig. 4.6C). A more complex translational regulation of Ferritin in the adult brain is put forward using these constructs. Indeed, overexpressing both of *GFP-Fer1HCH* and *mCherry-Fer2LCH* in the broader nervous system using *elav* promoter resulted in differential distribution of the fluorescent subunits in the brain and not in an absolute co-localization as expected (data not shown).

Insect Ferritins characterized so far have been studied exclusively in the secretory pathways of cells (Nichol and Locke, 1999). Ferritin's ability to be secreted is revisited *in vivo* using the newly devised tagged constructs. Overexpression of tagged constructs in the midgut cells reveals Fer2LCH's secretive nature as overexpressed myc-Fer2LCH trespasses into neighboring non-expressing wild-type tissue (Fig. 4.6D). On the other hand, FLAG-Fer1HCH remains confined within overexpressed tissue. Similar gain-of-function studies were performed in the developing eye. In contrast to-

Figure 4.6 Ferritin Assembles into a Non-Secretory Hetero-complex in the Developing Eye. **(A)** Schematic representation of tagged *ferritin* constructs. Tags were inserted immediately after predicted cleavage sites of the endoplasmic reticulum target sequences. *FLAG* and *EGFP* tags were inserted immediately following aspartatic acid 22 of *fer1HCH*. *myc* and *mCherry* tags were immediately inserted following cysteine 23 of *fer2LCH*. **(B-C)** mCherry-Fer2LCH is stained using a DsRed antibody (red) and GFP-Fer1HCH using a GFP antibody (green). DAPI is represented in blue. **(B)** Overexpression of mCherry-Fer2LCH and GFP-Fer1HCH using GMR-Gal4 promoter reveals an overlapping membrane-bound staining of both Ferritin subunits. **(C)** Overexpression of fluorescently tagged Ferritin in S2 cells using ubiquitous actin-Gal4 promoter further reveals a non-nuclear localization of the Ferritin complex, indicated by non-overlapping staining with DAPI. **(D-E)** myc-Fer2LCH is stained using a myc antibody (blue) and FLAG-Fer1HCH using a FLAG antibody (red). GFP labels wild-type tissue and overexpressed (gain-of-function) clones are represented by the absence of GFP (green). **(D1-D3)** Gain-of-function analysis in the larval midgut. FLAG-Fer1HCH is secluded in the overexpressed clones (**D3,** red) while myc-Fer2LCH (**D2**, blue) diffuses into neighboring wild-type tissue (**D1, green**). (**E1-E3)** Gain-of-function analysis in the third-instar eye imaginal disc. FLAG-Fer1HCH (**E3,** red) and myc-Fer2LCH (**E2**, blue) remain confined to the overexpressed clonal patches and do not diffuse into neighboring wild-type tissue (**E1,** green).

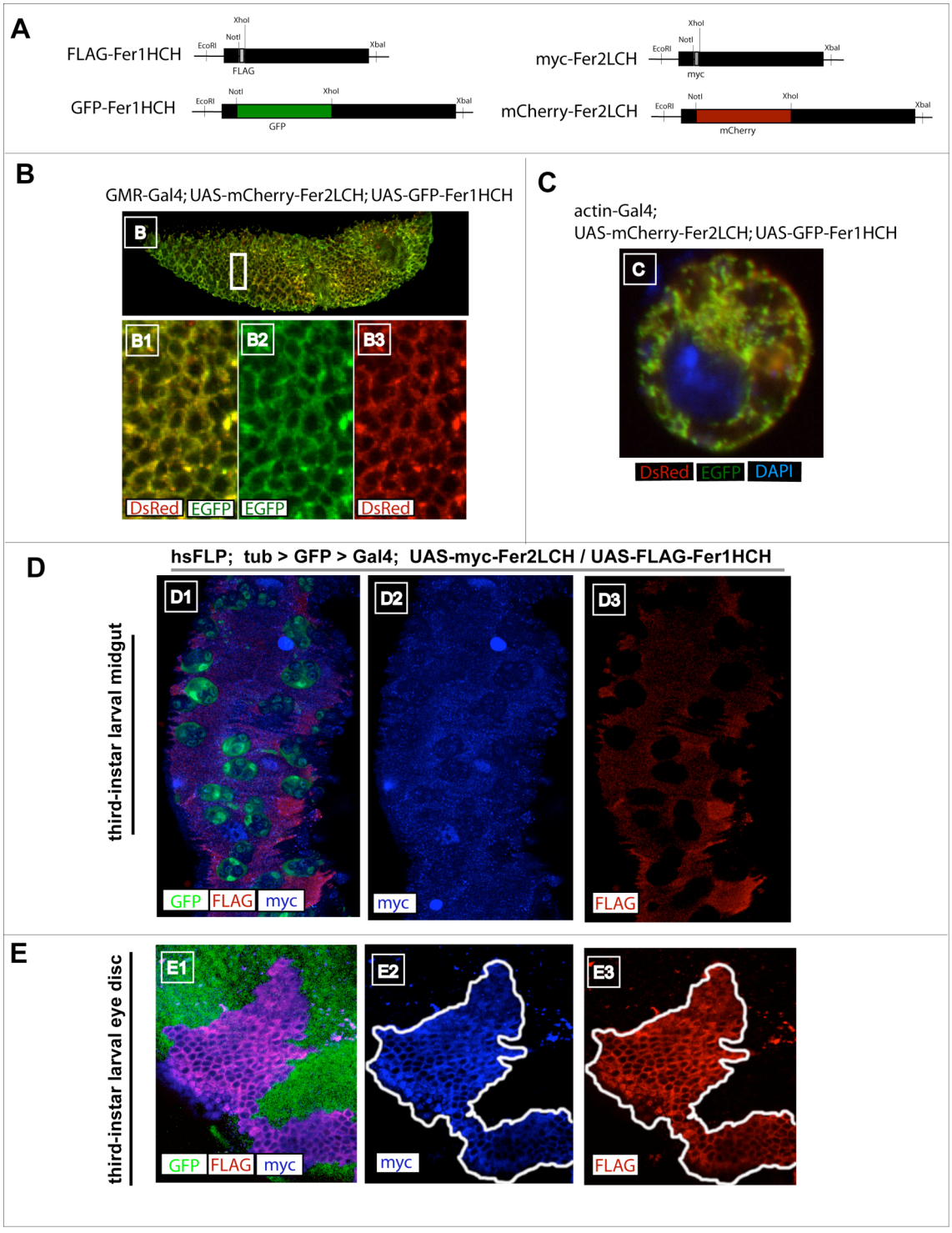

Figure 4.6 Ferritin Assembles into a Non-Secretory Hetero-complex in the Developing Eye

the midgut, a non-secreted form the Ferritin complex is revealed in the retina. Indeed, both FLAG-Fer1HCH and myc-Fer2LCH co-localize and remain exclusively within the gain-of-function clonal boundaries in the developing eye disc, thereby exhibiting no signs of secretive behavior (Fig. 4.6E).

4.4.5 Lack of Ferritin Triggers Retinal Cell Death During The Pupal Stages

To identify the earlier set of events leading to PRC loss in *ferritin*-deprived retinas, we looked for evidence of cell death early in development. In the third-instar eye imaginal disc, we generated loss-of-function *Def(3R)Fer* clones and first searched for differentiation defects. *svp* marks clusters of 4 developing PRCs, R1/R6 and R3/R4 pairs, in the developing third instar eye disc (Kanai et al., 2005). Comparison of *svp* staining in wild-type and *Def(3R)Fer* mutant tissue revealed no difference in differentiation of these sub-type of PRCs (Fig. 4.7A). We infer that PRC loss in *ferritin* mutant retinas is not due to differentiation defects but rather an ectopic death of differentiated PRCs.

In third instar larval eye disc, we stained *Def(3R)Fer* mutant clones and detected little to no caspase activation and thereby suspected that cell death occurred later in development (Fig. 4.7B). By 42-hour APF, a fixed

number of IOCs form a hexagonal array around each PRC cluster, comprising four cone cells, three bristle cells, two primary, six secondary and three tertiary pigment cells (*Chapter 1, section 1.10*). At this pupal stage, developmental IOC death is achieved and PRC are terminally differentiated (Mendes et al. 2006). Nevertheless, we observe cell death signals in mutant *Df(3R)Fer* PRCs (Fig. 4.7C). In whole-eye *Df(3R)Fer* mutant pupal eye discs at 42h APF, we detect cell death activation revealed by ectopic caspase activation in mosaic ommatidia. In whole-eye mutant for *Def(3R)Fer*, we further observe caspase activation in ommatidia. In addition, we detect missing PRCs in occasional ommatidia, IOC loss suggested by the misformed hexagonal-shaped ommatidial units, and the occasional collapse of entire ommatidia suggested by IOC aggregates (Fig. 4.7D). At the periphery of the 42h APF pupal eye disc, we reveal evidence of DNA damage in *Def(3R)Fer* mutant retinal cells (Fig. 4.7E).

4.4.6 *ferritin* Mutants Display Elevated Iron Levels and Oxidative Stress

In an effort to dissect mechanisms of Ferritin disruption-induced PRC death, we investigated iron levels in *ferritin* mutant retinas. Western blot analysis on fly heads reveals that overexpression of IRP-1A and IRP-1B

Figure 4.7 Ferritin-Deprived Cells Undergo Retinal Cell Death in Late Pupal Development. (A) *svp* is represented in red and *Def(3R)Fer* clones indicated by the absence of GFP (green). White line is used to demarcate the mutant clones from wild-type tissue **(A')**. *svp* expression in the eye imaginal disc does not reveal any difference in PRC differentiation patterns between wild-type and *Def(3R)Fer* mutant clones. **(B)** CM1 (red) staining in the eye imaginal disc reveals little cell death activation at this stage of development. A few CM1-positive cells are visible in the dorsal-anterior region of the eye imaginal disc in the PRC region **(B')**. **(C-C3)** The developing pupal eye disc at 42-hour APF displays caspase activation in *Def(3R)Fer* mutant PRCs (absence of green) revealed by the merge (white arrows) of CM1 staining (red) with ELAV (blue). CM1-positive PRCs are predominantly found in small clones and mosaic ommatidia. **(E-E3)** *Def(3R)Fer* whole clones at 42-hour APF reveal cell death activation in PRCs revealed by co-localization (white arrow) of CM1 (red) and ELAV (blue), ommatidia with missing PRCs (yellow circle) and ommatidial collapses suggested by the formation of IOC aggregates (yellow rectangle). **(F-F2)** TUNEL staining at the border of a 42h APF pupal eye reveal apoptotic retinal cells (TUNEL, red) in mutant *Def(3R)Fer* clones (absence of green).

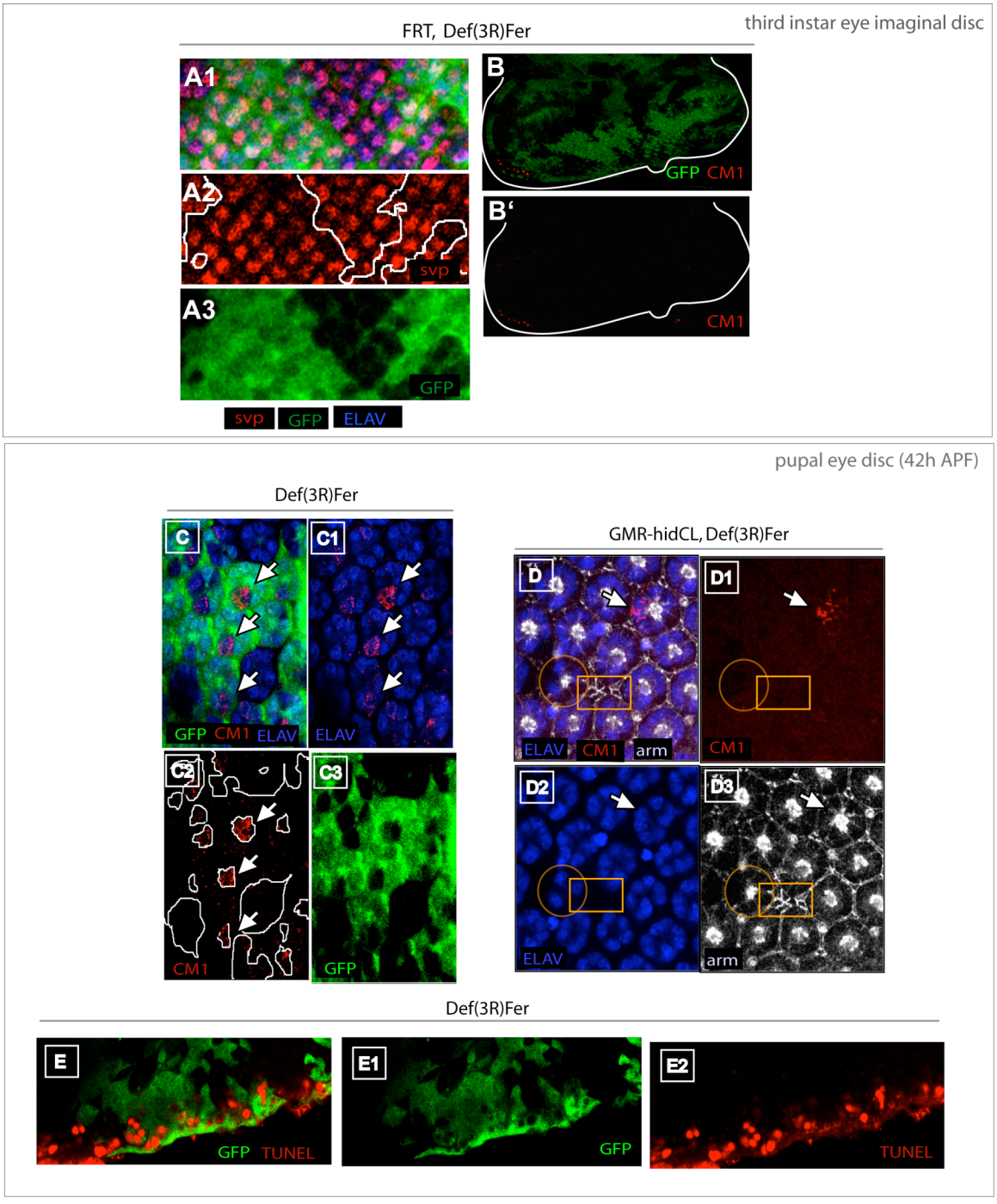

Figure 4.7 Ferritin-Deprived Cells Undergo Retinal Cell Death in Late Pupal Development

under GMR reduces basal levels of IRE-GFP (Fig. 4.8C). GFP expression on eye imaginal discs further validates that IRE-GFP's dependency of *Drosophila* IRPs. Indeed, IRP-1A overexpression reduced the levels of basal GFP to undetectable levels in the GMR region (Fig. 4.8F). We note that basal expression of IRE-GFP under GMR highlights increased iron levels of the morphogenetic furrow, where cells are arrested in cell cycle (Fig. 4.8D).

Using the IRE-GFP, we then examined iron levels in *Def(Fer)3R* mutant clones in the developing eye disc. In the third-instar eye imaginal disc, we do not observe any significant difference in iron distribution in *ferritin* mutant versus wild-type tissue (data not shown). However, at 42-hour APF, we detected a higher GFP expression in *ferritin* mutant PRC (Fig. 4.9A). We note that the intensity of GFP is proportional to the levels of the labile iron pool (LIP). Nevertheless, we also observe basal level of fluorescence in wild-type and heterozygous neighboring tissue. Seldom, we also observed heterozygous PRCs juxtaposed to mutant PRCs, often part of the same ommatidia, with a sharp increase in iron levels (Fig. 4.9A3).

Excess labile iron due to the lack of the Ferritin complex may participate in the generation of ROS and subsequent oxidative-mediated cell death. In an effort to understand the underlying pathway of *ferritin*-dependent PRC death, we then investigated oxidative stress levels in *ferritin*

mutants. To evaluate redox status in retina lacking the Ferritin complex, we first measured H_20_2 levels using the newly devised fluorescent-based sensor *HyPer*. While *HyPer* responded to exogenous 0.5μM H_20_2 administration to cultured eye discs, it did not reveal any significant differences in *Def(3R)Fer* clones (Appendix 6.4). However, iron accumulation in *ferritin* mutants is thought to participate in the Fenton reaction generating hydroxyl free radicals. Hence, we measured protein carbonylation, which is an irreversible oxidative modification that occurs when oxidative stress is elevated. Carbonylated proteins were revealed by the immunodetection of carbonyl groups in oxidized proteins (Levine et al., 1994). We found that protein oxidation levels are increased in whole eye homozygote mutant retinas for *fer1HCH*^{Pz0451} and *fer2LCH*^{Pz0035} compared to wild type retina (Fig. 4.9B).

In conclusion, we provide a comprehensive characterization of the Ferritin loss-of-function phenotype. We reveal an increase in labile iron, oxidative stress and caspase-mediated in *ferritin*-mutant terminally-differentiated PRCs.

Figure 4.8 Measuring the Labile Iron Pool and IRP-IRE Interactions *in vivo*. **(A)** Schematic representation of the IRE (blue) and IRP (gray) interaction. IRPs are cytoplasmic RNA-binding proteins involved in intracellular regulation of iron homeostasis. IRPs regulate expression of iron-regulated genes such as *fer1HCH, transferrin and succinate dehydrogenase (SdH)* at the mRNA level by interacting with a conserved RNA stem-loop structure termed the IRE, usually located in 5' UTRs. **(B)** Schematic representation of the IRE-GFP based construct to measure intracellular iron levels *in vivo* using GFP fluorescence. IRE, which regulates the translation of endogenous *fer1HCH* transcript in response to changes in iron concentration, is fused to a destabilized GFP and placed in a UAS vector. In low iron cellular conditions, IRP binds to IREs preventing GFP expression. In high iron cellular conditions, IRP disengages from IRE leading to GFP expression. **(C)** Western blot analysis reveals that overexpression of IRP-1A and IRP-1B under GMR, reduces IRE-GFP fluorescence to non-detectable levels comparable to *yw* and significantly lower to controls *GMR>GFP* and *GMR>IRE-GFP, lacZ*. **(D-G)** Overexpression of IRP-1A leads to a decrease in basal fluorescence of the IRE-GFP reporter **(F)** compared to *lacZ* control **(D)**. Overexpression of IRP-1A **(E)** or LacZ **(G)** display no significant differences when crossed to GMR>GFP.

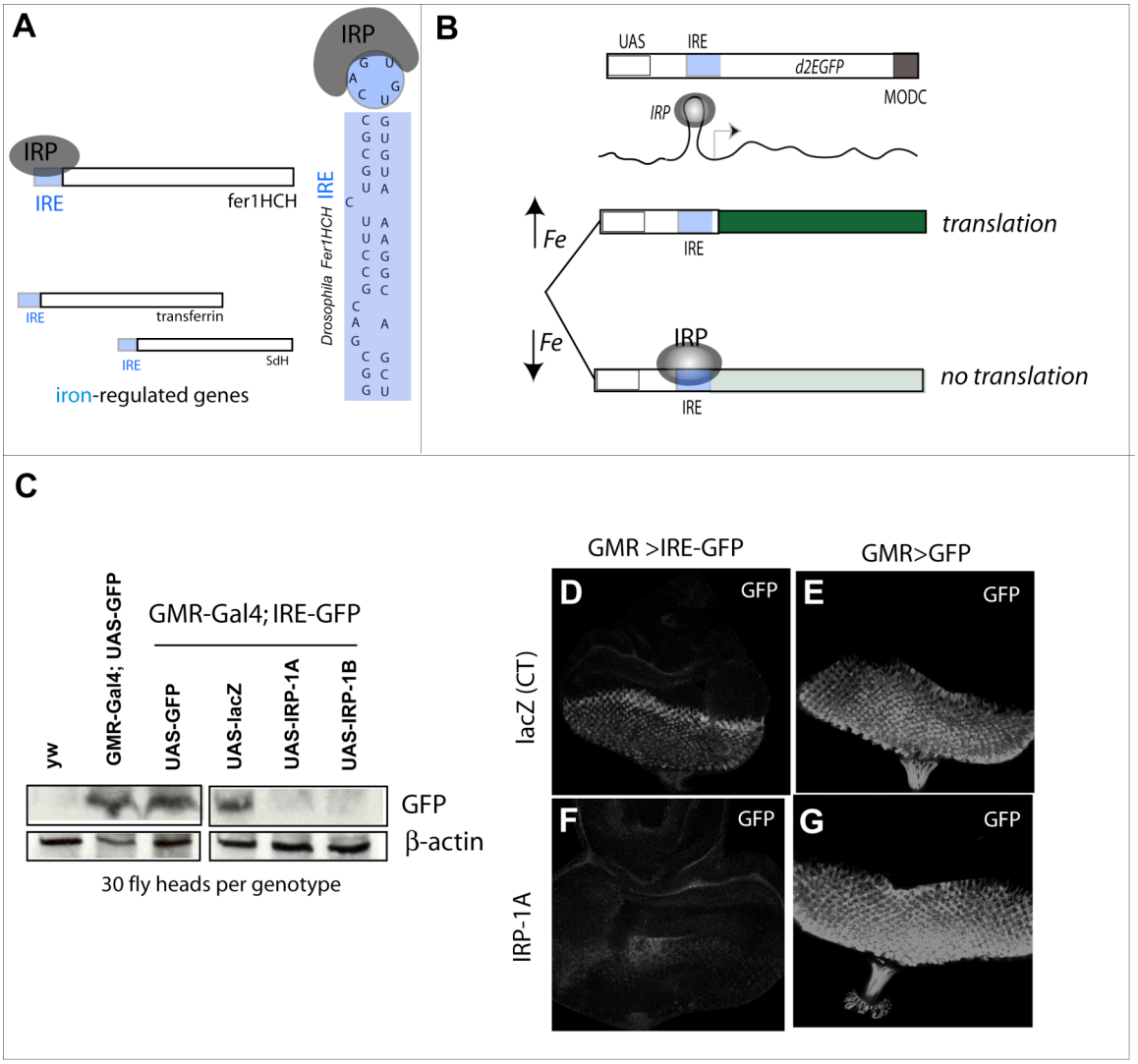

Figure 4.8 Measuring the Labile Iron Pool and IRP-IRE Interactions *in vivo*

Figure 4.9 Higher Levels of Iron and Oxidative Stress in *ferritin* Mutant Retinas. (A1-A3) The iron reporter IRE-GFP reveals higher levels of intracellular iron (**A3**, green) in PRCs **(A1**, blue) of *Def(3R)Fer* mutant clones (**A2**, absence of red). DsRed labels wild-type and heterozygous tissue Absence of DsRed reveals *Def(3R)Fer* mutant clones (**A2**). ELAV labels PRCs (**A1**). Note that wild-type and heterozygous PRCs display a basal GFP level and neighboring mutant clones also occasionally display higher levels of iron (green) indicated by white arrowheads. **(B)** Western blot analysis of protein extracts for wild-type and whole-eye retinas mutant for *fer2LCH*^{Pz0035} and *fer1HCH*^{Pz00451}. Samples were pretreated with DNPH allowing the reaction of DNPH with carbonylated proteins and the formation of DNP. Antibody immuno-staining against DNP reveals higher levels of protein carbonylation in *ferritin* mutant retinas indicated by high-weight molecular bands *(Image B, courtesy of Clemence Levet).*

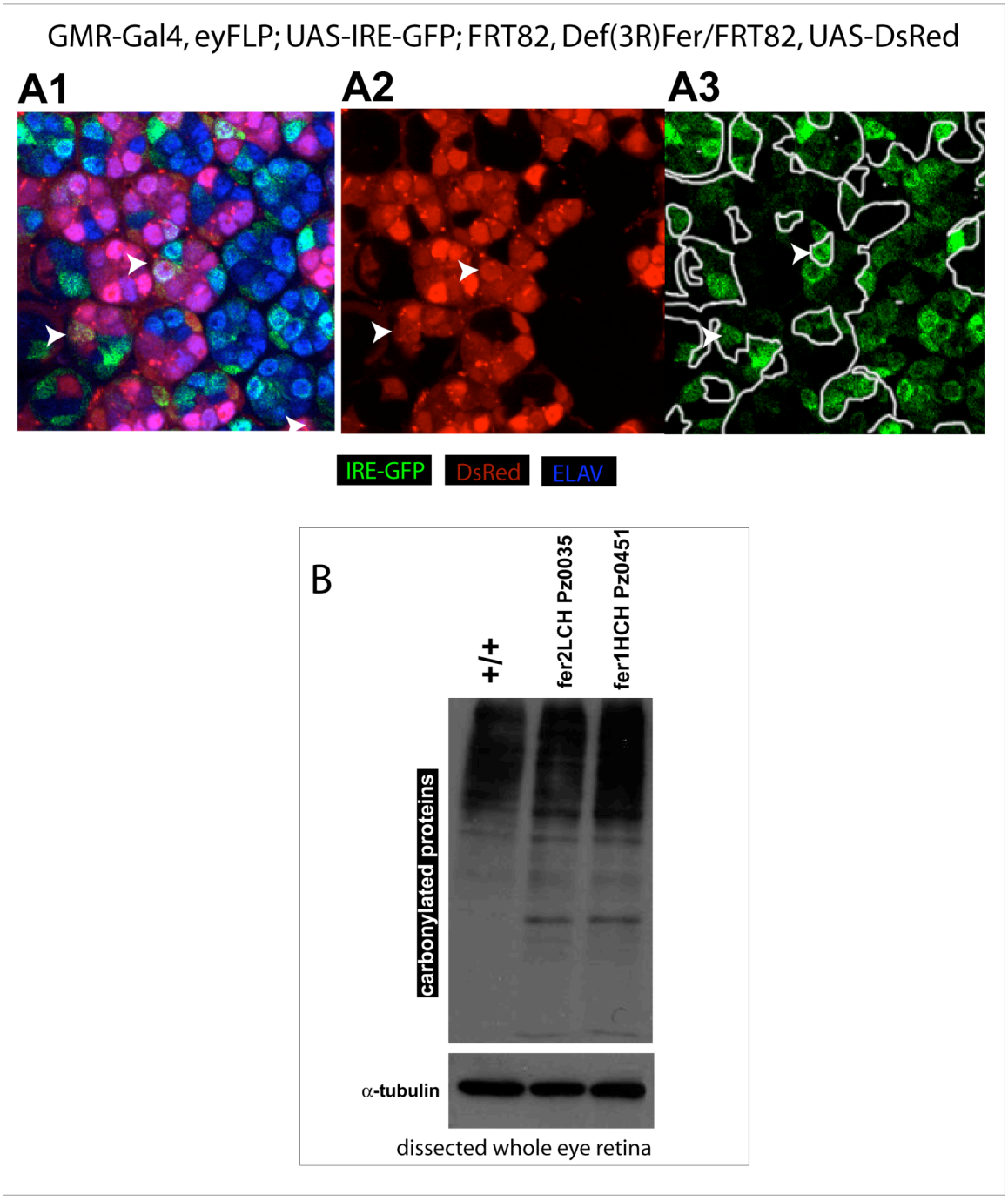

Figure 4.9 Higher Levels of Iron and Oxidative Stress in *ferritin* Mutant Retinas

4.5 Discussion

4.5.1 An *in vivo* Model for Iron-Induced Neuronal Cell Death

The involvement of iron in the progression of retinal and brain neurodegenerative diseases has been primarily suggested by correlative studies showing iron accumulation in a variety of pathological contexts and the attenuation of disease by overexpression of iron chelators and antioxidants. To our knowledge, there are no conclusive reports suggesting a causative role of iron in neurodegeneration via an activation of a caspase-dependent apoptotic pathway. In this study, we show that iron increase due to Ferritin disruption triggers caspase activation and caspase-dependent PRC death. Indeed, we revealed higher levels of labile iron, oxidative stress and caspase activation in terminally-staged PRCs of *ferritin* mutant retinas. Free reactive iron has been proposed to lead to iron-induced oxidative stress via the Fenton reaction. More specifically, ferrous iron, unbound to Ferritin, reacts with H_20_2 and generates very reactive hydroxyl radicals. These in turn selectively cause DNA oxidative damage. In our study, we reveal the presence of DNA damage in the *ferritin* loss-of-function developing retina. Comparatively, previous studies have also seen elevated iron levels and oxidative damage to nucleic acids in the nigral neurons of PD patients (Arosio and Levi, 2002). Moreover, the percentage of neurons expressing

activated caspase-3 was significantly higher in PD brain than control, suggesting that caspase-3 activation is a cause and not a consequence of apoptotic nigral cell death in PD (Hartmann et al., 2000). However, these studies linking iron and caspase activation remain correlative in disease. Our data indicates that unleashed labile iron in Ferritin mutants causatively activates caspase-dependent apoptotic signaling. Strikingly, our data demonstrates that iron overload consequences on PRC integrity are reverted by the overexpression of viral caspase inhibitor P35. These results suggest that the presence of P35 in neurons *in vivo* is protective against various types of iron-induced apoptosis and caspases may be an attractive potential target for preventing neuronal injury associated with elevated iron levels, such as AMD (caused by an excess of iron in the retinal pigment epithelium) (Chen et al., 2009).

As iron induces caspase activation, iron chelation, inherent to Ferritin regulation, conversely protects from apoptosis, by preventing the generation iron-induced oxidative stress. However, still much remains to be learned about how iron sequestration by Ferritin prevents neuronal injury. Studies on the role of the Ferritin complex in neurons have been conducted by studying the consequences of specific dominant-negative mutations, short RNA silencing hairpin as well as by evaluating the anti-apoptotic virtues of an

overexpressed complex on neurodegeneration. Seminal *in vivo* work on the mouse retina further revealed that the disruption of two other iron-binding ferroxidases, Cp and Heph, cause retinal iron overload and photoreceptor neuron degeneration with feature of age-related macular degeneration (AMD) (Hahn et al., 2004b). Here, we have generated the first ever loss-of-function of the entire and primary iron-storage Ferritin complex, genetically eliminating both subunits. We show that *in vivo* Ferritin disruption by genetic deletion affects survival of terminally-staged *Drosophila* PRCs.

A close examination of the retinal phenotype in the developing and adult *Drosophila* retina reveals that cell death features are especially prominent in mosaic ommatidia. We suggest that iron overload in entirely mutant ommatidia for the Ferritin complex may have already collapsed by earlier in development, resulting in an under-estimation of PRC loss in later stages. Indeed, the presence of IOC aggregates at 42-hour pupal stages in the developing retina suggests the demise of mutant PRCs leaving IOC clumps behind. We also propose that the abrupt iron level changes between wild-type and mutant cells may provide an environment prone to cell competition; wild-type tissue may participate in cell death signaling in neighboring *ferritin* mutant tissue. Further work is necessary to address these conjectures and assess the impact of iron overload over the course of pupal developing

in *ferritin*-deficient retinas. Work presented here has broader implication in understanding the specific signaling consequences of iron (de-) regulation and oxidative stress in age-dependent neurodegenerative processes.

4.5.2 JNK: A Missing Link between Iron and Cell Death?

The molecular link between iron-induced oxidative stress and caspase activation is still unclear. However, a likely candidate is JNK, which both responds to oxidative stress regulation and inputs into the apoptotic pathway. Indeed, ROS accumulation has been shown to activate JNK activation in both *Drosophila* and mammals. One proposed model for ROS-induced JNK activation provided evidence for the inactivation of JNK phosphatases of the MKP group by the oxidation of certain of its catalytic residues. Furthermore, JNK has been shown to induce apoptosis (Kamata et al., 2005). Furthermore, JNK is a primary mediator of TNFα-induced apoptosis. In *Drosophila*, the reduction of JNK signals, including DTraf1, rescues Reaper-induced apoptosis (Ryoo et al., 2002).

A link between Ferritin and JNK regulation has already been forwarded. Indeed, FHC upregulation has been shown to significantly decrease ROS accumulation, sustained JNK activation and subsequent cell death in a cell culture model of TNFα-induced apoptosis. Conversely, in the same study, FHC downregulation by RNAi hairpins triggered JNK

activation (Pham et al., 2004). An analysis on JNK activation and involvement in Ferritin-dependent PRC death is testable, by measuring phosphorylated JNK as well as probing the suppressive effects of JNK inhibitors and JNK dominant-negative mutants in *ferritin*-mutant retinas.

4.5.3 A Neuro-Specific and Non-Secreted Isoform of the Ferritin Complex

The *Drosophila* Ferritin complex has been shown to be endogenously expressed in the amnioserosa, and midgut. Our systematic expression analysis confirmed expression of Ferritin subunits in the gut and amnioserosa in embryonic and larval stages. Similar transcriptional expressions of Fer1HCH and Fer2LCH further suggested a co-dependent regulation of both subunits. Insects Ferritins, described as to date, are localized in the secretory pathway of cells; they can thereby secreted from and taken up by cells. Because *Drosophila* has no recognizable transferrin receptor, required for import of iron into cells, it was further suggested that secreted Ferritin could take on the role of transferrin-mediated iron transport. Hence, Ferritin could mediate and regulate the transport of iron from the site of absorption (the midgut) to the sites of utilization by virtually all tissues. Such a Ferritin-dependent mechanism has proven to be a key factor in the response of cells to iron exposure and could be the primary mechanism that

allow insects, notably mosquitoes, to defend against an intracellular iron overload (Dunkov and Georgieva, 2006; Dunkov et al., 2002; Nichol et al., 2002; Nichol and Locke, 1999).

Our gain-of-function analysis using tagged Ferritin constructs helped us to further dissect the secretive properties of Ferritin. Of the two subunits, we reveal that only Fer2LCH possesses secretive abilities in the midgut. Hence, this uncovers a complex mechanism of regulation of the Ferritin complex in the midgut. We propose that secreted Fer2LCH and Fer1HCH dependent on IRP/IRE system together constitute a two-layered coordinate regulatory system for proper Ferritin functionality in the *Drosophila* secretory pathway.

The presence of Ferritin in other tissues, notably the developing retina has yet to be described in insects. Furthermore, secreted insect Ferritins have not been shown to cross the blood-brain barrier (Dunkov and Georgieva, 2006). Hence, to function beyond the blood–retinal barrier, we propose that Ferritin must be expressed in the retina. Using expression and gain-of-function analyses, we have demonstrated the presence of a novel non-secreted Ferritin complex in the developing *Drosophila* retina. In contrast to the midgut, Ferritin subunits cooperatively form a non-secreted hetero-complex in the retina. Fer2LCH in the retina is therefore an

alternative isoform that similarly is restricted to the cytoplasm but does not contain a secretory signal. This implies the existence of unique Ferritin complex and iron regulation in the *Drosophila* nervous system. We make the analogy to the murine Cp, an iron-binding ferroxidase, which is produced by alternative splicing as either as a secreted protein in the blood or a membrane-linked protein in the retina (Patel and David, 1997).

4.5.4 LIP: A Determinant in Cellular Responses

Iron acts as a co-factor in proliferation, differentiation and apoptosis. The cellular labile iron pool (LIP) is a pool of chelatable (unbound to Ferritin complex) and redox-active iron, which is transitory and serves as a crossroad of cell iron metabolism and is dependent on the IRE/IRP regulatory system. Many attempts have been made to analyze the levels of LIP, notably using IRE/IRP bandshift assays (Kruszewski and Iwanenko, 2003). The most successful *in vivo* usage has been mammalian cell culture. For example, IRE-GFP has provided a few insights into iron regulation in the mitochondria in a cell culture-based system (Paradkar et al., 2009). Nevertheless, LIP management remains elusive across all lineages but a many studies point to its important to a variety of cellular responses. We introduce the first transgenic *in vivo* sensor to measure LIP. The iron sensor was successfully used to study the IRE-IRP regulatory system *in vivo* and

iron levels in different conditions. Using the transgenic sensor, we present novel findings regarding iron regulation in the developing *Drosophila* retina.

First, we note that IRP-1A was the only *Drosophila* IRP to show binding to IRE in the developing retina. Indeed, IRP-1B, previously described not to bind to IRE, was able to significantly reduce to non-detectable levels IRE-GFP basal levels, similarly to IRP-1A. Inference on the role of IRP-1B previously came primarily from overexpression studies in the muscle lineage and fat bodies (Lind et al., 2006). However, from our data, we speculate that IRP-1B may have particular importance in the developing retina and possibly in the regulation of iron in the broader *Drosophila* nervous system. This is supported by mammalian studies revealing that IRP-2 and not IRP-1 preferentially dominates post-transcriptional regulation of iron metabolism in the brain (Meyron-Holtz et al., 2004). Our data provides promising leads to further dissect the putative neuro-specific role taken on by IRP-1B in the *Drosophila* retina.

Second, we have identified a stronger basal expression of IRE-GFP in cells arrested at the morphogenetic furrow. A regulatory link between iron metabolism and the cell cycle has previously been evidenced in mammals. Mammalian cyclin inhibitors contain IRE sequences and iron depletion by iron chelating agents affects cell cycle progression in human T lymphocytes

(Lucas et al., 1995; Sanchez et al., 2006). Hence, basal activity of IRE-GFP using GMR reporter confirms a putative role of iron in *Drosophila* cell cycle progression and proliferation.

Finally, iron overload in *ferritin* mutant tissue compared to neighboring wild-tissue was demonstrated using the IRE-GFP sensor. Our studies highlight the distinctive single-cell resolution of the IRE-GFP, which is able to measure iron levels in individual PRCs. We observe a general significant increase in IRE-GFP in mutant PRCs. However, there are discrepancies in iron levels, as indicated by GFP fluorescence. Furthermore, we note occasional wild-type PRCs, juxtaposed to *ferritin*-deficient cells with high levels of iron. We infer the action of an uncharacterized transferrin receptor in the retina, coordinating iron transport, notably in conditions of iron overload, may be in play. Transferrin receptor-mediated iron transport may further alleviate PRC degeneration in *ferritin* mutant retinas. Finally, iron-induced apoptosis is particularly prominent in mosaic ommatidia, most likely to due abrupt iron level differences in juxtaposing PRCs.

In conclusion, the IRE-GFP transgenic further provides the first unique tool to survey iron levels in a variety of cellular processes as well as in response to iron treatment, cellular insults and pathological conditions (Habel and Jung, 2006; Yoo et al., 2004). In *Drosophila*, IRE-GFP presents

itself as an ideal *in vivo* tool to further dissect the endogenous role of iron in a variety of cellular processes, notably proliferation, differentiation, and cell death. Furthermore, the iron sensor will be vital to quantitatively assess the involvement of iron overload and oxidant-induced PRC loss in a variety of established neurodegeneration models, as is discussed in Chapter 5. We propose that the IRE-GFP may help determine what constitutes the varying thresholds, which may dictate iron's differential responses and roles in a time- and tissue-specific manner.

Iron chelation and overload have both been shown to trigger apoptosis so the use of iron for treating disease needs to be carefully administered. Understanding LIP management may prove to be crucial for treating cancer and neurodegenerative diseases. A selective release of iron may be appropriate for killing cancerous cells and for the development of new cancer treatments (Cazzola et al., 1990). Conversely, iron chelators may prove to be potential therapeutic target for neurodegenerative processes (Zecca et al., 2004).

5 FERRITIN AND IRON IN *DROSOPHILA* MODELS OF NEURODEGENERTION

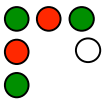

5.1 Summary

Iron must be carefully regulated in all cells, including those in the brain. Increased amounts of iron have been reported in many neurodegenerative disorders. Whether this increased iron contributes to neurodegeneration has been considered controversial. In Chapter 3, we validated a role of Ferritin in late pupal stages and showed that Ferritin mutations lead to caspase-dependent apoptosis in developing PRCs. In this chapter, the objective is to further investigate the survival role of Ferritin in adult PRCs under pathological neurodegenerative conditions. We show that the lack of the iron-storage complex, Ferritin, sensitizes PRCs exposed to a variety of stresses, implicating it as an important anti-apoptotic factor in adult neuronal viability. *ferritin* mutations dominantly enhance *dp53*-induced and aggravate light-induced PRC degeneration. In both conditions, the *ferritin* transcript is upregulated in the adult retina, revealing the importance of iron-storage proteins and iron sequestration in neurodegenerative progression. We further implicate Ferritin and the antioxidant response in ER stress-mediated neuroprotection. Finally, we reveal that free iron levels and *fer2LCH* transcript increases in select models of neurodegeneration in *Drosophila*, suggesting that iron may play a causative role in the neurodegenerative diseases. Work presented here

constitutes preliminary studies linking ferritin with neurodegeneration in the adult *Drosophila* retina.

5.2 Introduction

5.2.1 Iron Overload and Neurodegeneration

High levels of iron are of particular concern or the brain because of iron's intense oxidative metabolism, which generates large amounts of ROS and subsequent neurodegeneration. Iron misregulation has been implicated in a variety of diseases including PD, AD and HD. Patients affected with these types of diseases often display high levels of free iron and low levels of Ferritin in their brains (Dexter et al., 1990; Jellinger et al., 1990; Thomas and Jankovic, 2004). Senescent microglia, a hallmark in AD patients, were shown to be Ferritin-positive and less efficient in iron storage, thereby releasing free iron and causing significant neuronal damage (Lopes et al., 2008). In the brain of patients with PD, iron levels are elevated and the levels of iron-binding proteins are abnormal. Recent studies also suggest that an additional mechanism by which iron might contribute to PD is by inducing aggregation of the α-synuclein, a protein that accumulates in Lewy bodies (Barnham and Bush, 2008; Jellinger et al., 1990). Magnetic resonance imaging reveal increased basal ganglia iron levels in patients with

HD, and further showed that this increase occurred early in the disease process (Bartzokis et al., 1999; Berg and Youdim, 2006).

Mutations in iron metabolism genes have also been shown to cause neurodegeneration. A deficiency in *pantothenate kinase-2* (PANK2)-associated gene, a mitochondrial component important for generating panthothenate kinase, was suggested to trigger neurodegeneration and photoreceptor decline due to an increase in brain iron accumulation (Kuo et al., 2005). Friedrich Ataxia is an autosomal recessive ataxia, characterized by an increase in iron levels in the mitochondria and resulting from a mutation in mitochondrial iron-sulfur cluster *frataxin* gene (Gordon, 2000). Finally, patients with aceruloplasminemia, caused by mutation in ferroxidase *Cp* gene, have retinal degeneration and elevated retinal iron levels (Vassiliev et al., 2005).

Iron has been suspected to contribute to neurodegenerative diseases and neuronal cell death because ferrous (Fe^{2+}) labile iron is known to promote oxidative damage. Iron-binding proteins, primarily Ferritin are ferroxidases that facilitate the conversion of iron from a reactive ferrous (Fe^{3+}) to a stabilized ferric (Fe^{3+}) state. They are considered potent antioxidants, reducing oxidative stress by maintaining iron homeostasis.

5.2.2 A Crosstalk between ER Stress and Oxidative Stress

A common sign of many neurodegenerative diseases is the accumulation and deposits of misfolded proteins that affects various cell signaling systems as well as neuronal connectivity and cell death. Accumulation of misfolded proteins in the cell leads to ER stress. To cope with ER stress, cells trigger a specific response known as the unfolded protein response (UPR). The ER stress/UPR pathway and its function remain controversial, as it has been shown to both induce and protect from cell death. One hypothesis on what governs the switch between anti- or pro-apoptotic effects is the potency of the UPR. Mild UPR activation has been shown to protect murine-derived cells by inducing an antioxidant response. For example, the UPR counteracts TNFα-induced ROS and subsequent cell death by inhibiting glutathione levels (Xue et al., 2005). UPR has been suggested to regulate cell survival by upregulating Heme oxygenase-1 (HO-1), a cytoprotective protein that catalyzes the degradation of heme to iron (Liu et al., 2005).

In this chapter, we further explore the role of iron and Ferritin in a variety of neurodegenerative diseases. First, we analyzed whether *dp53*-induced PRC death and light-induced cell death were sensitized by

mutations in the Ferritin complex. Second, we explored the Ferritin response in ER stress conditions in mature *Drosophila* PRCs. Lastly, using both *fer2LCH*^{Pz0035} transcriptional reporter and the iron IRE-GFP sensor, described in Chapter 4, we assessed Ferritin and iron levels in AD, PD, HD and Tau *Drosophila* models of neurodegeneration.

5.3 Experimental Procedures

5.3.1 Fly Stocks and Genetics

ninaA^{E110V} and *ninaE*^{G6D} were kind gifts from Charles Zuker. *UAS-dp53* and *fer2LCH*^{Pz00035} were described in previous chapters. *UAS-Ab*^{42} (AD model) was a kind donation from Dr. Damian Crowther from the Cambridge Institute for Medical Research. *UAS-Htt* (HD model), *UAS-MJD*$^{tr\text{-}Q78}$ (Warrick et al., 1998) and *UAS-tau*^{R406W} (Wittmann et al., 2001)and *UAS-DJ-1A RNAi* (Yang et al., 2005) were used as models to study neurodegenerative diseases. *aβ*^{42} is an *amyloid beta* plaque of 42 amino acids mimicking *aβ* toxicity in the brains of AD patients. *htt*^{Q128} is the human *huntingtin* cDNA, encoding pathogenic polyQ expansion of 128 CAG repeats leading to abnormal protein conformation, and a hallmark feature in HD . *tau*^{R046W} encodes the human *tau* gene with R406W mutation leads to the accumulation of insoluble *tau* in the neurons of the brain and taupathologies

(Wittmann et al., 2001). *MJD*^{Q78} is a model for Machado-Joseph Disease characterized by the expansion of polyQ-repeats (Q78) leading to large aggregations within the cell (Warrick et al., 1998). *DJ-1A RNAi* silences *DJ-1A*, the *Drosophila* homologue of the familial PD-associated gene *DJ-1*, which plays an essential role in oxidative stress response and neuronal maintenance (Yang et al., 2005). Finally, *dPINK RNAi* down-regulates the *Drosophila P-Ten Induced Putative Kinase 1* (*dPINK*); human *PINK* mutations are linked to the autosomal recessive early onset familial form of PD (Wang et al., 2006).

5.3.2 β-galactosidase and DAPI Staining of Cryosections

Please refer to *Chapter 3, Experimental Procedures, 3.3.2*

5.3.3 Live Fluorescent Imaging of PRCs

Please refer to *Chapter 2, Experimental Procedures, 2.3.2*

5.3.4 Retinal Plastic Sections

Please refer to *Chapter 2, Experimental Procedures, 2.3.3*

5.3.5 Continuous Light Studies

Flies were placed in an illuminated incubator set to 25°C. The fluorescent light inside the door was used as the light source. The distance

from the light source to the fly vials was 12cm. The light intensities to which the flies were exposed ranged from 30 to 40 mW/cm depending on their locations within the vials. Flies were flipped into new fresh vials every 2 days so that the environment remained as constant as possible. Flies aged to 2 and 4 weeks were then sectioned following the Retinal Plastic Section protocol described in Chapter 2, *Exp. Proc 2.32*.

5.3.6 GFP Imaging and Quantification of Adult Eyes

Flies with genotype *GMR-Gal4; UAS-IRE-GFP* were crossed to a variety of neurodegeneration models and adult retina, at 1-day post-eclosure, were imaged using an upright GFP microscope and the Axiocam software. Ten adult eyes were imaged for each genotype and subsequently processed using *ImageJ* software to obtain total GFP fluorescence estimation. The fluorescence value, also referred to as the integrated density, was calculated for a designated outlined area of the eye. GFP fluorescence increase was calculated by normalizing integrated density values to control retina (*lacZ* control) basal fluorescence. Values are presented as percent increase of GFP fluorescence. All bar graphs are displayed with standard error values.

5.4 Results

5.4.1 Ferritin Protects from P53- and Light-Mediated PRC Degeneration

The PRC degeneration phenotype in *ferritin* mutant retinas is not visibly enhanced with age. However, the expression *fer2LCH* transcript increases in PRCs with age (Fig. 5.2G,H). Here, we uncover a novel requirement of Ferritin in adult PRCs subject to a variety of apoptotic stimuli.

The *P53* homolog in Drosophila, *dp53,* has been shown to play a role in radiation-induced apoptosis; it targets the apoptotic machinery via the IAP antagonist *reaper* (Brodsky et al., 2000). The overexpression of *dp53* in *Drosophila* eye disc caused cell death led to a rough eye phenotype (Jin et al., 2000). Furthermore, the ectopic expression of *dp53* under the control of the *rh1* promoter induces a progressive loss of outer PRCs (Mendes et al. unpublished) (Fig. 5.1C). P-element mutation, Pz^{0035}, in the *fer2LCH* locus, enhances *dp53*-induced cell death at day-3 post-eclosure. In contrast, wild-type and $fer2LCH^{Pz0035}$ do not display any missing PRCs (Fig. 5.1A-B). Further strengthening the genetic interaction between *dp53* ectopic expression and *fer2LCH* mutations, we observe an upregulation of the *fer2LCH* transcript at day-1 and day-3, indicated by the same P-element

mutation, which serves as a *lacZ* transcriptional reporter. Compared to control, *dp53*-stimulated retinas display stronger β-galactosidase staining at the level of the outer PRCs, indicative of *fer2LCH* transcript, in horizontal retinal sections. The upregulation is especially significant at day-3 post-eclosure. We note the loss of apical integrity and β-galactosidase-positive PRCs falling basally, indicative of PRC degeneration, stimulated by the overexpression of *dp53*, (Fig. 5.1G-H).

Light damage is a strong inducer of photo-oxidative stress and has also been shown to induce the overexpression of endogenous antioxidants to counteract oxidative stress (Chen et al., 2003). We therefore decided to investigate the sensitivity of *ferritin* whole-eye mutant retinas in constant light conditions. Retinas homozygous $fer2LCH^{Pz0035}$ and $fer1HCH^{Pz00451}$ exhibit PRC in 12-hour light/dark cycles. However this moderate PRC degeneration is exacerbated in constant light conditions (Fig. 5.2B,B',C,C'). This is indicated by the greater PRC loss and the increased presence of larger inter-cellular vacuoles in light conditions. We note that light also leads to retinal degeneration in wild-type retinas (Fig. 5.2A,A') but *ferritin* recessive mutant conditions dramatically enhance PRC degeneration at 2-weeks of age (Fig. 5.2B',C'). Similarly as *dp53* ectopic expression, continuous light exposure causes a strong induction of $fer2LCH^{Pz0035}$ reporter

Figure 5.1 Ferritin Mutations Dominantly Enhance PRC Death Induced by *dp53* Overexpression. Panel **A-D**, **F** and **H** represent retinas at 3-days post-eclosure. Retinal sections in panel **E-F** were taken at 1-day post-eclosure. **(A-D)** GFP live imaging (green) reveals that *dp53*-driven PRC degeneration under *rh1* **(C)** is enhanced by *fer2LCH*^{Pz0035} dominant mutations. Wild-type **(A)** and *fer2LCH*^{Pz0035}/+ heterozygous retinas **(B)** do not exhibit PRC loss. **(E-F)** *fer2LCH*^{Pz0035} *lacZ* transcriptional reporter visualized by X-Gal expression is upregulated when *dp53* is overexpressed in the outer PRCs under *rh1*. *fer2LCH* transcript upregulation is significantly increased at day-3 post-eclosure **(H)** compared to day-1 post-eclosure **(G)**. Conversely, overexpression of GFP (control) under *rh1* leads to little to no detectable upregulation at day-1 post-eclosure **(E)** of *fer2LCH*^{Pz0035} *lacZ* transcriptional reporter and a faint increase at day-3 post-eclosure **(F)**. Yellow arrows indicate X-Gal expression in outer PRCs and size of yellow arrow is proportional to strength of staining. X-Gal expression is represented in blue.

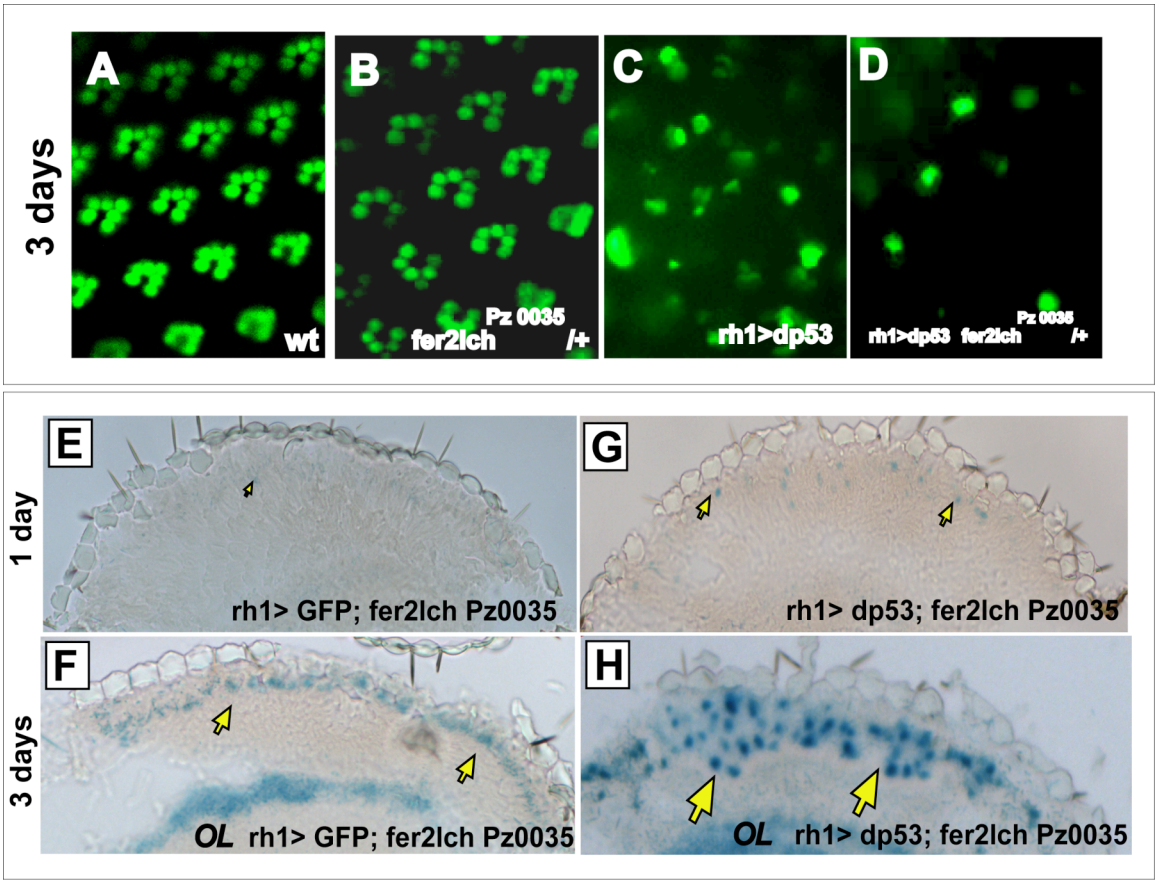

Figure 5.1 Ferritin Mutations Dominantly Enhance PRC Death Induced by *dp53* Overexpression

Figure 5.2 Constant Light Exposure Aggravates Ferritin-Dependent Retinal Degeneration. Retinal sections in panels **A-E**, **G** and **I** were taken at 2-weeks post-eclosure. Panels **H** and **J** were taken at 4-weeks post-eclosure. The red arrowheads highlight ommatidia with missing PRC degeneration and V denotes the presence of inter-cellular vacuoles. In panels **G-J**, yellow arrows point to PRC nuclei with X-gal staining, indicative of *fer2LCH* transcript expression. Size of yellow arrow is proportional to the intensity of X-Gal expression. (**A,C,E**) $fer2LCH^{Pz0035}$ (**C**) and $fer1HCH^{Pz0451}$ (**E**) whole-eye mutant retinal plastic sections reveal moderate degeneration in a normal 12-hour light/dark cycle. The red arrowheads highlight ommatidia with missing PRC degeneration. Wild-type retinas in 12-hour light/dark cycle exhibit no PRC degeneration (**A**). (**B,D,F**) $fer2LCH^{Pz0035}$ (B) and $fer1HCH^{Pz0451}$ (**D**) whole-eye mutant retinas are sensitive to light, as degeneration is aggravated in conditions of constant light exposure. The aggravated phenotype is revealed by an increase in PRC loss (red arrowheads) and large vacuoles (V). Wild-type retinas also exhibit moderate PRC degeneration (red arrowheads, V) in constant light conditions (**B**) but not as severe as in *ferritin* mutant retinas. (**G**, **H**) Flies reared in 12-hour light/dark cycles exhibit a progressive increase in *fer2LCH* transcript from 2-week (**G**) to 4-weeks (**H**). (I**, J**) Constant light exposure significantly upregulates significantly *fer2LCH* transcript at 2-weeks (**I**) and 4 weeks post-eclosure (**J**) compared to flies in 12-hour light/dark cycles (**G-H**). We also note the presence of PRC nuclei falling basally, indicate of retinal degeneration (yellow circles).

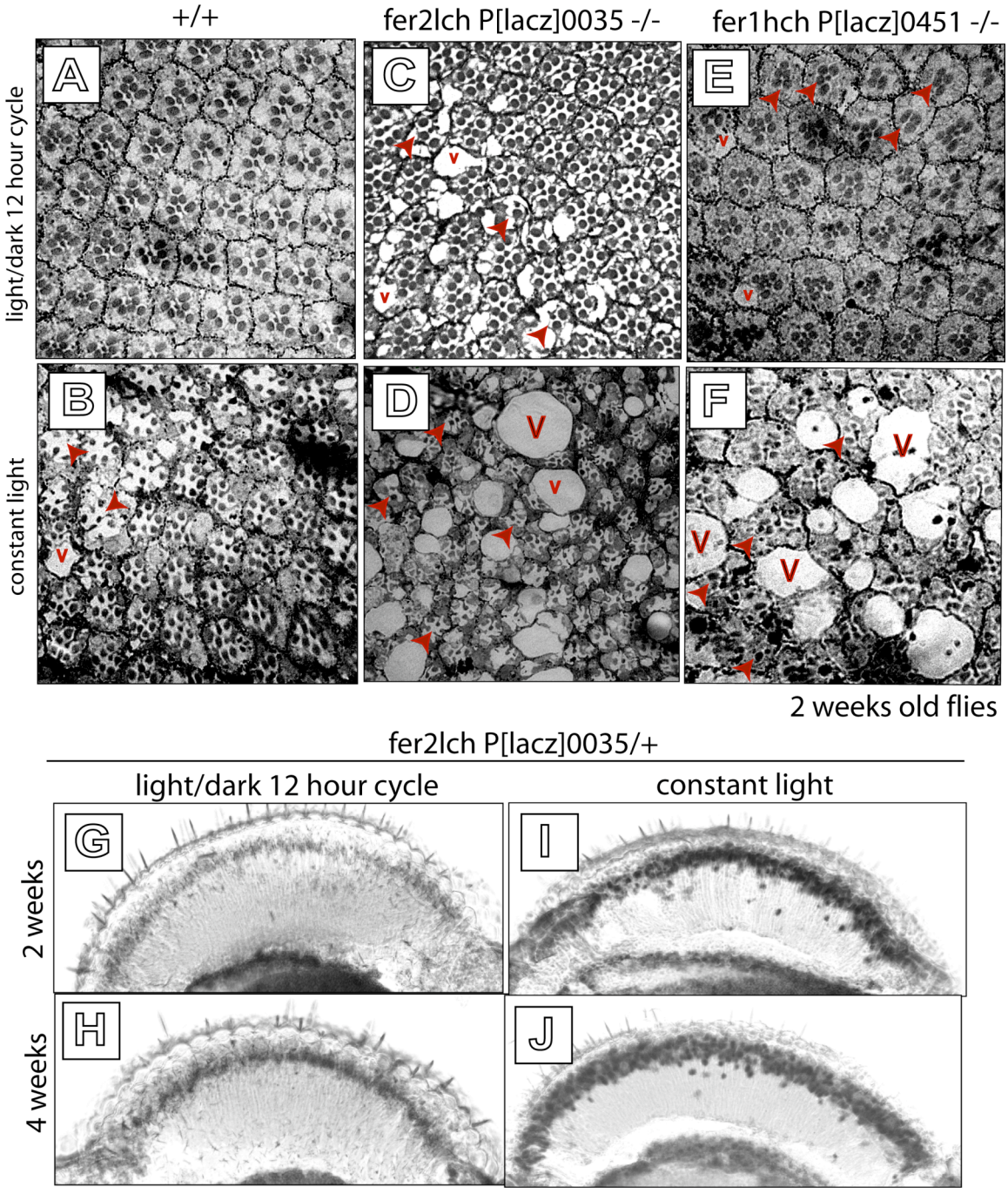

Figure 5.2 Constant Light Exposure Aggravates Ferritin-Dependent Retinal Degeneration

in PRCs in contrast to flies entrained in normal light and dark cycles (Fig. 5.2D,D',E,E').

5.4.2 ER stress Triggers a Ferritin Antioxidant Response

Recent work in the laboratory found that moderate ER stress protects PRC from apoptosis. It has been proposed that the UPR contributes to redox homeostasis after ER stress in mouse fibroblasts. We asked whether an antioxidant response is induced in *Drosophila* PRCs under ER stress. We found increased *fer2LCH* expression in nuclei of PRCs mutant for ER-resident genes, $ninaA^{E110V}$ or $rh1^{G69D}$ (Fig. 5.3A-D). Along with a *fer2LCH* increase, *ninaA* mutations trigger a mild UPR found to protect from a variety of apoptotic stimuli in PRCs including *dp53* and *reaper* (data not shown).

5.4.3 Ferritin and Iron In *Drosophila* Neurodegeneration Models

We further probe the pathological importance of iron-mediated stress in *Drosophila* models of neurodegeneration using the newly devised IRE-GFP sensor to measure the labile iron pool and $fer2LCH^{Pz0035}$ P-element allele to measure *fer2LCH* transcript levels. Adult retinas expressing neurodegenerative disease genes were assessed for an increase in IRE-GFP fluorescence. Compared to control, we observe very slight increases in the labile iron pool in $a\beta^{42}$, tau^{R406W} and *dPINK RNAi* models (Fig. 5.4A,C,F) -

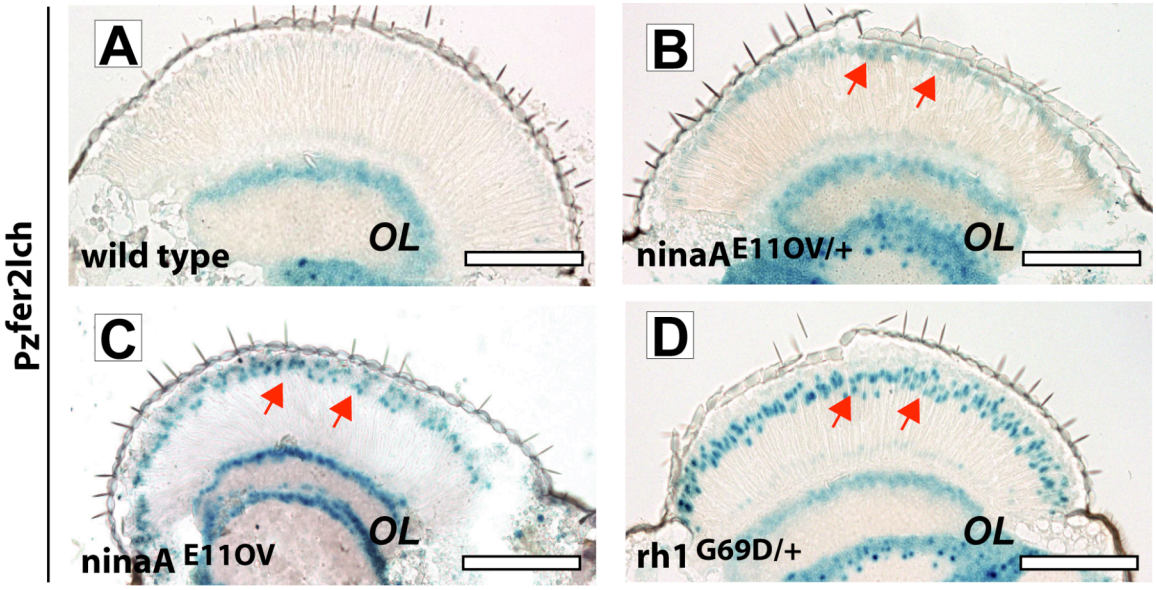

Figure 5.3 ER Triggers Upregulation of *fer2LCH* in Adult Retinas. (A) Horizontal retinal cyrosections stained for nuclear X-Gal (blue) activity. Red arrows point to X-Gal activity in outer PRC nuclei. **(A)** Wild-type retinas with $fer2LCH^{Pz0035}$ reveal little to no detectable X-gal staining in the PRC nuclei. **(B-D)** $ninaA^{E110V}$/+ **(B)**, $ninaA^{E110V}/ninaA^{E110V}$ **(C)**, and $rh1^{G69D}$/+ **(D)** exhibit an increase in X-Gal staining at the level of outer PRC nuclei (red arrows). Scale bar at 100μm. Images courtesy of (Mendes et al., 2009).

Figure 5.4 Ferritin and Iron Deregulation in *Drosophila* Neurodegeneration Models. (A-G) IRE-GFP iron reporter was crossed to neurodegeneration models under GMR and adult retinas were imaged to measure GFP intensity. Significant increases in IRE-GFP were visible in MJD^{Q78} **(D)** and *DJ-1A RNAi* (E) neurodegeneration models. tau^{R406W} **(C)** reveals a moderate upregulation of GFP. LacZ control (G), $a\beta^{142}$ (A), Htt^{128} **(B)** and *dPINK RNAi* **(F)** reveal little to undetectable GFP expression. **(H)** Quantification of GFP levels was performed using *ImageJ* software. Five retinas were used to calculate the average GFP levels and normalized to control (**G**, *lacZ*). Bar graph shows the percent increase of IRE-GFP for each model. Most significant increases are for MJD^{Q78} (~45%) and *DJ-1A RNAi* (~35%). **(I-J)** $fer2LCH^{Pz0035}$ LacZ reporter was crossed to established *Drosophila* neurodegeneration models to assess levels of *fer2LCH* transcript expression. Cryosections were performed on 1-week post-eclosure retinas. Significant increase in *fer2LCH* expression, based on X-Gal activity (red arrowheads), is most noticeable in MJD^{Q78} **(M)** and *DJ-1A RNAi* **(N)** neurodegeneration models. *fer2LCH* transcript is slightly increased in Htt^{128} **(K)** and tau^{R406W} **(L)** models. Control GFP, $a\beta^{142}$, and *dPINK RNAi* models **(I, J, O)** do not exhibit any detectable *fer2LCH* expression increase. Red arrowheads point to outer PRC regions with X-Gal expression. Htt^{128}: Huntington polyQ-128 (**HD** model), *DJ-1A*: **PD**-related gene, $a\beta^{142}$*:* amyloid-beta 142 (**AD** Model); tau^{R406W}, **Tau** pathology; *dPINK*, P-Ten Induced Kinase (**PD** model), MJD^{Q78}, Machado-Joseph Disease (**Ataxia** model).

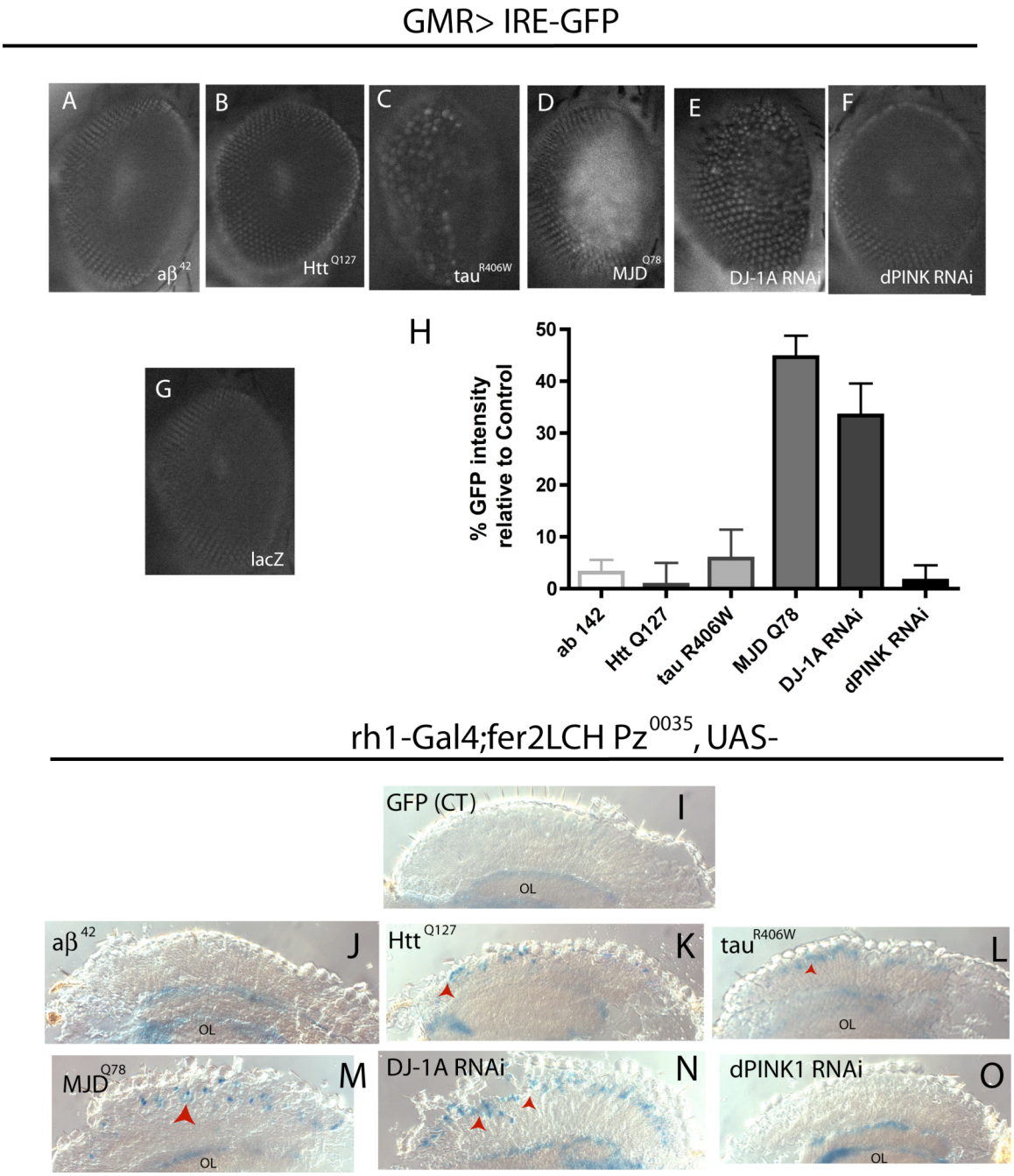

Figure 5.4 Ferritin and Iron Deregulation in *Drosophila* Neurodegeneration Models

and no real differences in htt^{Q178}-expressing flies (Fig. 5.4B); all variations which were not statistically significant (Fig. 5.4H). However, we detect a striking 30-40% approximate GFP increase in iron in *DJ-1A RNAi* and MJD^{Q178} (Fig. 5.4D,E,H) compared to GFP levels in *lacZ* control. A further *ferritin* expression profiling reveals that *fer2LCH* transcript is significantly upregulated in *DJ-1A RNAi*, MJD^{Q178} and htt^{Q127} neurodegenerative models (Fig. 5.4K,M,N).

5.5 Discussion

Previous studies have shown age-related increase in levels of iron in both mammals and *Drosophila* (Massie et al., 1985). As iron augments with age, iron management becomes an increasingly important issue. In this report, we corroborate these studies by revealing an increase in the transcript levels of *ferritin* increase in PRCs with age. We also confirm that iron management becomes increasingly important in stressed conditions as the mutations in the Ferritin complex increase *dp53*- and light-induced PRC degeneration.

It is widely accepted that P53 tumor suppressor restricts abnormal cells by the induction of growth arrest or by triggering apoptosis. Previous studies have shown that P53 is able to modulate iron homeostasis during growth arrest. Indeed, P53 induction decreases IRP binding to IRE, thereby

upregulating IRE-regulated genes such as Ferritin. These studies have suggested that P53 may expand the labile iron pool as part of their non pro-proliferative activity (Zhang et al., 2008). We confirm, using the newly developed IRE-GFP iron sensor, the higher levels of free iron in cells arrested at the morphogenetic furrow in *Drosophila* (Fig. 4.8D). Furthermore, iron-induced oxidative stress has been shown to selectively trigger oxidative DNA damage and it is well established that upon DNA damage, P53 is activated. Links between ROS and P53 has also previously been reported. P53 enhances cellular ROS by enhancing the transcription of pro-apoptotic genes at the mitochondria. However, P53 also protects the genome from oxidation by ROS by upregulating several antioxidant genes, including GPx and mitochondrial manganese (Mn) SOD2 (Hussain et al., 2004). The working model for P53 action is that low amounts of P53 can suppress ROS under normal physiological conditions but high P53 expression promotes ROS-induced apoptosis in conditions of profound pathological stress (Tomko et al., 2006).

Here, we reveal a link between P53 and Ferritin. P53 stimulates the upregulation of *ferritin* transcript, suggesting that the Ferritin complex is an important anti-apoptotic mechanism by which P53-stressed neurons try to relieve neurodegeneration. Collectively, a plausible explanation for the

enhancing effects of *ferritin* mutations on *dp53*-induced PRC death is that differentiated PRC neurons respond to the P53 by increasing their anti-oxidant potential through the up-regulation of a set of defense genes including Ferritin. Therefore, mutations in Ferritin reduce the antioxidant capacities of P53 and enhance its pro-apoptotic activity on PRCs.

Light has been shown to induce changes in gene expression, notably in the mouse retina. Of particular interest, light damage induces the upregulation of antioxidant genes, notably iron-binding proteins, ceruplasmin, methallthionein and HO-1 (Chen et al., 2003; Chen et al., 2004a; Chen et al., 2004b). Therefore, it has been suggested that these genes play a protective role in the acute retinal response to photo-oxidative stress. We reveal an upregulation of Ferritin in constant light conditions and an exacerbated light-induced retinal degeneration in the absence of a functional Ferritin complex. We speculate that the disruption of the Ferritin complex partially shuts down this antioxidant defense mechanism and increases neurodegeneration in the photic injury model. Overall, Ferritin and the broader anti-oxidant defense system are an important anti-apoptotic mechanism to attenuate *dp53*- and light-induced neurodegeneration.

We also found that Ferritin protect from ER stress, a common feature of neurodegenerative diseases. We propose that the inhibition of basal levels

of oxidative stress contributes to the protection of PRC submitted to ER stress. Our data strongly argue that ER stress can limit ROS accumulation by upregulating Ferritin. Intriguingly, ROS has shown to activate ER stress as well. Moreover, neurodegenerative diseases exhibit both ER stress and high levels of iron. Hence, we propose that iron management may be a decisive factor in the pro-survival or pro-apoptotic choice of ER-stress.

High iron concentrations in the brains of patients and the discovery of mutations in the genes associated with iron metabolism in the brain suggest that iron misregulation in the brain plays a part in neuronal death in some neurodegenerative disorders. The disrupted expression or function of proteins involved in iron metabolism increases the concentration of iron in the brain. Increased brain iron triggers a cascade of deleterious events that lead to neurodegeneration (Jellinger et al., 1990). Here, we provide preliminary studies indicating that Ferritin and iron deregulation occurs in select *Drosophila* models of neurodegeneration, notably MJD ataxia model and DJ-1A RNAi PD model. Indeed, we observe an increase in both *ferritin* transcript levels and free labile iron levels in both of these models. Interestingly, research into Friedrich's ataxia—a more common class of triplet mutation disorder than MJD—has identified a key role for metals in the pathogenesis of the disease, where the accumulation of iron in the

mitochondria of Friedreich's ataxia patients initiates a series of free radical mediated chain reaction well known for their ability to exert deleterious mutagenic effects on DNA structure (Gordon, 2000). As for DJ-1A RNAi, a model for PD, studies in mammals and *Drosophila* have revealed cellular accumulation of ROS, organismal hypersensitivity to oxidative stress and ultimately degeneration of neurons in the retina and the brain (Yang et al., 2005). Furthermore, high levels of iron and reduced levels of Ferritin stereotypically occur in PD patients. In our studies, we reveal an increase in iron indicated by IRE-GFP sensor and a significant upregulation of *fer2LCH* in *DJ-1A RNAi* retina. Based on these results, we hypothesize that labile iron may be the originating factor for ROS accumulation and underlining neuronal toxicity in the DJ-1A PD model. The causative role of iron in neurodegeneration is further inferred by the recent discoveries of IREs in the UTR regions of genes involved in disease. Of significance, we highlight recent studies revealing IREs in Alzheimer's APP and Parkinson's ASYN transcripts (Cahill et al., 2008) . Hence, iron metabolism and deregulation is inherently involved in AD and PD progressions.

Collectively, we infer that targeting iron-regulated pathway and using of iron chelators might provide a new approach for treating individuals with neurodegenerative disorders. In a murine model of PD, Ferritin

overexpression and metal chelators have been shown to improve dopaminergic neuronal loss in the substantia nigra of diseased mice (Kaur et al., 2003). Our studies attractively reveal the causative role of iron in pathological neurodegenerative conditions. We further highlight the usefulness of using *Drosophila* genetics, Ferritin mutations and the iron sensor as tools to further dissect iron's contribution to neurodegeneration, and finally settle the longstanding question of whether iron is a cause or merely a consequence of neuro-pathologies.

6 APPENDICES

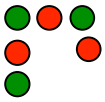

6.1 Choosing Fluorescent Genes: Criteria and Specifications

A substantial part of the work described relies on the development of fluorescent tools for PRC visualization (Chapter 2), the implementation of the genetic screens (Chapter 3) and the study of Ferritin function and iron regulation (Chapter 4,5). mCherry is the best general purpose red-monomer owing to its superior photostability. It was used to tag Fer2LCH and study *in vivo* it localization and regulation in the eye imaginal disc, larval midgut and S2 cells. tdTomato is twice the molecular weight of mCherry but shares a similar photostablity with the latter. However, it stands out for its higher brightness because of tandem dimer of two mRFP1 precursors and is very useful for *in vivo* live imaging. It was used for the red labeling *in vivo* of outer PRCs under *rh1* promoter Finally EGFP is less photostable than red fluorescent genes but harbors high brightness and is widely resorted to for *in vivo* imaging. It was used for tagging Fer1HCH subunit of the Ferritin complex and for the adaptation of the IRE-GFP and *HyPer* sensors to measure the free labile iron pool and hydrogen peroxide levels *in vivo*. The fluorescent proteins are presented in Table 6.1. All red fluorescent proteins were generated by random mutagenesis and dimerization of mRFP precursor.

Table 6.1 Specifications of Available Fluorescent Genes

Propeties of GFP and the RFP variants (derived from Table 1, *Shanar el al. 2005*)

Class	Protein	Excitation (nm)	Emission (nm)	Brightness	Photostability	pKa	Oligomerization
Red	mCherry	587	610	16	96	<4.5	Monomer
	tdTomato	554	581	95	98	4.7	Tandem dimer
	mStrawberry	574	596	26	15	<4.5	Monomer
	J-Red	584	610	8.8	13	5.0	Monomer
	DsRed-monomer	556	586	3.5	16	4.5	Monomer
Green	EGFP	487	509	39	0.69	6.0	Weak dimer

6.2 A PRC Gain-of-Function System: A Construct Gone Leaky!

Initial work in the lab focused on understanding the susceptibility of PRCs to apoptosis. We were particularly interested in understanding mechanisms of apoptosis in mosaic conditions. To achieve this, we developed tools to study loss-of-function of genes in PRCs described in Chapter 2. Moreover, we also attempted to develop gain-of-function PRC-specific tools to overexpress pro-apoptotic in a subset of PRCs. A principal question we sought to address was how does an overexpressed apoptotic stimulus in a subset of PRCs affect neighboring neighboring PRCs within the ommatidia and the integrity of the ommatidial unit? Furthermore, we planned to study the enhancing or suppressive effects of the overexpression in pro-apoptotic genes in the background of mutations of components of the apoptotic pathway. However, the construct was rendered unusable because of an observed leakiness passed the "Termination Codon". We expected that this could be due to the strength of the *rh1* promoter. However, further analysis is necessary to explain the 'leakiness'.

Figure 6.1 The Construct Design For Gain-of-Function Analysis in PRCs. (A) Schematic representation of the construct to generate gain-of-function clones in PRCs. Schematic representation of the construct to generate gain-of-function clones in PRCs. The construct was engineered based on *Flp-out* construct J33R '>hsp70(3')>' kindly provided by *Gary Struhl* (Struhl and Basler, 1993). The construct is composed of a minimal *rh1* promoter, $tdTomato^{ninaC}$ followed with a termination stop codon in between two FRT sites, and the *Gal4* sequence. Under normal conditions, *rh1* drives expression of *tdTomato* in outer PRCs. Upon *FLP* expression, *tdTomato* between two FRT sites is excised leading to the expression of Gal4 and any genes under the control of UAS. If the *Flp-out* construct is crossed to $UAS\text{-}GFP^{ninaC}$, GFP will be expressed in outer PRCs. This constructed was found to be 'leaky'. Indeed, even without FLP expression, Gal4 is weakly expressed suggesting read-through passed the 'termination codon'. The construct was hence rendered unusable for gain-of-function analysis. **(B)** Restriction map of Flp-out construct. **(C)** Flies harboring gain-of-function construct were crossed to *hs-FLP* and *UAS-GFP*. Upon clone induction, patterns in the eye reveal strong GFP expression in wild-type tissue and weak GFP in gain-of-function tissue (due to leakiness of construct) instead of GFP expression <u>only</u> in gain-of-function tissue. '>' refers to FRT sites.

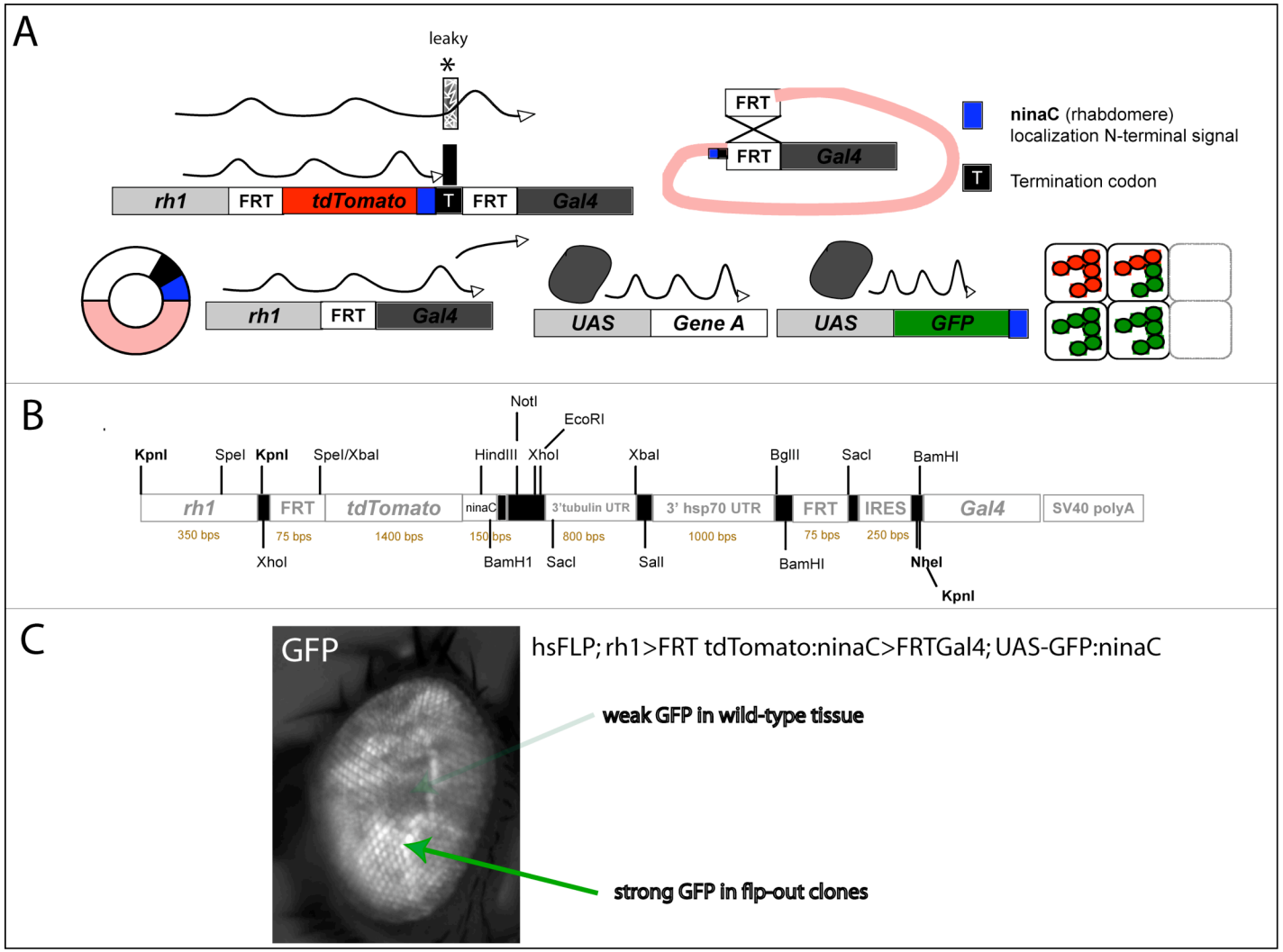

Figure 6.1 The Construct Design For Gain-of-Function Analysis in PRCs

6.3 Data Compilation of the PRC Recessive Screen and Secondary P35 Screen

We provide further details regarding the genetic screens described in Chapter 3. The genetic screen design, time estimation, and potential output were first estimated by performing a pilot screen using the UUCFRG lines on chromosome 3R. Subsequently, the complete PRC recessive screen was completed in collaboration with *Pierre Dourlen*, postdoctoral fellow in the Mollereau Laboratory, under my supervision and initial training during a 3-month summer internship in the laboratory. The Mollereau laboratory is currently completing the last stages of the P35 secondary (approximately 50 genes remaining) and analyzing a select number of candidates using tools described in Chapter 2. We present below the detailed crossing genetic schemes for the both screens performed (Fig. 6.2) and a list of selected examples of phenotypes from the PRC Recessive Screen (Fig. 6.3). We also provide a comprehensive list of 456 UUCFRG FRT-recombined alleles with their PRC phenotypes and corresponding P35 rescue or lack there of (Table 6.2).

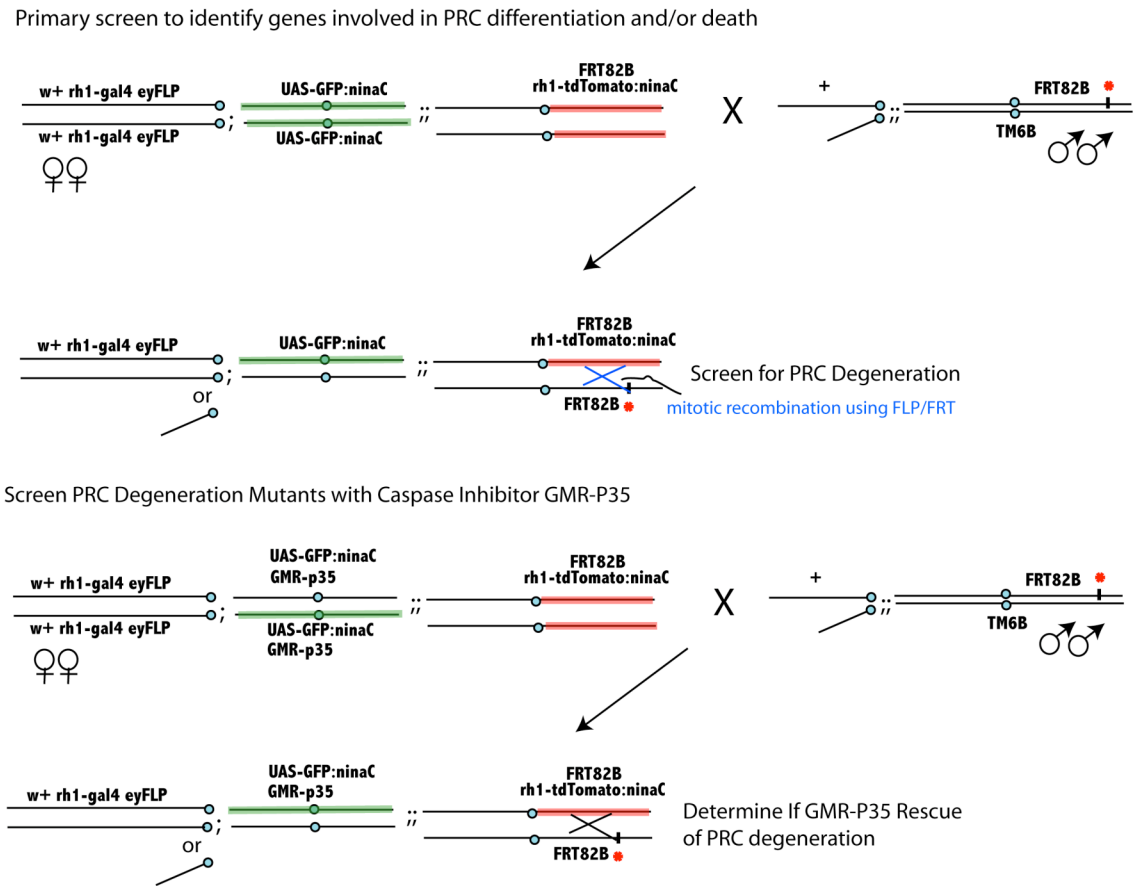

Figure 6.2 A Detailed Genetic Crossing Scheme for Primary PRC Recessive Screen and Secondary P35 Screen

Figure 6.3 Examples of PRC Recessive Screen Phenotypes. We present a selection of PRC phenotypes exhibiting morphology, chirality and expression defects. **(A)** *Glycogen Phosphorylase:* Mutant clones display randomized ommatidia orientation and polarity defects. **(B)** *NFSA (unknown gene):* Mutant clones display ectopic D-V axes (white lines). **(C)** *CG17090:* Mutant clones display *rh1* expression in inner PRCs. **(D)** *Anterior open, yan:* Mutant clones display ectopic outer PRCs leading to 'open configuration' of the ommatidia and loss of trapezoid ommatidial structure. **(E)** *Seven in absentia:* Mutant clones occasionally lead to missing inner PRCs causing 'clump' formation and loss of ommatidial trapezoid structure. **(F)** *Blistered*: Mutant clones display sub-divided rhabdomeres. **(G)** *Hsp70/90:* Mutant clones cause higher expression of *rh1* in PRCs (higher intensity of GFP). **(H)** *COP9 complex:* Mutant clones display abnormal disbanded rhabdomere morphology.

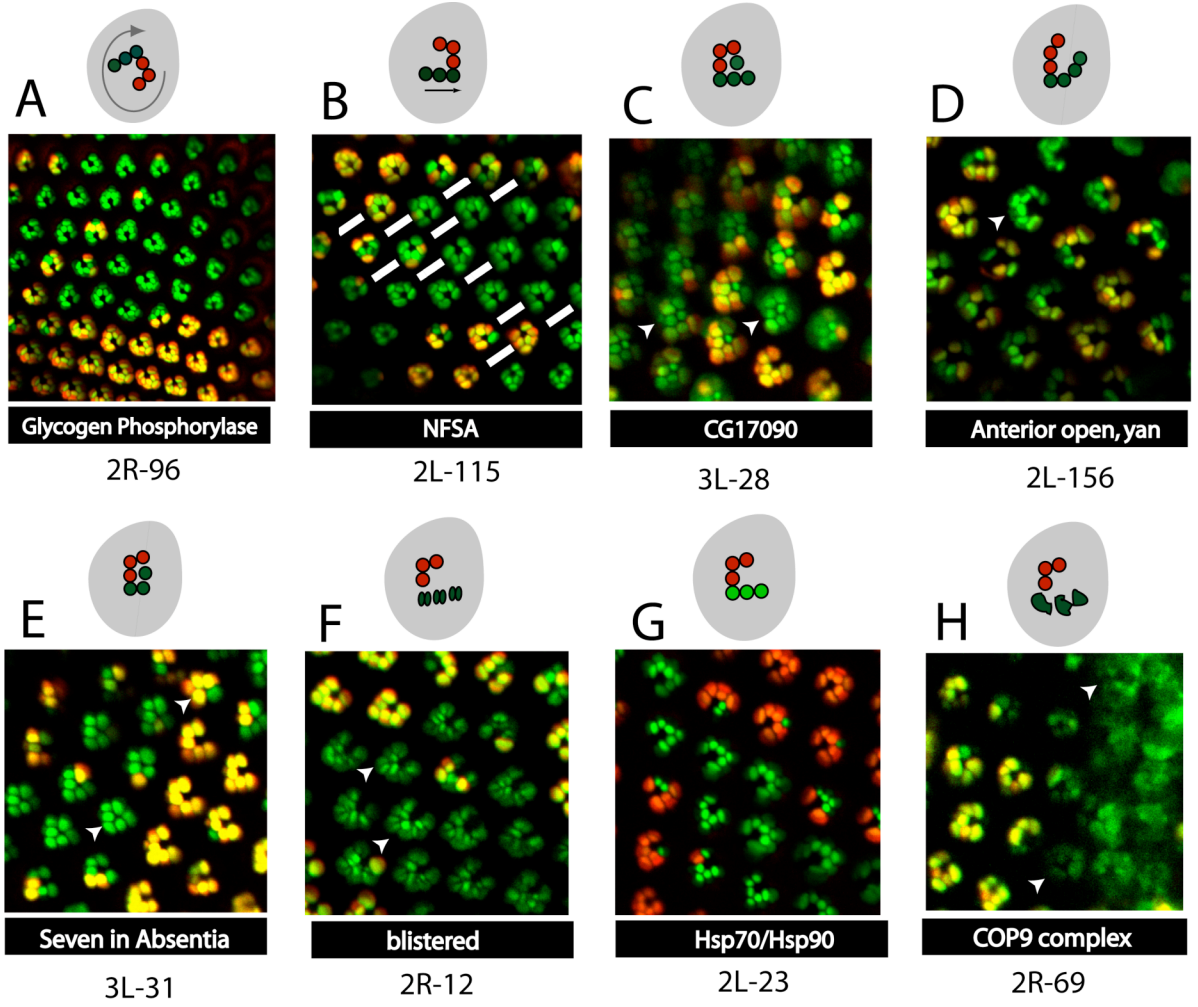

Figure 6.3 Examples of PRC Recessive Screen Phenotypes

Table 6.2 List of FRT UUCRFG Alleles and PRC Phenotypes. We include in tabular form the results of both genetic screens described in Chapter 3. We classify results by chromosomal arm (3L, 3R, 2L, 2R). The DG column refers to 'Degeneration' and indicates the level of PRC degeneration. **–** signifies no PRC degeneration, **+/-** represents both very mild and inconsistent pattern of PRC degeneration phenotypes. **+** represents moderate PRC degeneration phenotypes. The P35 rescue refers to the results from the secondary screen, during which 203 PRC degeneration phenotypes were screened for a P35 rescue. **–** signifies no rescues, **+/-** indicates partial rescue, **+** signifies complete rescue, ***** refers to PRC phenotypes with no degeneration and therefore not screened. Finally, **ND** for Non-Determined refers to genes yet to be screened (approximately 50 ND).

Table 6.2 List of FRT UUCRFG Alleles and PRC Phenotypes (23 pages: 252-274)

RE; UAS-GFP:ninaC; FRT80A, rh1-tdTomato:ninaC X 3L FRT80A UCLA FRT Lines								
Screen Stock #	P-element #	Insertion site	URCFG eye phenotype	Disrupted Gene 1	Disrupted Gene 2	PRC phenotype description	DG	p35 rescue
3L-1	10010	066D	wild-type	NFSA	-	*no defect*	-	*
3L-2	10017	062C02	wild-type	sallimus	-	*slight degeneration/polarity defects*	+	+
3L-3	10154	061C07	wild-type	bantam	-	*no defect*	-	*
3L-4	10156	061F04	wild-type	CG9187	SacI	*no defect*	-	*
3L-5	10162	062E07	wild-type	mishappen	ribosomal protein L8	*no defect*	+	-
3L-6	10166	065D03	wild-type	CG14821	-	*slight degeneration/polarity defects*	+/-	+
3L-7	10168	065E07	wild-type	Cdc27	-	*no defect*	-	*
3L-8	10173	067F01	wild-type	tonalli	-	*no defect*	-	*
3L-9	10175	070A03	rough	capricious	-	*high degeneration/polarity defects*	-	*
3L-10	10178	070C10	rough	26-29kD proteinase	-	*enlarged/deformed rhabdomeres*	+/-	-
3L-11	10186	074C01	wild-type	fringe connection	CG32174	*deformed/shrunken/elongated rhabdomeres*	+/-	+/-
3L-12	10199	078A05	rough	schizo	-	*high degeneration/polarity defects*	++	-
3L-13	10880	069D03-069D04	wild-type	mirror	-	*slight degeneration/deformed rhabdomeres*	+	-
3L-14	11791	077D01-077D02	rough	NFSA	-	*no defect*	-	*
3L-15	12061	061F06	wild-type	mitochondrial acyl carrier protein 1	-	*no defect*	-	*
3L-16	12064	063B11	rough	heat shock protein 83	-	*high degeneration/polarity defects*	++	-
3L-17	12070	065F10	rough	smallminded	-	*slight degeneration/polarity defects*	+/-	-
3L-18	12073	066D12	rough	CG32030 / Fhos	-	*high degeneration/polarity and align. defects*	++	N/A
3L-19	12077	067B05	rough	CG3967	SHC-adaptor protein	*high degeneration/polarity defects*	++	-
3L-20	12088	070F04	rough	trithorax-like	-	*high degeneration/polarity defects*	++	-
3L-21	12091	071E01	wild-type	C7427	-	*no defect*	-	*
3L-22	12092	071E01	wild-type	rhoGAP71E	-	*slight polarity/misorientation defects/occasional missing inner*	-	*
3L-23	12096	072E02	wild-type	mitochondrial ribosomal protein S34	-	*high degeneration/polarity defects*	++	-
3L-24	12097	073A01	wild-type	CG33158	CG32159	*no defect*	-	*

3L-25	12104	075C05-075C06	wild-type	MYPT-75D	-	*no defect*	-	*
3L-26	12105	075E04	wild-type	CG3902	-	*no defect*	-	*
3L-27	12430	074D01	wild-type	organic anion transporting polypeptide 74D	.	*no defect*	-	*
3L-28	12779	061C03	rough	CG17090	.	*inner express GFP/no polarity defects*	-	*
3L-29	12783	065D05	wild-type	sugarless	.	*no defect*	-	*
3L-30	12789	070C05	wild-type	Ral guanine nucleotide exchange factor 2	.	*elongated/shrunken rhabdomeres - age-dependent/slight polarity defects*	+/-	-
3L-31	12818	073D02	wild-type	seven in absentia	Rhodopsin 4	*missing PRCs inner and outer*	+	-
3L-32	12847	066B11	wild-type	Mediator complex subunit 24	-	*no defect*	-	*
3L-33	12854	073E04	wild-type	CG7728	CG6664	*no defect*	-	*
3L-34	13118	075E01	wild-type	ftz transcription factor 1	-	*no defect*	-	*
3L-35	13121	061C03	wild-type	CG17090	-	*age-dependent PRC degeneration/inner PRCs express GFP*	+	ND
3L-36	13203	077C01	wild-type	tribbles	-	*small single-cell clones with missing PRCs*	+	ND
3L-37	13309	070D04	rough	nuclear fallout	-	*PRC degeneration in small clones*	+	-
3L-38	13330	068A05	wild-type	JIL-1	-	*slight degeneration and distorted rhabdomeres*	+	-
3L-39	13338	067D02	wild-type	CG6685	Nedd2-like caspase	*no defect*	-	*
3L-40	13386	073C03	wild-type	Neurotactin	-	*no defect*	-	*
3L-41	13403	062C03	rough	sallimus	-	*slight PRC degeneration/polarity defects*	+	ND
3L-42	13437	066A20	wild-type	sunday driver	CG8268	*no defect*	-	*
3L-43	13452	069C05	rough	Transferrin 2	-	*misoriented PRCs/occasional PRC degeneration/polarity defects*	+	-
3L-44	13471	069C04	rough	sticky	-	*no defect*	-	*
3L-45	13648	074E04	wild-type	Protein on ecdysone puffs	-	*polarity defects*	-	*
3L-46	13677	067B01	rough	Peptidoglycan recognition protein LF	CG4347	*no defect*	-	*
3L-47	13723	064B02	wild-type	Cip4	-	*no defect*	-	*
3L-48	13744	076C04	wild-type	Guanylyl cyclase at 76C	-	*no defect*	-	*

3L-49	13914	064D02	wild-type	CG10630	-	*no defect*	-	*
3L-50	13941	077B02	wild-type	polo	-	*no defect*	-	*
3L-51	13944	066C12	rough	Cbl	-	*high PRC degeneration/polarity defects*	++	ND
3L-52	13979	063E01	wild-type	armitage	-	*no defect*	-	*
3L-53	14025	067F01	wild-type	tonalli	-	*no defect*	-	*
3L-54	14254	069C04	rough	vihar	-	*no defect*	-	*
3L-55	14266	078C02	wild-type	chromosome bows	-	*no defect*	-	*
3L-56	14279	062D07	wild-type	CG9004	-	*slight PRC degeneration*	+/-	-
3L-57	14501	067B06	rough	CG3911	-	*occasional ommatidia with missing PRCs*	+/-	ND
3L-58	14503	061B03	rough,glossy	mitochondrial ribosomal protein L17	-	*deformed rhabdomeres and (age-dependent) PRC degeneration*	++	ND
3L-59	14595	067C11-067D01	rough	CG8108	-	*slght PRC degeneration/polarity defects*	+	ND
3L-60	14607	067B10	wild-type	pathetic	-	*no defect*	-	*
3L-61	14608	061E02	wild-type	trio	CG9205	*no defect*	-	*
3L-62	14649	063B09	wild-type	CG12734	-	*no defect*	-	*
3L-63	14651	070C05	wild-type	Glued	-	*no defect*	-	*
3L-64	14878	070D04	wild-type	nuclear fallout	-	*no defect*	-	*
3L-65	14905	070D02	wild-type	nuclear fallout	nanchung	*no defect*	-	*

RE; UAS-GFP:ninaC; FRT82B, rh1-tdTomato:ninaC X 3R FRT82B UCLA FRT Lines

Screen Stock #	P-element #	Insertion site	URCFG eye phenotype	Disrupted Gene 1	Disrupted Gene 2	PRC phenotype description	DG	p35 rescue
3R-1	10216	083B04	rough	elongation initiation factor 5C	.	*mising inner/polarity defects/occasional missing outer*	+	-
3R-2	10217	083B06	wild-type	Another transcription unit	.	*no defect*	-	*
3R-3	10219	084B02	rough	CG1965	.	*no defect*	-	*
3R-4	10223	085A05	wild-type	Dihydroorotate dehydrogenase	.	*no defect*	-	*
3R-5	10228	085A05	wild-type	CG8036	.	*no defect*	-	*
3R-6	10235	085D11	rough	CG33936	.	*missing PRs but very small clones*	+	-
3R-7	10237	085F08	wild-type	mitochondrial transcription factor B2	CG11722	*no defect*	-	*

3R-8	10244	086E13	rough	C-terminal Src kinase	.	*no defect*	-	*
3R-9	10245	087E04	rough	CG8630	.	*no defect*	-	*
3R-10	10265	087F07	rough	B52 (spliceosome)	.	*high polarity defects/ missing PRCs*	++	-
3R-11	10279	088B01	wild-type	trithorax	.	*no defect*	-	*
3R-12	10290	088E11	glossy	MRG15	.	*polarity defects/high degeneration/shrunken-small rhabdomeres*	++	-
3R-13	10293	088F03	wild-type	CG14867	.	*no defect*	-	*
3R-14	10300	089B11-089B13	wild-type	sarah	.	*no defect*	-	*
3R-15	10301	089B17	wild-type	COP9 complex homolog subunit 5	.	*no defect*	-	*
3R-16	10305	089E11	wild-type	Daughters against dpp	.	*very minor PRC defects*	+/-	+
3R-17	10308	091F12	rough	vibrator	.	*complete missing ommatidia/massive degeneration*	++	-
3R-18	10312	093D09	rough	modifier of mdg4	.	*missing outer and sometimes inner PRCs/very slight polarity defects/newly formed D/V axis*	+	-
3R-19	10320	094C01	rough	Glutamate-cysteine ligase modifier subunit	.	*slight degeneration/polarity defects*	+	+
3R-20	10324	095F10	wild-type	crumbs	CG5715	*deformed/enlarged rhadomeres and occasional missing PRCs*	+	*
3R-21	10335	095F14	wild-type	CG5746	.	*no defect*	-	-
3R-22	10337	096B01	wild-type	CycB3	.	*no defect*	-	*
3R-23	10340	096B20	wild-type	Oligosaccharyl transferase 3	.	*no defect*	-	*
3R-24	10342	096C08-096C09	wild-type	NG	.	*no defect*	-	*
3R-25	10346	098F02	rough	Darkener of apricot	-	*high degeneration/polarity defects*	++	N/A
3R-26	10347	099A05-099A06	wild-type	string	-	*no defect*	-	*
3R-27	10348	099F01-099F02	wild-type	ND	-	*no defect*	-	*
3R-28	10349	099F06	wild-type	prolyl-4-hydroxylase-alpha EFB	-	*no defect*	-	*
3R-29	10350	100A06	wild-type	CG31012	-	*no defect*	-	*
3R-30	10354	100E01	wild-type	hephaestus	-	*no defect*	-	*
3R-31	10753	086E	wild-type	ND	-	*no defect*	-	*

3R-32	10896	090D-090E	wild-type	NG	-	*no defect*	-	*
3R-33	10932	090D-090E	wild-type	NFSA	-	*no defect*	-	*
3R-34	12117	088F03	wild-type	CG14867	-	*missing PRCs in small clones*	+	-
3R-35	12118	084C01	wild-type	Alhambra	-	*no defect*	-	*
3R-36	12124	085C03	rough	neuralized	-	*high degeneration/deformed rhabdomeres/polarity defects*	++	-
3R-37	12130	087D01-087D02	wild-type	NFSA	-	*PR missing in very small clones*	+	-
3R-38	12132	087E08	rough	CG8863	-	*massive degeneration/missing PRCs/polarity defects*	++	-
3R-39	12133	087F06	wild-type	squid	-	*massive degeneration or very small rhabdomeres*	++	-
3R-40	12135	088A04	wild-type	CG9924	-	*deformed/enlarged rhabdomeres/sometimes missing PRs*	+	-
3R-41	12137	088B01	rough	trithorax	-	*no defect*	-	
3R-42	12142	090F10	wild-type	14-3-3epsilon	-	*polarity defects and occasional missing inner PRCs*	+/-	-
3R-43	12143	091F04	wild-type	CG11779	nanos	*no defect*	-	-
3R-44	12144	091F12	rough	vibrator	-	*high degeneration/polarity defects*	++	ND
3R-45	12146	093A04	wild-type	Na pump α subunit	-	*no defect*	-	*
3R-46	12148	093B13	wild-type	Rab-protein 11	-	*no defect*	-	*
3R-47	12151	094A01	wild-type	held out wings	-	*no defect*	-	*
3R-48	12159	097B09	wild-type	scribbled	-	*no defect*	-	*
3R-49	12160	098E01-098E02	wild-type	CG10011	-	*no defect*	-	*
3R-50	12162	099D05	wild-type	similar	.	*no defect*	-	*
3R-51	12167	100D02	glossy	abnormal wing discs	.	*no defect*	-	*
3R-52	12304	089A04-089A05	wild-type	NFSA	.	*occasional missing PRCs*	+	+
3R-53	12410	099E04	wild-type	headcase	.	*enlarged/deformed rhabdomeres but degeneration variable*	-	*
3R-54	12827	090D01	wild-type	couch potato	.	*occasional PR missing*	+/-	-
3R-55	12947	093D04	wild-type	Heat shock RNA ω	.	*no defect*	-	*
3R-56	13052	092B02	wild-type	branchless	.	*no defect*	-	*
3R-57	13306	095C05	wild-type	NG	.	*no clones/cell lethal*	+	-
3R-58	13460	093C01	wild-type	CG5802	.	*slight degeneration/distorted rhabdomeres/age-dependent*	-	*

3R-59	13923	100B07	rough	CG1746	.	*no defect*	-	*
3R-60	13987	095F10	wild-type	crumbs	.	*no defect*	-	*
3R-61	14253	085B03	wild-type	polychaetoid	.	*no defect*	-	*
3R-62	14283	086E14	rough, glossy	CG14713	.	*no defect*	-	*
3R-63	14296	100C06	glossy	γ-coatomer protein	.	*high degeneration/no polarity defects*	++	ND
3R-64	14406	092F13	wild-type	CG17838	.	*no defect*	-	*
3R-65	14488	085D19	wild-type	CG8165	.	*missing PRCs in small clones*	+	-
3R-66	14640	099D03	wild-type	similar	.	*no defect*	-	*
3R-67	14736	093E08	wild-type	NG	.	*no defect*	-	*
3R-68	11483	99FD	wild-type	fer2LCH	.	*moderate PRC degeneration, especially in mosaic ommatidia*	+	+

RE; FRT40A, rh1-tdTomato:ninaC; UAS-GFP:ninaC X 2L FRT40A UCLA FRT Lines

Screen Stock #	P-element #	Insertion site	URCFG eye phenotype	Disrupted Gene 1	Disrupted Gene 2	PRC phenotype description	DG	p35 rescue
2L-1	10357	021F01-021F02	wild-type	NFSA	.	*deformed rhabdomeres*	+/-	+/-
2L-2	10359	035D02	wild-type	escargot	.	*minor defects (very small clones to none sometimes)*	-	*
2L-3	10362	035F01	rough	cropped	.	*missing PRCs, small rhabdomeres, polarity and alignment defects in large clones*	++	-
2L-4	10363	029E04-029E06	rough	raw	.	*ocassional missing PRCs and polarity defects but variable.*	+/-	-
2L-5	10367	021F01	wild-type	capulet	.	*minor to no defects*	-	
2L-6	10375	027C04	rough	Heterogeneous nuclear ribonucleoprotein at	.	*non-recoverable*	N/A	N/A
2L-7	10386	033A01-033A02	rough	crooked legs	.	*no clones (cell lethal)*	N/A	N/A
2L-8	10388	023C01-023C03	wild-type	lilliputian	.	*minor to no defects*	+/-	-
2L-9	10391	038B03-038B05	rough	nebbish	.	*missing PRCs and polarity defects, especially in large clones (small clones unaffected)*	+	-

2L-10	10403	026B02	wild-type	little imaginal discs	.	*slight PRC defects such as missing inner, polarity and deformed PRCs but not consistent*	+/-	-
2L-11	10435	031D01	rough	no mitochondrial derivative	.	*massive degeneration, wild-type seems to be affected (cell non-autonomous?)*	++	+/-
2L-12	10442	021B04-021B05	wild-type	kismet	.	*slight misalignment because maybe missing IOCs but minor defects/one more D-V axis*	-	*
2L-13	10446	033D01-033D02	wild-type	Rab-protein 6	.	*missing PRCs (but no rough eye), sometimes inner PRCs missing*	+	-
2L-14	10448	021B08	wild-type	U2 small nuclear riboprotein auxiliary factor 38	.	*rough eye occasionally. frequent missing outer/inner PRCs especially in very big clones and polarity defects. Small clones, only PR missing*	+	+
2L-15	10451	024E01	rough	turtle	.	*little defects/occasional missing PRCs but IOC mostly affected because misaligned/shifted ommatidia*	+/-	+
2L-16	10453	030A02-030A06	rough	taiman	.	*polarity and alignment defects/fused ommatidia seen once, missing PRCs*	+	-
2L-17	10457	023B06	rough	overgrown hematopoietic organs at 23B	.	*degeneration and rough eye but curiously very little PRC degeneration. Degeneration affects pigment/IOCs. Misalignment*	+/-	+/-
2L-18	10473	025C01	rough	viking	Collagen type IV	*minor to no defects*	-	*
2L-19	10474	023D03	wild-type	Mothers against dpp	.	*very little defects (occasional PRC missing in mosaic ommatidia but not always)*	+/-	-
2L-20	10476	031E01	wild-type	KDEL receptor	.	*minor to no defects*	-	*
2L-21	10479	025C01	wild-type	Collagen type IV	viking	*minor to defects*	-	*
2L-22	10481	023F05-023F06	wild-type	Thor	.	*minor defects*	-	*
2L-23	10483	021B08	rough	Hsp70/Hsp90 organizing protein homolog	.	*Occasionally PRC degeneration (not all eyes) Mutant PRs are brighter, smaller/bigger and sometimes missing*	+	-

2L-24	10490	024D04	rough	echinoid	.	*small clones. Alignment and polarity defects problems No PRC degeneration in large clones but*	+	-
2L-25	10506	026B02	rough	Eukaryotic initiation factor 4a	.	*massive PRC degeneration and smaller rhabdomeres. Very little wild PRCs (cell non-autonomous)*	++	-
2L-26	10508	037C01	wild-type	Dopa decarboxylase	.	*no defects*	-	*
2L-27	10512	038D01	rough,glossy	CG31680	.	*massive degeneration (not many wild-type PRCs). Deformed, missing PRCs. polarity defects in large clones (consq of DG?) but no in small clones.*	++	-
2L-28	10527	026D06-026D09	wild-type	Sec61α	.	*no defects*	-	*
2L-29	10539	033C04	wild-type	Threonyl-tRNA synthetase	.	*massive PRC degeneration, enlarged, smaller rhabdomeres/missing PRCs, no real polarity defects, wild-type eye (very interesting)*	++	+/-
2L-30	10553	027D05-027D07	wild-type	milton	.	*minor to no defects*	-	*
2L-31	10560	026D07-026D08	wild-type	Sec61α	.	*minor to no defects*	-	*
2L-32	10563	032B01	wild-type	porin	.	*minor defects, slight PRC degeneration, frequent 2/3 missing PRCs but some eyes with no defects*	+/-	-
2L-33	10568	028C07-028C09	wild-type	NFSA	.	*moderate PRC degeneration, polarity defects but no alignment defects (eye not rough)*	+	-
2L-34	10573	033F01-033F02	wild-type	CG5776	CG12292	*few missing PRCs and polarity defects in large clones, nearly no defects in small clones*	+/-	-
2L-35	10578	032C01	wild-type	piwi	.	*minor to no defects*	-	
2L-36	10580	023D05	wild-type	v(2)k05816	.	*from few missing PRCs to no defects.*	+/-	+
2L-37	10583	025D05	wild-type	vrille	.	*occasionally 1/2 missing PRCs but almost no defects*	+/-	-
2L-38	10617	031A02	wild-type	Pendulin	.	*minor to no defects*	-	*
2L-39	10625	030E01	wild-type	Bekka	CG5924	*minor to no defects*	-	*
2L-40	10630	021C02	wild-type	expanded	.	*no defects*	-	*

2L-41	10635	031B01	wild-type	maternal expression at 31B	.	*no defects*	-	*
2L-42	10644	031D08	wild-type	Ribonucleoside diphosphate reductase large subunit	.	*minor to no defects*	-	*
2L-43	10645	036C09	wild-type	Aac11	.	*large clones (few wt remaining) - occasional missing PRCs and slight polarity defects*	+/-	-
2L-44	10646	021B03	wild-type	split ends	.	*large clones (few wt remaining) - occasional missing PRCs and slight polarity defects*	+/-	-
2L-45	10651	021C02	wild-type	expanded	.	*very slight defects (almost none)*	+/-	-
2L-46	10652	034A01	wild-type	NG	.	*variable PRC degeneration (50% slight defects, 50% no defects)*	+/-	+
2L-47	10656	029C03	wild-type	A kinase anchor protein 200	.	*very little PRC defects*	+/-	+
2L-48	10665	034D01	wild-type	CG7364	.	*polarity defects/multiple D-V axes*	-	*
2L-49	10669	034A01	wild-type	kekkon-1	.	*no defects*	-	*
2L-50	10673	026D01	wild-type	CG9523	.	*slight PRC defects*	+	-
2L-51	10679	029D04	rough	Angiotensin-converting enzyme-related	.	*high PRC degeneration/small and enlarged rhabdomeres/in large clones sometimes no mutant PRCs left*	++	-
2L-52	10680	032E02	wild-type	CENP-ana	.	*minor to no defects/large clones/sometimes misalignment*	-	*
2L-53	10687	034B07	wild-type	Nnp-1	.	*variable PRC degeneration. Slight to none. Variable polarity defects and clones are often small*	+/-	-
2L-54	10690	034B06	wild-type	NG	.	*frequently missing PRCs*	+	+
2L-55	10692	022C03	wild-type	Glycogen phosphorylase	.	*massive polarity defects/randomized orientation of ommatidia and strong PRC degeneration*	++	-
2L-56	10758	030B	wild-type	ND	.	*very slight PRC defects*	+/-	-
2L-57	10794	024C01-024C02	wild-type	brother of odd with entrails limited	.	*occasioal missing PRCs in mosaic ommatidia but practically no defects*	+/-	-
2L-58	10838	024E05	wild-type	Trehalose-6-phosphate synthase 1	.	*very few missing PRCs*	+/-	+
2L-59	10863	031F04	wild-type	Myosin 31DF	.	*no defects*	-	*
2L-60	10879	039B03	wild-type	CG8678	.	*no defects*	-	*

2L-61	10910	029B02	wild-type	Ribosomal protein S13	.	*minor defects in mosaic ommatidia but practically no defects*	+/-	-
2L-62	10916	022B01-022B02	wild-type	CG17646	.	*very slight degeneration especially in mosaic ommatidia but practically no defects*	+/-	-
2L-63	10919	034E05-034E06	wild-type	rickets	.	*rhabdomeres may be slighly smaller but no real defects*	-	*
2L-64	10959	022C01	rough, glossy	CG31672	.	*small/bigger, deformed, missing PRCs*	++	-
2L-65	10965	023F03	rough, glossy	Pdsw	.	*small, disintegrated, deformed and missing PRCs*	++	N/A
2L-66	10972	027F04	wild-type	mir-275	.	*no defects*	-	*
2L-67	10973	025C01-025C02	wild-type	CG31917	.	*slight (consistent) PRC degeneration*	+/-	-
2L-68	10983	025B01	wild-type	CG3036	.	*no defects*	-	*
2L-69	10985	021B05	wild-type	kismet	.	*no defects*	-	*
2L-70	10986	038A07	wild-type	CG33316	.	*sometimes supernumeray (7) outer PRCs*	-	*
2L-71	10988	031F05	wild-type	Fatty acid (long chain) transport protein	.	*deformed, flattened rhabdomeres and moderate PRC degeneration. Age-dependent.*	+	+
2L-72	10995	036B01	wild-type	Myosin heavy chain	.	*blotches of fluorescence, morphogenesis of rhabdomere defects, some eyes have no clones,*	++	-
2L-73	10996	028B01	wild-type	NG	.	*no defects but occasionally supernumerary PRCs*	-	*
2L-74	10997	027C07	adult non-recover.	Coproporphyrinogen oxidase	.	*damaged rough eye, missing, smaller, bigger, deformed PRCs*	++	-
2L-75	11006	036C09	wild-type	dorsal	.	*no defects*	-	-
2L-76	11014	026D01	wild-type	CG9523	.	*deformed (smaller, larger, elongated) and missing PRCs*	+	-
2L-77	11017	025C06	wild-type	CG5828	polypeptide GalNAc transferase 5	*no defects*	-	*
2L-78	11023	021B05	wild-type	kismet	.	*no defects*	-	*
2L-79	11025	034A05	wild-type	NG	.	*no defects*	-	*
2L-80	11031	035F01	wild-type	heixuedian	.	*variable phenotype (slight PRC loss to no defects*	+/-	-

2L-81	11048	022A03	wild-type	Rieske iron-sulfur protein	.	*PRCs are deformed, enlarged and occasionally missing but moderate PRC degeneration.*	+	-
2L-82	11067	021C04-021C06	wild-type	expanded	.	*no defects*	-	*
2L-83	11071	032A05	wild-type	Ubiquitin conjugating enzyme 2	.	*variable phenotype. Missing PRCs sometimes, other retina no defects*	+/-	-
2L-84	11093	023F03	wild-type	Thor	.	*no defects*	-	*
2L-85	11094	021B07	wild-type	CG3645	.	*slight PRC degeneration but not always*	-	*
2L-86	11096	028E04	wild-type	Basigin	.	*variable phenotype (50% exhibit PRC loss and other 50% no defect)*	-	*
2L-87	11097	029E02	wild-type	Sema-1a	.	*no defects*	-	*
2L-88	11099	021E02	wild-type	CG2807	.	*no defects*	-	*
2L-89	11107	037A01-037A02	wild-type	NFSA	.	*no defects*	-	*
2L-90	11109	032D04	wild-type	Replication factor C 38kD subunit	.	*minor polarity/missing PRCs to no defects*	-	*
2L-91	11115	036A11	rough,glossy	Cytochrome c proximal	CG31782	*massive degeneration, enlarged-deformed mutant PRCs - alignment/polarity defects - sometimes no PRCs left in mutant*	++	-
2L-92	11119	030D01-030D02	wild-type	NG	.	*no defects*	-	ND
2L-93	11121	026F03-026F05	wild-type	CG11098	.	*no defects*	-	*
2L-94	11138	029B01	wild-type	CSN8	CG7627	*no defects*	-	*
2L-95	11139	036A10	wild-type	grapes	.	*minor to no defects*	-	*
2L-96	11147	032D02	wild-type	CG14914	.	*no defects*	-	ND
2L-97	11157	037B08	wild-type	CG10641	CG15168	*no defects*	-	*
2L-98	11166	021C02	rough	ebi	.	*missing/deformed PRCs (rough eye)*	++	-
2L-99	11174	036A04-036A05	wild-type	CG5953	.	*no defects*	-	*
2L-100	11186	021C02	wild-type	RNA polymerase I 135kD subunit	.	*slight PRC degeneration*	+/-	-
2L-101	11191	025D01	wild-type	thickveins	.	*minor to no defects*	+/-	-
2L-102	11212	024C05	rough	lethal (2) k16918	.	*massive PRC degeneration*	++	ND

2L-103	11216	028E04	wild-type	Basigin	.	*missing PRCs esp mosaic ommatidia*	+	ND
2L-104	11218	034A04	rough	Target of rapamycin	.	*"small" rhabdomeres and sometimes missing PRCs (age-dependent)*	+	ND
2L-105	12037	022D01	wild-type	NG	.	*slight PRC degeneration especially in mosaic ommatidia*	+/-	-
2L-106	12042	029F07	wild-type	rolling stone	.	*no defects*	-	*
2L-107	12170	022D04	wild-type	lethal (2) s5379	CG15387	*no defects*	-	*
2L-108	12173	035B08	rough	ND	.	*severe polarity _ alignment defects - "shaken" ommatidia - in small clones, missing PRCs especially (including inner PRCs) + polarity defects*	+	ND
2L-109	12177	035D04	wild-type	heixuedian	.	*minor to no defects*	+/-	ND
2L-110	12178	035F01	wild-type	PRL-1	.	*moderate degeneration - some no defects*	+/-	-
2L-111	12179	035F01	rough, glossy	mitochondrial ribosomal protein L4	.	*missing PRCs/deformed rhabdomeres/alignment defects (age-dependent)*	+	ND
2L-112	12308	021E01-021E02, 026D01-026D02	wild-type	NFSA	.	*normal-deformed-missing PRCs (age-dependent?)*	+/-	-
2L-113	12309	033A01-033A02	rough	NFSA	.	*missing PRCs to minor defects*	+/-	ND
2L-114	12310	023D01-023D02, 029A03-029A05	rough	NFSA	.	*slight PRC degeneration in clones*	+/-	-
2L-115	12384	032A04-032A05	wild-type	NFSA	.	*polarity defects/multiple D-V axes, no alignment problem*	-	ND
2L-116	12385	031E01-031E03	wild-type	NFSA	.	*PRC degeneration in most small clones*	+	ND
2L-117	12386	026B05-026B06	wild-type	NFSA	.	*slight to no defects*	-	*
2L-118	12388	031F01-031F02	wild-type	NFSA	.	*no defects*	-	*
2L-119	12745	021B05	wild-type	kismet	.	*variable phenotype - slight to frequent missing PRCs*	+/-	ND

2L-120	12752	030C05	wild-type	cAMP-dependent protein kinase 1	.	*slight to no defects*	-	*
2L-121	12809	035D04	wild-type	lethal (2) 35Di	.	*moderate PRC dgeenration - frequent missing PRCs - GFP sometimes brighter in mutant clones*	+	ND
2L-122	12894	023C05	wild-type	CG17259	.	*deformed, smaller, missing PRCs*	+	ND
2L-123	13013	025C05	wild-type	polypeptide GalNAc transferase 5	.	*massive PRC degeneration/no PRCs in most eyes*	++	ND
2L-124	13053	035D04	rough	Gliotactin	CG3793	*massive PRC degeneration (almost no PRCs left in clones)- rough eye*	++	ND
2L-125	13087	038C05	wild-type	spire	.	*no defects*	-	*
2L-126	13092	022B04	wild-type	CG7337	.	*slight PRC degeneration (1/2) esp. in mosaics*	+	-
2L-127	13097	026B05	rough	Kruppel homolog 1	.	*massive PRC degeneration (small eye)/no polarity defects*	++	ND
2L-128	13134	035F12	wild-type	chiffon	.	*GFP in inner PRCs but still trapezoidal shape*	+/-	ND
2L-129	13195	030B12	wild-type	glial cells missing	.	*no defects*	+/-	ND
2L-130	13692	032F02	rough	CG6509	.	*(age-dependent) PRC degeneration. Elongated/missing PRCs/polarity alignment defects- some R3-R4 differentiation defects*	+	ND
2L-131	13759	039D01	wild-type	NG	.	*occasional missing PRcs//slight polarity defects*	+	-
2L-132	13805	026D07	rough	CG9535	.	*massive PRC degeneration with no more mutant PRCs even post-eclosure*	++	ND
2L-133	13853	038A01	rough	Leukocyte-antigen-related-like	.	*age-dependent PRC degeneration starting post-eclosure. PRC degeneration increases with time.*	++	ND
2L-134	13942	037E04	wild-type	second mitotic wave missing	CG10189	*occasional deformed or missing PRCs/slight polarity defects*	+/-	ND
2L-135	13957	028C04	wild-type	Laminin B1	.	*no defects*	-	
2L-136	13964	025E05	wild-type	CG7277	CG31989	*high PRC degeneration*	++	ND
2L-137	13970	028E08	wild-type	CG31900	CG8552	*mutant PRCs have small rhabdomeres*	-	ND
2L-138	13976	023B08	rough	CG31694	.	*deformed and missing PRCs/some eyes - no more PRCs/polarity defects*	++	ND
2L-139	13978	038C06	rough	Arc-p34	.	*degeneration in small clones/distorted rhabdomeres/occasional*	+	ND

2L-140	14069	033F01	wild-type	NG	-	polarity/alignment defects/some rough eyes with large clones/slight PRC degeneration	+/-	-
2L-141	14090	022F04	wild-type	out at first	-	missing PRCs with occasional missing inner (clumps)	+	ND
2L-142	14201	032E02	wild-type	abrupt	.	nearly PRCs missing in some eyes. Large clones and non-autonomous effects. In small clones, no mutant PRCs left and rough eye	++	ND
2L-143	14263	030C09	rough	Inositol 1,4,5-triphosphate kinase 1	.	several eyes with no more PRCs. Degeneration (age-dependent)	++	ND
2L-144	14268	022F01	wild-type	decapentaplegic	.	missing PRCs and few eyes with practically no PRCs left. Non-automous effects?	++	ND
2L-145	14351	026B02	wild-type	infertile crescent	.	slight degeneration/polarity defects in small clones	+/-	ND
2L-146	14360	025D04	wild-type	NG	.	occasional missing PRCs	+/-	-
2L-147	14362	026B04	rough	CG9140	.	minor defects but occasional GFP in inner PRCs. Slight/occasional alignment problems	+/-	-
2L-148	14422	038E10	wild-type	CG9328	.	mutant rhabdomeres are lighter/smaller than wild-type. Minor defects - occasional missing inners	+/-	-
2L-149	14450	022F01-022E01	wild-type (rough?)	Rab-protein 5	.	missing inner/outer PRCs/maybe polarity defects	+	ND
2L-150	14465	036C07	rough	CG15141	.	polarity defects in large clones/massive (age-dependent) degeneration - small rhabdomeres	++	ND
2L-151	14473	026B04	wild-type	Kruppel homolog 2	.	occasional very small eyes with roughness but no real PRC degeneration	-	*
2L-152	14486	033D04	rough	CG5446	CG6388	no mutant PRC remaining even in post-eclosure flies. Age-dependent increase in severity.	++	-
2L-153	14493	036C07	wild-type	CLIP-190	.	massive PRC degeneration (rough and very small eyes)	++	-

2L-154	14594	022A06	rough,adult non-recoverable	CG31666	.	*massive PRC degeneration (rough eye)/deformed rhabdomeres*	++	-
2L-155	14597	037B06	wild-type	CG18397	.	*slight PRC degeneration*	+/-	*
2L-156	14633	022D01	rough	anterior open	.	*supernumerary (7) PRCs/missing PRCs occasionally and loss of trapezoid structure*	+	-
2L-157	14694	022F03	wild-type	transfer RNA:tyr1:22Fb	transfer RNA:tyr1:22Fa	*slight to moderate PRC degeneration/mixed phenotypes*	+	-
2L-158	14704	035F01	rough	cropped	.	*massive PRC/compelte ommaditia degeneration/polarity-alignment defect (consq DG?) - maybe cell non-autonomous defects*	++	-
2L-159	14711	036A02	wild-type	Tetratricopeptide repeat protein 2	.	*(age-dependent) PRC degeneration*	+	-
2L-160	14733	023E01	rough	CG3347	.	*slight PRC degeneration/slight polarity defects*	+/-	-
2L-161	14796	023A03	wild-type	Sensitized chromosome inheritance modifier 12	.	*slight PRC degeneration*	+/-	-
2L-162	14898	035B10	wild-type	vasa	.	*missing PRcs especially in mosaic ommatidia*	+	-
2L-163	14906	030C01	rough	NG	.	*(age-dependent) high PRC degeneration*	+	-

RE; FRT42D, rh1-tdTomato:ninaC; UAS-GFP:ninaC X 2R FRT42D UCLA FRT Lines

Screen Stock #	P-element #	Insertion site	URCFG eye phenotype	Disrupted Gene 1	Disrupted Gene 2	PRC phenotype description	DG	p35 rescue
2R-1	10181	057E08-057E9	wild-type	Misexpression suppressor of KSR 2	.	*very slight PRC degeneration*	+/-	-
2R-2	10200	055E01-055E02	rough	overgrown hematopoietic organs	.	*missing and elongated PRCs./no polarity defects*	+	-
2R-3	10358	045F06-046A01	wild-type	Matrix metalloproteinase 2	.	*distorted PRC morphology but no degeneration*	-	*

2R-4	10371	050C23-050D03	rough	mastermind	.	*polarity defects/supernumerary (7) PRCs/PRC degeneration/fused ommatidia*	+	-
2R-5	10373	057B03	wild-type	NFSA	.	*no defect*	-	*
2R-6	10376	051B06	rough	Sec61beta	.	*PRC degeneration and distorted/fuzzy rhabdomeres*	+	-
2R-7	10377	057B15-057B16	rough	shotgun	.	*high PRC degeneration and rhabdomere clumps*	++	-
2R-8	10380	051E01-051E02	wild-type	charlatan	.	*slight polarity defects but no PRC degeneration*	-	*
2R-9	10390	059E03	rough	Death caspase-1	.	*no defect*	-	*
2R-10	10392	060F05	wild-type	Kruppel	.	*no defect*	-	*
2R-11	10406	046B01	wild-type	dacapo	.	*no defect*	-	*
2R-12	10413	060C06-060C07	wild-type	blistered	.	*rhabdomeres seem to be sub-divided but ommatidia remain trapezoidal/ slight PRC degeneration*	+/-	-
2R-13	10420	060A05	wild-type	ken and barbie	Thiolase	*deformed/enlarged/missing PRCs/slight polarity defects*	++	+/-
2R-14	10431	057E01-057E06	wild-type	Syndecan	.	*no defects*	-	*
2R-15	10433	044E01-044E02	rough	lethal(2)44DEa	.	*slight PRC degeneration/small clones*	+/-	-
2R-16	10434	043E09-043E13	rough,glossy	CG30496	CG30493	*enlarged/missing/degenerating PRCs*	++	-
2R-17	10439	053C06-053C07	rough,glossy	Sema-2a	.	*deformed/enlarger/small PRCs/rhabdomeres/polarity defects - small clones*	++	-
2R-18	10447	048C01-048C02	wild-type	walrus	.	*deformed/missing/degenerating PRCs/polarity-alignment defects*	++	-
2R-19	10452	049F07	rough	Valyl-tRNA synthetase	.	*deformed/missing PRCs/polarity alignment defects*	++	-
2R-20	10455	059F01-059F04	wild-type	apontic	.	*no defect*	-	*
2R-21	10460	054E10-054F01	rough	grainy head	.	*polarity defects/inverted ommatidia/ D-V or A-P. no alignment defetcs. Few missing PRCs, sometimes problem of R3/R4 differentiation*	+/-	-

2R-22	10465	051C02	rough	Proteasome p44.5 subunit	.	*slight PRC degeneration/polarity defects but small clones*	+/-	-
2R-23	10467	043E01-043E03	wild-type	Cyt-b5	.	*no defect*	-	*
2R-24	10468	045A03	wild-type	CG8078	.	*no defect*	-	*
2R-25	10470	050C17	rough,glossy	Argonaute 1	.	*missing/deformed PRCs/missing entire ommatidia-massive (age-dependent?- degeneration/polarity defects in large clones (consq. DG)*	++	-
2R-26	10478	047D06-047E01	wild-type	schnurri	.	*no defect*	-	*
2R-27	10482	058F04-058F05	wild-type	jelly belly	.	*no defect*	-	*
2R-28	10485	056D07	wild-type	β-Tubulin at 56D	.	*no defect*	-	*
2R-29	10486	051B01-051B05	wild-type	ND	.	*no defect*	-	*
2R-30	10491	048F01	wild-type	Calmodulin	.	*no defect*	-	*
2R-31	10494	043F01	wild-type	lin-19-like	.	*polarity/alignement defects-inverted ommatidia/slight PRC degeneration*	-	*
2R-32	10497	054B01	wild-type	muscleblind	.	*no defect*	-	*
2R-33	10502	045F01	wild-type	mir-14	.	*no defect*	-	*
2R-34	10510	052D01	wild-type	NG	.	*no defect*	-	*
2R-35	10515	055B09	rough	lola like	.	*rough eye but no PRC degeneration/polarity-alignment defects*	-	*
2R-36	10521	049B01-049B02	wild-type	ND	.	*no defect*	-	*
2R-37	10524	044C02	wild-type	deadpan	.	*no defect*	-	*
2R-38	10525	046B01-046B02	wild-type	CG1648	.	*no defect*	-	*
2R-39	10541	054B01	wild-type	muscleblind	.	*frequently few missing PRCs, especially in big clones*	+	+
2R-40	10542	046F01-046F02	wild-type	gemini	.	*no defect*	-	*
2R-41	10543	049D07	wild-type	Aspartyl-tRNA synthetase	.	*no defect/maybe slight distorted rhabdomeres*	-	*
2R-42	10555	055C09	wild-type	CG30118	.	*no defect*	-	*

2R-43	10557	050E06	adult non-recoverable	Heat shock protein cognate 5	.	*degenerating/missing PRCs*	+	-
2R-44	10559	044F02	wild-type	Ryanodine receptor 44F	.	*no defect*	-	*
2R-45	10564	047A03-047A05	wild-type	midlife-crisis	.	*no defect*	-	*
2R-46	10569	050E01-050E02	wild-type	NG	.	*no defect*	-	*
2R-47	10570	046B04	wild-type	CG12924	CG1665	*missing PRCs in very small clones*	+	-
2R-48	10571	053D14	wild-type	CG6426	.	*no defect*	-	*
2R-49	10574	058D09	wild-type	meiotic W68	.	*no defect*	-	*
2R-50	10577	052C08	wild-type	lethal(2)k05713	.	*no defect*	-	*
2R-51	10612	046B01-046B02	wild-type	CG1472	.	*no defect*	-	*
2R-52	10615	056D09-056D11	wild-type	par-1	.	*no defect*	-	*
2R-53	10619	049E07	wild-type	Suppressor of zeste 2	.	*no defect*	-	*
2R-54	10622	051D05-051D06	wild-type	CG30475	atypical protein kinase C	*no defect*	-	*
2R-55	10629	053C09	rough	Cyclin-dependent kinase 4	.	*no defect*	-	*
2R-56	10631	048B02	wild-type	NG	.	*no defect*	-	*
2R-57	10660	053E02	wild-type	CG33455	vegetable	*no defect*	-	*
2R-58	10661	052A10	wild-type	Vha36	.	*no defect*	-	*
2R-59	10670	054C08	wild-type	CG14480	.	*no defect*	-	*
2R-60	10671	053E04	glossy	CG6796	.	*massive degeneration - inner/outer PRCs missing - polarity/alignment defects (consq of DG)*	++	-
2R-61	10672	054C01	wild-type	lethal (2) k07433	.	*slight PRC degeneration/slight polarity/alignement defects*	+/-	-
2R-62	10674	054E01	wild-type	CG6424	.	*no defect*	-	*
2R-63	10677	043F02	wild-type	ribonuclease H1	drosha	*moderate PRC degeneration/age-dependent?*	+	-
2R-64	10685	054F03-054F04	wild-type	three rows	.	*no defect*	-	*

2R-65	10688	049E06	rough	Posterior sex combs	.	*missing/deformed/enlarged rhabdomeres*	+	-
2R-66	10691	057A08	wild-type	rigor mortis	.	*no defect*	-	*
2R-67	10704	056F06-056F09	wild-type	18 wheeler	.	*no defect*	-	*
2R-68	10759	044F03	wild-type	G protein γ 1	CG13746	*no defect*	-	*
2R-69	10765	043F09	rough	COP9 complex homolog subunit 4	.	*very high PRC degeneration and sometimes very small clones*	++	-
2R-70	10772	050C14-050C17	rough	Argonaute 1	CG33184	*no defect*	-	*
2R-71	10790	044A02	wild-type	Nup44A	.	*no defect*	-	*
2R-72	10795	050C06-050C07	wild-type	CG6543	.	*no defect*	-	*
2R-73	10801	056C04	wild-type	coracle	.	*no defect*	-	*
2R-74	10803	053F08	wild-type	Glutathione S transferase S1	.	*no defect*	-	*
2R-75	10830	046C01	wild-type	CG12744	.	*no defect*	-	*
2R-76	10840	045F01-045F02	wild-type	NFSA	.	*no defect*	-	*
2R-77	10876	053D13-053D15	wild-type	NFSA	.	*no defect*	-	*
2R-78	10882	045F04	wild-type	CG1814	.	*no defect*	-	*
2R-79	10948	052E07	wild-type	spinster	.	*in small clones, missing PRcs. In large clones, no defects*	+/-	-
2R-80	10951	053D14	wild-type	Dek	.	*no defect*	-	*
2R-81	10953	057A06	wild-type	lethal(2)05510	.	*no defect*	-	*
2R-82	10955	054E01	wild-type	CG6424	.	*no defect*	-	*
2R-83	10982	045F01	rough	mir-14	.	*no defect*	-	*
2R-84	10990	046F06	wild-type	Hormone receptor-like in 46	.	*no defect*	-	*
2R-85	10992	057E08	wild-type	Misexpression suppressor of KSR 2	.	*no defect*	-	*
2R-86	10998	049D06	rough	bicaudal	.	*no defect*	-	ND
2R-87	11001	056F11	wild-type	Ate1	.	*no defect*	-	*
2R-88	11005	053F8	wild-type	Glutathione S transferase S1	.	*very slight PRC degeneration*	+/-	-
2R-89	11010	054B16	wild-type	methuselah-like 3	CG10764	*occasional mising PRCs*	+	-

2R-90	11015	045D04	rough	wunen-2	wunen	*masive degeneration and polarity defects*	++	+/-
2R-91	11021	054C01-054C02	rough,glossy	NFSA	.	*massive degeneration but small clones/no apparent polarity defects*	++	-
2R-92	11022	054E01	wild-type	CG6424	.	*no defect*	-	*
2R-93	11041	053E04	wild-type	Apaf-1-related-killer	.	*no defect*	-	*
2R-94	11042	054F01	wild-type	olf186-F	.	*slight polarity defects/occasional supernumerary (7) PRCs*	-	*
2R-95	11050	051B01	rough	tout-velu	.	*very slight PRC degeneration (yet rough eye phenotype)*	+/-	-
2R-96	11058	050E08	wild-type	Glycogen phosphorylase	.	*no defect*	-	*
2R-97	11059	045D05	wild-type	preli-like	.	*no defect*	-	*
2R-98	11066	053D11-053D13	wild-type	NFSA	.	*no defect*	-	*
2R-99	11072	052F04	rough	Lissencephaly-1	.	*missing and enlarged PRCs in small clones/(maybe) polarity defects*	+	-
2R-100	11074	058D04	wild-type	CG13506	.	*no defect*	-	*
2R-101	11077	053B01-053B02	wild-type	Kinesin heavy chain	.	*deformed and slight PRC degeneration*	+/-	+/-
2R-102	11084	053A03-053A04	wild-type	Kinesin heavy chain	.	*no defect*	-	*
2R-103	11090	045B03	rough	CG8026	.	*no defect*	-	*
2R-104	11095	053D14	wild-type	Dek	.	*no defect*	-	*
2R-105	11098	053E04-053E05	wild-type	Prosap	.	*no defect*	-	*
2R-106	11104	057C03	wild-type	X box binding protein-1	.	*no defect*	-	*
2R-107	11122	049F04	rough	Cap-G	tripeptidyl-peptidase II	*massive PRC degeneration/enlarged and smaller rhabdomeres*	++	-
2R-108	11128	054B04-054B05	wild-type	NFSA	.	*no defect*	-	*
2R-109	11133	048A03	rough	lethal (2) k14708	.	*no defect*	-	*
2R-110	11142	049B07	wild-type	unchained	.	*no defect*	-	*
2R-111	11144	050C19	wild-type	Cysteine proteinase-1	.	*no defect*	-	*
2R-112	11145	052E04	wild-type	Dystroglycan	.	*no defect*	-	*
2R-113	11150	053F02	wild-type	fat-spondin	teflon	*very small clones with occasional mising PRCs and polarity defects*	+/-	-

2R-114	11156	043B02	rough	costa	.	*high PRC degeneration/alignment and polarity defects/ occasional (7) supernumerary PRCs*	++	-
2R-115	11159	044F03	rough	Dynamitin	.	*very slight to no PRC degeneration/small clones*	+/-	-
2R-116	11161	057A05-057A06	wild-type	bancal	.	*very small (or no) clones with missing PRCs and polarity defects*	+	+
2R-117	11199	042E01	wild-type	visceral mesodermal armadillo-repeats	.	*very small (or no) clones with occasional PRC missing/cell-non autonomous effects*	+/-	-
2R-118	11202	051A04	rough	cleavage and polyadenylation specificity factor	.	*no defect*	-	*
2R-119	11207	044F12	wild-type	baboon	.	*alignment defects and divided/fused ommatidia. polarity defects in large clones/no missing PRCs*	-	*
2R-120	11208	056D07	wild-type	Ribosomal protein L11	.	*slight PRC degeneration in small clones*	+/-	-
2R-121	11217	058F04	wild-type	CG13512	.	*no defects*	-	*
2R-122	11225	049A09	rough	fused lobes	.	*occasional missing PRCs with slight alignment/polarity defects*	+/-	+
2R-123	12056	053C09	wild-type	Cyclin-dependent kinase 4	.	*no defect*	-	*
2R-124	12059	057A06	rough	bancal	.	*polarity and alignment defects with occasional missing and/or disorganized PRCs*	+/-	-
2R-125	12183	044A04-044A05	rough	NFSA	.	*polarity/alignment defects. Frequently supernumerary PRCs (7/8). Ommatidia lose trapezoid configuration. Very slight PRC*	+/-	-
2R-126	12184	044C01-044C02	wild-type	NFSA	.	*no defect*	-	*
2R-127	12188	050E04	rough,glossy	CG8479	.	*massive PRC degeneration, sometimes completely missing*	++	-
2R-128	12191	055C09	wild-type	scruin like at the midline	.	*no defect*	-	*
2R-129	12194	059C03	wild-type	lethal (2) k09913	.	*no defect*	-	*

2R-130	12196	059E01	wild-type	NG	.	*no defect*	-	*
2R-131	12198	060A16	wild-type	Peptidylglycine-α-hydroxylating monooxygenase	.	*missing or supernumerary PRCs/deformed ommatidia - split or fused ommatidia, slight polarity*	+/-	-
2R-132	12199	060B11-060B12	wild-type	Zinc finger protein RP-8	.	*slight polarity defects*	-	*
2R-133	12200	060C01	rough	spaghetti	.	*no defect*	-	*
2R-134	12201	060B05	adult non-recoverable	twinstar	.	*no defect*	-	*
2R-135	12204	060D03	wild-type	CG4589	.	*multiple D/V axes/polarity defects*	-	*
2R-136	12205	060D14	wild-type	Matrix metalloproteinase 1	.	*no defect*	-	*
2R-137	12206	060D05	rough,glossy	Nucleosome remodeling factor - 38kD	.	*missing and deformed PRCs/slight polarity defects*	+	-
2R-138	12208	060E05	wild-type	CG9047	.	*very slight PRC degeneration*	-	*
2R-139	12347	050C23	rough	mastermind	.	*deformed rhabdomeres but little PRC degeneration/slight polarity defects*	+/-	+
2R-140	12382	045D03-045D04	wild-type	wunen	.	*PRC degeneration/cell non-autonomous defects but sometimes no PRC degeneration - heterogenous*	+/-	+
2R-141	12387	048F01-048F06	rough	NFSA	.	*no defect*	-	*
2R-142	12389	060A11-060A12	wild-type	Calcium ATPase at 60A	.	*no defect*	-	*
2R-143	12391	052D09-052D10	wild-type	NFSA	.	*no defect*	-	*
2R-144	12394	058E03-058E05	wild-type	NFSA	.	*no defect*	-	*
2R-145	12444	054E09	wild-type	Ubiquitin conjugating enzyme 10	.	*no defect*	-	*
2R-146	12485	059A03	wild-type	jitterbug	.	*very slight PRC degeneration*	-	*
2R-147	12771	054B07	wild-type	Proteasome α subunit	.	*GFP expression very low in clones/affecting rh1 expression?*	-	*
2R-148	12849	050B06	rough	tripeptidyl-peptidase II	Cap-G	*(age-dependent) varying degree of PRC morphology (enlarged, small, missing)*	-	*

2R-149	12857	047D01	wild-type	pipsqueak	.	*no defect*	-	*
2R-150	12911	043B02	wild-type	CG11107	.	*no defect*	-	*
2R-151	13179	060F05	wild-type	Tyrosine kinase-related protein	.	*no defect*	-	*
2R-152	13212	044B03	rough	Pabp2	.	*(age-dependent) degeneration with varying degree of PRC degeneration*	+	-
2R-153	13265	049D07	rough	Aspartyl-tRNA synthetase	.	*(age-dependent) degeneration with missing and deformed PRs/polarity defects*	+	-
2R-154	13266	044E03	wild-type	conserved membrane protein at 44E	.	*no defect*	-	*
2R-155	13298	050E01	rough	combgap	.	*small clones/PRC degeneration - missing outer and inner PRCs*	+	-
2R-156	13335	044A04	rough	cul-4	.	*slight PRC degeneration/others no PRC degeneration - heterogenous*	+/-	-
2R-157	13519	057F08	wild-type	Tim10	.	*(age-dependent) slight PRC degeneration/no polarity defects*	+/-	-
2R-158	13673	060D14	wild-type	Matrix metalloproteinase 1	.	*no defect*	-	-

END

6.4 Design of Fly *HyPer*: An Genetically-Encoded H_20_2-sensor

In an effort to measure oxidative stress levels in *ferritin* mutants, we generated a genetically-encoded hydrogen peroxide sensor, *HyPer*, under the control of a UAS promoter in *Drosophila*. The sensor is based on *circularly permuted YFP* (*cpYFP*) and was previously shown to work in mammalian cells upon H_20_2 administration. Upon Apo2/Trail-induced apoptosis, *HyPer* was also able to detect an increase in H_20_2, which occurs in the cytoplasm in parallel with a drop in the mitochondrial transmembrane potential and a change in cell shape (Belousov et al., 2006). We have demonstrated the ability of the *HyPer* sensor to work in *Drosophila* tissue and thus, present the first *in vivo Drosophila* oxidative stress sensor. Upon 0.5μm H_20_2 addition, we detect about a 2-fold increase in *HyPer/cpYFP* fluorescence. However, in loss of function *ferritin Def(3R)Fer* clones, we did not detect any difference in H_20_2 levels compared to neighboring wild-type and heterozygous tissue (Fig. 7.2C). We infer by this negative result that Ferritin mutants generate other sub-types of ROS. Indeed, labile iron generated by the disruption of the Ferritin complex reacts with H_20_2 to generate hydroxyl radicals via the Fenton reaction. We confirm this as the protein carbonylation assay (Fig. 3.5) detects higher levels of oxidative events in whole-eye *ferritin* mutant retinas. While not applicable to the Ferritin

analysis, the *HyPer* sensor will undoubtedly be extremely useful to further study the endogenous role of oxidative stress in a variety of cellular process and developmental paradigms. It will also serve as an invaluable sensor for the detection of oxidative stress in a variety of cell death paradigms. For example, it may be very useful to address the role of the mitochondria (*Chapter 1, section 1.7*), the main determinant of oxidative stress, in *Drosophila* ectopic and developmental apoptotic paradigms.

Figure 6.4 *HyPer*: A Genetically-Encoded H_20_2 Sensor. (A) Schematic representation of *HyPer* engineered by inserting a *circularly permuted YFP* (*cpYFP*) into the H_20_2-sensing domain of prokaryotic (*E.coli*) *OxyR* peroxide sensor (Belousov et al., 2006). *HyPer* was inserted into a pUAST vector and used to assess H_20_2 levels in *Drosophila* tissue endogenously and under a variety of physiological and *ferritin* mutant conditions. **(B)** GMR>*HyPer* dissected eye imaginal discs reveal basal *HyPer* fluorescence (before). Administration of 0.5μm H_20_2 leads a eye disc cultured in S2 medium leads to an approximate 2-fold HyPer increase (after). Time-lapse imaging before (0-seconds) and after (10-seconds) further reveals *HyPer* increase upon addition of 0.5μm H_20_2. **(C)** Live-imaging of *Def(3R)Fer* clones (absence of red) and HyPer (green) reveals no apparent difference in HyPer (H_20_2) levels in wild-type versus mutant tissue. DsRed (red) denote wild-type and heterozygous tissue while absence of red marks the mutant tissue. **(D)** Expression of *HyPer* under the control of ubiquitous promoter, *arm-Gal4*, reveals endogenous patterns of oxidative stress in the third-instar larval eye disc and brain. In the eye disc, H_20_2 levels determined by *HyPer* seem to be increased in PRC region (black arrow). In the larval brain, punctuate fluorescence is observed in the mushroom bodies (white arrow) and in neurons of the ventral cord.

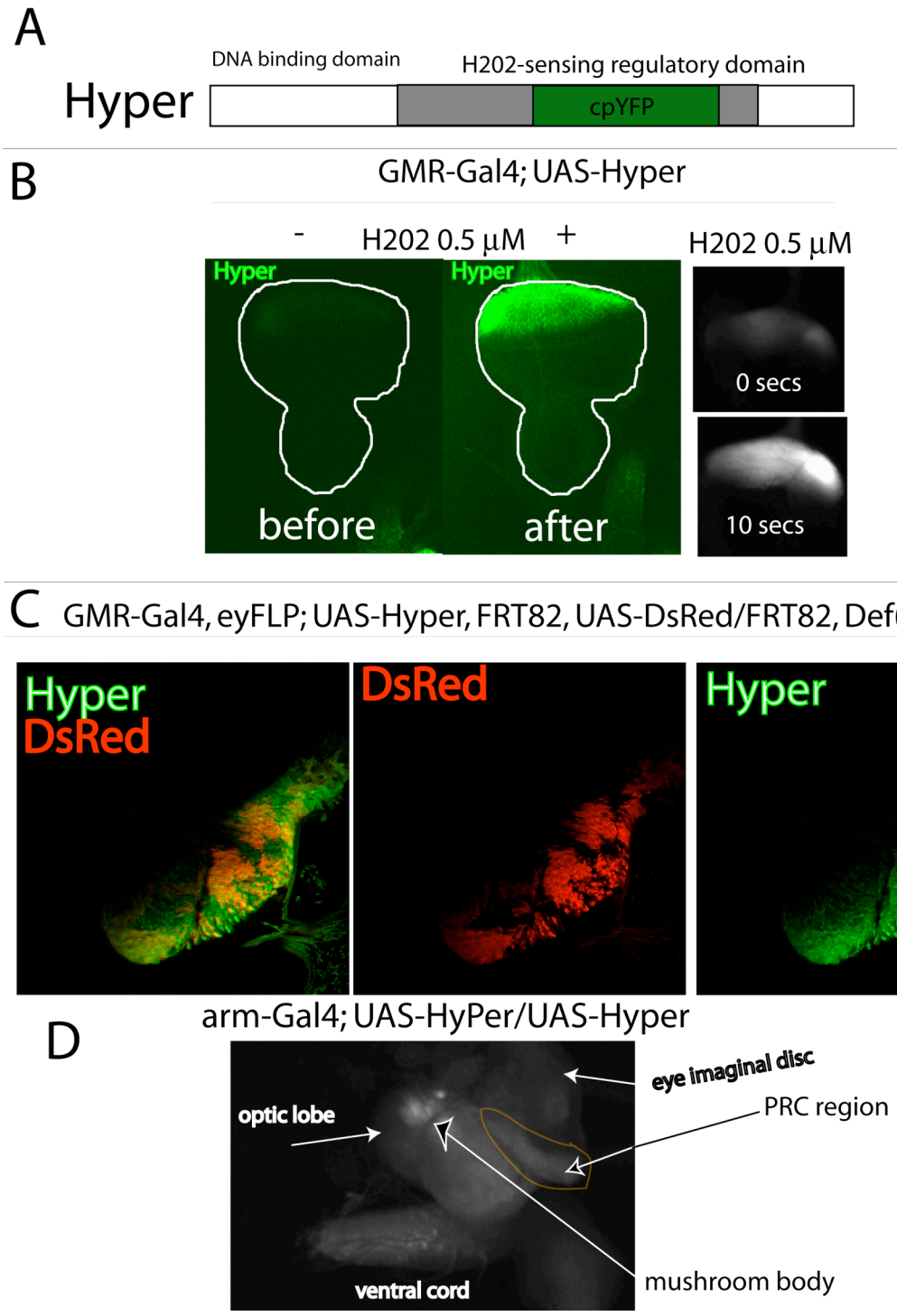

Figure 6.4 *HyPer*: A Genetically-Encoded H_20_2 Sensor

6.5 Larva with *fer2LCH* Mutations Display Evidence of Iron Accumulation

Flies with genotype *fer2LCH*$^{Pz:0035}$ recovered from the PRC recessive as mutants displaying moderate PRC degeneration, undergoes embryonic lethality in a homozygous state. However, in the preliminary phases of characterization of this P-element mutant, we observed first-instar 'escapers' that displayed distinct morphological features. Indeed, reddish-black aggregates, predominantly at the posterior edge of the larva, were observed and were hypothesized to be iron depositions. Further analysis using methods such as *Perl's* iron staining is required for demonstrating excess iron in homozygous *ferritin* mutant larva (Perl and Good, 1992).

Figure 6.5 Homozygous *fer2LCH Pz*^{0035} Larva Escapers. First instar 'escapers' display distinct morphological features in *fer2LCH Pz*^{0035} mutants. Reddish-black aggregates are predominantly at the posterior edge of the larva. Mutant larva also display mobility defects and die before reaching second or third instar larval stages.

6.6 PRC Degeneration Phenotype in *SOD* Null Mutants

In parallel to our analysis of *ferritin* mutants in PRCs, we analyzed other antioxidants to determine if they also displayed PRC degeneration. Previous studies have established that homozygous null mutation of *SOD*, SOD^{n108}, leads to higher levels of ROS, notably superoxide anions. We further reveal PRC degeneration and morphological defects using GFP live imaging. Similar mutations in *SOD* have been shown to occur in human Familial ALS (FALS), and have thereby, been used as a model to further understand the causes and pathogenesis of this diseases. Further analysis with caspase inhibitors such as P35 and analysis of cell death activity (CM1) is required to determine whether *SOD* mutations, similarly to *ferritin*, triggers caspase-dependent apoptosis in the *Drosophila* retina

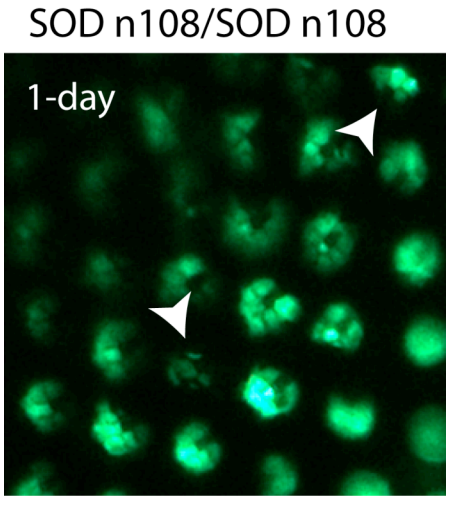

Figure 6.6 Antioxidant *SOD* Mutations Trigger PRC Degeneration –Using GFP live imaging, *SOD* null homozygotes at 1-day post-eclosure display internal disorganization of the ommatidial array and PRC degeneration revealed by smaller, abnormal and shrunken rhabdomeres (white arrows).

7 REFERENCES

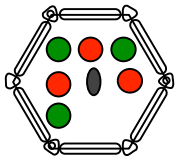

Abraham, M. C., Lu, Y. and Shaham, S. (2007). A morphologically conserved nonapoptotic program promotes linker cell death in Caenorhabditis elegans. *Dev Cell* **12**, 73-86.

Abrams, J. M., White, K., Fessler, L. I. and Steller, H. (1993). Programmed cell death during Drosophila embryogenesis. *Development* **117**, 29-43.

Agapite, J. and Steller, H. (2002). Genetic Analysis of Programmed Cell Death in *Drosophila melanogaster*. *Thesis, Massachusetts Institute of Technology*.

Ahmed, Y., Hayashi, S., Levine, A. and Wieschaus, E. (1998). Regulation of armadillo by a Drosophila APC inhibits neuronal apoptosis during retinal development. *Cell* **93**, 1171-82.

Albright, C. D., Borgman, C. and Craciunescu, C. N. (2003). Activation of a caspase-dependent oxidative damage response mediates TGFbeta1 apoptosis in rat hepatocytes. *Exp Mol Pathol* **74**, 256-61.

Ambrosini, G., Adida, C. and Altieri, D. C. (1997). A novel anti-apoptosis gene, survivin, expressed in cancer and lymphoma. *Nat Med* **3**, 917-21.

Andersen, J. K. (2004). Oxidative stress in neurodegeneration: cause or consequence? *Nat Med* **10 Suppl**, S18-25.

Anderson, P. R., Kirby, K., Hilliker, A. J. and Phillips, J. P. (2005). RNAi-mediated suppression of the mitochondrial iron chaperone, frataxin, in Drosophila. *Hum Mol Genet* **14**, 3397-405.

Andre, N. (2003). Hippocrates of Cos and apoptosis. *Lancet* **361**, 1306.

Arama, E., Agapite, J. and Steller, H. (2003). Caspase activity and a specific cytochrome C are required for sperm differentiation in Drosophila. *Dev Cell* **4**, 687-97.

Arama, E., Bader, M., Rieckhof, G. E. and Steller, H. (2007). A ubiquitin ligase complex regulates caspase activation during sperm differentiation in Drosophila. *PLoS Biol* **5**, e251.

Arama, E., Bader, M., Srivastava, M., Bergmann, A. and Steller, H. (2006). The two Drosophila cytochrome C proteins can function in both respiration and caspase activation. *EMBO J* **25**, 232-43.

Arosio, P. and Levi, S. (2002). Ferritin, iron homeostasis, and oxidative damage. *Free Radic Biol Med* **33**, 457-63.

Ashburner, M. and Bergman, C. M. (2005). Drosophila melanogaster: a case study of a model genomic sequence and its consequences. *Genome Res* **15**, 1661-7.

Bae, B. I., Xu, H., Igarashi, S., Fujimuro, M., Agrawal, N., Taya, Y., Hayward, S. D., Moran, T. H., Montell, C., Ross, C. A. et al. (2005). p53 mediates cellular dysfunction and behavioral abnormalities in Huntington's disease. *Neuron* **47**, 29-41.

Bantubungi, K., Jacquard, C., Greco, A., Pintor, A., Chtarto, A., Tai, K., Galas, M. C., Tenenbaum, L., Deglon, N., Popoli, P. et al. (2005). Minocycline in phenotypic models of Huntington's disease. *Neurobiol Dis* **18**, 206-17.

Barnham, K. J. and Bush, A. I. (2008). Metals in Alzheimer's and Parkinson's diseases. *Curr Opin Chem Biol* **12**, 222-8.

Barrio, R., de Celis, J. F., Bolshakov, S. and Kafatos, F. C. (1999). Identification of regulatory regions driving the expression of the Drosophila spalt complex at different developmental stages. *Dev Biol* **215**, 33-47.

Bartzokis, G., Cummings, J., Perlman, S., Hance, D. B. and Mintz, J. (1999). Increased basal ganglia iron levels in Huntington disease. *Arch Neurol* **56**, 569-74.

Beckman, J. S., Carson, M., Smith, C. D. and Koppenol, W. H. (1993). ALS, SOD and peroxynitrite. *Nature* **364**, 584.

Begemann, G., Michon, A. M., vd Voorn, L., Wepf, R. and Mlodzik, M. (1995). The Drosophila orphan nuclear receptor seven-up requires the Ras pathway for its function in photoreceptor determination. *Development* **121**, 225-35.

Bellen, H. J., Levis, R. W., Liao, G., He, Y., Carlson, J. W., Tsang, G., Evans-Holm, M., Hiesinger, P. R., Schulze, K. L., Rubin, G. M. et al. (2004). The BDGP gene disruption project: single transposon insertions associated with 40% of Drosophila genes. *Genetics* **167**, 761-81.

Belousov, V. V., Fradkov, A. F., Lukyanov, K. A., Staroverov, D. B., Shakhbazov, K. S., Terskikh, A. V. and Lukyanov, S. (2006). Genetically encoded fluorescent indicator for intracellular hydrogen peroxide. *Nat Methods* **3**, 281-6.

Berg, D. and Youdim, M. B. (2006). Role of iron in neurodegenerative disorders. *Top Magn Reson Imaging* **17**, 5-17.

Bergmann, A., Agapite, J., McCall, K. and Steller, H. (1998). The Drosophila gene hid is a direct molecular target of Ras-dependent survival signaling. *Cell* **95**, 331-41.

Bernal, A. and Kimbrell, D. A. (2000). Drosophila Thor participates in host immune defense and connects a translational regulator with innate immunity. *Proc Natl Acad Sci U S A* **97**, 6019-24.

Betz, A., Ryoo, H. D., Steller, H. and Darnell, J. E., Jr. (2008). STAT92E is a positive regulator of Drosophila inhibitor of apoptosis 1 (DIAP/1) and protects against radiation-induced apoptosis. *Proc Natl Acad Sci U S A* **105**, 13805-10.

Bilen, J. and Bonini, N. M. (2005). Drosophila as a model for human neurodegenerative disease. *Annu Rev Genet* **39**, 153-71.

Birnbaum, M. J., Clem, R. J. and Miller, L. K. (1994). An apoptosis-inhibiting gene from a nuclear polyhedrosis virus encoding a polypeptide with Cys/His sequence motifs. *J Virol* **68**, 2521-8.

Boyd, D., Jain, S. K., Crampton, J., Barrett, K. J. and Drysdale, J. (1984). Isolation and characterization of a cDNA clone for human ferritin heavy chain. *Proc Natl Acad Sci U S A* **81**, 4751-5.

Brachmann, C. B., Jassim, O. W., Wachsmuth, B. D. and Cagan, R. L. (2000). The Drosophila bcl-2 family member dBorg-1 functions in the apoptotic response to UV-irradiation. *Curr Biol* **10**, 547-50.

Brancolini, C., Sgorbissa, A. and Schneider, C. (1998). Proteolytic processing of the adherens junctions components beta-catenin and gamma-catenin/plakoglobin during apoptosis. *Cell Death Differ* **5**, 1042-50.

Brand, A. H. and Perrimon, N. (1993). Targeted gene expression as a means of altering cell fates and generating dominant phenotypes. *Development* **118**, 401-15.

Bratton, S. B., Walker, G., Srinivasula, S. M., Sun, X. M., Butterworth, M., Alnemri, E. S. and Cohen, G. M. (2001). Recruitment, activation and retention of caspases-9 and -3 by Apaf-1 apoptosome and associated XIAP complexes. *EMBO J* **20**, 998-1009.

Bredesen, D. E., Rao, R. V. and Mehlen, P. (2006). Cell death in the nervous system. *Nature* **443**, 796-802.

Brenner, S. (2003). Nature's gift to science (Nobel lecture). *Chembiochem* **4**, 683-7.

Brodsky, M. H., Nordstrom, W., Tsang, G., Kwan, E., Rubin, G. M. and Abrams, J. M. (2000). Drosophila p53 binds a damage response element at the reaper locus. *Cell* **101**, 103-13.

Broker, L. E., Kruyt, F. A. and Giaccone, G. (2005). Cell death independent of caspases: a review. *Clin Cancer Res* **11**, 3155-62.

Bump, N. J., Hackett, M., Hugunin, M., Seshagiri, S., Brady, K., Chen, P., Ferenz, C., Franklin, S., Ghayur, T., Li, P. et al. (1995). Inhibition of ICE family proteases by baculovirus antiapoptotic protein p35. *Science* **269**, 1885-8.

Cagan, R. L. and Ready, D. F. (1989a). Notch is required for successive cell decisions in the developing Drosophila retina. *Genes Dev* **3**, 1099-112.

Cagan, R. L. and Ready, D. F. (1989b). The emergence of order in the Drosophila pupal retina. *Dev Biol* **136**, 346-62.

Cahill, C. M., Lahiri, D. K., Huang, X. and Rogers, J. T. (2008). Amyloid precursor protein and alpha synuclein translation, implications for iron and inflammation in neurodegenerative diseases. *Biochim Biophys Acta*.

Casey, J. L., Hentze, M. W., Koeller, D. M., Caughman, S. W., Rouault, T. A., Klausner, R. D. and Harford, J. B. (1988). Iron-responsive elements: regulatory RNA sequences that control mRNA levels and translation. *Science* **240**, 924-8.

Cavodeassi, F., Diez Del Corral, R., Campuzano, S. and Dominguez, M. (1999). Compartments and organising boundaries in the Drosophila eye: the role of the homeodomain Iroquois proteins. *Development* **126**, 4933-42.

Cazzola, M., Bergamaschi, G., Dezza, L. and Arosio, P. (1990). Manipulations of cellular iron metabolism for modulating normal and malignant cell proliferation: achievements and prospects. *Blood* **75**, 1903-19.

Chai, J., Yan, N., Huh, J. R., Wu, J. W., Li, W., Hay, B. A. and Shi, Y. (2003). Molecular mechanism of Reaper-Grim-Hid-mediated suppression of DIAP1-dependent Dronc ubiquitination. *Nat Struct Biol* **10**, 892-8.

Challa, M., Malladi, S., Pellock, B. J., Dresnek, D., Varadarajan, S., Yin, Y. W., White, K. and Bratton, S. B. (2007). Drosophila Omi, a mitochondrial-localized IAP antagonist and proapoptotic serine protease. *EMBO J* **26**, 3144-56.

Chandrasekaran, V. and Beckendorf, S. K. (2003). senseless is necessary for the survival of embryonic salivary glands in Drosophila. *Development* **130**, 4719-28.

Chen, H., Lukas, T. J., Du, N., Suyeoka, G. and Neufeld, A. H. (2009). Dysfunction of the retinal pigment epithelium with age: increased iron decreases phagocytosis and lysosomal activity. *Invest Ophthalmol Vis Sci* **50**, 1895-902.

Chen, J. Call, G. B. Beyer, E. Bui, C. Cespedes, A. Chan, A. Chan, J. Chan, S. Chhabra, A. Dang, P. et al. (2005). Discovery-based science education: functional genomic dissection in Drosophila by undergraduate researchers. *PLoS Biol* **3**, e59.

Chen, L., Dentchev, T., Wong, R., Hahn, P., Wen, R., Bennett, J. and Dunaief, J. L. (2003). Increased expression of ceruloplasmin in the retina following photic injury. *Mol Vis* **9**, 151-8.

Chen, L., Wu, W., Dentchev, T., Wong, R. and Dunaief, J. L. (2004a). Increased metallothionein in light damaged mouse retinas. *Exp Eye Res* **79**, 287-93.

Chen, L., Wu, W., Dentchev, T., Zeng, Y., Wang, J., Tsui, I., Tobias, J. W., Bennett, J., Baldwin, D. and Dunaief, J. L. (2004b). Light damage induced changes in mouse retinal gene expression. *Exp Eye Res* **79**, 239-47.

Chen, M., Ona, V. O., Li, M., Ferrante, R. J., Fink, K. B., Zhu, S., Bian, J., Guo, L., Farrell, L. A., Hersch, S. M. et al. (2000). Minocycline inhibits caspase-1 and caspase-3 expression and delays mortality in a transgenic mouse model of Huntington disease. *Nat Med* **6**, 797-801.

Chen, P., Nordstrom, W., Gish, B. and Abrams, J. M. (1996). grim, a novel cell death gene in Drosophila. *Genes Dev* **10**, 1773-82.

Chen, Z., Naito, M., Hori, S., Mashima, T., Yamori, T. and Tsuruo, T. (1999). A human IAP-family gene, apollon, expressed in human brain cancer cells. *Biochem Biophys Res Commun* **264**, 847-54.

Cheresh, D. A. and Stupack, D. G. (2008). Regulation of angiogenesis: apoptotic cues from the ECM. *Oncogene* **27**, 6285-98.

Chew, S. K., Akdemir, F., Chen, P., Lu, W. J., Mills, K., Daish, T., Kumar, S., Rodriguez, A. and Abrams, J. M. (2004). The apical caspase dronc governs programmed and unprogrammed cell death in Drosophila. *Dev Cell* **7**, 897-907.

Chi, L., Ke, Y., Luo, C., Gozal, D. and Liu, R. (2007). Depletion of reduced glutathione enhances motor neuron degeneration in vitro and in vivo. *Neuroscience* **144**, 991-1003.

Chou, C. C., Gatti, R. A., Fuller, M. L., Concannon, P., Wong, A., Chada, S., Davis, R. C. and Salser, W. A. (1986). Structure and expression of ferritin genes in a human promyelocytic cell line that differentiates in vitro. *Mol Cell Biol* **6**, 566-73.

Chou, W. H., Hall, K. J., Wilson, D. B., Wideman, C. L., Townson, S. M., Chadwell, L. V. and Britt, S. G. (1996). Identification of a novel Drosophila opsin reveals specific patterning of the R7 and R8 photoreceptor cells. *Neuron* **17**, 1101-15.

Chou, W. H., Huber, A., Bentrop, J., Schulz, S., Schwab, K., Chadwell, L. V., Paulsen, R. and Britt, S. G. (1999). Patterning of the R7 and R8 photoreceptor cells of Drosophila: evidence for induced and default cell-fate specification. *Development* **126**, 607-16.

Chowdhury, I., Tharakan, B. and Bhat, G. K. (2006). Current concepts in apoptosis: the physiological suicide program revisited. *Cell Mol Biol Lett* **11**, 506-25.

Christich, A., Kauppila, S., Chen, P., Sogame, N., Ho, S. I. and Abrams, J. M. (2002). The damage-responsive Drosophila gene sickle encodes a novel IAP binding protein similar to but distinct from reaper, grim, and hid. *Curr Biol* **12**, 137-40.

Clark, I. E., Dodson, M. W., Jiang, C., Cao, J. H., Huh, J. R., Seol, J. H., Yoo, S. J., Hay, B. A. and Guo, M. (2006). Drosophila pink1 is required for mitochondrial function and interacts genetically with parkin. *Nature* **441**, 1162-6.

Clarke, P. G. and Clarke, S. (1996). Nineteenth century research on naturally occurring cell death and related phenomena. *Anat Embryol (Berl)* **193**, 81-99.

Claveria, C., Caminero, E., Martinez, A. C., Campuzano, S. and Torres, M. (2002). GH3, a novel proapoptotic domain in Drosophila Grim, promotes a mitochondrial death pathway. *EMBO J* **21**, 3327-36.

Clem, R. J., Fechheimer, M. and Miller, L. K. (1991). Prevention of apoptosis by a baculovirus gene during infection of insect cells. *Science* **254**, 1388-90.

Colussi, P. A., Quinn, L. M., Huang, D. C., Coombe, M., Read, S. H., Richardson, H. and Kumar, S. (2000). Debcl, a proapoptotic Bcl-2 homologue, is a component of the Drosophila melanogaster cell death machinery. *J Cell Biol* **148**, 703-14.

Conradt, B. and Horvitz, H. R. (1998). The C. elegans protein EGL-1 is required for programmed cell death and interacts with the Bcl-2-like protein CED-9. *Cell* **93**, 519-29.

Cook, T. and Desplan, C. (2001). Photoreceptor subtype specification: from flies to humans. *Semin Cell Dev Biol* **12**, 509-18.

Cooper, M. T. and Bray, S. J. (2000). R7 photoreceptor specification requires Notch activity. *Curr Biol* **10**, 1507-10.

Cordero, J., Jassim, O., Bao, S. and Cagan, R. (2004). A role for wingless in an early pupal cell death event that contributes to patterning the Drosophila eye. *Mech Dev* **121**, 1523-30.

Cregan, S. P., Fortin, A., MacLaurin, J. G., Callaghan, S. M., Cecconi, F., Yu, S. W., Dawson, T. M., Dawson, V. L., Park, D. S., Kroemer, G. et al. (2002). Apoptosis-inducing factor is involved in the regulation of caspase-independent neuronal cell death. *J Cell Biol* **158**, 507-17.

Crook, N. E., Clem, R. J. and Miller, L. K. (1993). An apoptosis-inhibiting baculovirus gene with a zinc finger-like motif. *J Virol* **67**, 2168-74.

Cunha-Oliveira, T., Rego, A. C., Cardoso, S. M., Borges, F., Swerdlow, R. H., Macedo, T. and de Oliveira, C. R. (2006). Mitochondrial dysfunction and caspase activation in rat cortical neurons treated with cocaine or amphetamine. *Brain Res* **1089**, 44-54.

Curtin, J. F., Donovan, M. and Cotter, T. G. (2002). Regulation and measurement of oxidative stress in apoptosis. *J Immunol Methods* **265**, 49-72.

Daish, T. J., Mills, K. and Kumar, S. (2004). Drosophila caspase DRONC is required for specific developmental cell death pathways and stress-induced apoptosis. *Dev Cell* **7**, 909-15.

Danial, N. N. and Korsmeyer, S. J. (2004). Cell death: critical control points. *Cell* **116**, 205-19.

de la Cova, C., Abril, M., Bellosta, P., Gallant, P. and Johnston, L. A. (2004). Drosophila myc regulates organ size by inducing cell competition. *Cell* **117**, 107-16.

Degterev, A., Boyce, M. and Yuan, J. (2003). A decade of caspases. *Oncogene* **22**, 8543-67.

Deveraux, Q. L., Roy, N., Stennicke, H. R., Van Arsdale, T., Zhou, Q., Srinivasula, S. M., Alnemri, E. S., Salvesen, G. S. and Reed, J. C. (1998). IAPs block apoptotic events induced by caspase-8 and cytochrome c by direct inhibition of distinct caspases. *EMBO J* **17**, 2215-23.

Dexter, D. T., Carayon, A., Javoy-Agid, F., Agid, Y., Wells, F. R., Daniel, S. E., Lees, A. J., Jenner, P. and Marsden, C. D. (1991). Alterations in the levels of iron, ferritin and other trace metals in Parkinson's disease and other neurodegenerative diseases affecting the basal ganglia. *Brain* **114 (Pt 4)**, 1953-75.

Dexter, D. T., Carayon, A., Vidailhet, M., Ruberg, M., Agid, F., Agid, Y., Lees, A. J., Wells, F. R., Jenner, P. and Marsden, C. D. (1990). Decreased ferritin levels in brain in Parkinson's disease. *J Neurochem* **55**, 16-20.

Dhaunsi, G. S., Kaur, J., Alsaeid, K., Turner, R. B. and Bitar, M. S. (2005). Very long chain fatty acids activate NADPH oxidase in human dermal fibroblasts. *Cell Biochem Funct* **23**, 65-8.

Dietzl, G., Chen, D., Schnorrer, F., Su, K. C., Barinova, Y., Fellner, M., Gasser, B., Kinsey, K., Oppel, S., Scheiblauer, S. et al. (2007). A genome-wide transgenic RNAi library for conditional gene inactivation in Drosophila. *Nature* **448**, 151-6.

Domingos, P. M., Mlodzik, M., Mendes, C. S., Brown, S., Steller, H. and Mollereau, B. (2004). Spalt transcription factors are required for R3/R4 specification and establishment of planar cell polarity in the Drosophila eye. *Development* **131**, 5695-702.

Dominguez, M. and de Celis, J. F. (1998). A dorsal/ventral boundary established by Notch controls growth and polarity in the Drosophila eye. *Nature* **396**, 276-8.

Dominguez, M., Wasserman, J. D. and Freeman, M. (1998). Multiple functions of the EGF receptor in Drosophila eye development. *Curr Biol* **8**, 1039-48.

Donepudi, M., Mac Sweeney, A., Briand, C. and Grutter, M. G. (2003). Insights into the regulatory mechanism for caspase-8 activation. *Mol Cell* **11**, 543-9.

Dorstyn, L. and Kumar, S. (2006). A cytochrome c-free fly apoptosome. *Cell Death Differ* **13**, 1049-51.

Dorstyn, L., Mills, K., Lazebnik, Y. and Kumar, S. (2004). The two cytochrome c species, DC3 and DC4, are not required for caspase activation and apoptosis in Drosophila cells. *J Cell Biol* **167**, 405-10.

Dorstyn, L., Read, S., Cakouros, D., Huh, J. R., Hay, B. A. and Kumar, S. (2002). The role of cytochrome c in caspase activation in Drosophila melanogaster cells. *J Cell Biol* **156**, 1089-98.

Doumanis, J., Dorstyn, L. and Kumar, S. (2007). Molecular determinants of the subcellular localization of the Drosophila Bcl-2 homologues DEBCL and BUFFY. *Cell Death Differ* **14**, 907-15.

Droge, W. (2002). Free radicals in the physiological control of cell function. *Physiol Rev* **82**, 47-95.

Droge, W. (2003). Oxidative stress and aging. *Adv Exp Med Biol* **543**, 191-200.

Du, Y., Ma, Z., Lin, S., Dodel, R. C., Gao, F., Bales, K. R., Triarhou, L. C., Chernet, E., Perry, K. W., Nelson, D. L. et al. (2001). Minocycline prevents nigrostriatal dopaminergic neurodegeneration in the MPTP model of Parkinson's disease. *Proc Natl Acad Sci U S A* **98**, 14669-74.

Duckett, C. S., Nava, V. E., Gedrich, R. W., Clem, R. J., Van Dongen, J. L., Gilfillan, M. C., Shiels, H., Hardwick, J. M. and Thompson, C. B. (1996). A conserved family of cellular genes related to the baculovirus iap gene and encoding apoptosis inhibitors. *EMBO J* **15**, 2685-94.

Dunkov, B. and Georgieva, T. (2006). Insect iron binding proteins: insights from the genomes. *Insect Biochem Mol Biol* **36**, 300-9.

Dunkov, B. C. and Georgieva, T. (1999). Organization of the ferritin genes in Drosophila melanogaster. *DNA Cell Biol* **18**, 937-44.

Dunkov, B. C., Georgieva, T., Yoshiga, T., Hall, M. and Law, J. H. (2002). Aedes aegypti ferritin heavy chain homologue: feeding of iron or blood influences message levels, lengths and subunit abundance. *J Insect Sci* **2**, 7.

Ellis, H. M. and Horvitz, H. R. (1986). Genetic control of programmed cell death in the nematode C. elegans. *Cell* **44**, 817-29.

Ellis, M. C., O'Neill, E. M. and Rubin, G. M. (1993). Expression of Drosophila glass protein and evidence for negative regulation of its activity in non-neuronal cells by another DNA-binding protein. *Development* **119**, 855-65.

Evan, G. I., Wyllie, A. H., Gilbert, C. S., Littlewood, T. D., Land, H., Brooks, M., Waters, C. M., Penn, L. Z. and Hancock, D. C. (1992). Induction of apoptosis in fibroblasts by c-myc protein. *Cell* **69**, 119-28.

Fernando, P., Kelly, J. F., Balazsi, K., Slack, R. S. and Megeney, L. A. (2002). Caspase 3 activity is required for skeletal muscle differentiation. *Proc Natl Acad Sci U S A* **99**, 11025-30.

Fisher, J., Devraj, K., Ingram, J., Slagle-Webb, B., Madhankumar, A. B., Liu, X., Klinger, M., Simpson, I. A. and Connor, J. R. (2007). Ferritin: a novel mechanism for delivery of iron to the brain and other organs. *Am J Physiol Cell Physiol* **293**, C641-9.

Fleury, C., Mignotte, B. and Vayssiere, J. L. (2002). Mitochondrial reactive oxygen species in cell death signaling. *Biochimie* **84**, 131-41.

Fortini, M. E. and Rubin, G. M. (1990). Analysis of cis-acting requirements of the Rh3 and Rh4 genes reveals a bipartite organization to rhodopsin promoters in Drosophila melanogaster. *Genes Dev* **4**, 444-63.

Franceschini, N., Kirschfeld, K. and Minke, B. (1981). Fluorescence of photoreceptor cells observed in vivo. *Science* **213**, 1264-7.

Freel, C. D., Richardson, D. A., Thomenius, M. J., Gan, E. C., Horn, S. R., Olson, M. R. and Kornbluth, S. (2008). Mitochondrial localization of Reaper to promote inhibitors of apoptosis protein degradation conferred by GH3 domain-lipid interactions. *J Biol Chem* **283**, 367-79.

Freeman, M. (1996). Reiterative use of the EGF receptor triggers differentiation of all cell types in the Drosophila eye. *Cell* **87**, 651-60.

Friesen, P. D. and Miller, L. K. (1987). Divergent transcription of early 35- and 94-kilodalton protein genes encoded by the HindIII K genome fragment of the baculovirus Autographa californica nuclear polyhedrosis virus. *J Virol* **61**, 2264-72.

Fuentes-Prior, P. and Salvesen, G. S. (2004). The protein structures that shape caspase activity, specificity, activation and inhibition. *Biochem J* **384**, 201-32.

Gafuik, C. and Steller, H. (2008). Identification and Characterization of a Viable ras Hypermorph in Drosophila. *Thesis, Rockefeller University*.

Georgieva, T., Dunkov, B. C., Harizanova, N., Ralchev, K. and Law, J. H. (1999). Iron availability dramatically alters the distribution of ferritin subunit messages in Drosophila melanogaster. *Proc Natl Acad Sci U S A* **96**, 2716-21.

Glickman, M. H. and Ciechanover, A. (2002). The ubiquitin-proteasome proteolytic pathway: destruction for the sake of construction. *Physiol Rev* **82**, 373-428.

Glucksmann, A. (1965). Cell death in normal development. *Arch Biol (Liege)* **76**, 419-37.

Godefroy, N., Lemaire, C., Renaud, F., Rincheval, V., Perez, S., Parvu-Ferecatu, I., Mignotte, B. and Vayssiere, J. L. (2004). p53 can promote mitochondria- and caspase-independent apoptosis. *Cell Death Differ* **11**, 785-7.

Golic, K. G. and Lindquist, S. (1989). The FLP recombinase of yeast catalyzes site-specific recombination in the Drosophila genome. *Cell* **59**, 499-509.

Goossen, B., Caughman, S. W., Harford, J. B., Klausner, R. D. and Hentze, M. W. (1990). Translational repression by a complex between the iron-responsive element of ferritin mRNA and its specific cytoplasmic binding protein is position-dependent in vivo. *EMBO J* **9**, 4127-33.

Gordon, N. (2000). Friedreich's ataxia and iron metabolism. *Brain Dev* **22**, 465-8.

Gottfried, Y., Rotem, A., Lotan, R., Steller, H. and Larisch, S. (2004). The mitochondrial ARTS protein promotes apoptosis through targeting XIAP. *EMBO J* **23**, 1627-35.

Goyal, L., McCall, K., Agapite, J., Hartwieg, E. and Steller, H. (2000). Induction of apoptosis by Drosophila reaper, hid and grim through inhibition of IAP function. *EMBO J* **19**, 589-97.

Grether, M. E., Abrams, J. M., Agapite, J., White, K. and Steller, H. (1995). The head involution defective gene of Drosophila melanogaster functions in programmed cell death. *Genes Dev* **9**, 1694-708.

Gu, S. and Rossi, J. J. (2005). Uncoupling of RNAi from active translation in mammalian cells. *RNA* **11**, 38-44.

Gutteridge, J. M. (1994). Hydroxyl radicals, iron, oxidative stress, and neurodegeneration. *Ann N Y Acad Sci* **738**, 201-13.

Habel, M. E. and Jung, D. (2006). Free radicals act as effectors in the growth inhibition and apoptosis of iron-treated Burkitt's lymphoma cells. *Free Radic Res* **40**, 789-97.

Hafen, E., Basler, K., Edstroem, J. E. and Rubin, G. M. (1987). Sevenless, a cell-specific homeotic gene of Drosophila, encodes a putative transmembrane receptor with a tyrosine kinase domain. *Science* **236**, 55-63.

Hahn, P., Dentchev, T., Qian, Y., Rouault, T., Harris, Z. L. and Dunaief, J. L. (2004a). Immunolocalization and regulation of iron handling proteins ferritin and ferroportin in the retina. *Mol Vis* **10**, 598-607.

Hahn, P., Qian, Y., Dentchev, T., Chen, L., Beard, J., Harris, Z. L. and Dunaief, J. L. (2004b). Disruption of ceruloplasmin and hephaestin in mice causes retinal iron overload and retinal degeneration with features of age-related macular degeneration. *Proc Natl Acad Sci U S A* **101**, 13850-5.

Haile, D. J. (1999). Regulation of genes of iron metabolism by the iron-response proteins. *Am J Med Sci* **318**, 230-40.

Halder, G., Callaerts, P. and Gehring, W. J. (1995). Induction of ectopic eyes by targeted expression of the eyeless gene in Drosophila. *Science* **267**, 1788-92.

Hales, K. G. (2004). The machinery of mitochondrial fusion, division, and distribution, and emerging connections to apoptosis. *Mitochondrion* **4**, 285-308.

Hamburger, A. E., West, A. P., Jr., Hamburger, Z. A., Hamburger, P. and Bjorkman, P. J. (2005). Crystal structure of a secreted insect ferritin reveals a symmetrical arrangement of heavy and light chains. *J Mol Biol* **349**, 558-69.

Hamburger, V. and Levi-Montalcini, R. (1949). Proliferation, differentiation and degeneration in the spinal ganglia of the chick embryo under normal and experimental conditions. *J Exp Zool* **111**, 457-501.

Harrison, P. M. and Arosio, P. (1996). The ferritins: molecular properties, iron storage function and cellular regulation. *Biochim Biophys Acta* **1275**, 161-203.

Hartmann, A., Hunot, S., Michel, P. P., Muriel, M. P., Vyas, S., Faucheux, B. A., Mouatt-Prigent, A., Turmel, H., Srinivasan, A., Ruberg, M. et al. (2000). Caspase-3: A vulnerability factor and final effector in apoptotic death of dopaminergic neurons in Parkinson's disease. *Proc Natl Acad Sci U S A* **97**, 2875-80.

Hay, B. A., Huh, J. R. and Guo, M. (2004). The genetics of cell death: approaches, insights and opportunities in Drosophila. *Nat Rev Genet* **5**, 911-22.

Hay, B. A., Wassarman, D. A. and Rubin, G. M. (1995). Drosophila homologs of baculovirus inhibitor of apoptosis proteins function to block cell death. *Cell* **83**, 1253-62.

Hay, B. A., Wolff, T. and Rubin, G. M. (1994). Expression of baculovirus P35 prevents cell death in Drosophila. *Development* **120**, 2121-9.

Hengartner, M. O., Ellis, R. E. and Horvitz, H. R. (1992). Caenorhabditis elegans gene ced-9 protects cells from programmed cell death. *Nature* **356**, 494-9.

Hengartner, M. O. and Horvitz, H. R. (1994). C. elegans cell survival gene ced-9 encodes a functional homolog of the mammalian proto-oncogene bcl-2. *Cell* **76**, 665-76.

Hentze, M. W., Caughman, S. W., Rouault, T. A., Barriocanal, J. G., Dancis, A., Harford, J. B. and Klausner, R. D. (1987). Identification of the iron-responsive element for the translational regulation of human ferritin mRNA. *Science* **238**, 1570-3.

Hentze, M. W., Keim, S., Papadopoulos, P., O'Brien, S., Modi, W., Drysdale, J., Leonard, W. J., Harford, J. B. and Klausner, R. D. (1986). Cloning, characterization, expression, and chromosomal localization of a human ferritin heavy-chain gene. *Proc Natl Acad Sci U S A* **83**, 7226-30.

Herman-Bachinsky, Y., Ryoo, H. D., Ciechanover, A. and Gonen, H. (2007). Regulation of the Drosophila ubiquitin ligase DIAP1 is mediated via several distinct ubiquitin system pathways. *Cell Death Differ* **14**, 861-71.

Ho, P. K. and Hawkins, C. J. (2005). Mammalian initiator apoptotic caspases. *FEBS J* **272**, 5436-53.

Hombria, J. C. and Sotillos, S. (2006). JAK/STAT signalling: STAT cannot play with Ken and Barbie. *Curr Biol* **16**, R98-100.

Horvitz, H. R. (2003). Worms, life, and death (Nobel lecture). *Chembiochem* **4**, 697-711.

Hu, S. and Yang, X. (2000). dFADD, a novel death domain-containing adapter protein for the Drosophila caspase DREDD. *J Biol Chem* **275**, 30761-4.

Huber, A., Schulz, S., Bentrop, J., Groell, C., Wolfrum, U. and Paulsen, R. (1997). Molecular cloning of Drosophila Rh6 rhodopsin: the visual pigment of a subset of R8 photoreceptor cells. *FEBS Lett* **406**, 6-10.

Huh, J. R., Foe, I., Muro, I., Chen, C. H., Seol, J. H., Yoo, S. J., Guo, M., Park, J. M. and Hay, B. A. (2007). The Drosophila inhibitor of apoptosis (IAP) DIAP2 is dispensable for cell survival, required for the innate immune response to gram-negative bacterial infection, and can be negatively regulated by the reaper/hid/grim family of IAP-binding apoptosis inducers. *J Biol Chem* **282**, 2056-68.

Hussain, S. P., Amstad, P., He, P., Robles, A., Lupold, S., Kaneko, I., Ichimiya, M., Sengupta, S., Mechanic, L., Okamura, S. et al. (2004). p53-induced up-regulation of MnSOD and GPx but not catalase increases oxidative stress and apoptosis. *Cancer Res* **64**, 2350-6.

Igaki, T., Kanda, H., Yamamoto-Goto, Y., Kanuka, H., Kuranaga, E., Aigaki, T. and Miura, M. (2002). Eiger, a TNF superfamily ligand that triggers the Drosophila JNK pathway. *EMBO J* **21**, 3009-18.

Igaki, T. and Miura, M. (2004). Role of Bcl-2 family members in invertebrates. *Biochim Biophys Acta* **1644**, 73-81.

Izaddoost, S., Nam, S. C., Bhat, M. A., Bellen, H. J. and Choi, K. W. (2002). Drosophila Crumbs is a positional cue in photoreceptor adherens junctions and rhabdomeres. *Nature* **416**, 178-83.

Jacobson, M. D., Weil, M. and Raff, M. C. (1997). Programmed cell death in animal development. *Cell* **88**, 347-54.

Jassim, O. W., Fink, J. L. and Cagan, R. L. (2003). Dmp53 protects the Drosophila retina during a developmentally regulated DNA damage response. *EMBO J* **22**, 5622-32.

Jellinger, K., Paulus, W., Grundke-Iqbal, I., Riederer, P. and Youdim, M. B. (1990). Brain iron and ferritin in Parkinson's and Alzheimer's diseases. *J Neural Transm Park Dis Dement Sect* **2**, 327-40.

Jin, S., Martinek, S., Joo, W. S., Wortman, J. R., Mirkovic, N., Sali, A., Yandell, M. D., Pavletich, N. P., Young, M. W. and Levine, A. J. (2000). Identification and characterization of a p53 homologue in Drosophila melanogaster. *Proc Natl Acad Sci U S A* **97**, 7301-6.

Joazeiro, C. A. and Weissman, A. M. (2000). RING finger proteins: mediators of ubiquitin ligase activity. *Cell* **102**, 549-52.

Kamata, H., Honda, S., Maeda, S., Chang, L., Hirata, H. and Karin, M. (2005). Reactive oxygen species promote TNFalpha-induced death and sustained JNK activation by inhibiting MAP kinase phosphatases. *Cell* **120**, 649-61.

Kanai, M. I., Okabe, M. and Hiromi, Y. (2005). seven-up Controls switching of transcription factors that specify temporal identities of Drosophila neuroblasts. *Dev Cell* **8**, 203-13.

Kanda, H., Igaki, T., Kanuka, H., Yagi, T. and Miura, M. (2002). Wengen, a member of the Drosophila tumor necrosis factor receptor superfamily, is required for Eiger signaling. *J Biol Chem* **277**, 28372-5.

Kanuka, H., Kuranaga, E., Takemoto, K., Hiratou, T., Okano, H. and Miura, M. (2005). Drosophila caspase transduces Shaggy/GSK-3beta kinase activity in neural precursor development. *EMBO J* **24**, 3793-806.

Kaufmann, S. H. and Hengartner, M. O. (2001). Programmed cell death: alive and well in the new millennium. *Trends Cell Biol* **11**, 526-34.

Kauppila, S., Maaty, W. S., Chen, P., Tomar, R. S., Eby, M. T., Chapo, J., Chew, S., Rathore, N., Zachariah, S., Sinha, S. K. et al. (2003). Eiger and its receptor, Wengen, comprise a TNF-like system in Drosophila. *Oncogene* **22**, 4860-7.

Kaur, D., Yantiri, F., Rajagopalan, S., Kumar, J., Mo, J. Q., Boonplueang, R., Viswanath, V., Jacobs, R., Yang, L., Beal, M. F. et al. (2003). Genetic or pharmacological iron chelation prevents MPTP-induced neurotoxicity in vivo: a novel therapy for Parkinson's disease. *Neuron* **37**, 899-909.

Kelso, R. J., Buszczak, M., Quinones, A. T., Castiblanco, C., Mazzalupo, S. and Cooley, L. (2004). Flytrap, a database documenting a GFP protein-trap insertion screen in Drosophila melanogaster. *Nucleic Acids Res* **32**, D418-20.

Kerr, J. F., Wyllie, A. H. and Currie, A. R. (1972). Apoptosis: a basic biological phenomenon with wide-ranging implications in tissue kinetics. *Br J Cancer* **26**, 239-57.

Kissel, H., Georgescu, M. M., Larisch, S., Manova, K., Hunnicutt, G. R. and Steller, H. (2005). The Sept4 septin locus is required for sperm terminal differentiation in mice. *Dev Cell* **8**, 353-64.

Koloteva, N., Muller, P. P. and McCarthy, J. E. (1997). The position dependence of translational regulation via RNA-RNA and RNA-protein interactions in the 5'-untranslated region of eukaryotic mRNA is a function of the thermodynamic competence of 40 S ribosomes in translational initiation. *J Biol Chem* **272**, 16531-9.

Kruszewski, M. and Iwanenko, T. (2003). Labile iron pool correlates with iron content in the nucleus and the formation of oxidative DNA damage in mouse lymphoma L5178Y cell lines. *Acta Biochim Pol* **50**, 211-5.

Kumar, J. P. and Ready, D. F. (1995). Rhodopsin plays an essential structural role in Drosophila photoreceptor development. *Development* **121**, 4359-70.

Kumar, S. and Doumanis, J. (2000). The fly caspases. *Cell Death Differ* **7**, 1039-44.

Kuo, Y. M., Duncan, J. L., Westaway, S. K., Yang, H., Nune, G., Xu, E. Y., Hayflick, S. J. and Gitschier, J. (2005). Deficiency of pantothenate kinase 2 (Pank2) in mice leads to retinal degeneration and azoospermia. *Hum Mol Genet* **14**, 49-57.

Kurada, P. and O'Tousa, J. E. (1995). Retinal degeneration caused by dominant rhodopsin mutations in Drosophila. *Neuron* **14**, 571-9.

Kurada, P. and White, K. (1998). Ras promotes cell survival in Drosophila by downregulating hid expression [see comments]. *Cell* **95**, 319-29.

Kuranaga, E. and Miura, M. (2007). Nonapoptotic functions of caspases: caspases as regulatory molecules for immunity and cell-fate determination. *Trends Cell Biol* **17**, 135-44.

Lamkanfi, M., Declercq, W., Kalai, M., Saelens, X. and Vandenabeele, P. (2002). Alice in caspase land. A phylogenetic analysis of caspases from worm to man. *Cell Death Differ* **9**, 358-61.

Lang, A. E. (2007). The progression of Parkinson disease: a hypothesis. *Neurology* **68**, 948-52.

Larisch, S., Yi, Y., Lotan, R., Kerner, H., Eimerl, S., Tony Parks, W., Gottfried, Y., Birkey Reffey, S., de Caestecker, M. P., Danielpour, D. et al. (2000). A novel mitochondrial septin-like protein, ARTS, mediates apoptosis dependent on its P-loop motif. *Nat Cell Biol* **2**, 915-21.

Lee, Y. S. and Carthew, R. W. (2003). Making a better RNAi vector for Drosophila: use of intron spacers. *Methods* **30**, 322-9.

Lehtinen, M. K., Yuan, Z., Boag, P. R., Yang, Y., Villen, J., Becker, E. B., DiBacco, S., de la Iglesia, N., Gygi, S., Blackwell, T. K. et al. (2006). A conserved MST-FOXO signaling pathway mediates oxidative-stress responses and extends life span. *Cell* **125**, 987-1001.

Lens, S. M., Vader, G. and Medema, R. H. (2006). The case for Survivin as mitotic regulator. *Curr Opin Cell Biol* **18**, 616-22.

Leulier, F., Lhocine, N., Lemaitre, B. and Meier, P. (2006). The Drosophila inhibitor of apoptosis protein DIAP2 functions in innate immunity and is essential to resist gram-negative bacterial infection. *Mol Cell Biol* **26**, 7821-31.

Levine, R. L., Williams, J. A., Stadtman, E. R. and Shacter, E. (1994). Carbonyl assays for determination of oxidatively modified proteins. *Methods Enzymol* **233**, 346-57.

Li, P., Allen, H., Banerjee, S., Franklin, S., Herzog, L., Johnston, C., McDowell, J., Paskind, M., Rodman, L., Salfeld, J. et al. (1995). Mice deficient in IL-1 beta-converting enzyme are defective in production of mature IL-1 beta and resistant to endotoxic shock. *Cell* **80**, 401-11.

Lind, M. I., Ekengren, S., Melefors, O. and Soderhall, K. (1998). Drosophila ferritin mRNA: alternative RNA splicing regulates the presence of the iron-responsive element. *FEBS Lett* **436**, 476-82.

Lind, M. I., Missirlis, F., Melefors, O., Uhrigshardt, H., Kirby, K., Phillips, J. P., Soderhall, K. and Rouault, T. A. (2006). Of two cytosolic aconitases expressed in Drosophila, only one functions as an iron-regulatory protein. *J Biol Chem* **281**, 18707-14.

Lipton, S. A. and Bossy-Wetzel, E. (2002). Dueling activities of AIF in cell death versus survival: DNA binding and redox activity. *Cell* **111**, 147-50.

Liu, X., Zou, H., Slaughter, C. and Wang, X. (1997). DFF, a heterodimeric protein that functions downstream of caspase-3 to trigger DNA fragmentation during apoptosis. *Cell* **89**, 175-84.

Liu, X. M., Peyton, K. J., Ensenat, D., Wang, H., Schafer, A. I., Alam, J. and Durante, W. (2005). Endoplasmic reticulum stress stimulates heme oxygenase-1 gene expression in vascular smooth muscle. Role in cell survival. *J Biol Chem* **280**, 872-7.

Lockshin, R. A. and Williams, C. M. (1965). Programmed Cell Death--I. Cytology of Degeneration in the Intersegmental Muscles of the Pernyi Silkmoth. *J Insect Physiol* **11**, 123-33.

Lohmann, I., McGinnis, N., Bodmer, M. and McGinnis, W. (2002). The Drosophila Hox gene deformed sculpts head morphology via direct regulation of the apoptosis activator reaper. *Cell* **110**, 457-66.

Lopes, K. O., Sparks, D. L. and Streit, W. J. (2008). Microglial dystrophy in the aged and Alzheimer's disease brain is associated with ferritin immunoreactivity. *Glia* **56**, 1048-60.

Lucas, J. J., Szepesi, A., Domenico, J., Takase, K., Tordai, A., Terada, N. and Gelfand, E. W. (1995). Effects of iron-depletion on cell cycle progression in normal human T lymphocytes: selective inhibition of the appearance of the cyclin A-associated component of the p33cdk2 kinase. *Blood* **86**, 2268-80.

Lukacsovich, T., Yuge, K., Awano, W., Asztalos, Z., Kondo, S., Juni, N. and Yamamoto, D. (2003). The ken and barbie gene encoding a putative transcription factor with a BTB domain and three zinc finger motifs functions in terminalia development of Drosophila. *Arch Insect Biochem Physiol* **54**, 77-94.

Luthi, A. U. and Martin, S. J. (2007). The CASBAH: a searchable database of caspase substrates. *Cell Death Differ* **14**, 641-50.

Lutz, R. J. (2000). Role of the BH3 (Bcl-2 homology 3) domain in the regulation of apoptosis and Bcl-2-related proteins. *Biochem Soc Trans* **28**, 51-6.

Macchi, P., Hemraj, I., Goetze, B., Grunewald, B., Mallardo, M. and Kiebler, M. A. (2003). A GFP-based system to uncouple mRNA transport from translation in a single living neuron. *Mol Biol Cell* **14**, 1570-82.

Macias, A., Romero, N. M., Martin, F., Suarez, L., Rosa, A. L. and Morata, G. (2004). PVF1/PVR signaling and apoptosis promotes the rotation and dorsal closure of the Drosophila male terminalia. *Int J Dev Biol* **48**, 1087-94.

Manjon, C., Sanchez-Herrero, E. and Suzanne, M. (2007). Sharp boundaries of Dpp signalling trigger local cell death required for Drosophila leg morphogenesis. *Nat Cell Biol* **9**, 57-63.

Massie, H. R., Aiello, V. R. and Williams, T. R. (1985). Iron accumulation during development and ageing of Drosophila. *Mech Ageing Dev* **29**, 215-20.

Mathiasen, I. S. and Jaattela, M. (2002). Triggering caspase-independent cell death to combat cancer. *Trends Mol Med* **8**, 212-20.

Matsumoto, H., Isono, K., Pye, Q. and Pak, W. L. (1987). Gene encoding cytoskeletal proteins in Drosophila rhabdomeres. *Proc Natl Acad Sci U S A* **84**, 985-9.

Mattson, M. P., Duan, W., Pedersen, W. A. and Culmsee, C. (2001). Neurodegenerative disorders and ischemic brain diseases. *Apoptosis* **6**, 69-81.

McCarthy, J. V. and Dixit, V. M. (1998). Apoptosis induced by Drosophila reaper and grim in a human system. Attenuation by inhibitor of apoptosis proteins (cIAPs). *J Biol Chem* **273**, 24009-15.

Mendes, C. S., Arama, E., Brown, S., Scherr, H., Srivastava, M., Bergmann, A., Steller, H. and Mollereau, B. (2006). Cytochrome c-d regulates developmental apoptosis in the Drosophila retina. *EMBO Rep* **7**, 933-9.

Mendes, C. S., Levet, C., Chatelain, G., Dourlen, P., Fouillet, A., Dichtel-Danjoy, M. L., Gambis, A., Ryoo, H. D., Steller, H. and Mollereau, B. (2009). ER stress protects from retinal degeneration. *EMBO J*.

Meyron-Holtz, E. G., Ghosh, M. C., Iwai, K., LaVaute, T., Brazzolotto, X., Berger, U. V., Land, W., Ollivierre-Wilson, H., Grinberg, A., Love, P. et al. (2004). Genetic ablations of iron regulatory proteins 1 and 2 reveal why iron regulatory protein 2 dominates iron homeostasis. *EMBO J* **23**, 386-95.

Micheau, O. and Tschopp, J. (2003). Induction of TNF receptor I-mediated apoptosis via two sequential signaling complexes. *Cell* **114**, 181-90.

Miller, A. C., Seymour, H., King, C. and Herman, T. G. (2008). Loss of seven-up from Drosophila R1/R6 photoreceptors reveals a stochastic fate choice that is normally biased by Notch. *Development* **135**, 707-15.

Miller, D. T. and Cagan, R. L. (1998). Local induction of patterning and programmed cell death in the developing Drosophila retina. *Development* **125**, 2327-35.

Missirlis, F., Hu, J., Kirby, K., Hilliker, A. J., Rouault, T. A. and Phillips, J. P. (2003). Compartment-specific protection of iron-sulfur proteins by superoxide dismutase. *J Biol Chem* **278**, 47365-9.

Missirlis, F., Kosmidis, S., Brody, T., Mavrakis, M., Holmberg, S., Odenwald, W. F., Skoulakis, E. M. and Rouault, T. A. (2007). Homeostatic mechanisms for iron storage revealed by genetic manipulations and live imaging of Drosophila ferritin. *Genetics* **177**, 89-100.

Mlodzik, M., Hiromi, Y., Weber, U., Goodman, C. S. and Rubin, G. M. (1990). The Drosophila seven-up gene, a member of the steroid receptor gene superfamily, controls photoreceptor cell fates. *Cell* **60**, 211-24.

Mollereau, B. and Domingos, P. M. (2005). Photoreceptor differentiation in Drosophila: from immature neurons to functional photoreceptors. *Dev Dyn* **232**, 585-92.

Mollereau, B., Dominguez, M., Webel, R., Colley, N. J., Keung, B., de Celis, J. F. and Desplan, C. (2001). Two-step process for photoreceptor formation in Drosophila. *Nature* **412**, 911-3.

Monserrate, J. P. and Brachmann, C. B. (2007). Identification of the death zone: a spatially restricted region for programmed cell death that sculpts the fly eye. *Cell Death Differ* **14**, 209-17.

Montell, C., Jones, K., Zuker, C. and Rubin, G. (1987). A second opsin gene expressed in the ultraviolet-sensitive R7 photoreceptor cells of Drosophila melanogaster. *J Neurosci* **7**, 1558-66.

Montell, C. and Rubin, G. M. (1988). The Drosophila ninaC locus encodes two photoreceptor cell specific proteins with domains homologous to protein kinases and the myosin heavy chain head. *Cell* **52**, 757-72.

Montell, D. J. (2006). A kinase gets caspases into shape. *Cell* **126**, 450-2.

Morey, M., Corominas, M. and Serras, F. (2003). DIAP1 suppresses ROS-induced apoptosis caused by impairment of the selD/sps1 homolog in Drosophila. *J Cell Sci* **116**, 4597-604.

Morizane, Y., Honda, R., Fukami, K. and Yasuda, H. (2005). X-linked inhibitor of apoptosis functions as ubiquitin ligase toward mature caspase-9 and cytosolic Smac/DIABLO. *J Biochem* **137**, 125-32.

Moses, K., Ellis, M. C. and Rubin, G. M. (1989). The glass gene encodes a zinc-finger protein required by Drosophila photoreceptor cells. *Nature* **340**, 531-6.

Moses, K. and Rubin, G. M. (1991). Glass encodes a site-specific DNA-binding protein that is regulated in response to positional signals in the developing Drosophila eye. *Genes Dev* **5**, 583-93.

Muckenthaler, M., Gunkel, N., Frishman, D., Cyrklaff, A., Tomancak, P. and Hentze, M. W. (1998). Iron-regulatory protein-1 (IRP-1) is highly conserved in two invertebrate species--characterization of IRP-1 homologues in Drosophila melanogaster and Caenorhabditis elegans. *Eur J Biochem* **254**, 230-7.

Muro, I., Hay, B. A. and Clem, R. J. (2002). The Drosophila DIAP1 protein is required to prevent accumulation of a continuously generated, processed form of the apical caspase DRONC. *J Biol Chem* **277**, 49644-50.

Newsome, T. P., Asling, B. and Dickson, B. J. (2000). Analysis of Drosophila photoreceptor axon guidance in eye-specific mosaics. *Development* **127**, 851-60.

Nichol, H., Law, J. H. and Winzerling, J. J. (2002). Iron metabolism in insects. *Annu Rev Entomol* **47**, 535-59.

Nichol, H. and Locke, M. (1999). Secreted ferritin subunits are of two kinds in insects molecular cloning of cDNAs encoding two major subunits of secreted ferritin from Calpodes ethlius. *Insect Biochem Mol Biol* **29**, 999-1013.

Nicholson, D. W. (1999). Caspase structure, proteolytic substrates, and function during apoptotic cell death. *Cell Death Differ* **6**, 1028-42.

Nishimura, I., Yang, Y. and Lu, B. (2004). PAR-1 kinase plays an initiator role in a temporally ordered phosphorylation process that confers tau toxicity in Drosophila. *Cell* **116**, 671-82.

O'Tousa, J. E., Baehr, W., Martin, R. L., Hirsh, J., Pak, W. L. and Applebury, M. L. (1985). The Drosophila ninaE gene encodes an opsin. *Cell* **40**, 839-50.

Olayioye, M. A., Kaufmann, H., Pakusch, M., Vaux, D. L., Lindeman, G. J. and Visvader, J. E. (2005). XIAP-deficiency leads to delayed lobuloalveolar development in the mammary gland. *Cell Death Differ* **12**, 87-90.

Owusu-Ansah, E., Yavari, A., Mandal, S. and Banerjee, U. (2008). Distinct mitochondrial retrograde signals control the G1-S cell cycle checkpoint. *Nat Genet* **40**, 356-61.

Papatsenko, D., Sheng, G. and Desplan, C. (1997). A new rhodopsin in R8 photoreceptors of Drosophila: evidence for coordinate expression with Rh3 in R7 cells. *Development* **124**, 1665-73.

Paradkar, P. N., Zumbrennen, K. B., Paw, B. H., Ward, D. M. and Kaplan, J. (2009). Regulation of mitochondrial iron import through differential turnover of mitoferrin 1 and mitoferrin 2. *Mol Cell Biol* **29**, 1007-16.

Park, H. H., Lo, Y. C., Lin, S. C., Wang, L., Yang, J. K. and Wu, H. (2007). The death domain superfamily in intracellular signaling of apoptosis and inflammation. *Annu Rev Immunol* **25**, 561-86.

Parks, A. L., Turner, F. R. and Muskavitch, M. A. (1995). Relationships between complex Delta expression and the specification of retinal cell fates during Drosophila eye development. *Mech Dev* **50**, 201-16.

Patel, B. N. and David, S. (1997). A novel glycosylphosphatidylinositol-anchored form of ceruloplasmin is expressed by mammalian astrocytes. *J Biol Chem* **272**, 20185-90.

Pellikka, M., Tanentzapf, G., Pinto, M., Smith, C., McGlade, C. J., Ready, D. F. and Tepass, U. (2002). Crumbs, the Drosophila homologue of human CRB1/RP12, is essential for photoreceptor morphogenesis. *Nature* **416**, 143-9.

Pereira, M. D., Eleutherio, E. C. and Panek, A. D. (2001). Acquisition of tolerance against oxidative damage in Saccharomyces cerevisiae. *BMC Microbiol* **1**, 11.

Perl, D. P. and Good, P. F. (1992). Comparative techniques for determining cellular iron distribution in brain tissues. *Ann Neurol* **32 Suppl**, S76-81.

Petcherski, A. G. and Kimble, J. (2000). Mastermind is a putative activator for Notch. *Curr Biol* **10**, R471-3.

Pham, C. G., Bubici, C., Zazzeroni, F., Papa, S., Jones, J., Alvarez, K., Jayawardena, S., De Smaele, E., Cong, R., Beaumont, C. et al. (2004). Ferritin heavy chain upregulation by NF-kappaB inhibits TNFalpha-induced apoptosis by suppressing reactive oxygen species. *Cell* **119**, 529-42.

Piccinelli, P. and Samuelsson, T. (2007). Evolution of the iron-responsive element. *RNA* **13**, 952-66.

Pichaud, F. and Desplan, C. (2001). A new visualization approach for identifying mutations that affect differentiation and organization of the Drosophila ommatidia. *Development* **128**, 815-26.

Plaza, S., Prince, F., Jaeger, J., Kloter, U., Flister, S., Benassayag, C., Cribbs, D. and Gehring, W. J. (2001). Molecular basis for the inhibition of Drosophila eye development by Antennapedia. *EMBO J* **20**, 802-11.

Porter, J. A., Hicks, J. L., Williams, D. S. and Montell, C. (1992). Differential localizations of and requirements for the two Drosophila ninaC kinase/myosins in photoreceptor cells. *J Cell Biol* **116**, 683-93.

Quinn, L., Coombe, M., Mills, K., Daish, T., Colussi, P., Kumar, S. and Richardson, H. (2003). Buffy, a Drosophila Bcl-2 protein, has anti-apoptotic and cell cycle inhibitory functions. *EMBO J* **22**, 3568-79.

Quinn, L. M. and Richardson, H. (2004). Bcl-2 in cell cycle regulation. *Cell Cycle* **3**, 7-9.

Rantnakumar, K. and Loiseau, P. (2002). P-element Enhancer Trap Screen: In Search of Genes Expressed in *Drosophila* Photoreceptors. (unpublished).

Ready, D. F., Hanson, T. E. and Benzer, S. (1976). Development of the Drosophila retina, a neurocrystalline lattice. *Dev Biol* **53**, 217-40.

Richter, B. W., Mir, S. S., Eiben, L. J., Lewis, J., Reffey, S. B., Frattini, A., Tian, L., Frank, S., Youle, R. J., Nelson, D. L. et al. (2001). Molecular cloning of ILP-2, a novel member of the inhibitor of apoptosis protein family. *Mol Cell Biol* **21**, 4292-301.

Riedl, S. J., Renatus, M., Schwarzenbacher, R., Zhou, Q., Sun, C., Fesik, S. W., Liddington, R. C. and Salvesen, G. S. (2001). Structural basis for the inhibition of caspase-3 by XIAP. *Cell* **104**, 791-800.

Robertson, H. M., Preston, C. R., Phillis, R. W., Johnson-Schlitz, D. M., Benz, W. K. and Engels, W. R. (1988). A stable genomic source of P element transposase in Drosophila melanogaster. *Genetics* **118**, 461-70.

Rodriguez, J. and Lazebnik, Y. (1999). Caspase-9 and APAF-1 form an active holoenzyme. *Genes Dev* **13**, 3179-84.

Rothe, M., Pan, M. G., Henzel, W. J., Ayres, T. M. and Goeddel, D. V. (1995). The TNFR2-TRAF signaling complex contains two novel proteins related to baculoviral inhibitor of apoptosis proteins. *Cell* **83**, 1243-52.

Rothenberger, S., Mullner, E. W. and Kuhn, L. C. (1990). The mRNA-binding protein which controls ferritin and transferrin receptor expression is conserved during evolution. *Nucleic Acids Res* **18**, 1175-9.

Rouault, T. A., Hentze, M. W., Caughman, S. W., Harford, J. B. and Klausner, R. D. (1988). Binding of a cytosolic protein to the iron-responsive element of human ferritin messenger RNA. *Science* **241**, 1207-10.

Roy, N., Deveraux, Q. L., Takahashi, R., Salvesen, G. S. and Reed, J. C. (1997). The c-IAP-1 and c-IAP-2 proteins are direct inhibitors of specific caspases. *EMBO J* **16**, 6914-25.

Rozman-Pungercar, J., Kopitar-Jerala, N., Bogyo, M., Turk, D., Vasiljeva, O., Stefe, I., Vandenabeele, P., Bromme, D., Puizdar, V., Fonovic, M. et al. (2003). Inhibition of papain-like cysteine proteases and legumain by caspase-specific inhibitors: when reaction mechanism is more important than specificity. *Cell Death Differ* **10**, 881-8.

Ryoo, H. D., Bergmann, A., Gonen, H., Ciechanover, A. and Steller, H. (2002). Regulation of Drosophila IAP1 degradation and apoptosis by reaper and ubcD1. *Nat Cell Biol* **4**, 432-8.

Ryoo, H. D., Gorenc, T. and Steller, H. (2004). Apoptotic cells can induce compensatory cell proliferation through the JNK and the Wingless signaling pathways. *Dev Cell* **7**, 491-501.

Sablina, A. A., Budanov, A. V., Ilyinskaya, G. V., Agapova, L. S., Kravchenko, J. E. and Chumakov, P. M. (2005). The antioxidant function of the p53 tumor suppressor. *Nat Med* **11**, 1306-13.

Sakahira, H., Enari, M. and Nagata, S. (1998). Cleavage of CAD inhibitor in CAD activation and DNA degradation during apoptosis. *Nature* **391**, 96-9.

Sanchez, M., Galy, B., Dandekar, T., Bengert, P., Vainshtein, Y., Stolte, J., Muckenthaler, M. U. and Hentze, M. W. (2006). Iron regulation and the cell cycle: identification of an iron-responsive element in the 3'-untranslated region of human cell division cycle 14A mRNA by a refined microarray-based screening strategy. *J Biol Chem* **281**, 22865-74.

Saunders, J. W., Jr. (1966). Death in embryonic systems. *Science* **154**, 604-12.

Sax, J. K. and El-Deiry, W. S. (2003). p53 downstream targets and chemosensitivity. *Cell Death Differ* **10**, 413-7.

Schaffer, J. E. and Lodish, H. F. (1994). Expression cloning and characterization of a novel adipocyte long chain fatty acid transport protein. *Cell* **79**, 427-36.

Schile, A. J., Garcia-Fernandez, M. and Steller, H. (2008). Regulation of apoptosis by XIAP ubiquitin-ligase activity. *Genes Dev* **22**, 2256-66.

Sepp, K. J. and Auld, V. J. (1999). Conversion of lacZ enhancer trap lines to GAL4 lines using targeted transposition in Drosophila melanogaster. *Genetics* **151**, 1093-101.

Seshagiri, S. and Miller, L. K. (1997). Caenorhabditis elegans CED-4 stimulates CED-3 processing and CED-3-induced apoptosis. *Curr Biol* **7**, 455-60.

Shaham, S. (1998). Identification of multiple Caenorhabditis elegans caspases and their potential roles in proteolytic cascades. *J Biol Chem* **273**, 35109-17.

Shaner, N. C., Campbell, R. E., Steinbach, P. A., Giepmans, B. N., Palmer, A. E. and Tsien, R. Y. (2004). Improved monomeric red, orange and yellow fluorescent proteins derived from Discosoma sp. red fluorescent protein. *Nat Biotechnol* **22**, 1567-72.

Shaner, N. C., Steinbach, P. A. and Tsien, R. Y. (2005). A guide to choosing fluorescent proteins. *Nat Methods* **2**, 905-9.

Shi, Y. (2002). Mechanisms of caspase activation and inhibition during apoptosis. *Mol Cell* **9**, 459-70.

Srinivasula, S. M., Datta, P., Fan, X. J., Fernandes-Alnemri, T., Huang, Z. and Alnemri, E. S. (2000). Molecular determinants of the caspase-promoting activity of Smac/DIABLO and its role in the death receptor pathway. *J Biol Chem* **275**, 36152-7.

Srinivasula, S. M., Datta, P., Kobayashi, M., Wu, J. W., Fujioka, M., Hegde, R., Zhang, Z., Mukattash, R., Fernandes-Alnemri, T., Shi, Y. et al. (2002). sickle, a novel Drosophila death gene in the reaper/hid/grim region, encodes an IAP-inhibitory protein. *Curr Biol* **12**, 125-30.

Srivastava, M., Scherr, H., Lackey, M., Xu, D., Chen, Z., Lu, J. and Bergmann, A. (2007). ARK, the Apaf-1 related killer in Drosophila, requires diverse domains for its apoptotic activity. *Cell Death Differ* **14**, 92-102.

Stark, W. S. and Thomas, C. F. (2004). Microscopy of multiple visual receptor types in Drosophila. *Mol Vis* **10**, 943-55.

Steller, H. (2008). Regulation of apoptosis in Drosophila. *Cell Death Differ* **15**, 1132-8.

Stowers, R. S. and Schwarz, T. L. (1999). A genetic method for generating Drosophila eyes composed exclusively of mitotic clones of a single genotype. *Genetics* **152**, 1631-9.

Struhl, G. and Basler, K. (1993). Organizing activity of wingless protein in Drosophila. *Cell* **72**, 527-40.

Suda, T., Takahashi, T., Golstein, P. and Nagata, S. (1993). Molecular cloning and expression of the Fas ligand, a novel member of the tumor necrosis factor family. *Cell* **75**, 1169-78.

Sulston, J. E. (1983). Neuronal cell lineages in the nematode Caenorhabditis elegans. *Cold Spring Harb Symp Quant Biol* **48 Pt 2**, 443-52.

Sulston, J. E. (2003). Caenorhabditis elegans: the cell lineage and beyond (Nobel lecture). *Chembiochem* **4**, 688-96.

Sulston, J. E. and Horvitz, H. R. (1977). Post-embryonic cell lineages of the nematode, Caenorhabditis elegans. *Dev Biol* **56**, 110-56.

Suzuki, Y., Nakabayashi, Y., Nakata, K., Reed, J. C. and Takahashi, R. (2001). X-linked inhibitor of apoptosis protein (XIAP) inhibits caspase-3 and -7 in distinct modes. *J Biol Chem* **276**, 27058-63.

Takahashi, A., Alnemri, E. S., Lazebnik, Y. A., Fernandes-Alnemri, T., Litwack, G., Moir, R. D., Goldman, R. D., Poirier, G. G., Kaufmann, S. H. and Earnshaw, W. C. (1996). Cleavage of lamin A by Mch2 alpha but not CPP32: multiple interleukin 1 beta-converting enzyme-related proteases with distinct substrate recognition properties are active in apoptosis. *Proc Natl Acad Sci U S A* **93**, 8395-400.

Tang, A. and Steller, H. (2007). Death By Frustration: How Defects in Cell Differentiation Trigger Apoptosis. *Thesis, Rockefeller University*.

Tanji, T. and Ip, Y. T. (2005). Regulators of the Toll and Imd pathways in the Drosophila innate immune response. *Trends Immunol* **26**, 193-8.

Tansley, K., Spear, F. G. and Glucksmann, A. (1937). The Effect of Gamma Rays on Cell Division in the Developing Rat Retina. *Br J Ophthalmol* **21**, 273-98.

Tawara, A. (1986). Transformation and cytotoxicity of iron in siderosis bulbi. *Invest Ophthalmol Vis Sci* **27**, 226-36.

Tenev, T., Zachariou, A., Wilson, R., Paul, A. and Meier, P. (2002). Jafrac2 is an IAP antagonist that promotes cell death by liberating Dronc from DIAP1. *EMBO J* **21**, 5118-29.

Teramoto, S., Tomita, T., Matsui, H., Ohga, E., Matsuse, T. and Ouchi, Y. (1999). Hydrogen peroxide-induced apoptosis and necrosis in human lung fibroblasts: protective roles of glutathione. *Jpn J Pharmacol* **79**, 33-40.

Thomas, F., Serratrice, G., Beguin, C., Aman, E. S., Pierre, J. L., Fontecave, M. and Laulhere, J. P. (1999). Calcein as a fluorescent probe for ferric iron. Application to iron nutrition in plant cells. *J Biol Chem* **274**, 13375-83.

Thomas, M. and Jankovic, J. (2004). Neurodegenerative disease and iron storage in the brain. *Curr Opin Neurol* **17**, 437-42.

Thompson, C. B. (1995). Apoptosis in the pathogenesis and treatment of disease. *Science* **267**, 1456-62.

Thompson, S. J., Loftus, L. T., Ashley, M. D. and Meller, R. (2008). Ubiquitin-proteasome system as a modulator of cell fate. *Curr Opin Pharmacol* **8**, 90-5.

Thornberry, N. A. and Lazebnik, Y. (1998). Caspases: enemies within. *Science* **281**, 1312-6.

Tittel, J. N. and Steller, H. (2000). A comparison of programmed cell death between species. *Genome Biol* **1**, REVIEWS0003.

Tomko, R. J., Jr., Bansal, P. and Lazo, J. S. (2006). Airing out an antioxidant role for the tumor suppressor p53. *Mol Interv* **6**, 23-5, 2.

Tomlinson, A. (1985). The cellular dynamics of pattern formation in the eye of Drosophila. *J Embryol Exp Morphol* **89**, 313-31.

Tomlinson, A. and Ready, D. F. (1986). Sevenless: A Cell-Specific Homeotic Mutation of the Drosophila Eye. *Science* **231**, 400-402.

Torti, F. M. and Torti, S. V. (2002). Regulation of ferritin genes and protein. *Blood* **99**, 3505-16.

Turk, B. and Stoka, V. (2007). Protease signalling in cell death: caspases versus cysteine cathepsins. *FEBS Lett* **581**, 2761-7.

Van Antwerp, D. J., Martin, S. J., Kafri, T., Green, D. R. and Verma, I. M. (1996). Suppression of TNF-alpha-induced apoptosis by NF-kappaB. *Science* **274**, 787-9.

Varkey, J., Chen, P., Jemmerson, R. and Abrams, J. M. (1999). Altered cytochrome c display precedes apoptotic cell death in Drosophila. *J Cell Biol* **144**, 701-10.

Vassiliev, V., Harris, Z. L. and Zatta, P. (2005). Ceruloplasmin in neurodegenerative diseases. *Brain Res Brain Res Rev* **49**, 633-40.

Vaux, D. L., Weissman, I. L. and Kim, S. K. (1992). Prevention of programmed cell death in Caenorhabditis elegans by human bcl-2. *Science* **258**, 1955-7.

Vucic, D., Stennicke, H. R., Pisabarro, M. T., Salvesen, G. S. and Dixit, V. M. (2000). ML-IAP, a novel inhibitor of apoptosis that is preferentially expressed in human melanomas. *Curr Biol* **10**, 1359-66.

Wang, D., Qian, L., Xiong, H., Liu, J., Neckameyer, W. S., Oldham, S., Xia, K., Wang, J., Bodmer, R. and Zhang, Z. (2006). Antioxidants protect PINK1-dependent dopaminergic neurons in Drosophila. *Proc Natl Acad Sci U S A* **103**, 13520-5.

Wang, M. C., Bohmann, D. and Jasper, H. (2003). JNK signaling confers tolerance to oxidative stress and extends lifespan in Drosophila. *Dev Cell* **5**, 811-6.

Warrick, J. M., Paulson, H. L., Gray-Board, G. L., Bui, Q. T., Fischbeck, K. H., Pittman, R. N. and Bonini, N. M. (1998). Expanded polyglutamine protein forms nuclear inclusions and causes neural degeneration in Drosophila. *Cell* **93**, 939-49.

White, K. (2000). Cell death: drosophila Apaf-1 - no longer in the (d)Ark. *Curr Biol* **10**, R167-9.

White, K., Grether, M. E., Abrams, J. M., Young, L., Farrell, K. and Steller, H. (1994). Genetic control of programmed cell death in Drosophila. *Science* **264**, 677-83.

White, K., Tahaoglu, E. and Steller, H. (1996). Cell killing by the Drosophila gene reaper. *Science* **271**, 805-7.

Whitworth, A. J., Theodore, D. A., Greene, J. C., Benes, H., Wes, P. D. and Pallanck, L. J. (2005). Increased glutathione S-transferase activity rescues dopaminergic neuron loss in a Drosophila model of Parkinson's disease. *Proc Natl Acad Sci U S A* **102**, 8024-9.

Wilkinson, J. C., Wilkinson, A. S., Galban, S., Csomos, R. A. and Duckett, C. S. (2008). Apoptosis-inducing factor is a target for ubiquitination through interaction with XIAP. *Mol Cell Biol* **28**, 237-47.

Wilson, R., Goyal, L., Ditzel, M., Zachariou, A., Baker, D. A., Agapite, J., Steller, H. and Meier, P. (2002). The DIAP1 RING finger mediates ubiquitination of Dronc and is indispensable for regulating apoptosis. *Nat Cell Biol* **4**, 445-50.

Wimmer, E. A., Cohen, S. M., Jackle, H. and Desplan, C. (1997). buttonhead does not contribute to a combinatorial code proposed for Drosophila head development. *Development* **124**, 1509-17.

Wing, J. P., Karres, J. S., Ogdahl, J. L., Zhou, L., Schwartz, L. M. and Nambu, J. R. (2002). Drosophila sickle is a novel grim-reaper cell death activator. *Curr Biol* **12**, 131-5.

Wittmann, C. W., Wszolek, M. F., Shulman, J. M., Salvaterra, P. M., Lewis, J., Hutton, M. and Feany, M. B. (2001). Tauopathy in Drosophila: neurodegeneration without neurofibrillary tangles. *Science* **293**, 711-4.

Wolff, T. and Ready, D. F. (1991). The beginning of pattern formation in the Drosophila compound eye: the morphogenetic furrow and the second mitotic wave. *Development* **113**, 841-50.

Wyllie, A. H., Kerr, J. F. and Currie, A. R. (1980). Cell death: the significance of apoptosis. *Int Rev Cytol* **68**, 251-306.

Xu, D., Li, Y., Arcaro, M., Lackey, M. and Bergmann, A. (2005). The CARD-carrying caspase Dronc is essential for most, but not all, developmental cell death in Drosophila. *Development* **132**, 2125-34.

Xu, Q., Kanthasamy, A. G. and Reddy, M. B. (2008). Neuroprotective effect of the natural iron chelator, phytic acid in a cell culture model of Parkinson's disease. *Toxicology* **245**, 101-8.

Xu, T. and Rubin, G. M. (1993). Analysis of genetic mosaics in developing and adult Drosophila tissues. *Development* **117**, 1223-37.

Xue, D. and Horvitz, H. R. (1995). Inhibition of the Caenorhabditis elegans cell-death protease CED-3 by a CED-3 cleavage site in baculovirus p35 protein. *Nature* **377**, 248-51.

Xue, D., Shaham, S. and Horvitz, H. R. (1996). The Caenorhabditis elegans cell-death protein CED-3 is a cysteine protease with substrate specificities similar to those of the human CPP32 protease. *Genes Dev* **10**, 1073-83.

Xue, X., Piao, J. H., Nakajima, A., Sakon-Komazawa, S., Kojima, Y., Mori, K., Yagita, H., Okumura, K., Harding, H. and Nakano, H. (2005). Tumor necrosis factor alpha (TNFalpha) induces the unfolded protein response (UPR) in a reactive oxygen species (ROS)-dependent fashion, and the UPR counteracts ROS accumulation by TNFalpha. *J Biol Chem* **280**, 33917-25.

Xue, Y., Daly, A., Yngvadottir, B., Liu, M., Coop, G., Kim, Y., Sabeti, P., Chen, Y., Stalker, J., Huckle, E. et al. (2006). Spread of an inactive form of caspase-12 in humans is due to recent positive selection. *Am J Hum Genet* **78**, 659-70.

Yan, N., Chai, J., Lee, E. S., Gu, L., Liu, Q., He, J., Wu, J. W., Kokel, D., Li, H., Hao, Q. et al. (2005). Structure of the CED-4-CED-9 complex provides insights into programmed cell death in Caenorhabditis elegans. *Nature* **437**, 831-7.

Yang, X., Chang, H. Y. and Baltimore, D. (1998). Essential role of CED-4 oligomerization in CED-3 activation and apoptosis. *Science* **281**, 1355-7.

Yang, Y., Dieter, M. Z., Chen, Y., Shertzer, H. G., Nebert, D. W. and Dalton, T. P. (2002). Initial characterization of the glutamate-cysteine ligase modifier subunit Gclm(-/-) knockout mouse. Novel model system for a severely compromised oxidative stress response. *J Biol Chem* **277**, 49446-52.

Yang, Y., Fang, S., Jensen, J. P., Weissman, A. M. and Ashwell, J. D. (2000). Ubiquitin protein ligase activity of IAPs and their degradation in proteasomes in response to apoptotic stimuli. *Science* **288**, 874-7.

Yang, Y., Gehrke, S., Haque, M. E., Imai, Y., Kosek, J., Yang, L., Beal, M. F., Nishimura, I., Wakamatsu, K., Ito, S. et al. (2005). Inactivation of Drosophila DJ-1 leads to impairments of oxidative stress response and phosphatidylinositol 3-kinase/Akt signaling. *Proc Natl Acad Sci U S A* **102**, 13670-5.

Yoo, S. J. (2005). Grim stimulates Diap1 poly-ubiquitination by binding to UbcD1. *Mol Cells* **20**, 446-51.

Yoo, Y. E., Hong, J. H., Hur, K. C., Oh, E. S. and Chung, J. M. (2004). Iron enhances NGF-induced neurite outgrowth in PC12 cells. *Mol Cells* **17**, 340-6.

Yu, S. Y., Yoo, S. J., Yang, L., Zapata, C., Srinivasan, A., Hay, B. A. and Baker, N. E. (2002). A pathway of signals regulating effector and initiator caspases in the developing Drosophila eye. *Development* **129**, 3269-78.

Yuan, J., Shaham, S., Ledoux, S., Ellis, H. M. and Horvitz, H. R. (1993). The C. elegans cell death gene ced-3 encodes a protein similar to mammalian interleukin-1 beta-converting enzyme. *Cell* **75**, 641-52.

Zachariou, A., Tenev, T., Goyal, L., Agapite, J., Steller, H. and Meier, P. (2003). IAP-antagonists exhibit non-redundant modes of action through differential DIAP1 binding. *EMBO J* **22**, 6642-52.

Zecca, L., Youdim, M. B., Riederer, P., Connor, J. R. and Crichton, R. R. (2004). Iron, brain ageing and neurodegenerative disorders. *Nat Rev Neurosci* **5**, 863-73.

Zermati, Y., Garrido, C., Amsellem, S., Fishelson, S., Bouscary, D., Valensi, F., Varet, B., Solary, E. and Hermine, O. (2001). Caspase activation is required for terminal erythroid differentiation. *J Exp Med* **193**, 247-54.

Zhang, F., Wang, W., Tsuji, Y., Torti, S. V. and Torti, F. M. (2008). Post-transcriptional modulation of iron homeostasis during p53-dependent growth arrest. *J Biol Chem* **283**, 33911-8.

Zhou, L., Schnitzler, A., Agapite, J., Schwartz, L. M., Steller, H. and Nambu, J. R. (1997). Cooperative functions of the reaper and head involution defective genes in the programmed cell death of Drosophila central nervous system midline cells. *Proc Natl Acad Sci U S A* **94**, 5131-6.

Zhou, L. and Steller, H. (2003). Distinct pathways mediate UV-induced apoptosis in Drosophila embryos. *Dev Cell* **4**, 599-605.

Zigmond, M. J. and Stricker, E. M. (1984). Parkinson's disease: studies with an animal model. *Life Sci* **35**, 5-18.

Zimmermann, K. C., Ricci, J. E., Droin, N. M. and Green, D. R. (2002). The role of ARK in stress-induced apoptosis in Drosophila cells. *J Cell Biol* **156**, 1077-87.

Zuker, C. S., Cowman, A. F. and Rubin, G. M. (1985). Isolation and structure of a rhodopsin gene from D. melanogaster. *Cell* **40**, 851-8.